CONTRIBUTION OF NOVEL MR IMAGING METHODS TO THE STAGING AND MANAGEMENT OF RECTAL CANCER

INÊS AFRODITE DA GLÓRIA PEREIRA SANTIAGO

Thesis to attain the degree of Doctor in Medicine
in the Specialty of Clinical Research
at the Faculdade de Ciências Médicas | NOVA Medical School da Universidade NOVA de Lisboa

September, 2021

CONTRIBUTION OF NOVEL MR IMAGING METHODS TO THE STAGING AND MANAGEMENT OF RECTAL CANCER

Inês Afrodite da Glória Pereira Santiago

Advisors:

Celso Matos, Director of the Radiology Department and Co-Director of Champalimaud Research at the Champalimaud Foundation

Noam Shemesh, Principal Investigator and Head of the Preclinical MR Imaging Facility at the Champalimaud Foundation

Tiago Bilhim, Interventional radiologist at the Centro Hospitalar Universitário de Lisboa Central and Invited Assistant Professor at Faculdade de Ciências Médicas | Nova Medical School da Universidade NOVA de Lisboa

Thesis to attain the degree of Doctor in Medicine
in the Specialty of Clinical Research

September, 2021

Table of contents

1. Abstract

The role of MR imaging in rectal cancer is well established in clinical practice but standard assessment has limitations. This thesis investigates new MR imaging methods and their diagnostic relevance in patient staging and management. It is divided in 2 parts: *Part I* focuses on lymph node staging and *Part II* focuses on the patterns of sustained clinical complete response after neoadjuvant therapy in locally-advanced rectal cancer patients.

Part I: Pelvic MR imaging is the pillar of rectal cancer staging and the basis for optimal multidisciplinary patient management. A thorough and systematic knowledge of the relevant anatomy, the key staging features and the particularities of early, low and mucinous tumours is mandatory for MR imaging interpretation and is provided as an educational review.

Lymph node status is one of the key staging features for risk stratification, but evaluation is hampered by limited MR imaging accuracy. Two new methodologies - Susceptibility Perturbation MR Imaging and Higher-order Diffusion MR Imaging - are introduced as original research. These methods were tested ex-vivo at ultra-high field (16.4 Tesla) in mesorectal lymph nodes and the mechanisms underlying the emerging contrasts were elucidated using quantitative histology. The experiments were then translated in-vivo upon patient staging in a clinical scanner (1.5 Tesla) and confronted with standard visual analysis by specialized radiologists.

Part 2: Locally-advanced rectal cancer patients may have no signs of viable tumour after neoadjuvant therapy. “Watch-and-Wait” programs were developed to place such patients under strict surveillance instead of submitting them to likely unnecessary mutilating surgery. MR imaging plays a fundamental role in the selection and follow-up of such patients and an educational review of the methods upon which they rely is provided.

To identify a clinical complete response in the early period after neoadjuvant therapy may be less important than to identify a clinical complete response that will be sustained over time, given complete responders that regrow present with a higher rate of distant metastases. Three new imaging patterns were reported for that purpose and are presented as original research – the split scar sign, the tumour scar depth angle difference and the scar thickness at second assessment.

Susceptibility Perturbation MR Imaging and Higher-order Diffusion MR Imaging may allow more accurate lymph node staging. As such, they may have the potential to improve risk stratification and patient selection for neoadjuvant therapy. The split scar sign, the scar depth angle difference and

the scar thickness at second assessment are simple tools to analyze on post-neoadjuvant therapy MR imaging that may aid in patient selection for “Watch-and-Wait” versus curative resection.

2. Acknowledgments

This work was carried out during my appointments as a researcher at the Preclinical MR imaging facility and as an assistant radiologist at the Imaging Department of the Champalimaud Foundation.

During my fundamental research experiments at the Preclinical MR imaging facility, all laboratory coworkers helped me substantially. Andrada Ianus was essential in the acquisition and post-processing analysis of our data. Paula Montesiños, Javier Sanchez and Nuno Loução from Philips Healthcare ® were fundamental for the clinical translation of our work. João Santinha from the Computational Clinical Imaging Group worked relentlessly in image co-registration. Joana Maia and Bruno Costa-Silva from the Systems Oncology Lab provided guidance for immunoflourescence. I am so grateful to all.

Regarding clinical research, I must thank my co-worker Maria João Barata in particular, and the whole technician team for their support. The collaboration of Nuno Figueiredo and Oriol Parés were fundamental. The surgeons Cisaltina Sobrinho, Vasco Geraldes and Carlos Leichsenring from Hospital Fernando Fonseca were essencial for patient recruitment. The availability of Antonio Galzerano, Rita Theias, Lara Castanheira, Alexandra Martins, Ana Santos, Antonio Beltran for specimen processing and histologic interpretation was noteworthy. Carlos Carvalho, as head of the Digestive Unit, orchestrated us as a colorectal cancer team. André Valente provided guidance through ethics committee requirements. I am immensely grateful to all, and also to Richard J Heald, for his nourishing curiosity, constant motivation and unconditional support.

I would like to thank Tiago Bilhim, my University tutor, who guided me through and supervised all my steps at Nova Medical School; and Noam Shemesh, my pre-clinical tutor, who used his geniality and extraordinary expertise in physics to find answers for my clinical questions, while introducing me to the astonishing world of preclinical MR imaging.

I am particularly grateful to my clinical tutor Celso Matos for devoting his outstanding professional expertise, his extraordinary interpersonal intelligence and his unceasing goodwill to elevate the quality of clinical practice and research in radiology. Celso Matos made way for this project while bridging my gaps and building me up as a radiologist and a researcher. I hope he continuous to do so for many years to come so that maybe one day I can do the same for others.

Finally, I would like to thank my family and friends for their cheerful support and understanding.

3. Publications

The material composing this thesis was published in international peer-reviewed journals and is listed below:

Original research:

1. Santiago I, Santinha J, Ianus A, Galzerano A, Theias R, Maia J, Barata M, Loução N, Costa-Silva B, Beltran A, Matos C, Shemesh N. Susceptibility Perturbation MRI Maps Tumor Infiltration into Mesorectal Lymph Nodes. Cancer Res. 2019. 1;79(9):2435-2444.

2. Santiago I, Barata M, Figueiredo N, Parés O, Henriques V, Galzerano A, Carvalho C, Matos C, Heald R. The split scar sign as an indicator of sustained complete response after neoadjuvant therapy in rectal cancer. Eur Radiol. 2020. 30(1):224-238.

3. Ianuş A, Santiago I, Galzerano A, Montesinos P, Loução N, Sanchez-Gonzalez J, Alexander DC, Matos C, Shemesh N. Higher-order diffusion MRI characterization of mesorectal lymph nodes in rectal cancer. Magn Reson Med. 2020. 84(1):348-364. *(Santiago I was co-responsible for the study design and was responsible for specimen processing, MR and histology image acquisition and image co-registration).*

4. Santiago I, Barata M, Figueiredo N, Parés O, Matos C. Early conformational changes at tumour bed and long term response after neoadjuvant therapy in rectal cancer. Eur J Radiol. 2021; 140:109742.

Educational reviews:

1. Santiago, I., Figueiredo, N., Parés, O. et al. MRI of rectal cancer—relevant anatomy and staging key points. Insights Imaging. 2020. 11(1):100.

2. Santiago I, Barata M, Figueiredo N, Fernandez L, Galzerano A, Parés O, Matos C. Re-staging and follow-up of rectal cancer patients with MR imaging when “Watch-and-Wait” is an option – A practical guide. Insights Imaging. 2021. 12:114.

4. PART I

LYMPH NODE STAGING WITH MR IMAGING

4.1 MRI of rectal cancer – Relevant anatomy and staging keypoints

Pelvic MR imaging is the pillar of rectal cancer staging and patient risk stratification. It therefore constitutes the basis for optimal multidisciplinary patient management. A thorough and systematic knowledge of the relevant anatomy, the key staging features and the particularities of early, low and mucinous tumours is mandatory for MR imaging interpretation and is provided in the following educational review.

Santiago *et al. Insights into Imaging* (2020) 11:100
https://doi.org/10.1186/s13244-020-00890-7

Insights into Imaging

EDUCATIONAL REVIEW Open Access

MRI of rectal cancer—relevant anatomy and staging key points

Inês Santiago[1,2,3*], Nuno Figueiredo[4], Oriol Parés[5] and Celso Matos[1,3]

Abstract

Rectal cancer has the eighth highest cancer incidence worldwide, and it is increasing in young individuals. However, in countries with a high human development index, mortality is decreasing, which may reflect better patient management, imaging being key. We rely on imaging to establish the great majority of clinical tumour features for therapeutic decision-making, namely tumour location, depth of invasion, lymph node involvement, circumferential resection margin status and extramural venous invasion. Despite major improvements in technique resulting in better image quality, and notwithstanding the dissemination of guidelines and examples of standardised reports, rectal cancer staging is still challenging on the day-to-day practice, and we believe there are three reasons. First, the normal posterior pelvic compartment anatomy and variants are not common knowledge to radiologists; second, not all rectal cancers fit in review paper models, namely the very early, the very low and the mucinous; and third, the key clinical tumour features may be tricky to analyse. In this review, we discuss the normal anatomy of the rectum and posterior compartment of the pelvis, systematise all rectal cancer staging key points and elaborate on the particularities of early, low and mucinous tumours. We also include our suggested reporting templates and a discussion of its comparison to the reporting templates provided by ESGAR and SAR.

Keywords: Anatomy, Anatomic variants, Rectum, Rectal cancer, Staging, Magnetic resonance

Key points

- Imaging is the pillar upon which therapeutic decisions are made in rectal cancer patients.
- Knowledge of normal anatomy and variants of the posterior pelvic compartment is mandatory for rectal cancer staging.
- We provide a roadmap for rectal cancer staging which includes anatomy and anatomic variants of the posterior pelvis, all key staging features and the particularities of early, low and mucinous tumours.

Background

Rectal cancer is one of the best examples of success of clinical research in the past 40 years. Total mesorectal excision (TME) alone, as opposed to blunt "pelvic rape", resulted in an increase in the 5-year cancer-specific survival rate from 38 to 68% [1]. The introduction of preoperative chemoradiation therapy in high-risk patients reduced local recurrence rates to 6% as opposed to 13% when given post-operatively [2]. We have slowly moved from specialty-centred decisions to generalised multidisciplinary patient management in which radiology became the pillar for risk stratification. In fact, with a differentiated multimodality treatment based on dedicated preoperative MR imaging, local recurrence has lost relevance compared to early diagnosis, treatment-related morbidity and metastatic disease prevention and control [3]. Despite major improvements in technique resulting in better image quality, and notwithstanding the dissemination of guidelines and examples of staging templates, rectal cancer staging is still challenging. It requires a

* Correspondence: ines.santiago@neuro.fchampalimaud.org
[1]Radiology Department, Champalimaud Foundation, Avenida Brasília, 1400-038 Lisbon, Portugal
[2]Nova Medical School, Campo Mártires da Pátria 130, 1169-056 Lisbon, Portugal
[3]Champalimaud Research, Champalimaud Foundation, Avenida Brasília, 1400-038 Lisbon, Portugal
Full list of author information is available at the end of the article

thorough convolution of radiologists with normal anatomy and technical pitfalls and a clear and systematised knowledge of the key imaging features of rectal cancer for decision-making. In this review, we have first focused on the normal anatomy of the posterior compartment of the pelvis, including the definitions of high/mid/low rectum, compartment boundaries, rectal blood supply and lymphatic drainage, and then systematised the staging key points, namely T staging and sub-staging, N staging and tumour deposits, M staging, circumferential margin of resection and extramural venous invasion. We have further included a discussion on the particularities of early, low and mucinous rectal cancers and provided our own staging templates. Even though no paper will ever replace validated experience and advice from senior experts, we aim to contribute to an easier and smoother training of interested radiologists.

Main Text

MR imaging of the normal rectum

From where up to where down

The rectum ends distally at the anorectal transition. The anorectal transition may be defined by 2 anatomic landmarks: the first is an abrupt increase in thickness of the inner muscular layer, corresponding to the upper limit of the internal sphincter of the anus (Fig. 1a) [4]. The other is the superior border of the puborectalis—the sling or U-shaped portion of the levator ani muscle complex (or "pelvic diaphragm")—which is anchored anteriorly to the inferior pubic ramus on each side of the symphysis pubis and posteriorly to the anococcygeal raphe (Fig. 1b) [5, 6].

The definition of the upper limit of the rectum is an intraoperative definition, corresponding to the lower limit of the large bowel that can be mobilised away from the spinal column. On MR imaging, it may correspond to the point of inflection between the more vertical rectum and the more horizontal rectosigmoid or "sigmoid take-off" [7–9] (Fig. 2a). The actual sigmoid starts at another more horizontal inflection, away from the lesser pelvis (Fig. 2b).

The rectum may be divided into 3 segments: upper, mid and low. The upper rectum is located above the lower limit of the anterior peritoneal reflection (see below) (Fig. 2a) [8]. The low rectum is surgically defined as the portion of the rectum that is less than 6 cm from the anal verge, visible on sagittal T2-WI as the lower limit of hypointense skin change (Fig. 2a) [10, 11]. The middle rectum is in between these two segments (Fig. 2a).

Keep in mind For standardization purposes, we recommend rectal cancer location measurements to be made based on the central axis of both the anal canal and rectum (Fig. 2a). Rectum definitions should be clear to the whole multidisciplinary team given older definitions are still frequently utilised. The latter include the distalmost 16 cm, 15 cm or 12 cm of the large bowel and the segment spanning from the anorectal transition to S3 or to the promontory [12].

The rectal wall

Although peristalsis, pulsation, breathing and susceptibility from bowel air may cause image artefacts, in optimal conditions, the layers of the rectal wall should be clearly defined. The mucosa is a thin, dark regular line on T2 (Fig. 3a). It is underlined by the T2-hyperintense fat-rich submucosa which is highly variable in thickness from patient to patient and also according to the degree of distension of the rectum (Fig. 3a). The muscularis propria is dark on T2 (similarly to skeletal muscle) and

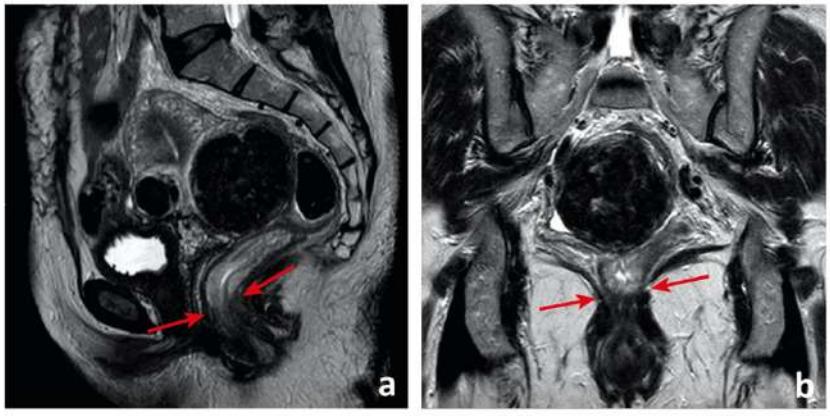

Fig. 1 The anorectal transition may be defined by the upper limit of the internal sphincter of the anus (between arrows in **a**), which is generally much thicker than the inner muscular layer of the *muscularis propria* of the rectum, or by the plane that intersects the superior border of the *puborectalis muscle* (between arrows in **b**), which may be asymmetric, as in the example depicted

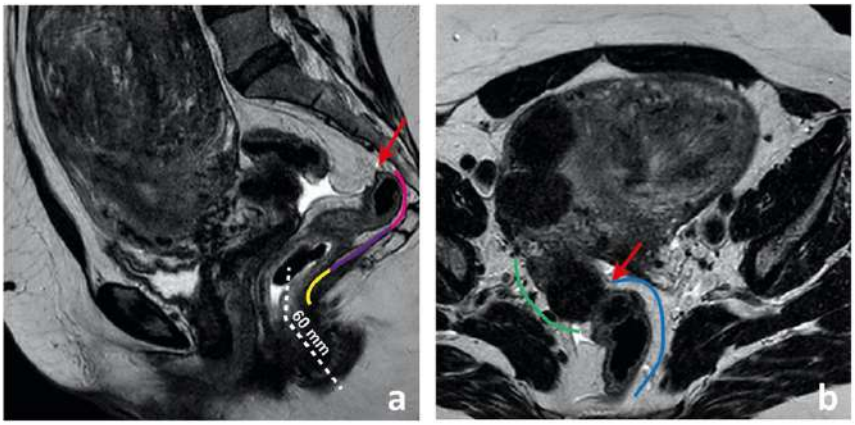

Fig. 2 The upper limit of the rectum corresponds on MR imaging to the point of inflexion between the more vertical rectum and the more horizontal sigmoid "take off" (arrow in **a**). The sigmoid starts at another more horizontal inflection, better visualised in the (oblique) axial plane (arrow in **b**). The low rectum is the segment located < 6 cm above the anal verge and above the anorectal transition (lined in yellow in **a**); the mid-rectum is located between the low rectum and the plane of the lowest point of the anterior peritoneal reflection (lined in purple in **a**); the high rectum is the segment above it and below the sigmoid "take-off" (lined in pink in **a**). The sigmoid "take-off" or rectosigmoid transition is lined in blue in **b**, while the actual sigmoid is lined in green

is composed of an inner circular layer and an outer longitudinal layer (Fig. 3a). Once again, its thickness varies according to the degree of distension of the rectum. The longitudinal layer of the muscularis propria is covered by the fat-rich mesorectum, which is highly variable in thickness according to body composition and unevenly distributed (Fig. 3a–d). Anteriorly, it may be very thin or even not visible, particularly in the 2 cm above the anorectal transition (Fig. 3c, d) [12].

Keep in mind A small enema before MR imaging may minimise susceptibility from bowel air [13]. Spasmolytic agents such as butylscopolamin or glucagon significantly reduce artefacts from peristalsis and may be administered to improve image quality in the absence of contraindications (Fig. 4) [13]. Our rectal cancer staging acquisition parameters at 1.5T are presented in Table 1.

The envelope

The rectum is out of the peritoneal cavity, and its serosa—the mesorectal fascia—is displaced radially to contain a large fatty cushion—the mesorectum. The mesorectal fascia is usually described as a pencil-drawn hypointense line on T2. However, it is a multi-layered envelope that presents with gaps, particularly at its lower antero-lateral aspect, which means that at some points it may not be visible and we must extrapolate its expected position (Fig. 5a) [14]. Also, it is juxtaposed to the parietal fascias, which contain the autonomic nerves [14]. As such, multiple pencil-drawn T2-hypointense lines may be apparent, in which case the innermost should be considered (Fig. 5b). The virtual space between the mesorectal fascia and the parietal fascias is the holy plane of rectal cancer surgery—the plane through which the surgeon must perform sharp dissection to obtain optimal oncologic results with minimal bleeding and autonomic nerve damage-related morbidity.

The parietal fascias have different names according to location. Anteriorly, in between the anterolateral neurovascular bundles and extending craniocaudally from the pelvic floor to the peritoneal reflection is the trapezoidal-shaped Dennonvillier fascia (Fig. 5c, d) [15]; posteriorly, covering the sacrum, is the presacral fascia (Fig. 5d); and extending between the mesorectal fascia and the presacral fascia at the level of S2/S4 is the Waldeyer's/rectosacral fascia (Fig. 5e). It divides the retrorectal space into superior and inferior compartments [14, 16–18].

Caudally, the mesorectal fascia is in continuity with the intersphicteric plane (Fig. 5f) [18]. Cranially, it is in continuity with the peritoneal reflection, which is lower anteriorly, of intermediate height laterally and higher posteriorly. The most relevant reference while staging rectal cancer is the anterior peritoneal reflection, which we should look for in the plane immediately below any pelvic small bowel loops and the sigmoid take-off. Its appearance on (oblique) axial plane is that of a seagull or V-shaped T2-hypointense line infolding (Fig. 6a). On mid-sagittal plane, this T2-hypointense line extends roughly horizontally from the anterior rectal wall to the roof of the mesorectal fascia, most commonly at the level of the torus uterinus in women or superior bladder in men (Fig. 6b) [19, 20]. The posterior peritoneal

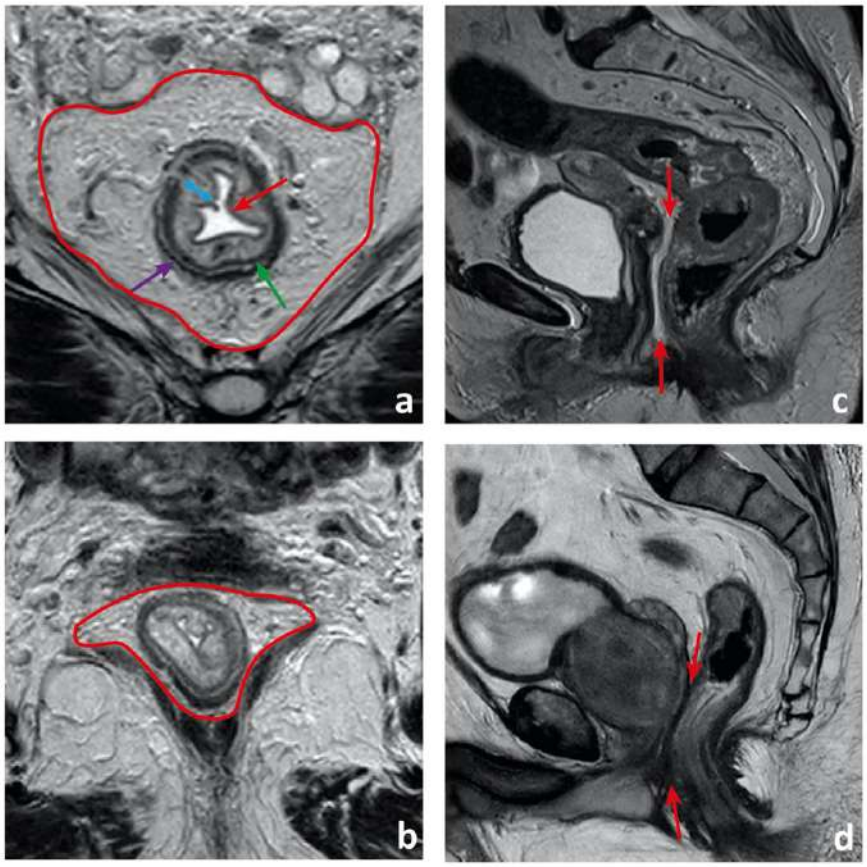

Fig. 3 The rectal wall. The mucosa is visible on T2-weighted imaging as a regular thin (≈ 1 mm) hypointense line delimiting the lumen (red arrow in **a**). The submucosa is hyperintense and of variable thickness (double-headed blue arrow in **a**). It may not be visible when the rectum is distended. The *muscularis propria* is composed of an inner circular layer (green arrow in **a**) and an outer longitudinal layer (purple arrow in **a**) which may be separated by a thin layer of fat, as in the example shown. Lying externally to it is a cushion of mesorectal fat (delimited in red in **a**) that tappers inferiorly (delimited in red in **c**) and anteriorly, where it can be thin (between arrows in **c**) or even invisible (between arrows in **d**), in which case the mid/low rectum appears juxtaposed to the Dennonvillier fascia

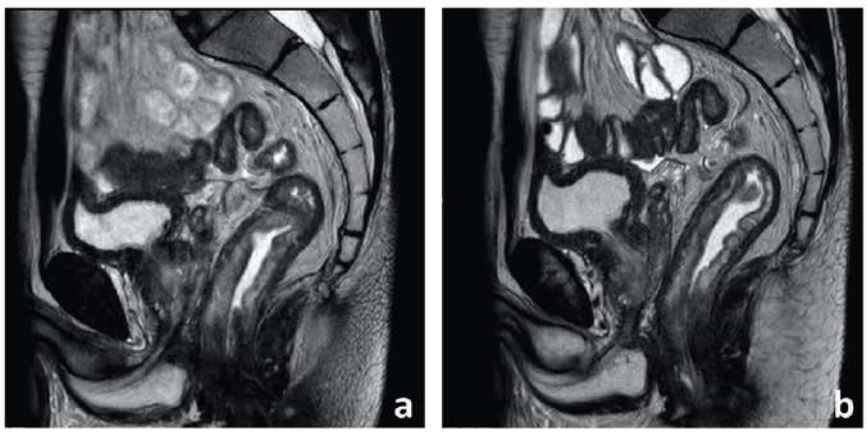

Fig. 4 Sagittal T2-weighted images before (**a**) and 5 min after (**b**) IV administration of a spasmolytic agent (butylscopolamine 20 mg). Notice how the walls of the rectum and small bowel are much better defined due to limited peristalsis

Table 1 MR acquisition parameters at a 1.5 T Ingenia Philips Healthcare®, Best, The Netherlands equipment

Parameter	Oblique axial T2-weighted turbo spin-echo*	Oblique coronal T2-weighted turbo spin-echo	Sagittal T2-weighted turbo spin-echo	Single-shot spin-echo echo-planar diffusion-weighted+	2D T1-weighted gradient-echo
Echo time (ms)	85	100	100	90	10
Repetition time (ms)	5692	2000	2660	4288	683
Echo train length	18	16	21	–	–
Slice thickness (mm)	3	3	3	5	5
Gap (mm)	0.3	0.3	0	0	1
Matrix	416 × 465	200 × 179	252 × 223	76 × 65	292 × 300
Field-of-view (mm)	250 × 328	160 × 160	200 × 200	200 × 200	290 × 348
In-plane resolution (mm^2)	0.6 × 0.7	0.8 × 0.8	0.8 × 0.9	2.6 × 3.01	1 × 1.16
Signal averages	1	2	2	7	1

*Oblique axial scans are acquired perpendicular to the long axis of the rectal wall at tumour location
+Spectral pre-saturation with inversion recovery is utilised for fat saturation. *B* values of 0 and 1400 s/mm^2 are employed

reflection is located most commonly 1 to 4 cm below S1–S2 and corresponds to the upper limit of the rectum [21, 22]. It is not easily identified.

Keep in mind The anterior peritoneal reflection can easily be identified whenever there is a small amount of free peritoneal fluid because in the supine position it will accumulate at the deepest point of the rectovesical or rectouterine pouch, exactly where the peritoneum "reflects" (Fig. 6c). The height of the anterior peritoneal reflection is variable, and it may not be visible in > 10–25% of cases [19, 20].

The blood supply

Arterial blood arrives at the rectum through 4 routes. The main route is the superior rectal artery, which is the continuation of the inferior mesenteric artery when it crosses the left common/internal iliac artery (Fig. 7a) [22]. The middle rectal arteries are inconsistent (present in 36–57% of cases) and highly variable. They may be unilateral, double or treble and may arise from the internal iliac or one of its branches [22–24]. They usually reach the mesorectum through either its antero-lateral or postero-lateral aspect, roughly 6 cm above the pelvic floor (Fig. 7b) [22]. The inferior rectal arteries originate from the internal pudendal arteries below the levator ani muscle, cross the ischioanal fossa anteromedially and irrigate the distal rectum, anal canal and internal and external anal sphincters (Fig. 7c) [24]. The middle sacral artery courses inferiorly along the surface of the lumbo-sacral vertebrae, within the presacral space and usually contributes with small vessels to the posterior surface of the rectum (Fig. 7d) [24]. The 4 rectal arterial routes communicate extensively through intramural anastomosis. However, in the posterior and inferior portion of the low rectum, there is a relatively vessel-deficient area which may explain why most anastomotic leaks after low anterior resections (LAR) occur in this location (Fig. 8) [22].

The venous drainage takes place through both an outer muscularis plexus that extends longitudinally from the anterior peritoneal reflexion down to the *levatior ani*, and an inner submucosal plexus which runs through the whole extension of the rectum and continues down to the anus [22]. Both plexus anastomose superiorly give rise to the superior rectal vein, draining the roughly upper 2/3 of the rectum into the portal circulation through the inferior mesenteric vein [22]. Inferiorly, the inner plexus becomes the inferior rectal vein. A middle rectal vein may be found in about 32.6%, usually unilaterally and rarely accompanied by a middle rectal artery. Inferior and middle rectal veins drain roughly the distal 1/3 of the rectum into the systemic circulation through the internal iliac vein [22, 25].

Keep in mind Surgeons may find information on the presence of middle rectal artery(ies) and vein(s), their route and calibre useful to prevent unexpected bleeding, and as such, we should provide that information on staging reports. The fact that the lower 1/3 of the rectum drains into the systemic circulation rather than the portal circulation may at least partially justify the higher rate of lung metastasis in patients with low rectal cancer [26].

The lymphatic drainage

The intramural lymphatic network drains to extramural lymphatics that in general follow the course of blood vessels [24]. Along the course of lymphatics within the mesorectum, we find a variable number of lymph nodes (mean 6.8 to 73.7 in surgical TME specimens with varied disease processes, surgical technique and pathology processing) [27–30]. Their size ranges between 2 and 10 mm in normal subjects, and they are more numerous

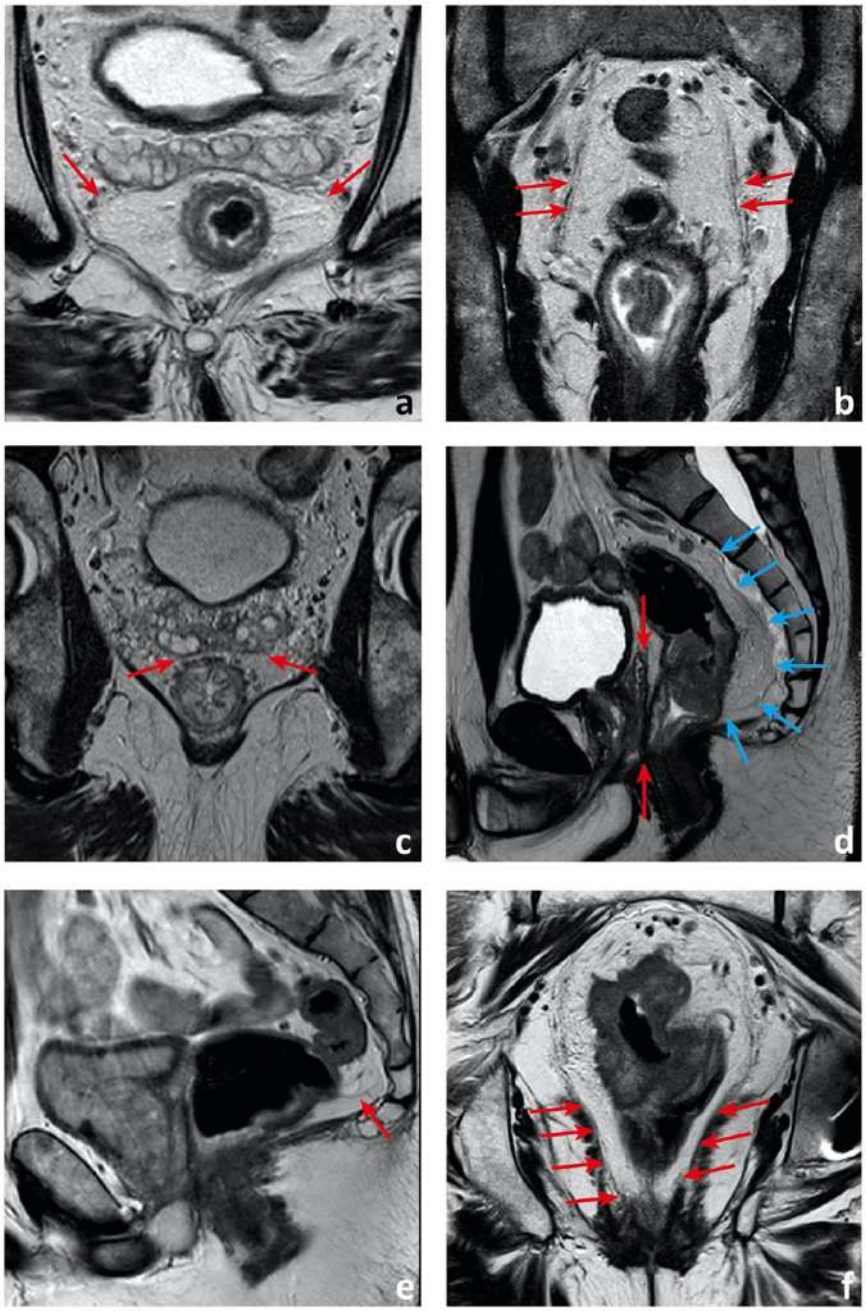

Fig. 5 The mesorectal fascia may present with gaps, particularly anterolaterally (arrows in **a**). It is a multilayered envelope and as such multiple hypointense lines may be apparent (arrows in **b**). Anteriorly, in between the neurovascular bundles, extending from the peritoneal reflection down to the pelvic floor, the mesorectal fascia is juxtaposed to the Dennonvillier fascia (between red arrows in **c** and **d**). Posteriorly, it is juxtaposed to the presacral fascia (blue arrows in **d**). Sometimes, the presacral compartment is divided by the Waldeyers fascia (arrow in **e**) into superior and inferior compartments. Inferiorly, the mesorectal fascia tappers and is "lost" within the intersphincteric plane (arrows in **f**)

and larger in the upper and posterior mesorectum (Fig. 9) [27–30]. Normal/reactive lymph nodes on T2-WI MR imaging appear homogeneous in 48 to 88% and with smooth, sharply demarcated borders in 80 to 94% of cases [31, 32]. In approximately 70% of cases, they will show a smooth and regular, uninterrupted chemical shift effect on T2-WI in the phase encoding direction, likely the result from the sharp interface between the water-rich subcapsular sinus

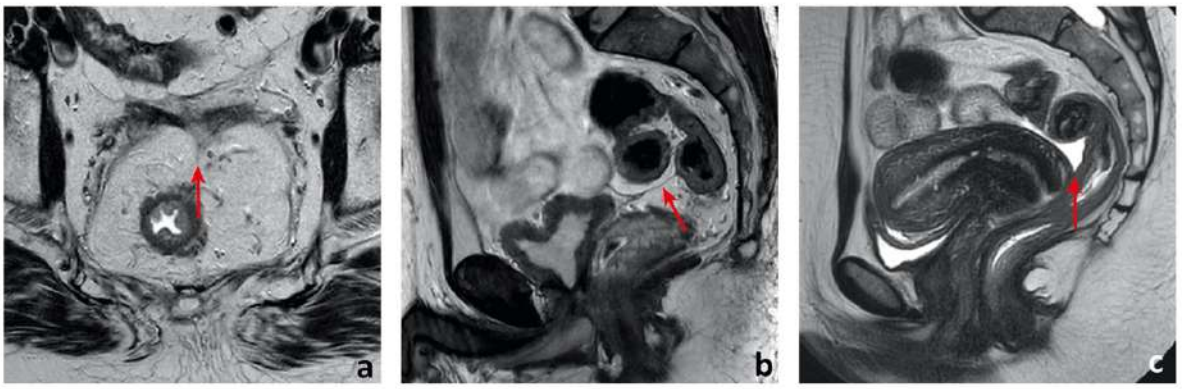

Fig. 6 The peritoneal reflection, when visible, may present with a seagull or V-shaped appearance on the (oblique) axial plane (arrow in **a**). The sagittal plane is depicted as a hypointense line extending from the rectal wall to the roof of the mesorectal fascia (arrow in **b**). It is more easily identified whenever there is a small amount of peritoneal effusion, which will accumulate immediately above it (arrow in **c**)

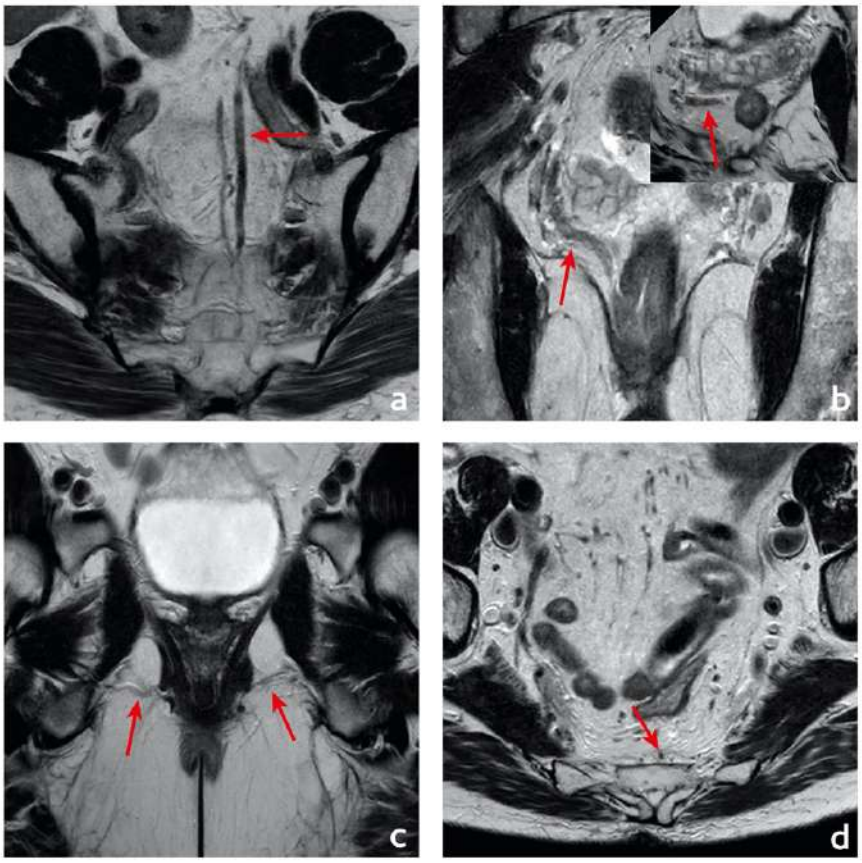

Fig. 7 The rectum's arterial supply has 3 to 4 routes. The main route is the superior rectal artery (arrow in **a**). The middle rectal arteries are inconsistent but may be present in up to 57% of cases. In **b**, a large calibre right middle rectal artery (arrow) arising from the internal iliac artery pierces the mesorectal fascia at its anterolateral aspect. The inferior rectal arteries originate from the internal pudendal arteries, are usually small in caliber and cross the ischioanal fossae towards the anal canal (arrows in **c**). The middle sacral artery courses down along the lumbosacral vertebrae, within the presacral space (arrow in **d**)

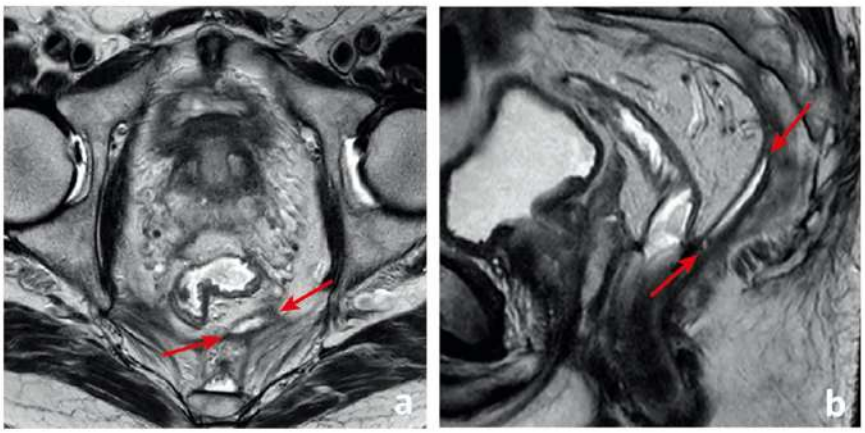

Fig. 8 Patient who underwent low anterior resection for rectal cancer presented with a posterior colorectal anastomotic leak which became a chronic fluid collection (between arrows in **a** and **b**)

and the mesorectal fat (Fig. 10) [32]. Lymph nodes located within the mesorectum, along the inferior and superior rectal vessels, along the inferior mesenteric vessels and along the internal iliac vessels and their branches are considered regional.

Keep in mind Although considered regional by the AJCC, internal iliac lymph nodes, commonly referred to as "lateral pelvic lymph nodes", are outside of the "circumferential margin of resection" in rectal cancer surgery and as such pose different management challenges (see below).

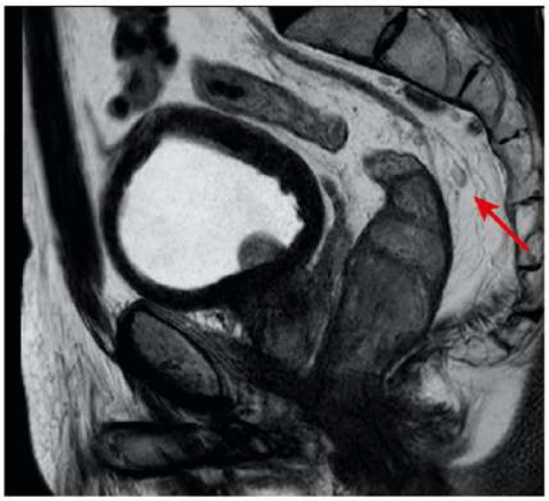

Fig. 9 Normal distribution of lymph nodes in the mesorectum (sagital minimum intensity projection). Lymph nodes are more numerous and larger in the high posterior mesorectum (arrow points to the largest lymph node but a few more are visible upstream)

Staging rectal cancer

The primary—T stage

We find reading the endoscopy report carefully to aid in the interpretation of the images—we should check whether the gastroenterologist found a suspicious focus in a benign polyp or a clearly malignant infiltration of the rectal wall and pay special attention to the lesions' shape description, estimated location, size and circumference of involvement. Also, we believe DWI may help locate small primary tumours, given on high *b* value images they will present most commonly with high signal intensity, but high-resolution T2-weighted imaging (T2-WI) perpendicular to the long axis of the tumour is the pillar of T staging given it provides the highest rectal wall layer detail. The maximum depth of tumour invasion will determine the MR imaging T stage (mrT) (Figs. 11 and 12).

Although NCCN guidelines consider any tumour ≥ mrT3 eligible for neoadjuvant therapy, in many European countries, mrT3 sub-classification according to the depth of invasion beyond muscularis propria is incorporated in the decision-making framework (Fig. 11) [33, 34]. Neoadjuvant therapy is, according to European (ESMO) guidelines, reserved for tumours > mrT3b which pose a higher risk of local recurrence (23.6% vs 10.4%) [34]. Reported MR imaging accuracy for the assessment of T stage is variable, ranging from 66 to 94% using pathology as a reference standard [35, 36]. The main difficulty is the differentiation between T2 and T3, and discriminating between the two is particularly relevant on low tumours given the much thinner cushion of mesorectal fat and consequent proximity to sphincter complex and middle pelvic compartment structures [35, 36]. T2 tumours may present with desmoplastic reaction leading to overstaging as T3. Desmoplasia tends to present as thin spiculae of T2-hypointensity surrounding invaded muscularis propria,

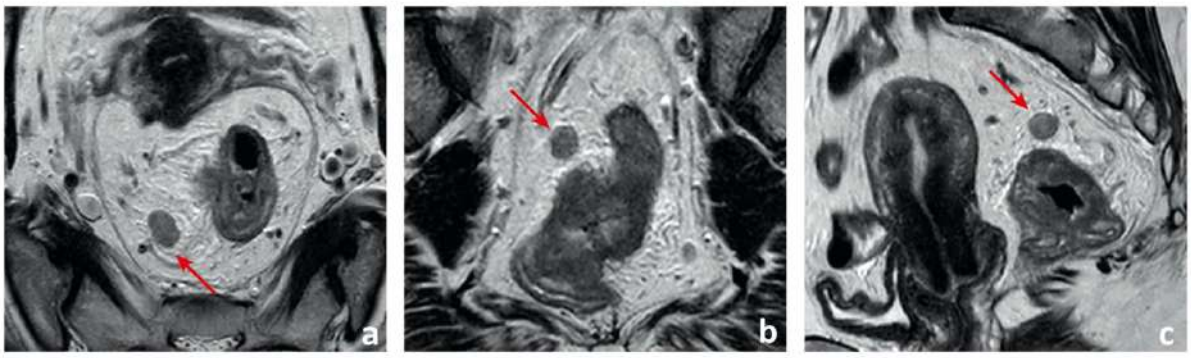

Fig. 10 Patient staged as mrT3a/b mrN2b due to multiple bulky lymph nodes in the mesorectum of which one is depicted, measuring 13 mm in the long axis and 10 mm in the short axis. The patient underwent surgery and was a pT3N0. While carefully reviewing the lymph node appearance on T2-WI, we notice they all presented with well-defined borders, homogeneous signal intensity and a preserved chemical shift effect

whereas T3 tumours usually present with a broad-based or nodular T2-intermediate-signal front at mesorectal fat [37].

Keep in mind The maximum depth of invasion tends to occur at the tumour's centre, and in large tumours, orientation of the slices perperdicular to it may be the most useful. On the other hand, it is common for the tumour's periphery to overhang the rectal wall into the lumen (Fig. 12c, d, f).

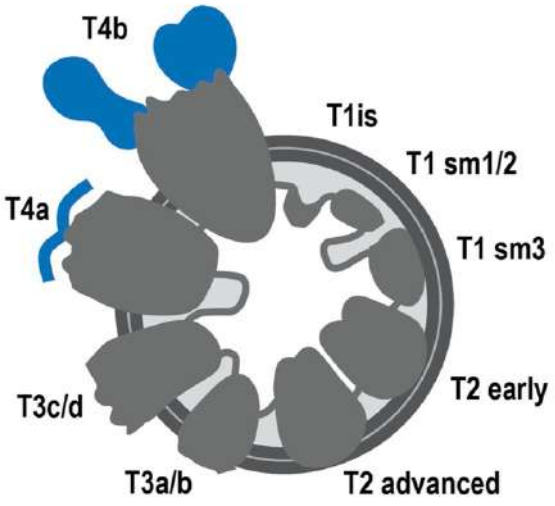

Fig. 11 T stages and substages. T1is: tumour in situ; T1sm1/2: tumour invades the submucosa, but not its full thickness; T1sm3: tumour invades the full thickness of the submucosa; T2 early: tumour focally invades the *muscularis propria*; T2 advanced: tumour invades the full thickness of the *muscularis propria*; T3a: tumour extends < 1 mm into the mesorectal fat; T3b: tumour extends between 1 and 5 mm into the mesorectal fat; T3c: tumour extends between 5 and 15 mm into the mesorectal fat; T3d: tumour extends > 15 mm into the mesorectal fat; T4a: tumour invades the peritoneum; T4b: tumour invades adjacent organs

The circumferential margin of resection

The circumferential margin of resection (CRM) is the plane where surgeons must dissect in order to perform a standardised total mesorectal excision (TME). It corresponds to the full circumference of the mesorectal fascia and, in tumours extending down into the anal canal, to the intersphincteric plane, with which the mesorectal fascia is in continuity inferiorly. The minimum distance between the tumour and the circumferential margin of resection on high-resolution T2-WI acquired perpendicular to its long axis should be recorded, as well as its location and extent. CRM is considered involved if the tumour lies < 1 mm from it (Fig. 13a) [38]. Although MR imaging was considered very accurate and reliable at predicting a clear margin in 2 seminal studies by Brown et al. and Beets-Tan et al., in a large meta-analysis, the sensitivity and specificity for margin involvement using a 1-mm cutoff were of only 76% and 88% respectively [39–41]. Margin involvement at MR imaging is associated with higher local recurrence rates (20% vs 7.1%), worse overall survival (42.2% vs 62.2%) and disease-free survival (47.3% vs 67.2%) [39, 42]. It is considered an indication for neoadjuvant therapy by both NCCN and ESMO guidelines [33, 34].

The extramural venous invasion

Extramural venous invasion (EMVI) on the histopathology of rectal cancer surgery specimens is an independent predictor of local recurrence, distant recurrence and worse overall survival [43]. MR imaging may detect EMVI with low sensitivity (62%) but high specificity (88%), using pathology as the gold standard [43]. It is depicted as intermediate signal intensity within vessels, with or without associated expansion and contour irregularity. It is generally in continuity with the primary tumour, but discontinuous mrEMVI may also be observed. The likelihood of mrEMVI may be graded based on an ordinal scale by Smith et al., grades 3 and 4,

Santiago *et al. Insights into Imaging* (2020) 11:100

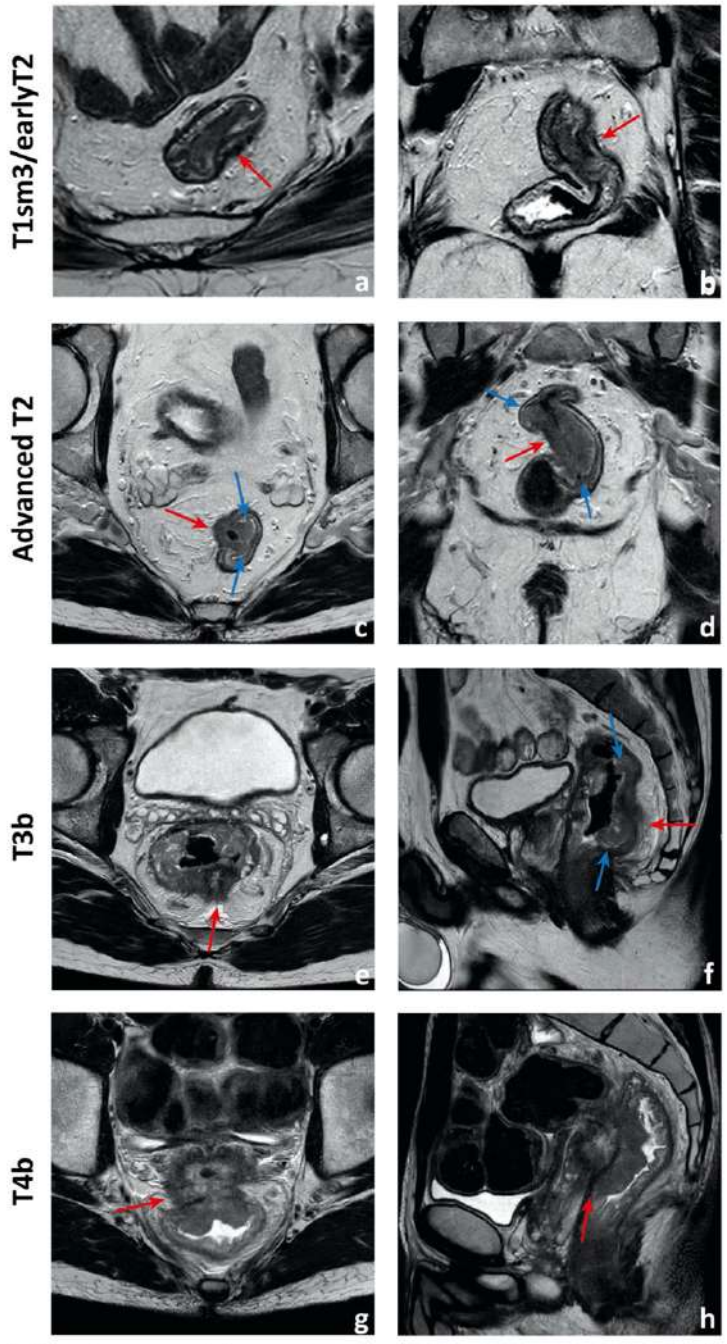

Fig. 12 Examples of differently T-staged tumours. **a**, **b** Arrows point to an early polypoid tumour occupying the full depth of the submucosa centrally and therefore staged clinically as mrT1sm3/early T2. Total mesorectal excision was performed, and at pathology, it corresponded to a T1sm3. **c**, **d** This ulcerated tumour extends in depth through the full thickness of the *muscularis propria* and was therefore staged as an MR advanced T2 (red arrows), which was confirmed at pathology. Notice how the periphery of the tumour overhangs the rectal wall both in the axial and coronal planes (blue arrows). **e**, **f** This mid-high, sub-circumferential rectal cancer extends 4 mm into the mesorectal fat at its most central area (red arrows) and was therefore staged as T3b. Notice the overhanging edges on the sagittal plane (blue arrows in **f**). **g**, **h** An anterior mid-high rectal cancer crosses the Denonvillier fascia and the peritoneal reflection to invade the seminal vesicles in this male patient, corresponding to an mrT4b. The patient underwent chemoradiation and is currently under palliative treatment due to distant metastatic disease

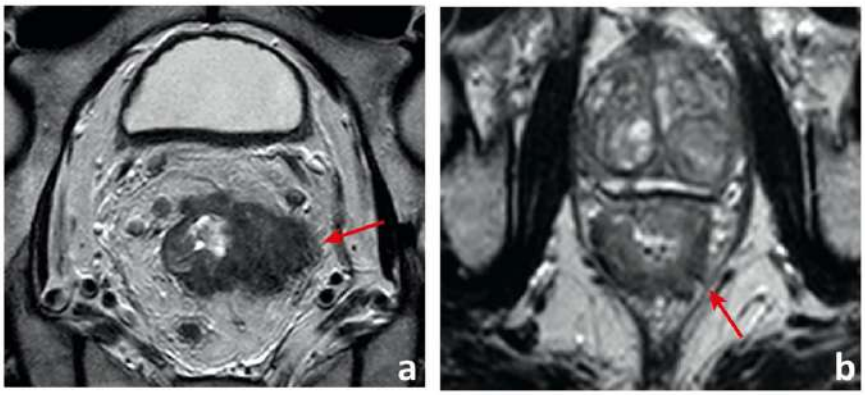

Fig. 13 Circumferential margin of resection involvement. **a** A T3d tumour invades the mesorectal fascia on the left side (arrow). **b** A 1–2 mm fat plane between this mrT3b low rectal cancer and the sphincter complex (arrow) is observed and as such the circumferential margin of resection may be considered free

characterised by the presence of intermediate signal intensity within vessels (Fig. 14), being associated with a lower relapse-free survival (35% vs 74%) [43, 44] and a higher risk of synchronous (OR 5.68; 95 CI 3.75–8.61) and metachronous (OR 3.91; 95 CI 2.61–5.86) metastasis [45]. Its presence is considered an indication for neoadjuvant therapy according to ESMO guidelines [34]. It is not part of the NCCN guidelines [33].

Lymph node involvement and tumour deposits

In rectal cancer patients, nearly 48% of positive lymph nodes are ≤ 5 mm. As such, size criteria to identify nodal

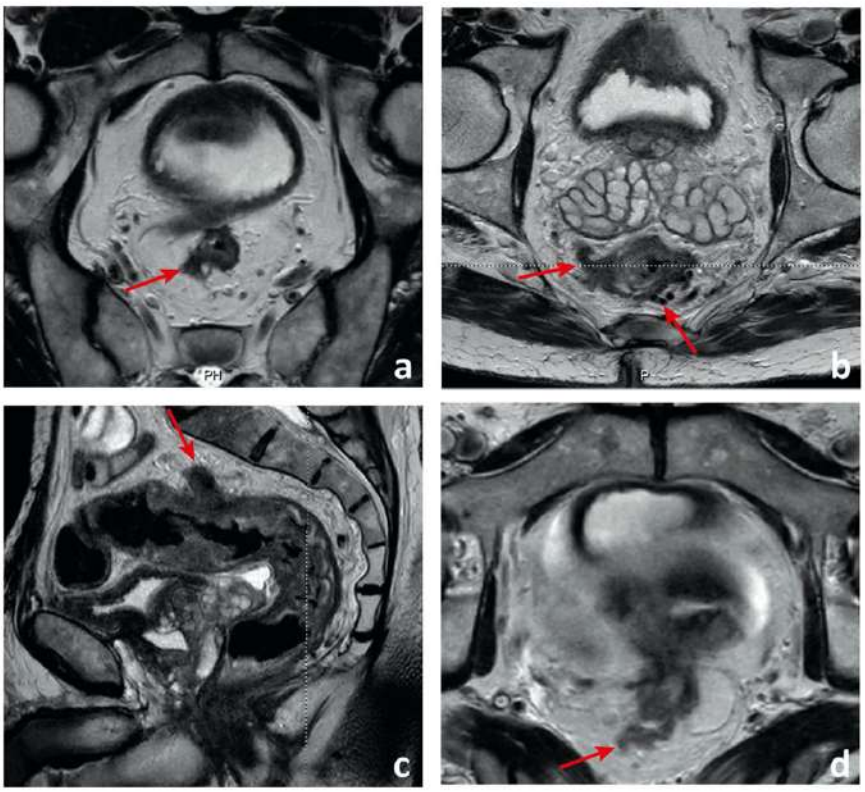

Fig. 14 MR extramural venous invasion (mrEMVI) is characterised by the presence of intermediate signal intensity tumour signal within vessels, which may be expanded (arrows in **a** to **d**) with (arrow in **a**) or without contour irregularity

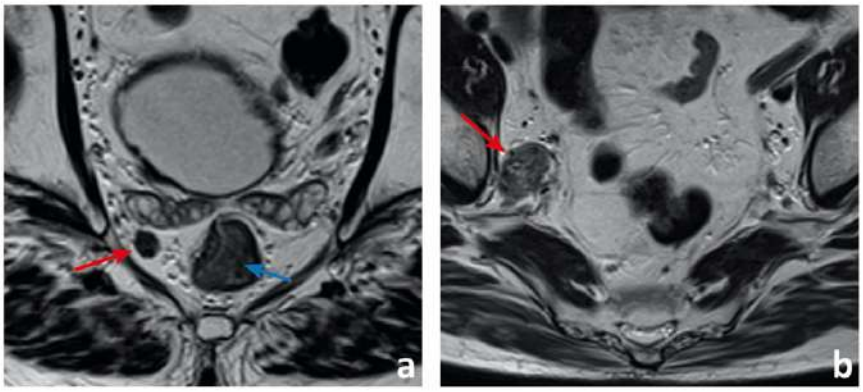

Fig. 15 **a** This patient presents with a polypoid tumour (blue arrow in **a**) located 7 cm above the anal verge. Tumour is underlined by a clear, uninterrupted, hyperintense submucosal fat plane and may as such be staged as mrT1 sm1/2. The patient also presented with a hypointense round lymph node in the mesorectum (red arrow), at tumour plane, 10 o'clock, with a slightly irregular contour anterolaterally. A very bulky, irregularly contoured, heterogeneous lymphadenopathy was found in the obturator space of the right lateral pelvic sidewall. The patient was selected for chemoradiation therapy

involvement are not reliable [27–30, 46]. Although normal lymph nodes are more numerous and larger in the upper and posterior mesorectum (Fig. 9), the incidence of nodal metastases is the same in anterior, lateral and posterior locations [27–30]. Regional positive lymph nodes in a more cranial location are associated with a higher risk of distant metastases [46]. Advanced T stage is associated with a higher number of positive lymph nodes, particularly small in size [46]. Most involved lymph nodes occur within the 1 cm proximal and the 1 cm distal to the tumour [47], and further spread occurs cranially in more than 90% of cases [48–50]. In the case of rectal cancers at the level of or below the peritoneal reflection, particularly ≥ T3, further spread may also occur to the lateral pelvic compartments [30, 51]. In fact, the lower the tumour, the more likely lateral spread is, going from 11.4% between 4 and 6 cm from the anal verge to 33.3% below 4 cm (Fig. 15) [51].

For nodes in the lateral pelvis, mostly size criteria have been tested, with variable cutoffs and variable outcomes [52–56]. According to research by the Lateral Node Study Consortium, in the particular case of cT3/4 low tumours, lateral lymph nodes with a short axis of at least 7 mm on staging MR have a significantly higher risk of lateral recurrence and lateral lymph node dissection in such cases may reduce lateral recurrences significantly [57]. For nodes > 3 mm in the mesorectum, contour irregularity, signal heterogeneity and interruption or absence of chemical shift artefact on T2-WI are the most

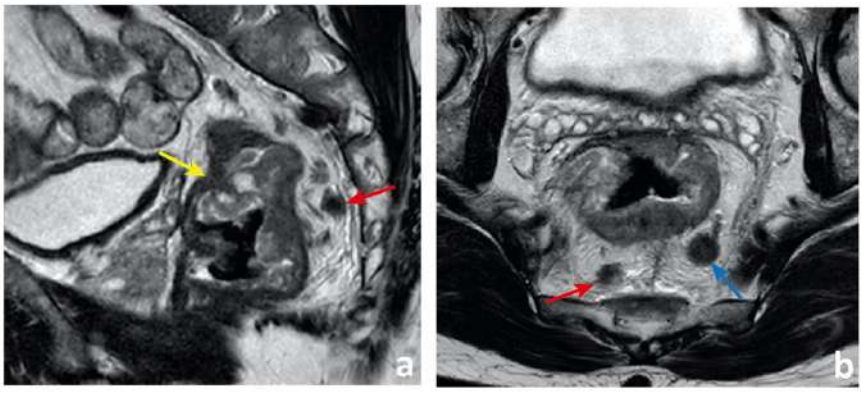

Fig. 16 This patient with a large T3 MRF+ rectal cancer (yellow arrow in **a**) presents with a hypointense, highly irregular, intermediate-to-low signal intensity nodule in the mesorectum (red arrows in **a** and **b**) that does not interrupt the course of a vein but is irregular enough for us to admit the possibility of an extranodal deposit (mrENTD). The patient also presented with a round, hypointense slightly heterogeneous and slightly irregularly contoured lesion which we believe to be a lymphadenopathy (blue arrow in **b**)

reliable criteria for tumour infiltration [31, 32, 39]. No reliable criteria exist for nodes smaller than that [31, 39]. N staging based on MR imaging may be reported symmetrically to the TNM staging system.

Tumour deposits are defined according to AJCC 2018 as discrete tumour nodules in the rectal cancer pathology specimen within the lymphatic drainage area of the primary tumour without identifiable lymphatic, vascular or neural tissue, irrespective of their morphology [58]. If a vessel wall/remnant is identified, the lesion should be classified as lymphovascular invasion, further subclassified as either lymphatic or venous. If neural structures are identified, the lesion should be classified as perineural invasion. Tumour deposits are found in 3.3% of rectal cancer specimens without lymph node involvement, in which case N1c should be recorded (TNM classification), but when lymph nodes are positive, tumour deposits are not to be added to the total positive lymph node count. Lord et al. are currently studying the differentiation of extranodal tumour deposits (mrENTDs) from involved lymph nodes on MR imaging—the subject of an ongoing clinical trial named COMET [59]. Their imaging definition is quite different from the pathologic definition described above [59]. mr-ENTDs are described as comet-shaped nodules of tumour which appear to directly interrupt the course of a vein (Fig. 16) [59].

Although T stage now prevails, lymph node positivity on MR imaging is still considered an indication for neoadjuvant therapy according to NCCN guidelines, whereas ESMO guidelines admit surgery upfront for N positive patients without involvement of the circumferential margin of resection or mrEMVI, preferably ≤ T3a-b [33, 34].

Keep in mind In the authors' perspective, the differentiation between positive lymph nodes with extracapsular extension, ENTDs and discontinuous EMVI on MR imaging may be difficult. Evidence suggests all of these entities entail a worse outcome compared to confined lymph node involvement. As such, pointing extranodal

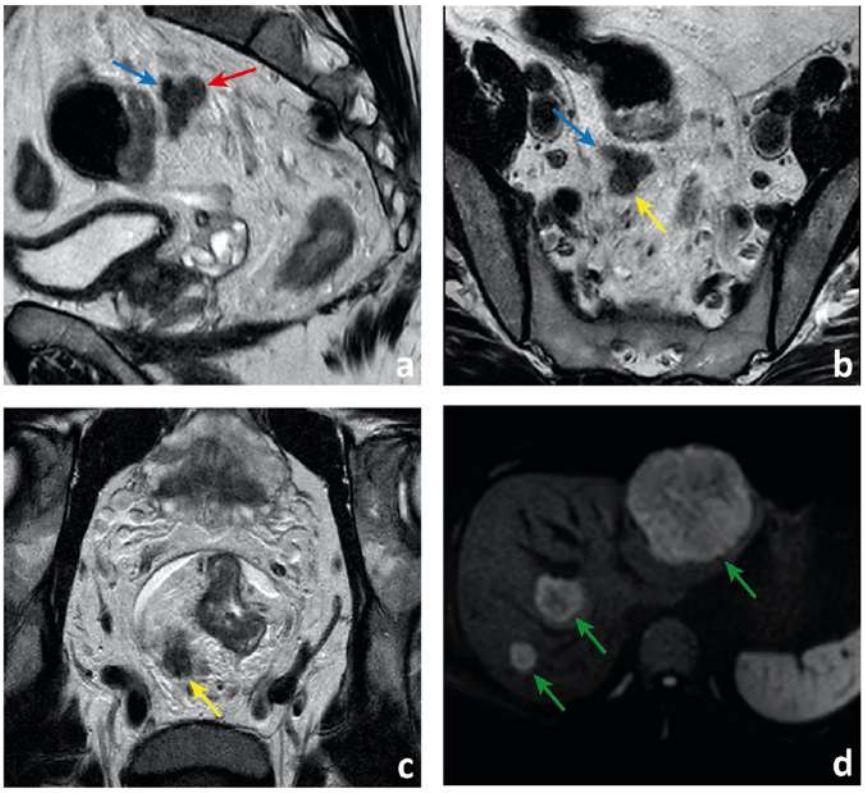

Fig. 17 A patient with an mrT3d MRF+ high rectal cancer also presents with a very irregular hypointense lesion in the high mesorectum (red arrow in **a**) that appears to both interrupt the course of a vein suggesting mrENTD (blue arrow in **a**) and to grow within it suggesting discontinuous mrEMVI (blue arrow in **b**). It is also in continuity with a round, irregular and heterogeneous structure appearing to be a positive lymph node with extracapsular extension (yellow arrows in **b** and **c**). The patient presented with synchronous metastatic liver disease, visible on b900 DWI (green arrows in **d**)

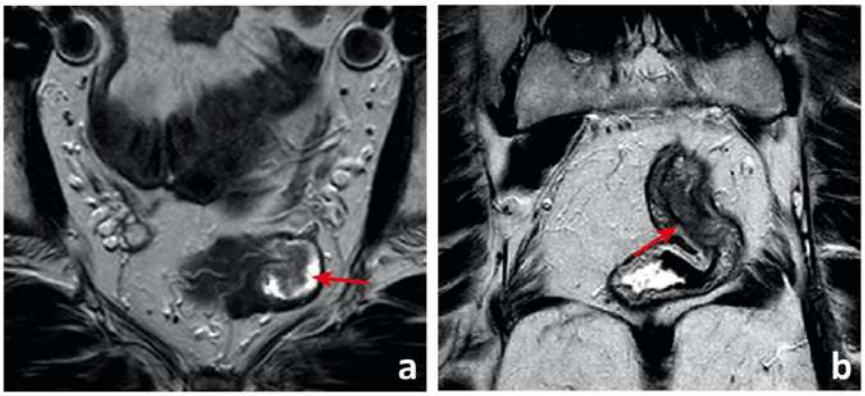

Fig. 18 Two different patients with two different early rectal cancers are depicted in **a** and **b**. In **a**, a thin submucosal fat plane is observed between the intermediate signal intensity tumour and the tented *muscularis propria*. Tumour may therefore be staged as mrT1sm1/2. Pathology of the total mesorectal excision specimen revealed a pT1sm1; in **b**, the tumour abuts the inner circular layer of the *muscularis propria* and may therefore be staged as mrT1sm3/earlyT2. Pathology of the total mesorectal excision specimen revealed a pT1sm3

tumour on staging reports may be more important than matching its exact pathologic diagnosis (Fig. 17) [60].

The specific scenarios

The very early rectal cancers

Very early rectal cancers, defined as low grade (G1/G2) cT1 cN0 cEMVI- tumours [33], can be subclassified based on the depth of invasion of the submucosa, tumours with < 1 mm of submucosal invasion having a practically null risk of lymph node metastasis [61]. This means transanal endoscopic microsurgery (TEM) can provide similar outcomes to TME in these patients, with much reduced morbidity and mortality [34]. The risk of lymph node metastases in cT1 tumours extending beyond 1 mm is relatively low (≅ 10%), particularly if G1/G2, V0, L0 [34, 62] and TEM may still be a reasonable upfront approach. MR imaging may have a role in the selection of these patients: Balyasnikova et al. could differentiate patients with either no evidence of submucosal invasion or a visibly spared ≥ 1 mm submucosa (mrT1 sm1/2)—considered eligible for TEM, from patients with no visibly spared submucosa or partially preserved muscularis (mrT1 sm3/earlyT2), with an accuracy of 89% and a good interobserver agreement (k = 0.74) [62]. Results of a larger UK multi-institutional trial (SPECC) are now awaited. MR imaging may also help assess lymph node involvement upfront and monitor recurrence after TEM. Fig. 18 depicts examples of both mrT1sm1/2 and mrT1sm3/earlyT2.

The low rectal cancers

A tumour with its lower edge less than 6 cm above the anal verge is considered a low rectal cancer [63](Fig. 19). Its prognosis is worse, with higher rates of local recurrence and poorer survival [63]. These figures may result from the inferior mesorectal tapering and closer proximity of tumours to the pelvic floor and middle pelvic compartment structures, requiring more mutilating surgical procedures and being associated with higher rates of margin positivity [64]. A specific MR imaging staging system was developed by Shihab et al. to address the particularities of low rectal cancer and aid in surgery planning [63, 65, 66]. According to it, tumours confined to the bowel wall not extending through its full thickness are considered mrLR1, tumours replacing the muscle coat but not reaching the intersphinteric plane are considered mrLR2, tumours invading the intersphincteric plane or lying within 1 mm to the levator muscle are considered mrLR3 and tumours invading the external anal sphincter and being within 1 mm

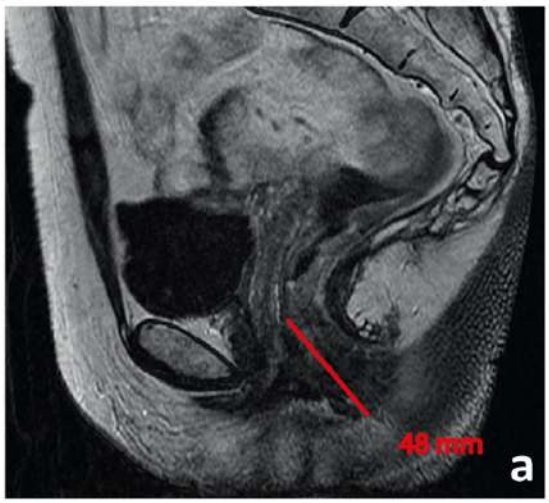

Fig. 19 A low rectal cancer is depicted with its lower edge 48 mm above the anal verge. Measurement is made from the central axis of the anus to the central axis of the rectum at the plane of the lower edge of the tumour

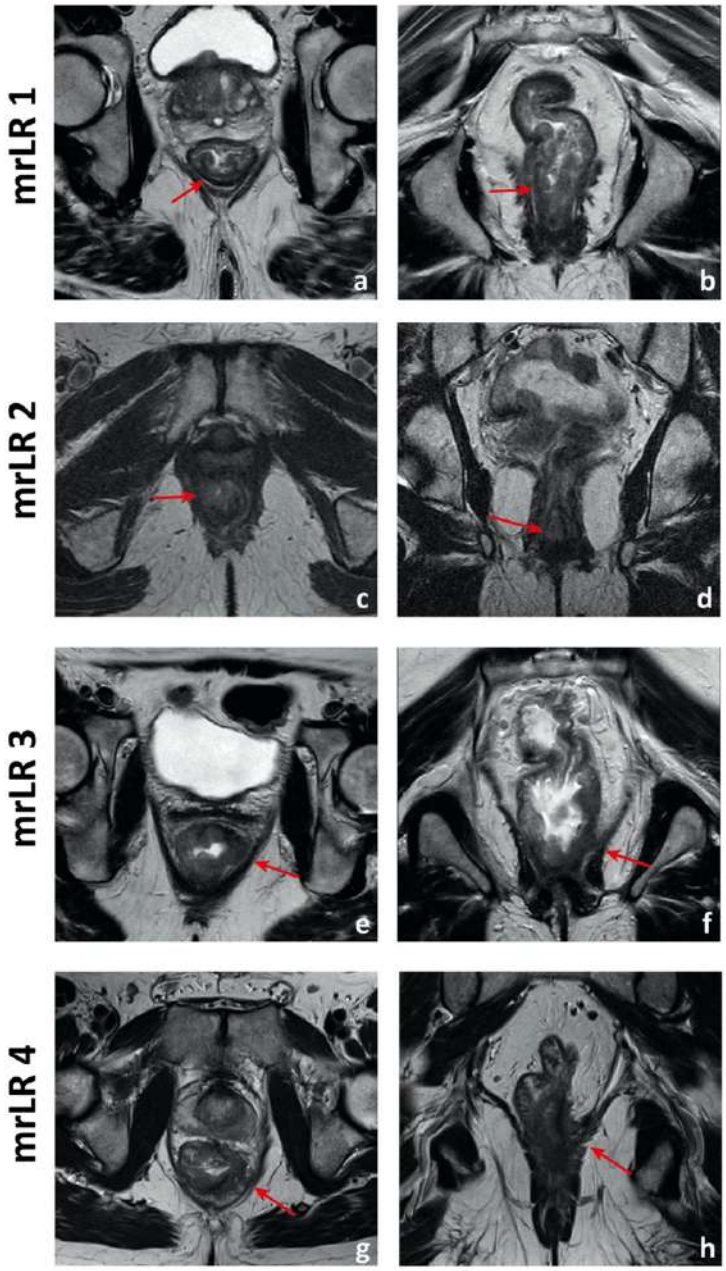

Fig. 20 Four low rectal cancers from 4 different patients are depicted. In **a** and **b**, a posterior mrT1sm3/early T2 tumour is depicted. It is classified as LR1 according to the low rectal cancer classification given it does not extend through the full thickness of the rectal wall. In **c** and **d**, a right anterior quadrant mrT2 tumour extending inferiorly into the anal canal is depicted, which invades the full thickness of the internal anal sphincter without extending into the intersphincteric plane—mrLR2. In **e** and **f**, a T3 tumour extending into the low mesorectum to within 1 mm of the left levator muscle is classified as mrLR3; in **g** and **h**, a low tumour extends through the mesorectal fat reaching the left levator muscle, therefore classified as mrLR4

and beyond the levator muscle, with or without invading adjacent structures, are considered mrLR4 (Fig. 20) [66]. mrLR1 tumours confined to the low rectum may be approached by LAR, in which the mesorectum is removed en bloc down to the pelvic floor. mrLR1 tumours extending into the anal canal may be approached with a LAR + intersphincteric dissection [4]. Low colorectal anastomosis or coloanal anastomosis may be performed upon favourable sphincter competence in these procedures, to avoid a permanent stoma, but the rate of

anastomotic leak and pelvic sepsis is increased and may significantly reduce patient quality of life. mrLR2 may be approached with standard abdominoperineal excision (SAPE), also known as an intersphincteric APE, in which the distal colon, rectum and anal sphincter are removed en bloc [4, 67]. When surgical treatment is considered for mrLR3-4, an extralevator abdominoperineal excision (ELAPE) is oncologically safer (less chance of R1 resection), in which dissection along the mesorectal fascia ends caudally at the levator origin and is met by a perineal dissection along the outer surface of the levators [4, 68]. ELAPE is associated with lower perforation and margin involvement rates, and consequent lower local recurrence rates than SAPE, albeit at the cost of higher perineal

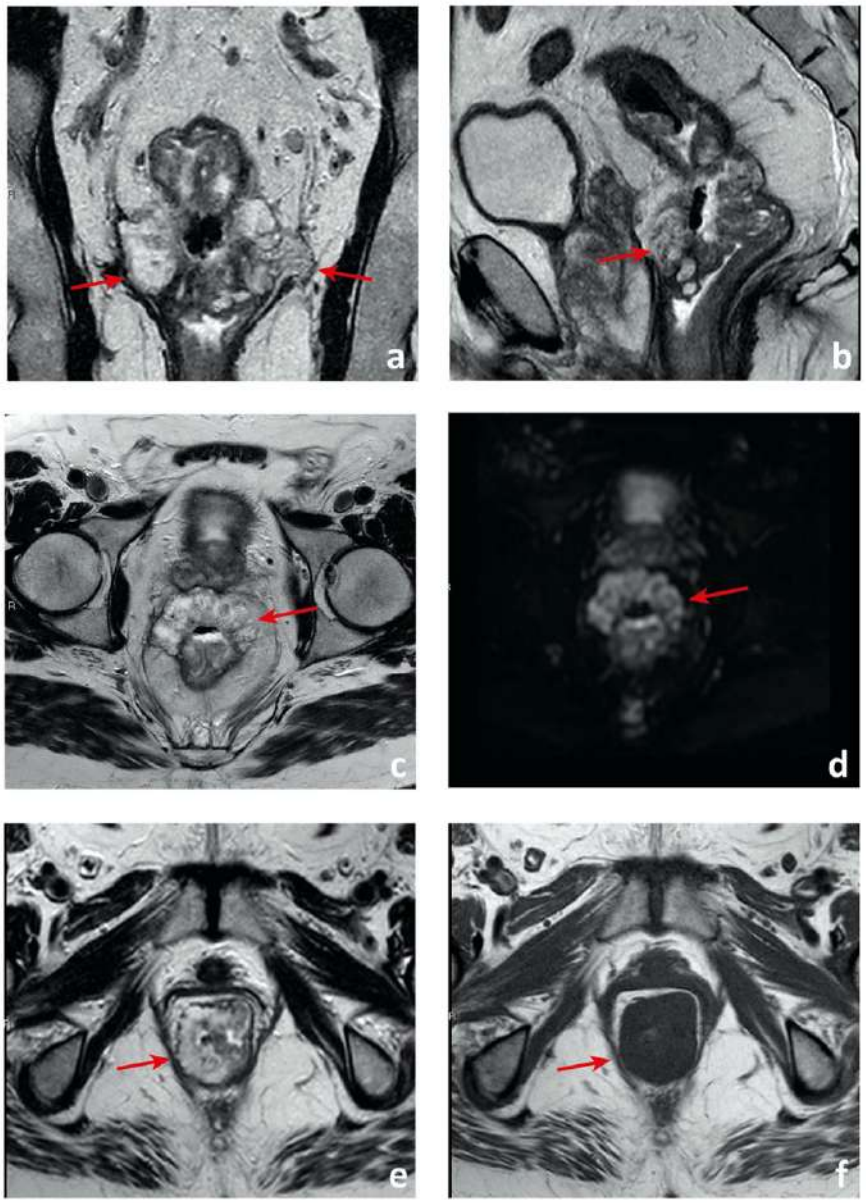

Fig. 21 In **a** to **c**, we observe a low/mid rectal cancer with a predominance of high signal intensity in accordance with a mucinous histologic subtype. It presents with bilateral (arrows in **a**) and anterior (arrow in **b**) transgression of the mesorectal fascia, extending into the pelvic sidewall and middle pelvic compartment, respectively. It may not be easy to define its exact boundaries due to the approximation of signal intensity to that of fat (arrow in **c**). b0 DWI images are fat-suppressed T2-WI and may aid in the distinction (arrow in **d**). T1WI may work even better, namely to define or exclude a fat plane between tumour and circumferential margin of resection. In **e**, a low mucinous rectal cancer appears to invade the levator muscle on T2-WI but in the corresponding T1WI (**f**), we see a thin fat plane between the two.

morbidity [68]. For tumours located both above and below the puborectalis sling or located anteriorly, at the level of the prostate, pelvic exenteration may be more appropriate [69]. In the particular case of very low rectal tumours (< 4 cm from the anal verge), mrT > 2 may by itself be an indication for neoadjuvant therapy according to European guidelines, whereas for higher locations, it may be reserved for mr > T3b if good quality TME can be assured [33]. Examples of mrLR1 - 4 are given in Fig. 20.

Keep in mind In low rectal tumours, additional oblique axial and coronal T2-WI planes perpendicular and parallel to the long axis of the anal canal, respectively, should be acquired when needed. The anal verge may be identified on sagittal T2-WI as the lower limit of the perianal hypointense skin change (Fig. 19).

The mucinous rectal cancers

Mucinous adenocarcinomas comprise 10–20% of all rectal cancers, tend to affect younger patients and are

Pelvic MRI for mid/high rectal cancer staging

Clinical information

.....

Technique

High resolution T2-WI in sagittal, oblique axial and oblique coronal planes, and oblique axial DWI were acquired after a small enema (...) and spasmolytic agent administration (...).

Results

The tumour is infiltrative / polypoid and not / partially / clearly mucinous.

It´s caudal edge is located ....mm above the anal verge and ....mm above the anoorectal transition.

It is ....mm in lenght and its cranial edge is located ....mm above / at the level of / ....mm below the anterior peritoneal reflection.

It extends from .... to .... o´clock and is confined to the mucosa. / invades part of the submucosa. / invades the whole submucosa. / invades part of the muscularis propria. / invades the whole muscularis propria. / extends ....mm beyond the muscularis propria.

Its deepest edge is located at .... o´clock, within ....mm of the CRM. / reaching the CRM. / extending beyond the CRM to invade .....

The peritumoural area shows a non-nodular pattern, without adjacent vessels. / minimal signal intensity changes not adjacent vessels. / signal intensity changes adjacent to normal-calibre vessel(s). / intermediate signal within vessel(s) with slight expansion. / vessel(s) with irregular contour and clear tumoural signal.

There are no / .... suspicious mesorectal lymph nodes ,none of which reaching the CRM, / ,.... of which invading the CRM at .....,

none of which being superior hemorrhoidal/mesenteric / ....of which being superior hemorrhoidal/mesenteric and none less than 5 cm below the tumour. / .... less than 5 cm below the tumour.

In the pelvic sidewalls (PSW), we find no suspicious lymph nodes. / .... suspicious lymph nodes at ....

There are no tumour deposits. / is one tumour deposit at .... / are ... tumour deposits at ....

We find no relevant additional pelvic findings.
There are the following additional relevant pelvic findings: .... (to include anatomic variants such as middle rectal veins/arteries and their entrance in the mesorectum)

Conclusion

Tumour located ....mm above the anorectal transition, mrT.... mrEMVI.... mrN.... (PSW....) CRM....

.....(include relevant considerations such as tumour implants in addition to N+, discontinuous mrEMVI outside the pelvis, high suspicious lymph nodes, metastases, etc).....

Fig. 22 A standardised report proforma for mid/high rectal cancer staging is depicted. In blue, a single option should be chosen per field

Pelvic MRI for low rectal cancer staging

Clinical information

.....

Technique

High resolution T2-WI in sagittal, oblique axial and oblique coronal planes, and oblique axial DWI were acquired after a small enema (...) and spasmolitic agent administration (...).

Results

The tumour is infiltrative / polypoid and not / partially / clearly mucinous.

It´s caudal edge is located ....mm above / at the level of the anal verge and ....mm above / at the level of / ....mm below the anorectal transition.

It is ....mm in lenght and its cranial edge is located ....mm above / at the level of / ....mm below the anterior peritoneal reflection.

It extends from ....to....o´clock and appears confined to the mucosa. / its deepest edge is located between ....and....o´clock, where it

invades part of the submucosa.
invades the whole submucosa.
invades part of the muscularis propria/interna sphincter.
invades the whole muscularis propria/internal sphincter.
invades the intersphincteric plane / is within 1 mm of the levator.
invades the external sphincter / levator.
extends .... mm beyond the external sphincter/levator, into the left/right/both ischioanal space(s).
invades the prostate/urogenital diafragm/penile bulb/vagina.

The peritumoural area shows a non-nodular pattern, without adjacent vessels. / minimal signal intensity changes not adjacent vessels. / signal intensity changes adjacent to normal-calibre vessel(s). / intermediate signal within vessel(s) with slight expansion. / vessel(s) with irregular contour and clear tumoural signal.

There are no / .... suspicious mesorectal lymph nodes, / none of which reaching the CRM. / ....of which invading the CRM at .....

and none of which being superior hemorrhoidal/mesenteric.
and ....of which being superior hemorrhoidal/mesenteric.

In the pelvic sidewalls (PSW), we find no suspicious lymph nodes. / one suspicious lymph node at ..... / .... suspicious lymph nodes at .....

There are no extranodal tumour deposits. / is one extranodal tumour deposit at ..... / are ... extranodal tumour deposits at .....

We find no relevant additional pelvic findings.
There are the following additional relevant pelvic findings: ..... (to include anatomic variants such as middle rectal veins/arteries and their entrance in the mesorectum)

Conclusion

Tumour between ..... and ..... o´clock, staged as mrLR.... mrT.... mrEMVI.... mrN.... (PSW....)

...(include relevant considerations such as extension of deepest edge, tumour implants in addition to N+, discontinuous mrEMVI outside the pelvis, high suspicious lymph nodes, metastases, etc)....

Fig. 23 A standardised report proforma for low rectal cancer staging is depicted. In blue, a single option should be chosen per field

defined histologically by the presence of extracellular mucin in more than 50% of the tumour stroma [69]. There is an association with a history of inflammatory bowel disease and pelvic radiotherapy [69]. This histologic subtype may be associated with a higher T stage upon diagnosis, a greater risk of metachronous metastases and a worse response to chemoradiation, but results regarding the impact on overall survival are conflicting [70, 71]. Although the definition is histologic, it may be that mucinous tumours are more efficiently detected on T2-WI MR imaging than on endoscopic biopsy, imaging definition being more than 50% high signal intensity areas within the tumour—areas with a signal intensity similar to or brighter than that of the mesorectal fat [69, 71]. MR imaging-detected mucinous tumours carry a similarly worse prognosis relative to histology, with

poorer responses to chemoradiation and worse disease-free survival [69] (Fig. 21).

Keep in mind Whenever in doubt, DWI b0 may be useful for the distinction between fat signal, which will be suppressed, and mucin, which will remain bright. Also, we find high-resolution T1-WI may help define the boundary between mucin and fat (Fig. 21).

Rectal cancer staging templates

Figures 22 and 23 depict our suggested templates for the staging of mid/high and low rectal cancers respectively. In this section, we discuss the small deviations from SAR and ESGAR consensus guidelines and their reasoning.

Our patients routinely perform a small enema shortly before MR imaging to empty the rectum, which significantly reduces susceptibility artefacts due to air content, improvement being particularly relevant for DWI [72]. Intravenous butilscopolamine is also administered routinely at our centre in the absence of contraindications, between scout and (oblique axial) T2-WI acquisitions, to minimise artefacts due to peristalsis. Neither the use of small enema nor the use of spasmolytic agents has reached consensus by SAR or ESGAR expert panels and is therefore considered optional according to their respective guidelines [13, 73].

Our acquisition protocol is exhibited in Table 1. We routinely perform DWI in staging examinations to help locate small lesions and to serve as a baseline for response assessment. Although DWI is a recommended sequence according to SAR consensus guidelines, it is considered optional upon staging according to ESGAR consensus guidelines [73, 74]. We do not administer intravenous contrast for rectal cancer staging, which is optional according to both guidelines. The exception is a suspicion of pelvic sepsis or fistulization, in which case we find contrast very helpful to delineate abscesses and fistulous tracts respectively. We include an unenhanced T1 sequence, as recommended by SAR [13, 73], which provides an overview of the whole pelvis and may help characterize incidental bone ou genito-urinary lesions. It may also help delimit mucinous tumours, as discussed in the "The mucinous rectal cancers" section.

With respect to staging key points, all of our patients are staged with MR imaging unless an absolute contraindication is known, even early tumours, and as such, we have decided to include early tumour sub-staging in our templates as by Balyasnikova et al. [62], which is not part of either SAR or ESGAR consensus guidelines [13, 73]. Also, we have kept the mrLR classification for low rectal tumours [66] given it is well known by our multidisciplinary team. Even though the specific mrLR term is not utilised in the templates by SAR or ESGAR, the depth of invasion subclass options for low tumours is presented similarly in both [13, 73]. We have used the 5-point scale by Smith et al. [43] for mrEMVI assessment since the very beginning of our practice, and we find it helpful for less experienced radiologists. As such, we kept it, whereas SAR and ESGAR have adopted a simpler 3-point and 2-point scale for that purpose, respectively [13, 73]. Finally, our templates leave node involvement interpretation open, whereas both SAR and ESGAR reporting templates adopt strict mixed size-morphology criteria [13, 73]. The reason for this deviation is our own node-by-node analysis experience based on such criteria, which we found suboptimal [74]. We rely on morphologic criteria irrespective of size, namely shape, contour, heterogeneity and chemical shift effect, as explained in the "Lymph node involvement and tumour deposits" section.

Conclusions

Pelvic MR imaging is the pillar of clinical rectal cancer staging and the basis for optimal multidisciplinary patient management decision-making. A thorough and systematic knowledge of the relevant normal anatomy and variants, of the key staging imaging features and of the particularities of early, low and mucinous tumours is mandatory for rectal cancer staging MR image interpretation.

Abbreviations

AJCC: American Joint Committee on Cancer; CRM: Circumferential margin of resection; DWI: Diffusion-weighted imaging; EMVI: Extramural venous invasion; ENTD: Extranodal tumour deposit; ESMO: European Society of Medical Oncology; MR: Magnetic resonance; NCCN: National comprehensive cancer network; OR: Odds ratio; T2-WI: T2-weighted imaging; TEM: Transanal endoscopic microsurgery; TME: Total mesorectal excision; TNM: Tumour node metastases staging system

Acknowledgements

We would like to thank all the staff from the Radiology Department and the Digestive Unit of the Champalimaud Foundation Clinical Centre.

Authors' contributions

Inês Santiago contributed for the elaboration, critical revision and review of the intellectual content of the manuscript. Nuno Figueiredo, Oriol Parés and Celso Matos contributed to the critical revision and review of the intellectual content of the manuscript. The authors read and approved the final manuscript.

Funding

The authors declare no funding was obtained for this paper.

Availability of data and materials

Not applicable.

Ethics approval and consent to participate

Not applicable.

Consent for publication

Not applicable.

Competing interests

The authors declare that they have no financial or non-financial competing interests.

Author details
[1]Radiology Department, Champalimaud Foundation, Avenida Brasília, 1400-038 Lisbon, Portugal. [2]Nova Medical School, Campo Mártires da Pátria 130, 1169-056 Lisbon, Portugal. [3]Champalimaud Research, Champalimaud Foundation, Avenida Brasília, 1400-038 Lisbon, Portugal. [4]Colorectal Surgery, Digestive Unit, Champalimaud Foundation, Avenida Brasília, 1400-038 Lisbon, Portugal. [5]Radiation Oncology Department, Champalimaud Foundation, Avenida Brasília, 1400-038 Lisbon, Portugal.

Received: 25 March 2020 Accepted: 26 June 2020
Published online: 03 September 2020

References

1. Heald RJ, Moran BJ, Ryall RD, Sexton R, MacFarlane JK (1998) Rectal cancer: the Basingstoke experience of total mesorectal excision, 1978-1997. Arch Surg 133(8):894–899
2. Sauer R, Becker H, Hohenberger W et al (2004) Preoperative versus postoperative chemoradiotherapy for rectal cancer. N Engl J Med 351:1731–1740
3. Engelen S, Maas M, Lahaye M et al (2003) Modern multidisciplinary treatment of rectal cancer based on staging with magnetic resonance imaging leads to excellent local control, but distant control remains a challenge. Eur J Cancer 49(10):2311–2320
4. Nougaret S, Reinhold C, Hisham WM, Rouanet P, Bibeau F, Brown G (2013) The use of MR imaging in treatment planning for patients with rectal carcinoma: have you checked the "DISTANCE"? Radiology 268(2):330–344
5. Herschorn S (2004) Female pelvic floor anatomy: the pelvic floor, supporting structures, and pelvic organs. Rev Urol 6(Suppl 5):S2–S10
6. Wallner C (2008) Is the puborectalis muscle part of the levator ani muscle? Dis Colon Rectum 51(7):1165–1166
7. D'Souza N, Lord A, Shaw A et al (2020) The sigmoid take-off: an anatomical imaging definition of the rectum validated on specimen analysis. Eur J Surg Oncol. https://doi.org/10.1016/j.ejso.2020.01.008
8. D'Souza N, de Neree tot Babberich N, d'Hoore A et al (2019) Definition of the rectum: an international, expert-based Delphi consensus. Ann Surg 270(6):955–959
9. D'Souza N, Balyasnikova S, Tudyka V et al (2018) Variation in landmarks for the rectum: an MRI study. Colorectal Dis 20(10):O304–O309
10. Dimitriou N, Michail O, Moris D, Griniatsos J (2015) Low rectal cancer: sphincter preserving techniques-selection of patients, techniques and outcomes. World J Gastrointest Oncol 7(7):55–70
11. Nagtegaal I, Van De Velde C, Marijnen C, van Krieken JH, Quirke P (2005) Low rectal cancer: a call for a change of approach in abdominoperineal resection. J Clin Oncol 23(36):9257–9264
12. Kenig J, Richter P (2013) Definition of the rectum and level of the peritoneal reflection-still a matter of debate? Wideochir Inne Tech Maloinwazyjne 8(3): 183–186
13. Beets-Tan R, Lambregts D, Maas M et al (2018) Magnetic resonance imaging for clinical management of rectal cancer: updated recommendations from the 2016 European Society of Gastrointestinal and Abdominal Radiology (ESGAR) consensus meeting. Eur Radiol 28:1465–1475
14. Lee JM, Kim NK (2018) Essential anatomy of the anorectum for colorectal surgeons focused on the gross anatomy and histologic findings. Ann Coloproctol 34(2):59–71
15. Lindsey I, Guy R, Warren B, Mortensen NM (2000) Anatomy of Denonviliers' fascia and pelvic nerves, impotence, and implications for the colorectal surgeon. Br J Surg 87(10):1288–1299
16. Jin Z, Peng J, Zhu Q, Yin L (2011) Waldeyer's fascia: anatomical location and relationship to neighboring fasciae in retrorectal space. Surg Radiol Anat 33(10):851–854
17. García-Armengol J, García-Botello S, Martinez-Soriano F, Roig JV, Lledó S (2008) Review of the anatomic concepts in relation to the retrorectal space and endopelvic fascia: Waldeyer's fascia and the rectosacral fascia. Colorectal Dis 10(3):298–302
18. Kraima A, West N, Treanor D et al (2015) Understanding the surgical pitfalls in total mesorectal excision: investigating the histology of the perirectal fascia and the pelvic autonomic nerves. Eur J Surg Oncol 41(12):1621–1629
19. Yiqun S, Tong T, Fangqi L et al (2016) Recognition of anterior peritoneal reflections and their relationship with rectal tumors using rectal Magnetic Resonance Imaging. Medicine (Baltimore) 95(9):e2889
20. Gollub M, Maas M, Weiser M et al (2013) Recognition of the anterior peritoneal reflection at rectal MRI. AJR Am J Roentgenol 200(1):97–101
21. Torkzad M, Blomqvist L (2005) The mesorectum: morphometric assessment with magnetic resonance imaging. Eur Radiol 15:1184–1191
22. Nikolouzakis T, Mariolis-Sapsakos T, Triantopoulou C et al (2019) Detailed and applied anatomy for improved rectal cancer treatment. Ann Gastroenterol 32(5):431–440
23. Raman S, Horton K, Fishman E (2013) MDCT and CT angiography evaluation of rectal bleeding: the role of volume visualization. AJR Am J Roentgenol 201(3):589–597
24. Naidoo N, Lazarus L, Singh B, Satyapal K (2018) Clinical relevance of the arterial supply to the proximal rectum. Eur J Anat 22(1):67–73
25. Sakorafas G, Zouros E, Peros G (2006) Applied vascular anatomy of the colon and rectum: clinical implications for the surgical oncologist. Surg Oncol 15(4):243–255
26. Pan H, Zhao G, An Q, Xiao G (2018) Pulmonary metastasis in rectal cancer: a retrospective study of clinicopathological characteristics of 404 patients in Chinese cohort. BMJ Open 8(2):e019614
27. Canessa C, Badía F, Fierro S, Fiol V, Háyek G (2001) Anatomic study of the lymph nodes of the mesorectum. Dis Colon Rectum 44(9):1333–1336
28. Thakur S, Somashekar U, Chandrakar S, Sharma D (2011) Anatomic study of distribution, numbers, and size of lymph nodes in mesorectum in Indians: a autopsy study. Int J Surg Pathol 19(3):315–320
29. Topor B, Acland R, Kolodko V, Galandiuk S (2003) Mesorectal lymph nodes: their location and distribution within the mesorectum. Dis Colon Rectum 46(6):779–785
30. Steup W, Moriya Y, Van de Velde C (2002) Patterns of lymphatic spread in rectal cancer. a topographical analysis on lymph node metastases. Eur J Cancer 38(7):911–918
31. Brown G, Richards C, Bourne M et al (2003) Morphologic predictors of lymph node status in rectal cancer with use of high-spatial-resolution MR imaging with histopathologic comparison. Radiology 227(2):371–377
32. Zhang H, Zhang C, Zheng Z et al (2017) Chemical shift effect predicting lymph node status in rectal cancer using high-resolution MR imaging with node-for-node matched histopathological validation. Eur Radiol 27(9):3845–3855
33. National Comprehensive Cancer Network. Rectal Cancer (Version 1.2020). http://www.nccn.org/professionals/physician_gls/pdf/bone.pdf. .
34. Glynne-Jones R, Wyrwics L, Tiret E et al (2017) Rectal cancer: ESMO clinical practice guidelines for diagnosis, treatment and follow-up. Ann Oncol 28(Suppl 4):iv22–iv40
35. Videhult P, Smedh K, Lundin P, Kraaz W (2007) Magnetic resonance imaging for preoperative staging of rectal cancer in clinical practice: high accuracy in predicting circumferential margin with clinical benefit. Colorectal Dis 9(5): 412–419
36. Brown G, Radcliffe A, Newcombe R, Dallimore NS, Bourne MW, Williams GT (2003) Preoperative assessment of prognostic factors in rectal cancer using high-resolution magnetic resonance imaging. Br J Surg. 90(3):355–364
37. Taylor F, Swift R, Blomqvist L, Brown G (2008) A systematic approach to the interpretation of preoperative staging MRI for rectal cancer. AJR Am J Roentgenol 191(6):1827–1835
38. MERCURY study group (2006) Diagnostic accuracy of preoperative magnetic resonance imaging in predicting curative resection of rectal cancer: prospective observational study. BMJ 333(7572):779
39. Hunter C, Brown G (2016) Preoperative staging of rectal cancer: a review of imaging techniques. Expert Rev Gastroenterol Hepatol 10(9):1011–1025
40. Beets-Tan R, Beets G, Vliegen R et al (2001) Accuracy of magnetic resonance imaging in prediction of tumour-free resection margin in rectal cancer surgery. Lancet 357(9255):497–504 33
41. Xie H, Zhou X, Zhuo Z, Che S, Xie L, Fu W (2014) Effectiveness of MRI for the assessment of mesorectal fascia involvement in patients with rectal cancer: a systematic review and meta-analysis. Dig Surg 31(2):123–134
42. Taylor F, Quirke P, Heald R et al (2014) Preoperative magnetic resonance imaging assessment of circumferential resection margin predicts disease-free survival and local recurrence: 5-year follow- up results of the MERCURY study. J Clin Oncol 32(1):34–43
43. Smith N, Barbachano Y, Norman A, Swift RI, Abulafi AM, Brown G (2008) Prognostic significance of magnetic resonance imaging-detected extramural vascular invasion in rectal cancer. Br J Surg 95(2):229–236
44. Sohn B, Lim JS, Kim H et al (2015) MRI-detected extramural vascular invasion is an independent prognostic factor for synchronous metastasis in patients with rectal cancer. Eur Radiol 25(5):1347–1355

45. Sohn B, Lim J, Kim H et al (2015) MRI-detected extramural vascular invasion is an independent prognostic factor for synchronous metastasis in patients with rectal cancer. Eur Radiol 25(5):1347–1355
46. Yao Y, Wang L, Liu Y, Li JY, Gu J (2011) Lymph node distribution and pattern of metastases in the mesorectum following total mesorectal excision using the modified fat clearing technique. J Clin Pathol 64(12): 1073–1077
47. Cserni G, Tarján M, Bori R (2001) Distance of lymph nodes from the tumour, an important feature in colorectal cancer specimens. Arch Pathol Lab Med 125(2):246–249
48. Koh D, Brown G, Temple L et al (2005) Distribution of mesorectal lymph nodes in rectal cancer: in vivo MR imaging compared with histopathological examination. Initial observations. Eur Radiol 15(8):1650–1657
49. Zheng Y, Zhou Z, Li L et al (2007) Distribution and patterns of lymph nodes metastases and micrometastases in the mesorectum of rectal cancer. J Surg Oncol 96(3):213–219
50. Engelen S, Beets-Tan R, Lahaye M, Kessels AG, Beets GL (2008) Location of involved mesorectal and extramesorectal lymph nodes in patients with primary rectal cancer: preoperative assessment with MR imaging. Eur J Surg Oncol 34(7):776–781
51. Morikawa E, Yasutomi M, Shindou K et al (1994) Distribution of metastatic lymph nodes in colorectal cancer by the modified clearing method. Dis Colon Rectum. 37(3):219–223
52. Gulevski S, Russell M, Buchwald P (2019) Significance, diagnosis and treatment of lateral lymph nodes in rectal cancer: a systematic review. Int J Surg Open 21:73–82
53. Kim H, Choi G, Park J et al (2017) Optimal treatment strategies for clinically suspicious lateral pelvic lymph node metastasis in rectal cancer. Oncotarget 8(59):100724–100733
54. Atef Y, Koedam T, van Oostendorp S, Bonjer HJ, Wijsmuller AR, Tuynman JB (2019) Lateral pelvic lymph node metastases in rectal cancer: a systematic review. World J Surg 43(12):3198–3206
55. Ogawa S, Hida J, Ike H et al (2017) Prediction of lateral pelvic lymph node metastasis from lower rectal cancer using magnetic resonance imaging and risk factors for metastasis: multicenter study of the lymph node committee of the Japanese society for cancer of the colon and rectum. Int J Colorectal Dis 32(10):1479–1487
56. Ogura A, Konishi T, Beets G et al (2019) Lateral nodal features on restaging magnetic resonance imaging associated with lateral local recurrence in low rectal cancer after neoadjuvant chemoradiotherapy or radiotherapy. JAMA Surg 3:e192172
57. Ogura A, Konishi T, Cunningham C et al (2019) Neoadjuvant (chemo)radiotherapy with total mesorectal excision only is not sufficient to prevent lateral local recurrence in enlarged nodes: results of the multicenter lateral node study of patients with low ct3/4 rectal cancer. J Clin Oncol. 37(1):33–43
58. Amin M, Edge S, Greene F et al (2017) AJCC Cancer Staging Manual, 8th edn. Springer, New York
59. Lord A, D'Souza N, Shaw A (2019) The current status of nodal staging in rectal cancer. Current Colorectal Cancer Reports 15:143–148
60. Resch A, Langner C (2013) Lymph node staging in colorectal cancer: old controversies and recent advances. World J Gastroenterol 19(46):8515–8526
61. Kitajima K, Fujimori T, Fuji S et al (2004) Correlations between lymph node metastasis and depth of submucosal invasion in submucosal invasive colorectal carcinoma: a Japanese collaborative study. J Gastroenterol 39(6): 534–543
62. Balyasnikova S, Read J, Wotherspoon A et al (2017) Diagnostic accuracy of high-resolution MRI as a method to predict potentially safe endoscopic and surgical planes in patients with early rectal cancer. BMJ Open Gastroenterol 4(1):e000151
63. Battersby N, How P, Moran B et al (2016) Prospective Validation of a Low Rectal Cancer Magnetic Resonance Imaging Staging System and Development of a Local Recurrence Risk Stratification Model: the MERCURY II study. Ann Surg 263(4):751–760
64. Nagtegaal I, van de Velde C, Marijnen C, van Krieken JH, Quirke P (2005) Low rectal cancer: a call for a change of approach in abdominoperineal resection. J Clin Oncol 23(36):9257–9264
65. Shihab O, How P, West N et al (2011) Can a novel MRI staging system for low rectal cancer aid surgical planning? Dis Colon Rectum 54(10):1260–1264
66. Salerno G, Daniels I, Moran B, Heald RJ, Thomas K, Brown G (2009) Magnetic resonance imaging prediction of an involved surgical resection margin in low rectal cancer. Dis Colon Rectum 52:632–639
67. Perry B, Connaughton J (2007) Abdominoperineal resection: how is it done and what are the results? Clin Colon Rectal Surg 20(3):213–220
68. How P, West N, Brown G (2014) An MRI-based assessment of standard and extralevator abdominoperineal excision specimens: time for a patient tailored approach? Ann Surg Oncol 21:822–828
69. Yu S, Chand M, Tait D, Brown G (2014) Magnetic resonance imaging defined mucinous rectal carcinoma is an independent imaging biomarker for poor prognosis and poor response to preoperative chemoradiotherapy. Eur J Cancer 50(5):920–927
70. Horvat N, Hope T, Pickhardt P, Petkovska I (2019) Mucinous rectal cancer: concepts and imaging challenges. Abdom Radiol (NY) 44(11):3569–3580
71. Wnorowski A, Menias C, Pickhardt P, Kim DH, Hara AK, Lubner MG (2019) Mucin-containing rectal carcinomas: overview of unique clinical and imaging features. AJR Am J Roentgenol 213(1):26–34
72. van Griethuysen J, Bus E, Hauptmann M et al (2018) Gas-induced susceptibility artefacts on diffusion-weighted MRI of the rectum at 1.5 T - effect of applying a micro-enema to improve image quality. Eur J Radiol 99: 131–137
73. Gollub M, Arya S, Beets-Tan R et al (2018) Use of magnetic resonance imaging in rectal cancer patients: Society of Abdominal Radiology (SAR) rectal cancer disease-focused panel (DFP) recommendations 2017. Abdom Radiol (NY) 43(11):2893–2902
74. Santiago I, Santinha J, Ianus A et al (2019) Susceptibility perturbation MRI (SPI) maps tumor infiltration into mesorectal lymph nodes. Cancer Res 79(9): 2435–2444

Publisher's Note

4.2. Why is there a need to improve lymph node staging?

Lymph node involvement is one of the key determinants of patient prognosis in oncology. It corresponds to the middle letter (N) of the widespread TNM (tumour – lymph nodes – metastasis) staging system defined by the American Joint Committee on Cancer and the International Union Against Cancer. Prognostic stratification based on TNM relies on the evaluation of the extension of the primary tumour and on the count of involved locoregional lymph nodes within the surgically resected specimen. However, in the particular case of rectal cancer, before submitting a patient to a potentially mutilating and morbid surgery, a question arises: Will this patient benefit from neoadjuvant radiotherapy and/or chemotherapy? The answer relies on MR imaging-based risk stratification and guidelines are available to establish which patients present with locally-advanced rectal cancer. They have at least two things in common: Lymph node involvement is part of the equation, and patients with rectal cancer considered locally-advanced have an indication for neoadjuvant therapy [its beneficial and superior impact compared to post-operative regimens on local recurrence and disease-free survival has been demonstrated in several seminal randomized clinical trials (1-6)]. On the other hand, non-locally-advanced rectal cancer patients will not benefit from neoadjuvant therapy - they will pointlessly endure significant adverse effects, surgery will be delayed and become technically more difficult, and they will more likely suffer from post-operative morbidity than if they go straight to surgery.

Standard MR imaging is quite accurate regarding two of the major pillars for risk stratification - T stage and mesorectal fascia involvement (7,8). However, with respect to lymph node involvement, performance is poor and in a large multicentric study involving 100.211 patients has even been compared to flipping a coin (8,9). Diagnostic performance may improve significantly with injectable contrast agents such as the strictly intravascular Gadofosveset® or the ultrasmall superparamagnetic iron oxide particles (USPIO), both with AuROC above 0.90 (10,11). The latter are captured by macrophages and transported to normal lymphatic tissue. T2* weighted gradient echo images will then detect a decrease in signal intensity in normal lymphatic tissue due to local field inhomogeneity induced by iron, whereas in tumour tissue, such signal decrease will not be observed (11). However, despite impressive reported results, these contrasts are cumbersome to use, have relevant adverse effects and are not commercially available (11).

Gradient echo MR imaging may also be used without USPIO administration for the differentiation between benign and malignant lymph nodes. The physiological reasoning is that macrophages

naturally engulf endogenous magnetic field disturbing substances, namely blood degradation products, whereas cancer cells do not (12,13). Another promising technique, which explores the restriction to the movement of water molecules, is diffusion weighted MR imaging (DWI). Dense, cell-rich tumour contains more barriers to the diffusion of water than sparsely cellular normal tissue. This property has been explored extensively in human imaging. However, normal lymphatic tissue is also characterized by high cellularity and the apparent diffusion coefficient (ADC), the simplest and best-known quantitative DWI-derived parameter, shows a significant overlap between benign and malignant lymph nodes. New and more elaborate post-processing DWI models are now available that may make way for a better understanding of tissue architecture and for a more accurate differential diagnosis (14).

The purpose of the following original research is to explore new acquisition and post-processing methods using gradient echo and diffusion-weighted MR Imaging for lymph node classification in rectal cancer.

References

1) Sebag-Montefiore D, Stephens R, Steele R et al. Preoperative radiotherapy versus selective postoperative chemoradiotherapy in patients with rectal cancer (MRC CR07 and NCIC-CTG C016): a multicentre, randomised trial. Lancet. 2009. 373(9666):811-820.

2) Kapiteijn E, Marijnen C, Nagtegaal I et al. Preoperative radiotherapy combined with total mesorectal excision for resectable rectal cancer. N Engl J Med. 2001. 345(9):638-646.

3) Sauer R, Becker H, Hohenberger W et al. Preoperative versus postoperative chemoradiotherapy for rectal cancer. N Engl J Med. 2004. 351(17):1731-1740.

4) Cedermark B, Dahlberg M, Glimelius B et al. Swedish Rectal Cancer Trial. Improved survival with preoperative radiotherapy in resectable rectal cancer. N Engl J Med. 1997. 336(14):980-987.

5) Sauer R, Liersch T, Merkel S et al. Preoperative versus postoperative chemoradiotherapy for locally advanced rectal cancer: results of the German CAO/ARO/AIO-94 randomized phase III trial after a median follow-up of 11 years. J Clin Oncol. 2012. 30(16):1926-1933.

6) Rödel C, Graeven U, Fietkau R et al. German Rectal Cancer Study Group. Oxaliplatin added to fluorouracil-based preoperative chemoradiotherapy and postoperative chemotherapy of locally advanced rectal cancer (the German CAO/ARO/AIO-04 study): final results of the multicentre, open-label, randomised, phase 3 trial. Lancet Oncol. 2015. 16(8):979-89.

7) Zhang G, Cai Y, Xu G. Diagnostic Accuracy of MRI for Assessment of T Category and Circumferential Resection Margin Involvement in Patients with Rectal Cancer: A Meta-Analysis. Dis Colon Rectum. 2016. 59(8):789-99.

8) Al-Sukhni E, Milot L, Fruitman M et al. Diagnostic accuracy of MRI for assessment of T category, lymph node metastases, and circumferential resection margin involvement in patients with rectal cancer: a systematic review and meta-analysis. Ann Surg Oncol. 2012. 19(7):2212-23.

9) Brouwer N, Stijns R, Lemmens V et al. Clinical lymph node staging in colorectal cancer; a flip of the coin? Eur J Surg Oncol. 2018. 44(8):1241–6.

10) Lambregts D, Beets G, Maas M et al. Accuracy of gadofosveset-enhanced MRI for nodal staging and restaging in rectal cancer. Ann Surg. 2011. 253:539–45.

11) Wu L, Cao Y, Liao C et al. Diagnostic performance of USPIO-enhanced MRI for lymph-node metastases in different body regions: a meta-analysis. Eur J Radiol. 2011. 80(2):582-9.

12) Korteweg M, Zwanenburg J, Hoogduin J et al. Dissected Sentinel Lymph Nodes of Breast Cancer Patients: Characterization with High-Spatial-Resolution 7-T MR Imaging. Radiology. 2011. 261:127–135.

13) Li C, Meng S, Yang X et al. The Value of T2 in Differentiating Metastatic from Benign Axillary Lymph Nodes in Patients with Breast Cancer - A Preliminary In Vivo Study. PLOSONE. 2014:9(1).*

14) Panagiotaki E, Chan R, Dikaios N et al. Microstructural Characterization of Normal and Malignant Human Prostate Tissue with Vascular, Extracellular, and Restricted Diffusion for Cytometry in Tumours Magnetic Resonance Imaging. Invest Radiol. 2015. 50(4):218-227.

4.3. Susceptibility perturbation imaging maps tumor infiltration into mesorectal lymph nodes

Translational Science

Cancer Research

Susceptibility Perturbation MRI Maps Tumor Infiltration into Mesorectal Lymph Nodes

Inês Santiago[1,2,3], João Santinha[4], Andrada Ianus[1,5], Antonio Galzerano[6], Rita Theias[7], Joana Maia[8], Maria J. Barata[2], Nuno Loução[9], Bruno Costa-Silva[8], Antonio Beltran[6], Celso Matos[2], and Noam Shemesh[1]

Abstract

Noninvasive characterization of lymph node involvement in cancer is an enduring onerous challenge. In rectal cancer, pathologic lymph node status constitutes the most important determinant of local recurrence and overall survival, and patients with involved lymph nodes may benefit from preoperative chemo and/or radiotherapy. However, knowledge of lymph node status before surgery is currently hampered by limited imaging accuracy. Here, we introduce Susceptibility-Perturbation MRI (SPI) as a novel source of contrast to map malignant infiltration into mesorectal lymph nodes. SPI involves multigradient echo (MGE) signal decays presenting a nonmonoexponential nature, which we show is sensitive to the underlying microstructure via susceptibility perturbations. Using numerical simulations, we predicted that the large cell morphology and the high cellularity of tumor within affected mesorectal lymph nodes would induce signature SPI decays. We validated this prediction in mesorectal lymph nodes excised from total mesorectal excision specimens of patients with rectal cancer using ultrahigh field (16.4 T) MRI. SPI signals distinguished benign from malignant nodal tissue, both qualitatively and quantitatively, and our histologic analyses confirmed cellularity and cell size were the likely underlying sources for the differences observed. SPI was then adapted to a clinical 1.5 T scanner, added to patients' staging protocol, and compared with conventional assessment by two expert radiologists. Nonmonoexponential decays, similar to those observed in the *ex vivo* study, were demonstrated, and SPI classified lymph nodes more accurately than standard high-resolution T_2-weighted imaging assessment. These findings suggest this simple, yet highly informative, method can improve rectal cancer patient selection for neoadjuvant therapy.

Significance: These findings introduce an MRI methodology tailored to detect magnetic susceptibility perturbations induced by subtle alterations in tissue microstructure.

Introduction

In rectal cancer, pathologic lymph node status of the mesorectum constitutes the most important determinant of local recurrence and overall survival (1). Standard assessment is based on hematoxylin and eosin (H&E)-stained slides (1), which can identify malignancy based on the contrast between small, roughly round, and loosely-packed leucocytes and much larger, goblet-shaped, tightly packed malignant epithelial cells. This information becomes available only with radical surgery; however, preoperative neoadjuvant chemoradiation therapy is associated with lower incidences of local relapse in patients with high-risk features, including lymph node positivity, when compared with postoperative regimens (6% vs. 13% at 5 years; ref. 2). This justifies the need for accurate preoperative noninvasive imaging-based lymph node characterization.

MRI is safe, noninvasive, and benefits from extremely versatile physics, giving rise to a multitude of contrast mechanisms, which, in turn, can highlight different aspects of biological tissue. One of the most important sources of MRI contrast is dephasing in the transverse plane, typically characterized by a time constant T_2–the spin–spin relaxation. T_2 is affected by alkali cation composition and tissue microstructure and has been shown to be capable of differentiating between normal tissue and malignant tumors since the very beginning of magnetic resonance experiments in tissues (3). Indeed, T_2-weighted MRI (T2-WI) remains the gold standard for pelvic staging in rectal cancer, but it is unfortunately very limited with respect to lymph node involvement (4, 5). However, more generally, the MRI signal can be sensitized to transverse dephasing induced by local field variations arising from susceptibility distributions. In this case, the transverse relaxation constant is described by $1/T_2^* = 1/T_2 + 1/T_2'$, where T_2' characterizes the additional source of dephasing (6). Divalent calcium or trivalent iron cations, as well as tissue oxygenation, are important

[1]Neuroplasticity and Neural Activity Lab, Champalimaud Research, Champalimaud Centre for the Unknown, Lisbon, Portugal. [2]Radiology Department, Champalimaud Centre for the Unknown, Lisbon, Portugal. [3]Nova Medical School, Campo Mártires da Pátria, Lisbon, Portugal. [4]Computational Clinical Imaging Group, Champalimaud Centre for the Unknown, Lisbon, Portugal. [5]Centre for Medical Imaging Computing, Department of Computer Science, University College London, London, United Kingdom. [6]Pathology Department, Champalimaud Centre for the Unknown, Lisbon, Portugal. [7]Pathology Department, Hospital Fernando Fonseca, Amadora, Portugal. [8]Systems Oncology Lab, Champalimaud Research, Champalimaud Centre for the Unknown, Lisbon, Portugal. [9]Philips Healthcare Iberia, Madrid, Spain.

Note: Supplementary data for this article are available at Cancer Research Online (http://cancerres.aacrjournals.org/).

Corresponding Author: Noam Shemesh, Champalimaud Research, Champalimaud Centre for the Unknown, Av. Brasilia, Lisbon 1400-038, Portugal. Phone: 3512-1048-0000 ext. 4467; E-mail: noam.shemesh@neuro.fchampalimaud.org

doi: 10.1158/0008-5472.CAN-18-3682

sources of susceptibility-induced local field variations and their characterization is routinely performed using T_2^*-sensitive sequences such as gradient-echo MRI. Interestingly, gradient echo MRI has been also performed in the context of lymph node characterization. A study on dissected axillary lymph nodes at 7T demonstrated that the T_2^* of metastatic lymph nodes was distinct from that of benign nodes (7). A subsequent similar study performed *in vivo* at 3T reached similar conclusions (8), although the mechanism underlying these T_2^* variations remains to be elucidated.

T_2^* is a "generic" parameter, which can only be accurately estimated in the (approximately) linear, low echo-time regime of a multigradient echo (MGE) signal decay. This generic linear decay with the log of the signal decay is quite "featureless"; rather dramatic changes in susceptibility would be required to induce a significant variation in the T_2^*. However, the underlying physics (9–11) suggests that in most realistic scenarios, magnetic fields would be distributed according to susceptibility-driven perturbations leading to nonexponential (9) and even nonmonotonic (10) signals, which potentially reflect microstructural tissue properties. Curiously, the vast majority of studies assumed that it is sufficient to measure the "linear" component at short echo times, and only very few studies ventured toward measuring the full MGE decay up to longer echo times (TE), which could reflect the underlying susceptibility perturbations much better. Indeed, the few studies that have measured the full MGE decay have discovered that much more detailed information could be potentially extracted. For example, Chen and colleagues reconstructed the shape and orientation of white matter substructures and their arrangement relative to one another in humans at 3T from multiexponential MGE decays measured up to long TEs (9). Nunes and colleagues probed *ex vivo* rat spinal cords at 16.4 T and found nonexponential, and nonmonotonic MGE decays, which were simply modeled by two compartments (axons + extraaxonal space), leading to axon density quantification (10). Qian and colleagues scanned tibial cartilage explants at 3T and classified different types of MGE decays, where the short T_2^* component differentiated diseased from healthy cartilage successfully, while the monoexponential T_2^* model did not (11).

Normal lymph nodes are composed of a relatively uniform and loose distribution of small lymphocytes. In contrast, malignancy is characterized by the presence of tightly-packed large malignant epithelial cells. Because susceptibility-driven magnetic field distributions depend on the underlying compartment sizes, we hypothesized that MGE signals could reflect these intrinsic susceptibility disturbances and distinguish tumor-infiltrated from normal nodal tissue. We term this long-echo MGE approach Susceptibility Perturbation MR Imaging (SPI) because it probes susceptibility perturbations due to microstructure. We tested SPI using numerical simulations and ultrahigh magnetic field MRI experiments (16.4 T) in mesorectal lymph nodes extracted from the surgical specimens of patients with rectal cancer. We elucidated the mechanisms underlying the emerging SPI contrasts using quantitative histologic analysis. Finally, we translated the experiment to an *in vivo* 1.5 T scanner, upon patient staging, for clinical applicability assessment, in which the SPI contrast was again observed. Our findings indicate that SPI is superior to the current standard methodology for lymph node involvement characterization *in vivo*.

Materials and Methods

Simulations

Numerical simulations were performed to predict whether changes in cellularity could affect MGE decays. To this end, we simulated susceptibility-driven magnetic field distribution maps arising from randomly packed spheres with different distributions of cell sizes and intracellular volume fractions. The magnetic field distribution for an individual sphere of radius R located at position (x_0,y_0,z_0) in a 3D mesh (x,y,z) is given in Eq. A (12, 13):

$$\Delta B^{sph}(x,y,z) = B_0 \begin{cases} \frac{1}{3}\chi R^3 \frac{(2(z-z_0)^2-(x-x_0)^2-(y-y_0)^2)}{((z-z_0)^2+(x-x_0)^2+(y-y_0)^2)^{5/2}} & \text{outside the sphere} \\ 0 & \text{inside the sphere} \end{cases} \quad (A)$$

Following others (14), in this study we used a susceptibility difference of $\chi = 6 \times 10^{-7}$ (14) in all simulations.

Guided by our histology assessment, we designed two tissue configurations corresponding to the microstructure of benign and malignant tissue, respectively. The benign tissue configuration employed a distribution of spherical radii corresponding to a lognormal distribution of areas with a mean of 12.2 μm^2 and SD of 6.1 μm^2 packed in a $50 \times 50 \times 50\ \mu m^3$ cube with intracellular volume fraction of 24%. For the malignant tissue configuration, we used a similar lognormal distribution, but now with a mean of 92.7 μm^2 and SD of 49.8 μm^2, packed in a $50 \times 50 \times 50\ \mu m^3$ volume with 61% intracellular volume fraction. Once the configurations were set, the field map $\Delta B(x,y,z)$ was calculated as the sum over the contributions of all individual spheres within each substrate.

Once the field maps were produced for every substrate, the MGE signal in the simulated "voxel" could be calculated by simply summing across the entire "voxel", as represented in Eq. B:

$$S_{MGE}(TE) = \iiint_{x,y,z} \exp(i\gamma\Delta B(x,y,z) \cdot TE) \quad (B)$$

Ultrahigh field SPI of *ex vivo* lymph nodes

Institutional setting and lymph node harvesting. This study was approved by the institutional ethics committee and written informed consent was obtained from twenty-five consecutive patients with rectal cancer that agreed to participate in the study. Six of these patients were excluded because they underwent neoadjuvant therapy and another three were excluded because they chose to be operated in a different institution. Sixteen patients underwent surgery without neoadjuvant therapy and their total mesorectal excision specimens were immersed in a 4% formaldehyde solution for 72 hours. During macroscopic specimen processing, the otherwise discarded halves of lymph nodes present in more than 1 cut slice, approximately 5 mm in thickness, were collected and labeled to match the halves sent for pathologic staging, which was performed by a gastrointestinal pathologist (8 years of experience), according to the cancer protocol defined by the College of American Pathologists (https://www.cap.org/protocols-and-guidelines/cancer-reporting-tools/cancer-protocol-templates). Pathologic staging resulted in the exclusion of an additional 5 patients with node-negative disease. A total of 11 patients were included (mean age 61.6 years, 5 males).

Acquisition protocol at 16.4T

Retrieved lymph node "halves" from each patient were grouped in benign/malignant pairs based on the information from pathologic staging, preferably originating from the same histopathologic block and with a similar size. Prior to scanning, the nodes were washed with a 1% PBS solution for 24 hours and then immersed in Flourinert within a 10 mm NMR tube.

The preclinical MRI images were acquired at 37°C on a 16.4T Bruker Aeon Ascend Scanner (Bruker Biospin) using a Micro5 probe with a gradient system capable of producing up to 3,000 mT/m in all directions. An MGE acquisition was performed with the following parameters: 50 echo times starting at 1.6 ms with 1.4 ms interval, repetition time of 1,500 ms, flip angle of 50°, slice thickness of 0.3 mm, a field-of-view of 12 × 12 mm^2, and matrix size of 120 × 120, leading to an in-plane resolution of 0.1 × 0.1 mm^2. The acquisition bandwidth was set to 125 kHz and 25 signal averages were acquired, leading to a total scan time of 1 hour 12 minutes per node.

Histopathologic analysis for validation of the MRI findings

The scanned "halves" of lymph nodes were embedded in paraffin and 6 consecutive 4 μm slices were cut every 50 μm using a Leica RM2245 microtome (Leica Biosystems) in a plane parallel to the cut surface of the node, similarly to the MRI acquisition. One slice per interval was stained with H&E and analyzed by the gastrointestinal pathologist (8 years of experience) using a Zeiss Axio Lab A1, (Carl Zeiss Microscopy GmbH) with a 40× amplification. The analysis of the scanned "halves" resulted in reclassification of 3 previously defined benign nodes as malignant. Given they all originated from patients already classified as N+, this did not impact patient management. In total, we scanned and analyzed 29 benign and 35 malignant lymph nodes.

In four representative lymph nodes, the remaining 4-μm slices were used for additional characterization: Pearls coloration (Iron Staining Kit, Ventana Medical Systems, Inc.) was used to quantify iron-containing MR-field–disturbing particles; an antibody against CD45 (CD45, QBEnd/10, Leica Biosystems) was used to mark leucocytes; and multicytokeratin AE1/AE3 (Leica Biosystems) was used to mark adenocarcinoma cells.

MR image analysis

Multigradient echo datasets were denoised in Matlab (Mathworks) using Marchenko–Pastur principle component analysis (15) with a window size of 7 × 7. Benign and malignant histology-matched regions-of-interest (ROI) were defined by a dedicated radiologist (10 years of experience). Three ROIs were placed per node, in the most representative slice; in malignant nodes, malignant areas were selected on the basis of MR-histology coregistration (see subtopic below). The mean signal value per node was computed for each TE. Although SPI in principle leads to a field distribution, we here simplified the complex expressions by assuming that one, two, or three components would be sufficient to describe the signal decay. In the multiexponential models, one compartment was arbitrarily assumed to be on resonance while the others exhibited a frequency shift. The signal expressions for 1-compartment, 2-compartment, and 3-compartment models are given in Eqs. C, D, and E, respectively.

$$S_{1c} = S_0 \exp(-TE/T_2^*) \quad \text{(C)}$$

$$S_{2c} = S_0 \left| f^a \exp\left(-\frac{TE}{T_2^{*a}}\right) + (1-f^a)\exp\left(-TE\left(\frac{1}{T_2^{*b}} + i\Delta\omega^b\right)\right)\right| \quad \text{(D)}$$

$$S_{3c} = S_0 \left| f^a \exp\left(-\frac{TE}{T_2^{*a}}\right) + f^b \exp\left(-TE\left(\frac{1}{T_2^{*b}} + i\Delta\omega^b\right)\right) + (1-f^a-f^b)\exp\left(-TE\left(\frac{1}{T_2^{*c}} + i\Delta\omega^c\right)\right)\right| \quad \text{(E)}$$

where TE is the echo time, S_0 is the signal at TE = 0, and T_2^{*i} is the relaxation time of compartment i, which has a volume fraction f^i and frequency shift $\Delta\omega^i$.

Voxel-by-voxel fitting of the signal models above to the experimental data were performed for the whole dataset.

MR-pathology coregistration

Histology H&E slides were scanned at a Philips Ultrafast Scanner 1.6 (Philips Healthcare), stacked into a volume, and registered to MGE images using SimpleElastix (16). For the stacking step, a 2D-rigid pairwise registration was performed, in which a set of 3 to 6 corresponding control points were defined on each pair of histology images and the translations and rotations were estimated using adaptive stochastic gradient descent, minimizing both the advanced Mattes mutual information and the corresponding points Euclidean distance metric. The registration of a given stack to the MGE images utilized a 3D-rigid registration scheme with 6 to 12 corresponding control points defined in the two volumes and optimized using adaptive stochastic gradient descent that minimized both the advanced mattes mutual information and the corresponding points Euclidean distance metric.

Histology quantification

With the purpose of understanding the parametric differences encountered between benign and malignant lymph node tissue, we analyzed histology H&E slides and obtained measurements of cellularity and cell size. To ensure histology measurements were as representative as possible, we first selected the single H&E slide from the volume stack that best matched the MGE image in which the ROIs were placed. The selection was based on specific contour and inner landmarks that could be found in both MGE and scanned H&E images at low magnification (×0.03). Then, from each MGE-ROI–matching histology area and at higher magnification (×0.42), 3 random 50 × 50 μm fields were selected and a Cell Detection Tool (QuPath) was employed to quantify cell number, nucleus area, and cell area.

Statistical analysis

Signal decay models were compared on the basis of Bayesian Information Criterion (BIC), which describes the goodness of fit, penalizing for increasing number in model parameters, as

represented in Eq. F.

$$BIC = \ln(N)k - 2\ln(\hat{L}) \quad \text{(F)}$$

where N is the number of data points, k is the number of model parameters (1 for monoexponential decay, 4 for biexponential decay, and 7 for triexponential decay), and $\ln(\hat{L})$ is the maximum value of the log likelihood function of the model. Specifically, $\ln(\hat{L})$ is the negative of the sum of squared differences between the model prediction and the measured data, which was also used as objective function for nonlinear fitting of the models.

For all parameters extracted from the models, comparison between benign and malignant was based on the Mann–Whitney *U* test, given data were not normally distributed. An $\alpha < 0.05$ was considered as the statistical significance threshold.

Spearman rank correlation coefficient was the test used to establish the statistical dependence between the rankings of model parameters and histology metrics. Bonferroni correction was employed to account for multiple comparisons.

Translation of SPI to the clinic, *in vivo* at 1.5 T

This study was also approved by the institution's ethics committee and written informed consent was obtained. In 8 participating patients, butylscopolamine 20 mg was administered intravenously to minimize bowel movement and a stereotactic body radiotherapy pressure belt with manual pump insufflated to 20–40 mmHg (Orfit Industries) was used to minimize respiratory movement artifacts. A MGE sequence with the following parameters was added to the staging pelvic MRI, which was performed on a 1.5 T Clinical Scanner (Ingenia, Philips Healthcare): 32 TEs were acquired starting at 2.37 ms with a 2.37 ms interval; repetition time of 1971 ms; flip angle of 55°; slice thickness of 4 mm; field of view of 20 × 20 cm^2, matrix size of 480 × 480, bandwidth of 431 Hz, and 2 signal averages, leading to an in-plane resolution of 0.42 × 0.42 mm^2 and a total acquisition time of 11 minutes 19 seconds.

Whole-node ROIs were defined for all visible lymph nodes on the single slice with the largest surface by a general radiologist (11 years of experience). Mapping during specimen processing allowed 36 benign and 27 malignant lymph nodes originating from the 6 patients subsequently selected for surgery without preoperative therapy at multidisciplinary team meeting (mean age, 61.7 years; 4 males) to be matched to MGE images (2 patients were excluded because they underwent neoadjuvant therapy). Models were fitted to the median magnitude signal of each lymph node, given the reduced number of voxels per node and deviation from normality of the distribution of signal intensities. Two radiologists dedicated to gastrointestinal and abdominal imaging (10 and 13 years of experience), blinded to pathology results, independently performed a node-by-node classification in the corresponding axial, coronal, and sagittal high-resolution T_2-WI in accordance with the ESGAR 2016 recommendations for nodal staging (17). Reliability of the T_2-WI–based analysis was estimated using the intraclass correlation coefficient (<0.40 = poor; 0.40 to 0.59 = Fair; 0.60 to 0.74 = good; 0.75 to 1.00 = excellent). The SPI and T_2-WI analysis and their combination were compared using logistic regression. The statistical significance of the differences between the corresponding areas under the ROC curves (AuROC) were tested using the De Long Test.

Results

Simulations

Our first goal was to simulate whether microstructural changes induced by the infiltration of malignant cells into lymph nodes would produce significant perturbations to magnetic field distributions. Figure 1A and B simulate the spatial distribution of magnetic fields in the "benign" substrate (small spheres, low volume fraction) and "malignant" substrate (infiltration of large spheres, with large volume fraction), respectively. Importantly,

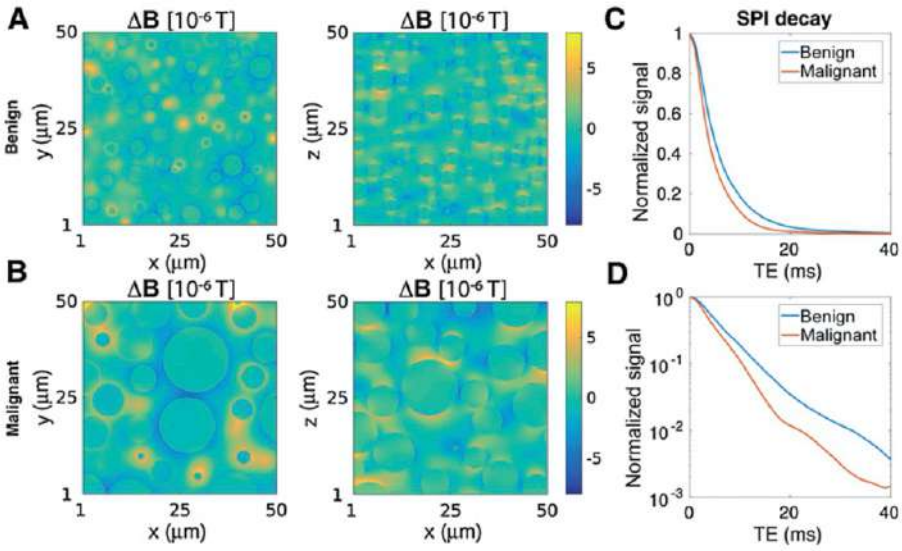

Figure 1.
Spatial distribution of the magnetic field induced by a distribution of spherical cells corresponding to benign tissue over a 50 × 50 μm^2 field of view in the XY and XZ planes (**A**) and malignant tissue over a 50 × 50 μm^2 field of view in the XY and XZ planes (**B**). **C,** Normalized signal decay as a function of TE for the two substrates corresponding to benign and malignant tissue. **D,** Normalized log signal decay as a function of TE for the same two substrates.

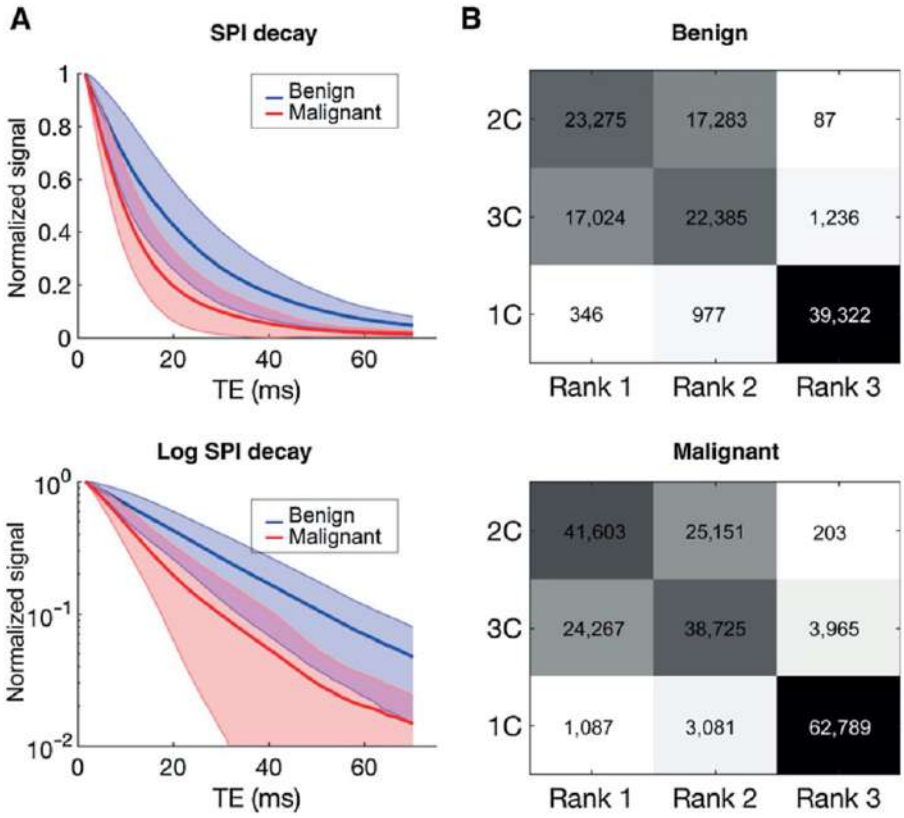

Figure 2.
A, Normalized average signal and log average signal with increasing TE of benign ($n = 29$) and malignant ($n = 35$) lymph node datasets. Shaded areas represent the SD limits. **B,** Number of entries per rank of voxel-by-voxel analysis using BIC for benign and malignant lymph nodes. Notice 2-compartment model ranked first and 1-compartment model ranked last in most instances for both benign and malignant datasets.

these field distributions give rise to a nonmonoexponential MGE signal decay (Fig. 1C, note the signal oscillation), which is more evident perhaps in the logarithmic plot (Fig. 1D). Perhaps even more importantly, these simulations predict a slower decay for small spheres with low volume fraction (benign tissue) and a faster decay for larger spheres with high volume fraction (malignant tissue), suggesting that MGE measurements could inform about tissue microstructure.

Ultrahigh field SPI of *ex vivo* lymph nodes

To test the validity of the above predictions and investigate whether SPI could distinguish between normal nodal tissue and nodal tissue infiltrated by malignancy, we performed ultrahigh field *ex vivo* experiments with very high spatial and TE resolution on 29 benign and 35 malignant lymph nodes (64 lymph nodes in total). Figure 2A shows that the normalized MGE signal decay for both benign and malignant tissue is indeed nonmonoexponential. TE-dependent differences between the signal decay of the different groups are already apparent from the raw data (Fig. 2A). A BIC analysis for model selection (e.g., between Eqs. A, B, and C) reveals that the 2-compartment model represents the data better than a 1- or 3-compartment model in the vast majority of voxels (Fig. 2B).

Figure 2A also reveals clear and dramatically different SPI decays for benign and malignant tissue: while the former decays slowly, the latter decays much more rapidly.

Given that the 2-compartment model was selected from the BIC values, further analysis was focused on this model. The median values of T_2^*a were significantly shorter in malignant tissue, by a factor of approximately 2 (malignant = 15.05 ms; benign = 29.59 ms; $P = 1 \times 10^{-4}$), as were the median values of T_2^*b, by a factor of approximately 2.3 (malignant = 10.71 ms; benign = 24.64 ms; $P = 1 \times 10^{-4}$). In addition, in absolute value, the median frequency shift $\Delta\Omega$ was significantly larger in malignant tissue, by a factor of approximately 1.6 (malignant = −0.08 rad; benign = −0.05 rad; $P = 8 \times 10^{-4}$). The fraction of the first component did not exhibit a significant difference between tissues (malignant = 0.62; benign = 0.66; $P = 0.097$). Figure 3 depicts these measurement differences as boxplots.

We next turn to the histologic analyses, where striking microstructural differences were found. In benign nodal tissue, the predominant cell type—lymphocyte—is small, round, and practically devoid of visible cytoplasm. Adenocarcinoma cells, on the other hand, are cytoplasm-rich and much larger. When quantified, we found that cell size, both in terms of nuclear area (benign: $\bar{x} = 12.36$ and $\sigma_{\bar{x}} = 0.99$ μm^2; malignant: $\bar{x} = 23.77$ and $\sigma_{\bar{x}} = 4.16$ μm^2; $P = 5.99 \times 10^{-7}$) and total cell area (benign: $\bar{x} = 12.36$ and $\sigma_{\bar{x}} = 0.99$ μm^2; malignant: $\bar{x} = 104.34$ and $\sigma_{\bar{x}} = 23.53$ μm^2; $P = 2.23 \times 10^{-8}$), was higher in malignant tissue while the mean number of cells per surface area was much lower (benign: $\bar{x} = 19.91 \times 10^{-3}$ and $\sigma_{\bar{x}} = 2.69 \times 10^{-3}$ cells/μm^2; malignant: $\bar{x} = 6.62 \times 10^{-3}$ and $\sigma_{\bar{x}} = 3.73 \times 10^{-3}$ cells/μm^2; $P = 5 \times 10^{-3}$). We also directly correlated SPI parameters with the cellularity and cell size by registering MR images with the histologic slices (Fig. 4A). We found significant correlations between T_2^*b, our best-performing parameter, and both number of cells

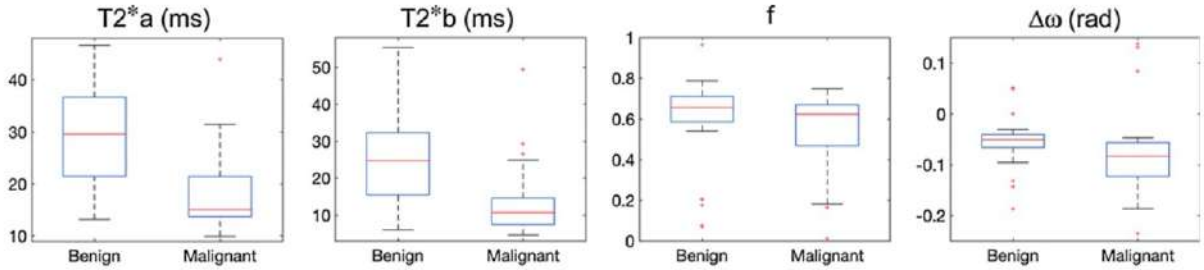

Figure 3.
Boxplots depicting the measurement differences for the 2-compartment model-derived parameters. Significant differences between benign and malignant lymph nodes were found for T_2*a, T_2*b, and $\Delta\Omega$, but not for f.

per surface area ($\rho = 0.52$, considered moderate; $P = 9.18 \times 10^{-6}$) and mean nuclear area ($\rho = -0.56$, considered moderate; $P = 1.14 \times 10^{-6}$; Fig. 4B).

We also noted a variety of infiltration patterns in malignant lymph nodes, namely cellular areas (those constituted by tightly packed malignant cells), areas of necrosis and areas of tumor-induced desmoplasia. These patterns tend to coexist in malignant lymph nodes in varying proportions but when selective ROIs were placed in relatively "pure" areas, we discovered that areas with tightly packed malignant cells tended to produce a slower MGE signal decay compared with areas characterized by desmoplesia or necrosis but still, the decay occurred much faster than in benign nodal tissue (Fig. 5). To investigate the mechanism underlying the SPI decay differences, we performed staining for different markers (Fig. 5). Importantly, no iron particle accumulation was found in the selected fields neither in benign nor in malignant nodes, suggesting iron is not involved in the contrasts obtained in this study.

Translation of SPI to the clinic, *in vivo* at 1.5 T

We next aimed to assess the clinical applicability of SPI for mesorectal lymph node characterization prospectively, upon rectal cancer staging. The nonmonoexponential nature of the MGE signal decay was evidenced for both benign ($n = 36$) and malignant ($n = 27$) lymph node datasets (63 lymph nodes in total), and again revealed radically different decay characteristics: the benign nodes had a much slower decay compared with the malignant. Figure 6 shows SPI decays from a benign and a malignant node and in from Supplementary Fig. S1, the corresponding full extent of TEs is displayed.

The BIC analysis ranked the biexponential model first and the monoexponential model last in most instances. Differences in the parameter values derived from the biexponential model are presented in Figure 7A. T_2*a carried differences between benign and malignant lymph nodes with statistical significance (malignant: median = 50.86 ms; iqr = 20.84 ms; benign: median = 58.87 ms; iqr = 29.50 ms; $P = 0.02$), as did T_2*b (malignant: median = 2.96 ms; iqr = 0.73 ms; benign:

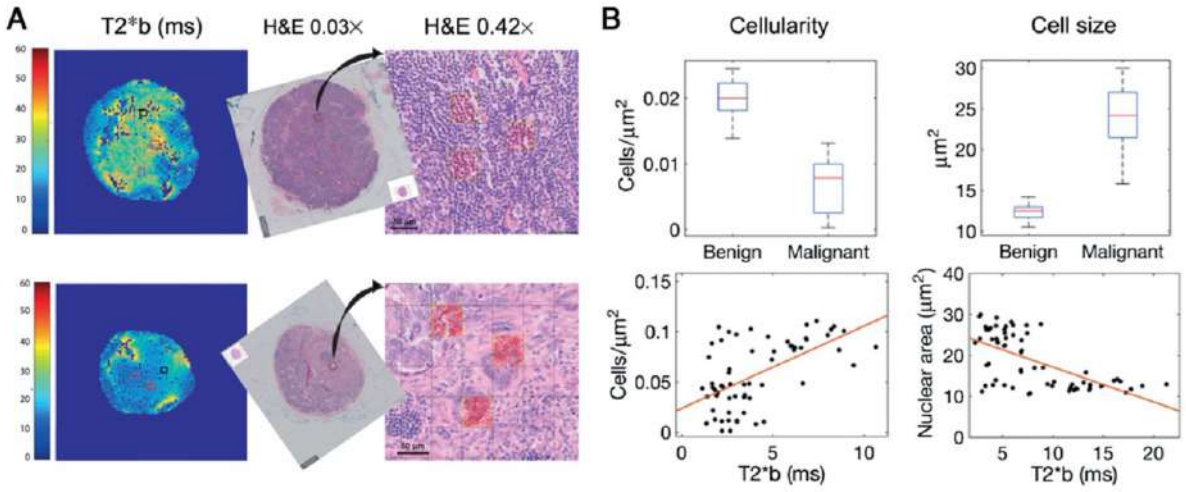

Figure 4.
A, T_2*b parametric maps and corresponding QuPath cell detection tool applications are exemplified for a benign (top) and a malignant lymph node (bottom). **B,** Cellularity and cell size differences between benign and malignant lymph nodes are depicted in the boxplot above and Spearman correlations between them and T_2*b are depicted in the scatterplot below ($\rho = 0.52$ for cells/µm² and $\rho = -0.56$ for nuclear area, both considered moderate and both with $P < 0.01$).

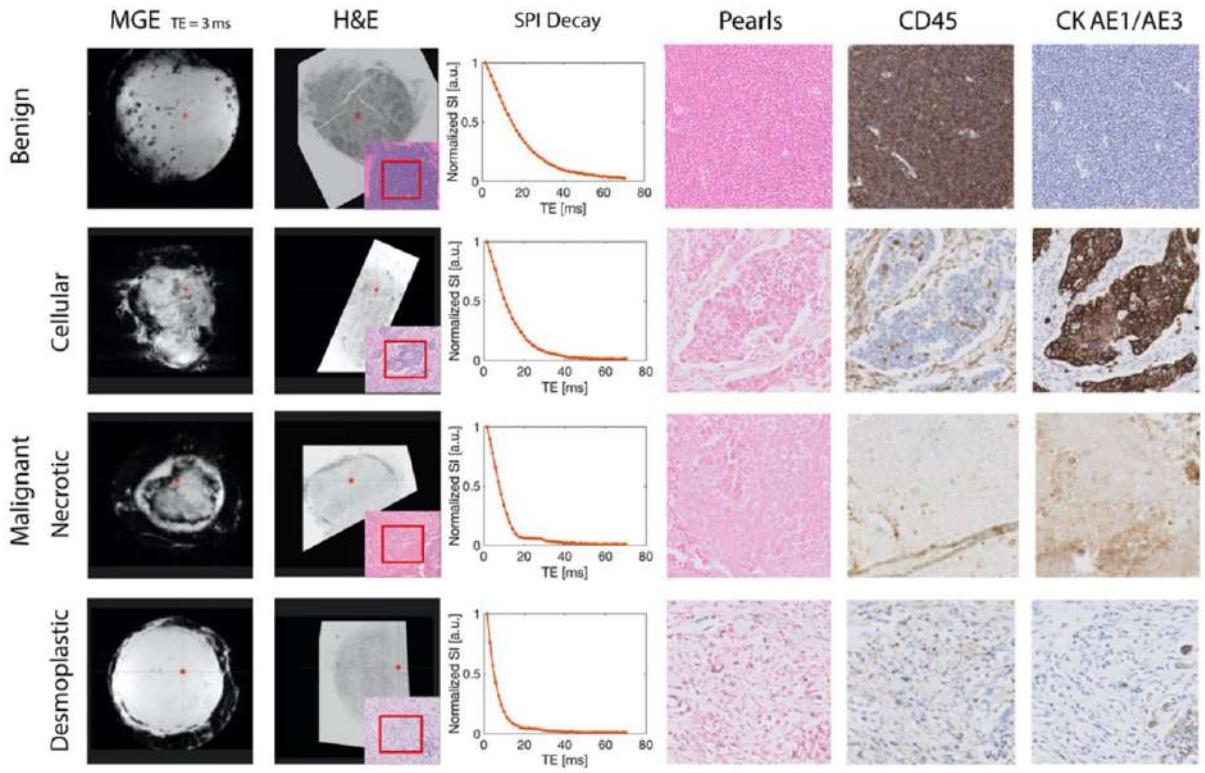

Figure 5.

When selective ROIs were defined, clear variations in SPI decay behavior were present. Highly cellular areas in secondary follicles from benign nodal tissue show a slower initial decline, whereas in tumor tissue, this decline tends to occur much faster and a clear oscillation between 20 and 40 ms becomes apparent. Pearls coloration was negative in all selected fields (iron particles stained in dark blue using Pearls coloration). CD45 is expressed in the cellular membrane of all leucocytes and benign lymph node tissue stains heavily, as expected. CK AE1/AE3 is a cytokeratin combination expressed in epithelial cells, including malignancies of epithelial origin such as colorectal adenocarcinoma. Although all malignant lymph node areas were positive, the area of high cellularity shows more pronounced staining, and the corresponding early decay slope is higher when compared with other malignant patterns.

median = 3.59 ms; iqr = 6.17 ms; $P = 3 \times 10^{-3}$). Both T_2*a and T_2*b were shorter in malignant lymph nodes, in accordance with the *ex vivo* data. For a cutoff of 58.5 ms, T_2*a presented with an AuROC of 0.70 and for a cutoff of 53.2, T_2*b presented with an AuROC of 0.76. The combination of T_2*a + T_2*b resulted in an AuROC of 0.79 (Fig. 7C). The performance of these metrics was superior to both that of T_2* derived from the monoexponential model (0.64) and that of the T_2-WI–based analysis (0.67 and 0.69 for the two radiologists observing the data, ICC = 0.70, considered good). Adding the T_2*a + b SPI analysis to the T_2-WI assessment increased the AuROC from 0.65 to 0.80 for Reader 1 and from 0.66 to 0.87 for Reader 2 (Fig. 7C). The observed increase was statistically significant ($P = 8.6 \times 10^{-4}$ and $P = 3 \times 10^{-4}$ for Readers 1 and 2, respectively). However, the performance of the combination was not significantly improved when compared with the plain T_2*a + b SPI analysis ($P = 0.90$ and $P = 0.26$ for Readers 1 and 2, respectively).

Discussion

Lymph node staging is crucial for clinical decision-making in the great majority of malignancies. In the particular case of rectal cancer, lymph node involvement before surgery may be considered an indication for neoadjuvant therapy (18) but lymph node classification is limited on the basis of standard imaging, namely high-resolution T_2-weighted MRI (4, 5). Lymph node characterization can be improved using nontargeted imaging agent methods such as MR lymphography with USPIO nanoparticles, which have been applied with very high accuracy (19, 20, 21) and AuROC above 0.90 (22, 23). Very good results have also been reported using Gadofosveset, a gadolinium-based intravascular contrast agent (AuROC curve of 0.96; ref. 24). The drawback of these techniques is that they involve the administration of exogenous contrast agents with their implicit adverse reactions. Moreover, these contrast agents are not available for clinical use, making these techniques impractical.

In this study, we hypothesized that the microstructural changes associated with tumor infiltration—namely, the presence of malignant epithelial cells, much larger and more densely packed than native leucocytes—would cause susceptibility-induced magnetic field perturbations that could be picked up using SPI—an MGE sequence acquired up to very long TEs. Our histology-inspired numerical simulations clearly revealed that the hypothesis is viable and that MGE signal decays nonexponentially with

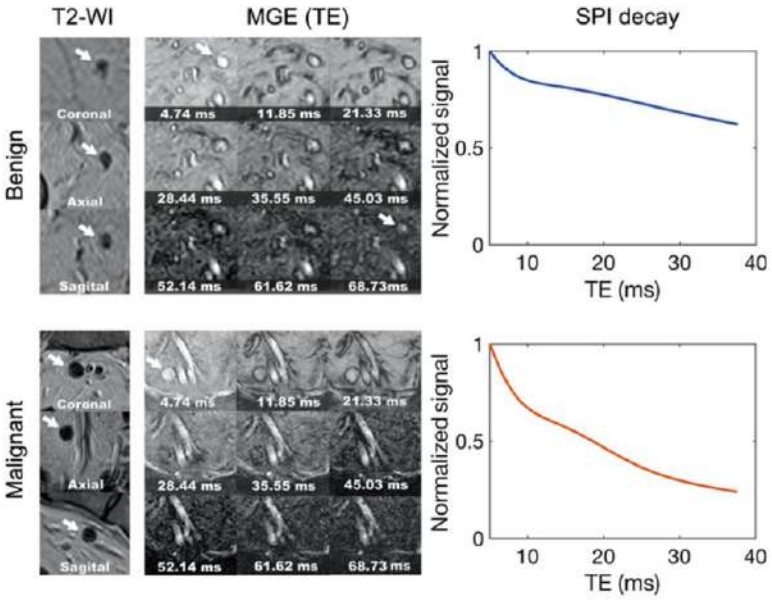

Figure 6.
Examples of a benign and malignant lymph node as depicted in multiplanar high-resolution T_2-WI and MGE clinical images with increasing TE (only 9 TEs were depicted for simplicity, but the full range of TEs is presented in Supplementary Fig. S1). A clearly faster loss of signal intensity with increasing TE is observed in the malignant lymph node. The corresponding single-slice whole-node ROI-based decay curves again show nonmonoexponential behavior.

potentially oscillating features. We then applied SPI at ultrahigh field 16.4 T MRI to perform a "virtual histology" with sufficient resolution to actually resolve infiltrated regions versus normal node tissue. Our experimental findings further corroborated our hypothesis: the SPI decays in the 64 lymph nodes dissected from the total mesorectal excision specimens of patients with rectal cancer were dramatically different in benign and malignant tissue, both with respect to the phenomenological signal decay, which was slower for normal nodes, but also quantitatively, from the ensuing extracted parameters. Interestingly, we found three different types of malignant infiltration into the lymph nodes. Patterns included clumps of adenocarcinoma cells tightly packed together, areas of desmoplastic reaction, and areas of necrosis/cystic degeneration. These patterns tend to coexist in varying proportions within and across lymph nodes but we were able to show, albeit qualitatively only, that the three different kinds of infiltration may be characterized by different SPI curves. While the prognostic impact of these histologic divergences is unknown, it may be worth exploring in the future to further assist in the decision-making framework.

To simplify the SPI analysis, we assumed that a small number of components could be fit to the data. T_2*b (the component with longer relaxation time) evidenced the most significantly different values and was much shorter in tumor tissue, though

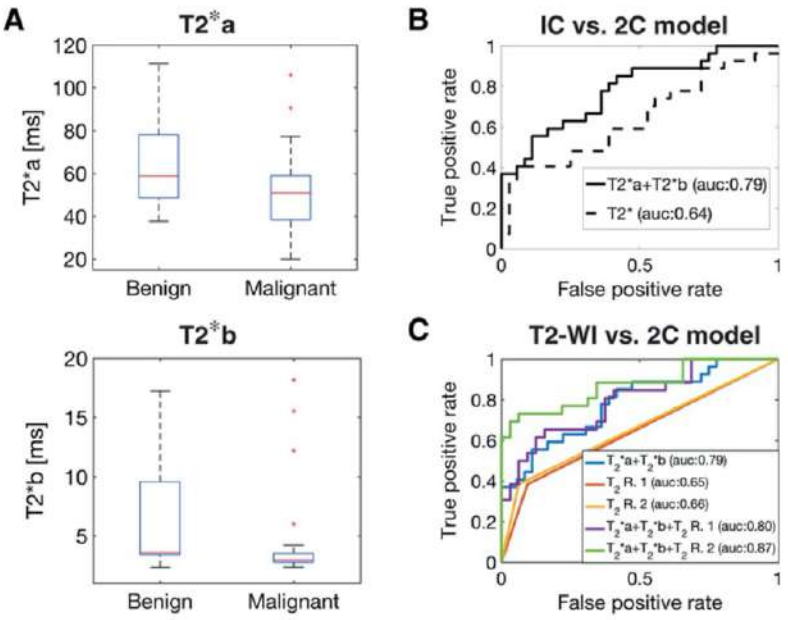

Figure 7.
A, Boxplots depict the significant differences in 2-compartment model-derived parameter values from the clinical dataset. **B,** ROC curves for monoexponential T_2* and biexponential T_2*a + b are also depicted, in which a clearly higher AuROC is present for the bi-compartmental model assessment. **C,** ROC curves for T_2-WI and T_2*a + b SPI analysis are shown, as well as their combination. The combination of the T_2-WI assessment with the SPI analysis performs best, showing the highest AuROC.

T_2*a was also significantly shorter. In absolute value, the frequency shift ($\Delta\Omega$) in tumor was higher, which is in line with the shorter relaxation rates observed.

The final step in the *ex vivo* part of the study was corroborating the working hypothesis using histology. Our histology quantification data indicated that microstructural features, namely cellularity and cell size, influenced the extracted SPI parameters. Judging by Pearl coloration, which was negative in both benign and malignant nodes studied, iron particle accumulation does not appear to be the source for the observed differences in the signal decays. Importantly, the shortening of both T_2* components observed in tumor *ex vivo* were also evidenced in malignant nodes *in vivo*. This suggests that oxygenation state, flow effects, or tissue preparation are unlikely explanations for our results. All these lend further credence to our hypothesis: the microstructure itself induces the capability of differentiating between infiltrated and benign node tissue.

It could be argued that these results, which were obtained at such high magnetic fields, would not necessarily be translatable to the lower magnetic fields existing in clinical settings. However, although it could be expected that the field distribution strongly depends on the strength of the magnetic field, it is worth noting that the MGE phase, which governs the nonmonoexponential decay observed above, goes as $\varphi_{MGE} = \gamma\Delta B \cdot TE$, which suggests that the lower ΔB can be compensated for with higher TE, and still obtain the same phase. We therefore translated the experiment to the clinical setting and scanned 63 mesorectal lymph nodes in patients with rectal cancer both with SPI and the contemporary state-of-the-art high resolution T_2-WI evaluated by two expert radiologists according to current guidelines (17). We found that, in accordance with the *ex vivo* experiment, the MGE signal is nonmonoexponential and, in some cases, also nonmonotonic, and it was best characterized by a biexponential model. We further found that in most instances, T_2*a and T_2*b values were significantly lower in malignant lymph nodes. The differences were somewhat less pronounced than in the *ex vivo* experiment, which may be justified by the smaller field strength and by the use of whole-node ROIs, required due to the constraints in clinical image resolution. Still, SPI parameters performed better than visual assessment by expert radiologists, with a higher sensitivity and no loss in specificity. We were therefore able to show that the simple SPI experiment provides indeed information on the microstructure also *in vivo* and adds value to current standard evaluation based on T2-WI. Even though results were slightly inferior to those reported for USPIO and Gadofosveset-enhanced MR imaging, unlike the latter, SPI is a simple, readily available, and adverse-effect–free method that can easily complement T_2-WI during staging pelvic MRI of patients. It should be noted that SPI is expected to have a better performance at 3T or even higher fields that may become more clinically relevant in the future. The separability of the curves is expected to be enhanced with increasing field, as the T_2*s shorten and the phase shifts increase due to stronger susceptibility perturbation (25–27). Moreover, an increase in signal to noise ratio could facilitate higher resolution for characterizing smaller nodes.

This study of course also had several limitations. First, no lymph node tissue could be retrieved from very small lymph nodes (<3 mm), which biased our sample for larger nodes in both *in vivo* and *ex vivo* experiments. Second, a large heterogeneity in the signal intensity decay patterns of malignant datasets was found. However, these reflected to some extent an inherent variability in tumor-spreading patterns, which as previously stated is hypothesized to carry relevant prognostic information. Third, the numerical simulations were somewhat simplified: the two tissue types assumed ideally spherical cells and that susceptibility does not vary between substrates. In addition, when computing the MRI signal, diffusion effects were ignored, that is, the static dephasing regime was assumed (12, 13). Nevertheless, the simulated signal in this toy model showed similar trends to measured data, suggesting that differences in cellular size and packing density play an important role in the observed SPI contrast.

Finally, it is worth reflecting on the translation of these findings to other lymph nodes not necessarily originating from the mesorectum of patients with rectal cancer. They might be particularly useful for urologic cancers such as prostate and bladder, for which high-mordibity–associated lateral pelvic lymph node dissection is still performed for staging purposes or based on indirect nomogram predictive model scoring rather than strictly to patients with lymph node involvement documented noninvasively (28, 29).

Conclusion

SPI accurately characterizes lymph node tissue and improves specificity toward microstructural characterization. At least in part, the quantitative differences in the extracted parameters were explained by differences in cellularity and cell size between the tissues, as opposed to iron content or oxygenation state. Using the same methodology and without the need for exogenous contrast administration, we found concordant results *in vivo* at 1.5T. When compared with expert visual assessment based on T_2-WI, SPI increased the accuracy of lymph node characterization upon clinical staging, with a significant improvement in sensitivity and no loss in specificity. It may therefore be of added value for patient selection for neoadjuvant therapy. The results given here are a first step that bodes well for future studies aiming to generalize SPI as a lymph-node–specific biomarker.

Disclosure of Potential Conflicts of Interest

No potential conflicts of interest were disclosed.

Authors' Contributions

Conception and design: I. Santiago, A. Beltran, N. Shemesh
Development of methodology: I. Santiago, J. Santinha, A. Ianus, A. Galzerano, N. Loução, B. Costa-Silva, A. Beltran, N. Shemesh
Acquisition of data (provided animals, acquired and managed patients, provided facilities, etc.): I. Santiago, R. Theias, N. Loução, A. Beltran, N. Shemesh
Analysis and interpretation of data (e.g., statistical analysis, biostatistics, computational analysis): I. Santiago, J. Santinha, A. Ianus, M. J. Barata,
Writing, review, and/or revision of the manuscript: I. Santiago, J. Santinha, A. Ianus, A. Galzerano, M. J. Barata, A. Beltran, C. Matos, N. Shemesh
Administrative, technical, or material support (i.e., reporting or organizing data, constructing databases): J. Maia, N. Shemesh
Study supervision: N. Shemesh
Others (simulations): A. Ianus
Others (pathology assessment): A. Galzerano
Others (macroscopy search for lymph nodes in surgical specimen and optical microscopy analysis of lymph nodes): R. Theias

Acknowledgments

The authors would like to thank the following for their contributions: Lara Castanheira, Alexandra Ferreira, and Ana Santos from the Pathology

Department of the Champalimaud Centre for the Unknown; Paula Montesinos, and Javier Gonzalez-Sanchez from Philips Healthcare Iberia; Nuno Figueiredo and José Filipe Cunha from the Digestive Unit of the Champalimaud Centre for the Unknown; Carlos Leichsenring, Vasco Geraldes, and Cisaltina Sobrinho from the Department of Surgery of the Hospital Fernando Fonseca, EPE; Maria Lisitskaya, a fellow radiologist at the Computational Clinical Imaging Group, Champalimaud Centre for the Unknown; Nickolas Papanikolaou from the Computational Clinical Imaging Group, Champalimaud Centre for the Unknown; all the staff from the Radiology Department of the Champalimaud Centre for the Unknown; and the researchers from the Neuroplasticity and Neural Activity MRI Lab, Champalimaud Centre for the Unknown. This study was funded by EPSRC grants from the Champalimaud Centre for the Unknown (EP/M020533/1 and EP/N018702/1 to A. Ianus).

The costs of publication of this article were defrayed in part by the payment of page charges. This article must therefore be hereby marked *advertisement* in accordance with 18 U.S.C. Section 1734 solely to indicate this fact.

Received November 27, 2018; revised February 13, 2019; accepted March 15, 2019; published first March 20, 2019.

References

1. Yao YF, Wang L, Liu YQ, Li JY, Gu J. Lymph node distribution and pattern of metastases in the mesorectum following total mesorectal excision using the modified fat clearing technique J Clin Pathol 2011; 64:1073–7.
2. Sauer R, Becker H, Hohenberger W, Rodel C, Wittekind C, Fietkau R, et al. Preoperative versus postoperative chemoradiotherapy for rectal cancer. N Engl J Med 2004;351:1731–40.
3. Damadian R. Tumour detection by nuclear magnetic resonance. Science 1971;171:1151–3.
4. Jhaveri K, Hosseini-Nik H. MRI of rectal cancer: an overview and update on recent advances. Am J Roentgenol 2015;205:42–55.
5. Bipat S, Glas AS, Slors FJ, Zwinderman AH, Bossuyt PM, Stoker J. Rectal cancer: local staging and assessment of lymph node involvement with endoluminal US, CT, and MR imaging—a meta-analysis. Radiology 2004; 232:773–83.
6. Chavhan GB, Babyn PS, Thomas B, Shroff M, Haacke EM. Principles, techniques, and applications of T2*-based MR imaging and its special applications. Radiographics 2009;29:1433–49.
7. Korteweg MA, Zwanenburge JJM, Hoogduin JM, van der Bosch MAAJ, van Diest PJ, van Hillegersberg R, et al. Dissected sentinel lymph nodes of breast cancer patients: characterization with high-spatial-resolution 7-T MR imaging. Radiology 2011;261:127–35.
8. Li C, Meng S, Yang X, Wang J, Hu J. The value of T2* in differentiation metastatic from benign axillary lymph nodes in patients with breast cancer – a preliminary *in vivo* study. PloS One 2014;9: e84038.
9. Chen WC, Foxley S, Miller KL. Detecting microstructural properties of white matter based on compartmentalization of magnetic susceptibility. NeuroImage 2013;70:1–9.
10. Nunes D, Cruz TL, Jespersen SN, Shemesh N. Mapping axonal density and average diameter in white matter using non-monotonic time-dependent gradient-echo MRI. J Magn Reson 2017;277: 117–30.
11. Qian Y, Williams AA, Chu CR, Boada FE. Multicomponent T2* mapping of knee cartilage: technical feasibility ex vivo. Magn Reson Med 2010;64: 1427–32.
12. Weisskoff R, Zuo CS, Boxerman JL, Rosen BR. Microscopic susceptibility variation and transverse relaxation: theory and experiment. Magn Reson Med 1994;31:601–10.
13. Salomir R, de Senneville BD, Moonen CTW. A fast calculation method for magnetic field inhomogeneity due to an arbitrary distribution of bulk susceptibility. Magn Reson Eng 2003;19B:26–34.
14. Kashevskii BE, Kashevskii SB, Prokhorov IV, Aleksandrova EN, Istomin YuP. Magnetophoresis and the magnetic susceptibility of HeLa tumor cells. Biophysics 2006;51:902–7.
15. Veraart J, Novikov DS, Christiaens D, Ades-Aron B, Sijbers J, Fieremans E. Denoising of diffusion MRI using random matrix theory. Neuroimage 2016;142:394–406.
16. Marstal K, Berendsen F, Staring M, Klein S. SimpleElastix: a user-friendly, multi-lingual library for medical image registration. International Workshop on Biomedical Image Registration (WBIR). Las Vegas, NV: 2016. Available from: https://www.opensourceimaging.org/project/simpleelastix/.
17. Beets-Tan RGH, Lambregts DMJ, Maas M, Bipat S, Barbaro B, Curvo-Semedo L, et al. Magnetic resonance imaging for clinical management of rectal cancer: updated recommendations from the 2016 European Society of Gastrointestinal and Abdominal Radiology (ESGAR) consensus meeting. Eur Radiol 2018;28:1465–75.
18. Benson AB, Venook AP, Al-Hawary MM, Cederquist L, Chen YJ, Ciombor KK, et al. Rectal cancer, version 2.2018, NCCN clinical practice guidelines in oncology. J Natl Compr Cnc Netw 2018;16:874–901.
19. Koh DM, Brown G, Collins DJ. Nanoparticles in rectal cancer imaging. Cancer Biomarkers 2009;5:89–98.
20. Wu L, Cao Y, Liao C, Huang J, Gao F. Diagnostic performance of USPIO-enhanced MRI for lymph-node metastases in different body regions: a meta-analysis. Eur J Radiol 2011;80:582–9.
21. Torabi M, Aquino SL, Harisinghani MG. Current concepts in lymph node imaging. J Nucl Med 2004;45:1509–18.
22. Rockall AG, Sohaib SA, Harisinghani MG, Babar SA, Singh N, Jeyarajah AR, et al. Diagnostic performance of nanoparticle-enhanced magnetic resonance imaging in the diagnosis of lymph node metastases in patients with endometrial and cervical cancer. J Clin Oncol 2005;23: 2813–21.
23. Sigal R, Vogl T, Casselman J, Moulin G, Veillon F, Hermans R, et al. Lymph node metastases from head and neck squamous cell carcinoma: MR imaging with ultrasmall superparamagnetic iron oxide particles (Sinerem MR) – results of a phase-III multicenter clinical trial Eur Radiol2002;12: 1104–13.
24. Lambregts DM, Beets GL, Maas M, Kessels AG, Bakers FC, Cappendijk VC, et al. Accuracy of gadofosveset-enhanced MRI for nodal staging and restaging in rectal cancer. Ann Surg 2011;253:539–45.
25. Kiselev VG. Larmor frequency in heterogeneous media. J Magn Reson 2019; 299:168–175.
26. He X, Yablonskiy DA. Biophysical mechanisms of phase contrast in gradient echo MRI. Proc Nat Acad Sci USA 2009;106:13558–63.
27. Sati P, van Gelderen P, Silva AC, Reich DS, Merkle H, de Zwart JA, et al. Micro-compartment specific T2 relaxation in the brain. NeuroImage 2013;77:268–78.
28. Porpiglia F, Manfredi M, Mele F, Bertolo R, Bollito E, Gned D, et al. Indication to pelvic lymph nodes dissection for prostate cancer: the role of multiparametric magnetic resonance imaging when the risk of lymph nodes invasion according to Briganti updated nomogram is <5. Prostate Cancer Prostatic Dis 2018;21:85–91.
29. Sundi D, Svatek RS, Nielsen ME, Schoenberg MP, Bivalacqua TJ. Extent of pelvic lymph node dissection during radical cystectomy: is bigger better? Rev Urol 2014;16:159–66.

4.4. Higher-order diffusion MRI characterization of mesorectal lymph nodes in rectal cancer

FULL PAPER

Magnetic Resonance in Medicine

Higher-order diffusion MRI characterization of mesorectal lymph nodes in rectal cancer

Andrada Ianuş[1,2] | **Ines Santiago**[3,4] | **Antonio Galzerano**[3] | **Paula Montesinos**[5] | **Nuno Loução**[5] | **Javier Sanchez-Gonzalez**[5] | **Daniel C. Alexander**[2] | **Celso Matos**[1,3] | **Noam Shemesh**[1]

[1]Champalimaud Research, Champalimaud Centre for the Unknown, Lisbon, Portugal
[2]Centre for Medical Image Computing, University College London, London, United Kingdom
[3]Champalimaud Clinical Centre, Champalimaud Centre for the Unknown, Lisbon, Portugal
[4]Nova Medical School, Lisbon, Portugal
[5]Philips Healthcare Iberia, Madrid, Spain

Correspondence
Andrada Ianuş, Champalimaud Research, Champalimaud Centre for the Unknown, Lisbon, Portugal, Avenida Brasilia, 1400-038 Lisbon, Portugal.
Email: andrada.ianus@neuro.fchampalimaud.org

Funding information
Champalimaud Centre for the Unknown; NIHR UCLH Biomedical Research Centre; Engineering and Physical Sciences Research Council, Grant/Award Number: EP/M020533/1 and EP/N018702/1; Philips Healthcare Iberia

Purpose: Mesorectal lymph node staging plays an important role in treatment decision making. Here, we explore the benefit of higher-order diffusion MRI models accounting for non-Gaussian diffusion effects to classify mesorectal lymph nodes both 1) ex vivo at ultrahigh field correlated with histology and 2) in vivo in a clinical scanner upon patient staging.

Methods: The preclinical investigation included 54 mesorectal lymph nodes, which were scanned at 16.4 T with an extensive diffusion MRI acquisition. Eight diffusion models were compared in terms of goodness of fit, lymph node classification ability, and histology correlation. In the clinical part of this study, 10 rectal cancer patients were scanned with diffusion MRI at 1.5 T, and 72 lymph nodes were analyzed with Apparent Diffusion Coefficient (ADC), Intravoxel Incoherent Motion (IVIM), Kurtosis, and IVIM-Kurtosis.

Results: Compartment models including restricted and anisotropic diffusion improved the preclinical data fit, as well as the lymph node classification, compared to standard ADC. The comparison with histology revealed only moderate correlations, and the highest values were observed between diffusion anisotropy metrics and cell area fraction. In the clinical study, the diffusivity from IVIM-Kurtosis was the only metric showing significant differences between benign (0.80 ± 0.30 $\mu m^2/ms$) and malignant (1.02 ± 0.41 $\mu m^2/ms$, $P = .03$) nodes. IVIM-Kurtosis also yielded the largest area under the receiver operating characteristic curve (0.73) and significantly improved the node differentiation when added to the standard visual analysis by experts based on T_2-weighted imaging.

Conclusion: Higher-order diffusion MRI models perform better than standard ADC and may be of added value for mesorectal lymph node classification in rectal cancer patients.

KEYWORDS

compartment models, diagnostic accuracy study, diffusion MRI, higher-order models, IVIM, kurtosis, lymph node imaging, rectal cancer

1 | INTRODUCTION

Characterizing the involvement of lymph nodes is a very important prognostic marker in rectal cancer patients because it determines the local recurrence and overall survival rates.[1] To date, the gold standard for lymph node characterization is histology of the surgical specimen using hematoxylin and eosin (H&E) staining to highlight differences in cellular structure between normal lymphatic tissue and tumor.[1] However, preoperative characterization is beneficial because neoadjuvant chemoradiation has been shown to decrease the incidence of local relapse in high-risk patients,[2] such as those with lymph node involvement. Thus, there is a clinical need for accurate preoperative, preferably noninvasive, imaging techniques for lymph node characterization.[3]

MRI plays an important role in noninvasive imaging, including in cancer detection and staging.[4] In the case of rectal cancer staging, T_2-weighted MRI can be considered the contemporary gold standard for determining lymph node involvement. Unfortunately, T_2-weighted MRI, whether based on size thresholds or morphologic characteristics such as shape, contour, and heterogeneity, has been shown to be quite a blunt tool with respect to lymph node characterization.[5-7] Other contrasts, such as dynamic contrast enhancement,[8] susceptibility contrast,[9] or diffusion-weighted imaging,[10] have also been proposed for lymph nodes characterization, with variable degrees of success.

Diffusion MRI (dMRI) is becoming an increasingly attractive modality, providing a noninvasive, indirect characterization of tissue microstructure.[11,12] The simplest dMRI metric, namely apparent diffusion coefficient (ADC), has been widely used for cancer imaging[13] as a biomarker reflecting increased cellularity in malignant tumors.[14] For lymph node characterization, ADC has shown variable performance. For instance, some studies of cervical and axillary lymph nodes show that ADC is a promising technique for determining lymph node involvement,[15,16] whereas other studies, for example, in cervical and perigastric lymph nodes, show a low accuracy of ADC for benign/malignant differentiation.[17,18] In rectal cancer, an accuracy of ~70% for lymph node involvement has been previously reported for ADC.[19] Because ADC assumes a single isotropic water pool that exhibits isotropic Gaussian diffusion, it lacks specificity to the underlying changes in tissue microstructure and cannot differentiate between variations in cell size, cellularity, orientation distribution, etc. This is also reflected in a variable correlation of ADC with histology data.[14]

Higher-order dMRI models, which account for non-Gaussian diffusion, have been proposed to better characterize the diffusion properties in complex tissue microstructures. Diffusion kurtosis[20] accounts for the signal departure from a monoexponential decay at high b-values and has been successfully applied for cancer imaging, improving the differentiation of both primary tumors[21,22] as well as lymph nodes,[23-25] compared to ADC. To separate the effects of tissue perfusion and diffusion, the intravoxel incoherent motion (IVIM)[26] captures the fast signal decay at low b-values due to flow effects, and in many cases it provided better tumor characterization compared to ADC.[27] For rectal cancer, IVIM also improved lymph node differentiation,[28,29] although the results are not consistent between the 2 studies. Combining IVIM and kurtosis can provide insight into both perfusion and non-Gaussian diffusion effects and has shown potential for differentiating various tumors[30,31] as well as lymph nodes in the head and neck region[32]; however, to our knowledge it has not been employed thus far to image lymph nodes involved in rectal cancer.

To further enhance the specificity of dMRI-derived parameters to the underlying microstructure, recently proposed higher-order dMRI techniques[33-40] employ biophysical compartment models of various (assumed) tissue features to fit the dMRI measurements, usually acquired at multiple b-values and diffusion times. Such approaches showed enhanced ability over ADC to explain the diffusion measurements and differentiate between benign and malignant tumors in various cancer types such as xenograft colorectal tumors,[33] prostate cancer,[37,41-44] breast cancer,[40] and gliomas.[45,46] Moreover, the estimated dMRI parameters for restriction size and volume fraction correlated well with histology measurements.[33,41,47] Compartment models have also been employed in a preliminary study to characterize diffusion in lymph node tissue ex vivo,[48] showing that models that include restriction and anisotropy provide the best fit to the data; however, only 3 samples were included, and a direct link to tissue microstructure through histological validation was not presented.

Here, we aimed to investigate whether a diffusion modeling approach could characterize lymph node structure and define lymph node involvement in rectal cancer. To this end, in the first part we performed an ex vivo study at ultrahigh field MRI employing a rich dMRI protocol on lymph nodes extracted from the surgical specimens of rectal cancer patients. In this dataset, we compared various higher-order diffusion models in terms of signal characterization as well as node differentiation capability. We also correlated various diffusion metrics with quantitative histology features, which to our knowledge has not been studied so far. In the second part, we employed a clinically feasible dMRI acquisition and modeling approach at 1.5 T to characterize higher-order diffusion properties of mesorectal lymph nodes in rectal cancer patients upon staging and investigated its benefit for node differentiation compared to standard T_2-weighted qualitative assessment by expert radiologists.

2 | METHODS

2.1 | Part 1: Ex vivo imaging of lymph nodes at ultrahigh field

The ex vivo study aims to investigate the diffusion properties of benign and malignant lymph node tissue and their relationship with histological features in rectal cancer patients that were staged as N+; that is, at least 1 lymph node has been classified as malignant following the pathological examination.

2.2 | Institutional setting and lymph node harvesting

This study was approved by the institutional ethics committee, and informed consent was obtained from all participating patients. Sixteen patients underwent surgery without neoadjuvant therapy, and mesorectal specimens were excised and immersed in a 4% formaldehyde solution for 72 h. Lymph nodes present in more than 1 cut slice (~5 mm thickness) were extracted and processed as follows: half was sent for pathologic staging performed by a gastrointestinal pathologist (8 years of experience); and the other half, which is normally discarded, was used for this study's ex vivo scanning. Following the pathologic results, 5 additional patients with node-negative disease were excluded.

Prior to scanning, lymph node "halves" were washed with a 1% phosphate-buffered saline solution for 24 h and then mounted in a 10 mm NMR tube filled with Flourinert (Sigma - Aldrich Quimica S.L., Lisbon, Portugal), preferably grouped in pairs of similar size and originating from the same histopathologic block. In total, 75 nodes were scanned. Insufficient image quality due to susceptibility artifacts and/or image distortions retrospectively related to inadequate shimming, poor specimen preparation reflected by a highly inhomogeneous H&E staining in pathology, as well as accidental sample mishandling resulted in the exclusion of 14 benign and 7 malignant nodes, as detailed in the Supporting Information Figure S1. Thus, the final analysis included 54 nodes (31 malignant) originating from 9 patients (mean age 63.2 years, 6 males).

2.3 | Histopathologic analysis for comparison with MRI

To match histology to MRI, the scanned lymph nodes were embedded in paraffin and sliced parallel to cut surface every 50 μm using a Leica RM2245 microtome (Leica Biosystems. Newcastle, UK). One slice per interval was stained with H&E and analyzed using a Zeiss Axio Lab A1 (Carl Zeiss Microscopy GmbH, Jena, Germany) with a 40× amplification.

2.4 | Diffusion MRI acquisition protocol at 16.4T

The ex vivo MRI images were acquired on a 16.4T Bruker Aeon Ascend scanner interfaced with an AVANCE IIIHD console and operating a Micro5 probe (Bruker BioSpin GmbH, Rheinstetten, Germany) with a gradient system capable of producing up to 3000 mT/m in all directions. A 10 mm birdcage coil was used for signal reception, and RF transmission and samples were scanned at 37°C. The diffusion-weighted images were acquired in Stimulated Echo Acquisition Mode (STEAM) using standard line-by-line readout with imaging parameters detailed in Table 1A. Single diffusion encoding sequences with 6 gradient directions and duration $\delta = 1$ ms were acquired at 4 b-values up to 2000 s/mm^2 and multiple diffusion times Δ from 5 to 150 ms, as detailed in Table 1A, leading to a total scan time of ~6 h per node.

2.5 | MR image analysis

Diffusion-weighted images were analyzed in MatLab R2017b (MathWorks, Natick, MA). The acquired data was first normalized for each Δ to account for T_1 relaxation effects, due to different mixing times in the STEAM sequence. Then, 8 diffusion models were fitted voxel-wise. The models included standard representations, such as ADC, diffusion tensor (DT), and diffusion kurtosis, as well as several 2-compartment models that account for anisotropic and/or restricted diffusion. In particular, the following models were considered (using the nomenclature in Ref. [49]): BallBall, BallSphere, ZeppelinBall, ZeppelinSphere, and BallFiniteCylinder, where "ball" describes isotropic Gaussian diffusion (a single ball compartment is equivalent to ADC); "zeppelin" describes a cylindrically symmetric anisotropic Gaussian diffusion tensor;

TABLE 1 Imaging parameters for (A) preclinical dMRI acquisition at 16.4T with stimulated echo preparation and line-by-line readout and (B) clinical dMRI acquisition at 1.5T with spin-echo preparation and multi-shot EPI readout

(A)	**Preclinical Scan Parameters**		
Parameter			
TE (ms)	6.5		
TR (ms)	2800		
Slice thickness (mm)	0.7		
In-plane resolution (mm^2)	0.14×0.14		
Matrix size	70×70		
Bandwidth (kHz)	34.722		
Gradient duration (ms)	1		
No. gradient directions	6		
b-values (s/mm^2)	0, 500, 1000		0, 1500, 2000
Signal averages	1		2
Diffusion time (ms)	5, 10, 20, 40, 70, 100, 150		10, 20, 30, 50
Mixing time (ms)	2.2, 7.2, 17.2, 37.2, 67.2, 97.2, 147.2		7.2, 17.2, 27.2, 47.2
(B)	**Clinical Scan Parameters**		
Parameter	**Small b-values**	**Medium b-values**	**High b-values**
TE (ms)	65	65	65
TR (ms)	3,550	3,755	9,561
Flip angle	90	90	90
Slice thickness (mm)	5	5	5
Gap (mm)	0	0	0
Matrix	128×126	128×126	128×126
FOV (mm)	320×320	320×320	320×320
In-plane resolution (mm^2)	2.5×2.5	2.5×2.5	2.5×2.5
Signal averages	1	1	2
EPI factor	63	63	63
Bandwidth (kHz)	29.1	21.7	21.7
dB/dt (T/s)	91.5	41.2	41.2
Acquisition duration	2 min 26 s	2 min 34 s	15 min 09 s
Fat suppression	SPAIR	SPAIR	SPAIR
Halfscan factor	0.696	0.696	0.667
b-values	0, 50, 100, 200	0, 500, 1000	0, 1500, 2000, 2500
Gradient duration (ms)	15	16.6	16.9
Diffusion time (ms)	35.7	32.5	32.8

Abbreviations: EPI, echo planar imaging; FOV, field of view; SPAIR, SPectral Attenuated Inversion Recovery .
Significance of bold values are 0.05.

and "sphere" describes isotropic, restricted diffusion. When fitting models with restriction, the same diffusivity for the restricted and Gaussian compartments was assumed.[50] Details regarding the compartment models, specific parameter ranges, and model assumptions are given in Supporting Information Table S1. For restricted diffusion, we used the signal expressions derived in Ref. 51 based on the Gaussian phase distribution approximation[52] for STEAM diffusion sequences.[53-55]

2.6 | Experiment 1: Information-based comparison of DW-MRI models

The models were compared based on the Bayesian Information Criterion (BIC) that accounts for goodness of fit and penalizes increasing number of model parameters:

$$BIC = \ln(N)\,k - 2\ln(\hat{L}),$$

where N is the number of data points; k is the number of model parameters; and $\ln(\hat{L})$ is the maximum value of the log likelihood function of the model, which accounts for Rician noise.[51]

The BIC was computed voxel-wise for each model, and then the models were compared based on the number of voxels where they occupy a certain rank.

2.7 | Experiment 2: Differentiation between benign and malignant nodes based on dMRI models

Next, we investigated the model parameter differences between benign and malignant lymph nodes for the standard DT model as well as the best-fitting model (ZeppelinSphere).

To study the ability of differentiating between benign and malignant nodes, we performed a receiver operating characteristic (ROC) analysis for the standard models (Ball, Kurtosis and Tensor), as well as for the best-fitting ZeppelinSphere model. The following model parameters are included in the analysis for each diffusion model. Ball: diffusivity (D); Kurtosis: D and kurtosis (k); Tensor: mean diffusivity (MD) and fractional anisotropy (FA); ZeppelinSphere: D, FA of the zeppelin compartment, fraction (f_{sphere}) and radius (R_{sphere}) of spherical compartment. The ROC analysis was performed with 2 sets of histogram features for each model parameter: median values across each node and median plus interquartile range (IQR).

2.8 | Experiment 3: Correlation between quantitative histology and dMRI metrics

To investigate the link between parameters derived from dMRI data and histological features, we analyzed histology H&E slides and quantified the following parameters: cell count, average nuclear area, average cell area, and cell area fraction. To ensure a relevant comparison between histology and MRI, the best-matching H&E slice based on contour and visible landmarks was selected. Then, the histological features were quantified in a 420 × 560 μm^2 field using a cell detection tool (QuPath, Belfast, UK).

A similarly sized ROI was placed in the dMRI images by a radiologist with 8 years of experience. Then, we quantified the correlation between the mean parameter values of the diffusion models and the histological features in the given ROIs. Specifically, we analyzed the parameters of DTI and the best-fitting ZeppelinSphere model. For the latter, we have excluded from the correlation analysis N = 97/1120 voxels, for which the estimated R_{sphere} reached the upper limit imposed during fitting. See Supporting Information Table S1.

2.9 | Part 2: Clinical imaging at 1.5 T

The clinical study aims to investigate the benefit of including dMRI to differentiate between benign and malignant lymph nodes for rectal cancer patient staging.

2.10 | Institutional setting

The clinical study was also carried out with the approval of the institution´s ethics committee. A total of 10 patients previously diagnosed with rectal cancer (mean age of 64.9 years, 5 males) were enrolled after obtaining written informed consent. The imaging was performed on a 1.5T scanner (Ingenia, Philips Healthcare, Best, The Netherlands) with the diffusion acquisition added to the clinical staging pelvic MRI. A spasmolytic agent was administered butylscopolamine (20 mg) and a pressure belt was utilized (Orfit Industries, Wijnegem, Belgium) to minimize bowel and respiratory movement artefacts, respectively.

2.11 | Image acquisition and data analysis

The diffusion data was acquired using a Torso XL surface coil (Ingenia, Philips Healthcare, Best, The Netherlands) with multi-shot spin-echo EPI, with the acquisition parameters detailed in Table 1B. The diffusion acquisition was split in 3 parts, with small b-values (50, 100, 200 s/mm^2), medium b-values (500, 1000 s/mm^2), and high b-values (1500, 2000, 2500 s/mm^2), with imaging parameters detailed Table 1B. The sequences were split to minimize the TE of the acquisition (65 ms) because previous visual optimization showed it plays an important role for image contrast. To achieve this TE time for the high b-values, the TR was increased to 9.5 s to satisfy duty cycle constraints. Thus, by separating the sequences, the TR for the small and medium *b*-values could be lower to allow an overall shorter acquisition time (TR of 3.5 and 3.7 for small and medium b-values, respectively). Moreover, splitting the sequences allowed for multiple B_0 values (in this case 3), which were beneficial for the delineation of the ROIs to minimize the effects of motion. The data was acquired in 3 orthogonal directions averaged on the scanner.

In total, 76 lymph nodes were delineated by a radiologist (8 years of experience) and matched to pathology during macroscopy. The process consisted of sequential slicing of the specimen, followed by positioning and numbering of the cut slices to match the MR imaging acquisition and dyeing of the extracted lymph nodes based on their radial position. Due to motion artifacts, 4 nodes were excluded, leaving 72 nodes (14 malignant). Whole-node ROIs were defined on the high b-value images and copied to the low and medium b-value data sets. When necessary, the ROIs were slightly translated to account for motion during the

acquisition. The average ROI signal for each b-value was normalized to the ROI average of the b_0 images in the respective set. The normalized signal decay was fitted with 4 diffusion models, which can be used to characterize the diffusion properties of the tissue given the in vivo clinical acquisition. Thus, ADC was fitted to the measurements with medium b-values; IVIM was fitted to the measurements with small and medium b-values; kurtosis was fitted to the sets with medium and high b-values; and IVIM-kurtosis was fitted to the entire data set. Details regarding the the models are given in Supporting Information Table S2. In the clinical study, only models of isotropic diffusion without an explicit representation of restriction were fitted because the acquired data did not have enough directional information for anisotropic models or diffusion times for models of restricted diffusion. On the other hand, the models included IVIM effects to account for perfusion.

We investigated the parameter differences between benign and malignant nodes and then employed a ROC analysis to compare the differentiation ability of the best performing model (IVIM + Kurtosis) with the standard T_2-weighted classification performed by 2 experienced radiologists on a subset of 56 lymph nodes.

2.12 | Statistical analysis

To investigate the parameter differences between benign and malignant nodes, we employed a mixed effect linear model with the diffusion metrics as response variable and the malignancy status as predictor variable. The model accounts for the hierarchical structure of the data. In the voxel-wise analysis of the ex vivo dataset, there is a 3-level hierarchy, with the voxels grouped by lymph node and by patient. In the ROI analysis of the clinical data, there is a 2-level hierarchy, with the whole node ROI values grouped by patient.

To assess the differentiation ability of different models, we employ a ROC analysis. Specifically, we used the *perfcurve* function in MatLab R2017b (MathWorks), following a multivariate linear regression. Differences between ROC curves were assessed using the DeLong test.[56]

3 | RESULTS

3.1 | Part 1: Ex vivo imaging of lymph nodes at ultrahigh field

3.1.1 | Experiment 1: Information-based comparison of dMRI models

The first experiment compared the goodness of fit of different diffusion models according to their BIC values. Figure 1A illustrates the model ranking for benign (left) and malignant nodes (right). The models are listed in decreasing order of their performance from the top to the bottom of the plots. The results show that models including anisotropy and restriction consistently rank higher both for benign and malignant nodes. Figure 1B presents maps of the best-fitting model for a benign and a malignant node. A spatial variability of the best-fitting model pattern can be observed, which reflects the underlying structure, with the ZeppelinSphere model providing the best fit in the nodal parenchyma, whereas the tensor model provides the best fit in the nodal capsule. This pattern is consistent for other nodes where the capsule is visible (data not shown).

Figure 2 shows example datasets for 2 voxels from a benign (left) and a malignant (right) lymph node, which were fitted with the (A) tensor model and (B) ZeppelinSphere model. In both node types, the ZeppelinSphere model fit (solid lines) better captured the trends in the experimental data (symbols) compared with the tensor model, as expected from the results presented in Figure 1. The data also shows a higher spread of the measured signal in the diffusion time dimension for the malignant voxel compared to the benign voxel. The time-dependence pattern is variable across nodes. Nevertheless, on average malignant nodes exhibit stronger diffusion time dependence compared to benign nodes.

3.1.2 | Experiment 2: Differentiation between benign and malignant nodes based on dMRI models

The next analysis targeted the ability of different model parameters to differentiate between benign and malignant nodes. For the standard DT model, when analyzing the voxelwise parameters from all nodes, both MD and FA show significant differences between benign and malignant nodes, with lower MD and higher FA in malignant nodes ($P < .01$ in both cases), as illustrated in Supporting Information Figure S2. The results for the best-fitting ZeppelinSphere model are presented in Figure 3. Parameter maps of D, FA of the zeppelin compartment, f_{sphere}, and R_{sphere} are shown in panel A. Parameter differences between benign and malignant nodes are shown in panel B. D shows a significant decrease between benign and malignant nodes ($P < .01$), whereas FA and f_{sphere} show a significant increase ($P < .01$). The sphere radius does not evidence any statistically significant difference between the groups.

Figure 4 presents the ROC curves of 4 diffusion models (Ball, Kurtosis, Tensor and ZeppelinSphere), based only on median parameter values (4A) or median and IQR values (4B). When analyzing only the median values, the areas under curve (AUC) for all models considered were between 0.7 and 0.8, with the ZeppelinSphere showing a higher AUC (0.79). However, this difference was not significant based on the DeLong test.[56] When including the IQR of the

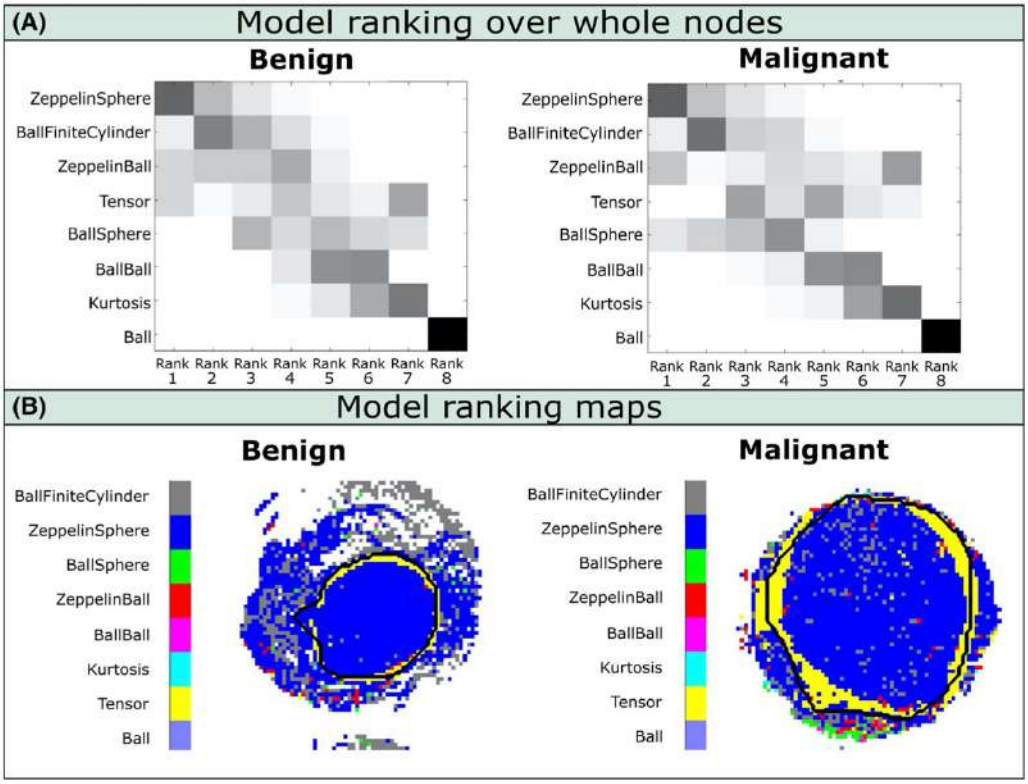

FIGURE 1 (A) Model ranking for benign (left) and malignant (right) lymph nodes. The models are fitted voxelwise, and the gray scale reflects the frequency with which a model occupies a certain rank. Thus, the model on top provides the best fit in most of voxels, whereas the model on the bottom provides the worst fit in most of voxels. The models are roughly ordered according to how many times they provide a certain rank, from best (top) to worst (bottom). (B) Maps showing the best-fitting model in each voxel of a benign (left) and malignant (right) node

parameters, a significant increase ($P < .01$) in the classification ability of the Tensor and ZeppelinSphere models was observed (AUC of 0.93 and 0.95, respectively). We have further tested whether the Tensor model fitted to a single shell acquisition ($b = 1000$ s/mm^2, $\Delta = 5$ ms) could also provide a good differentiation between benign and malignant nodes. The ROC analysis showed similar values of the AUC (0.78 and 0.92 for median and median + IQR, respectively); although slightly smaller, these are not significantly different from the ZeppelinSphere results. These results, together with the fact that including the IQR for the ADC and BallSphere models does not result in a significant increase in the AUC (data not shown), suggest that both anisotropy and its heterogeneity in the malignant lymph nodes play an important role for the classification.

3.1.3 | Experiment 3: Correlation between quantitative histology and dMRI metrics

Figure 5 summarizes the results of the quantitative histology analysis, based on corresponding ROIs drawn on microscopy and MRI images, as presented in Figure 5A,B. The results show statistically significant differences ($P << .01$) between the benign and malignant lymph nodes for all the histological features included in the analysis (cellularity, average nuclear area, average cell area, cell area fraction).

Figure 6 shows the significant correlation between dMRI-derived metrics and the histology features described above. The correlations for the Tensor parameters are depicted in Figure 6A. MD showed a weak positive correlation with cell count ($r = 0.34$, $P = .014$) and weak negative correlations with nuclear area ($r = -0.38$, $P = .006$), cell area ($r = -0.39$, $P = 3.4E\text{-}3$), and cell area fraction ($r = -0.36$, $P = .011$). FA exhibited a moderate positive correlation with nuclear area ($r = 0.57$, $P = 1.5E\text{-}5$) and cell area fraction ($r = 0.59$, $P = 4.4E\text{-}6$). The correlations for the ZeppelinSphere model parameters are depicted in Figure 6B. Zeppelin FA showed a moderate positive correlation with nuclear area ($r = 0.59$, $P = 7.2E\text{-}6$) and with cell area fraction ($r = 0.66$, $P = 1.7E\text{-}7$). R_{sphere} exhibited a moderate positive correlation with cell count ($r = 0.46$, $P = 7.7E\text{-}4$), and a moderate negative correlation with cell area ($r = -0.44$, $P = 1.6E\text{-}3$) and the corresponding cell radius

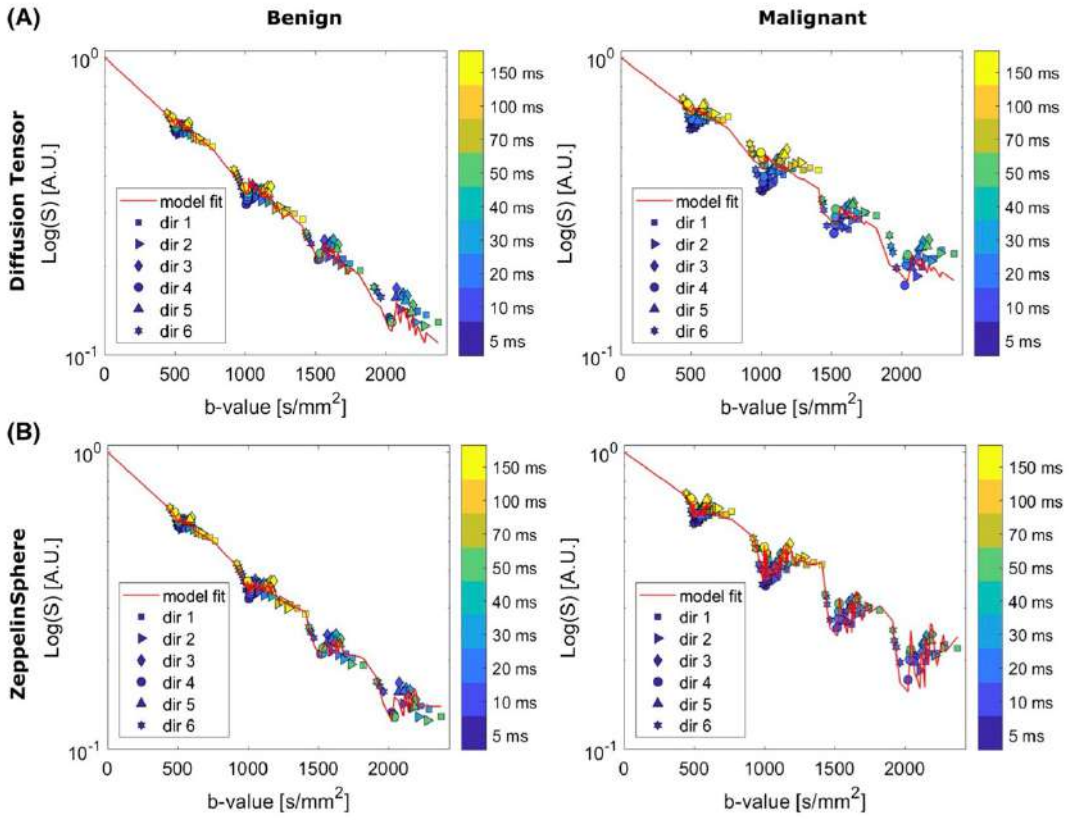

FIGURE 2 Example of voxelwise model fitting for (A) tensor and (B) ZeppelinSphere models in a benign and a malignant node. The different symbols show different gradient directions, and the color encodes different diffusion times. The red line shows the model fit to the data

(r = −0.42, P = 2.4E-3). For D the correlation coefficients were smaller than 0.3. Another feature of this dataset is a large variability of the estimated parameters in the benign lymph nodes, especially for the diffusivities and sphere radius, which has a direct impact on the observed correlations.

3.2 | Part 2: Clinical imaging at 1.5T

This section presents the analysis of the clinical dMRI data acquired at 1.5T. In total, 72 lymph nodes, which originated from 10 patients with rectal cancer and without neoadjuvant therapy, were analyzed.

Figure 7A,B illustrate examples of diffusion-weighted images and ROI selection for a benign and a malignant node, respectively, and Figure 7C plots the average signal decay separated by the malignancy types. The decay curves in Figure 7C clearly revealed a faster decay for malignant nodes and a slower decay for benign nodes, which are also reflected in the model parameters presented in Figure 8 and Table 2.

Figure 8A shows box plots of the parameter values for ADC, IVIM, Kurtosis, and IVIM-Kurtosis estimated in benign and malignant nodes. ADC values were higher in malignant nodes compared with benign nodes; however, the difference was not statistically significant (P = .26). The only parameter, which reached a statistically significant threshold, was the diffusivity (D) estimated from the IVIM-Kurtosis model (P = .03), which has higher values in the malignant nodes. The diffusivity values from the IVIM and Kurtosis models were also higher in malignant nodes; however, the differences were not statistically significant (P = .11 and 0.22 for IVIM and Kurtosis, respectively). The pseudo-diffusivities from the IVIM and IVIM-Kurtosis models are lower in malignant nodes compared to benign nodes, with P values of 0.07 and 0.24, respectively. The kurtosis values in malignant nodes were also lower than in benign nodes; however, the difference was not statistically significant (P = .12 for the Kurtosis model and P = .32 for the IVIM-Kurtosis model).

Figure 8B presents the ROC analysis, which compared the 4 diffusion models in terms of differentiating between benign and malignant lymph nodes. ADC is the worst performing model, with an AUC value of 0.60, whereas IVIM-Kurtosis is the best performing model with an AUC of 0.73; however, the difference does not reach statistical significance according to the DeLong test (P = .19).[56] Figure 8C shows that

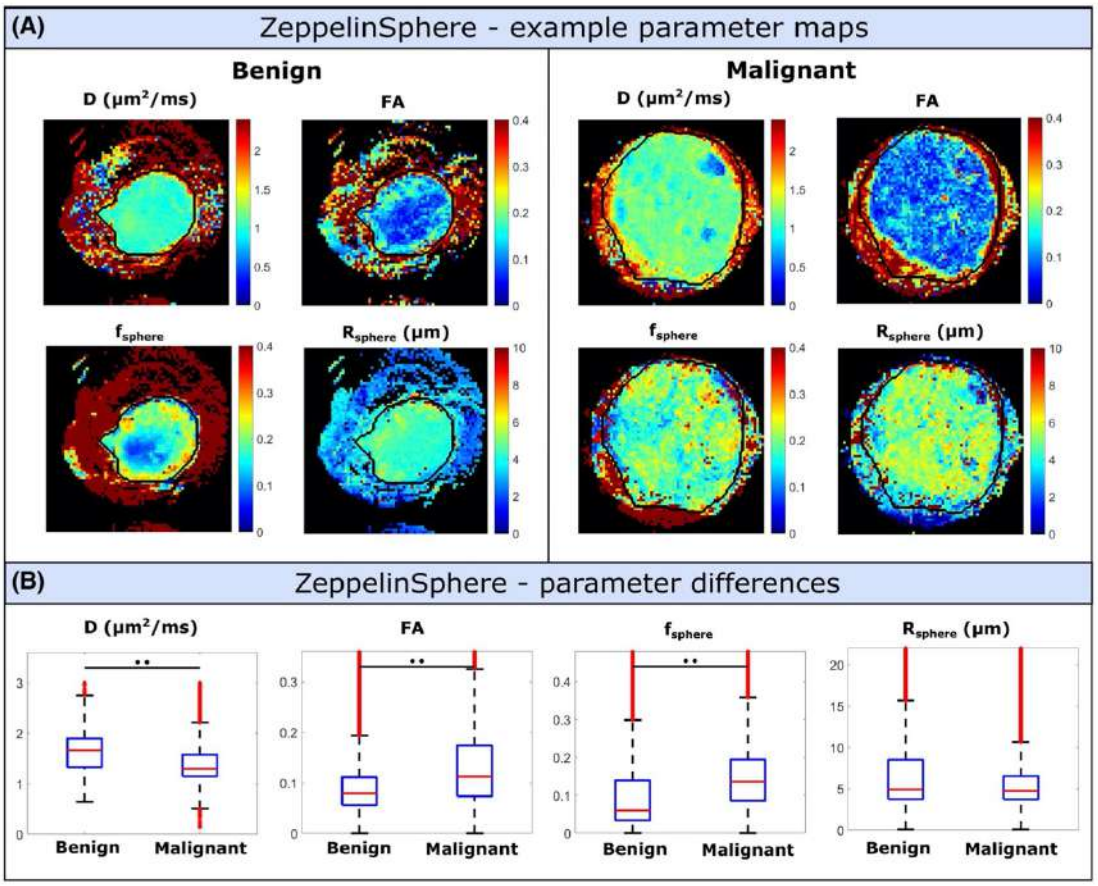

FIGURE 3 (A) Parameter maps derived from the ZeppelinSphere model (D, FA of the zeppelin compartment, f_{sphere}, and R_{sphere}) for a benign and malignant lymph node. (B) D, FA, f_{sphere}, and R_{sphere} comparison for benign and malignant nodes.

IVIM-Kurtosis also provides a better differentiation between benign and malignant nodes (AUC = 0.80) compared to the standard clinical T_2 classification based on the European Society of Gastrointestinal and Abdominal Radiology 2016 criteria[57] (AUC = 0.74 for reader 1; AUC = 0.59 for reader 2), which takes into consideration lymph node size, shape, contour, and heterogeneity. Moreover, combining IVIM-Kurtosis and T_2 results significantly improves the classification compared to T_2-weighted images alone ($P = .08$ for reader 1; $P = 0.007$ for reader 2).

4 | DISCUSSION

Characterizing lymph nodes in vivo and noninvasively is of high relevance given the importance of lymph node staging in rectal cancer patient treatment planning.[2] Because lymph node microstructural changes play an important role in malignancy,[1] and given that diffusion MRI can portray at least some microsctructural properties, we hypothesized that dMRI could be used to distinguish malignant from benign nodes.

In the first part of this study, lymph nodes underwent extensive dMRI experiments at ultrahigh field MRI, leading to a rich and robust dataset with excellent resolution to which 8 different compartment models were fitted. An important finding of the preclinical study is that models including restriction and anisotropy best explain the measured data for both benign and malignant nodes (Figure 3), a result in agreement with preliminary data from Ref. 48. Spatial variations of the diffusion patterns are also observed. Thus, the lymph node capsule exhibited higher anisotropy and lower restriction compared with the lymph node parenchyma, with the diffusion tensor being the best-fitting model. The tensor MD and FA are higher in the capsule compared to the parenchyma, as illustrated in Supporting Information Figure S4. This probably reflects the inherent capsule composition, which is relatively paucicellular (dominant cell being the fusiform fibroblast) and extracellular matrix-rich, with long extracellular matrix molecules, predominantly of collagen and elastin. In addition to providing a better fit to the data, the higher-order models also improved the differentiation between benign and malignant nodes (Figure 4), better capturing

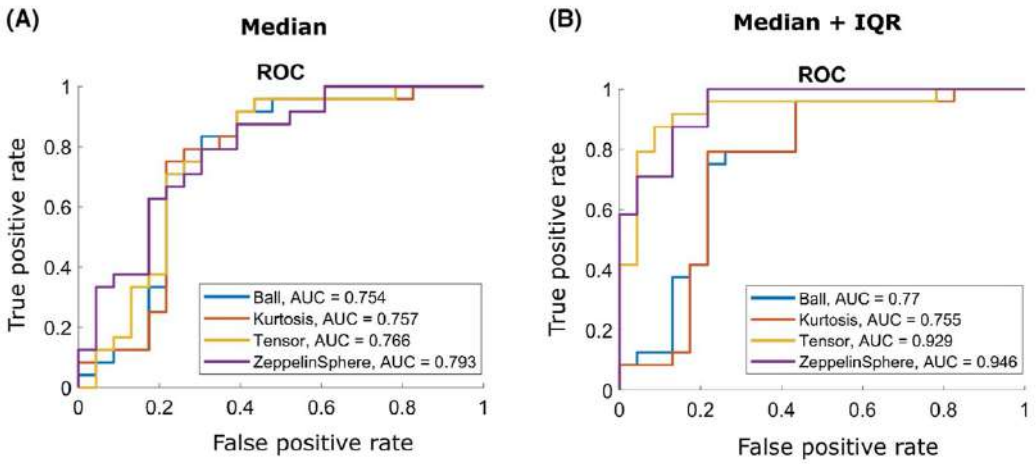

FIGURE 4 ROC curves for the ball, kurtosis, tensor, and ZeppelinSphere model when including for each model parameter the (A) median values and (B) median values and IQR. IQR, interquartile range; ROC, receiver operating characteristic

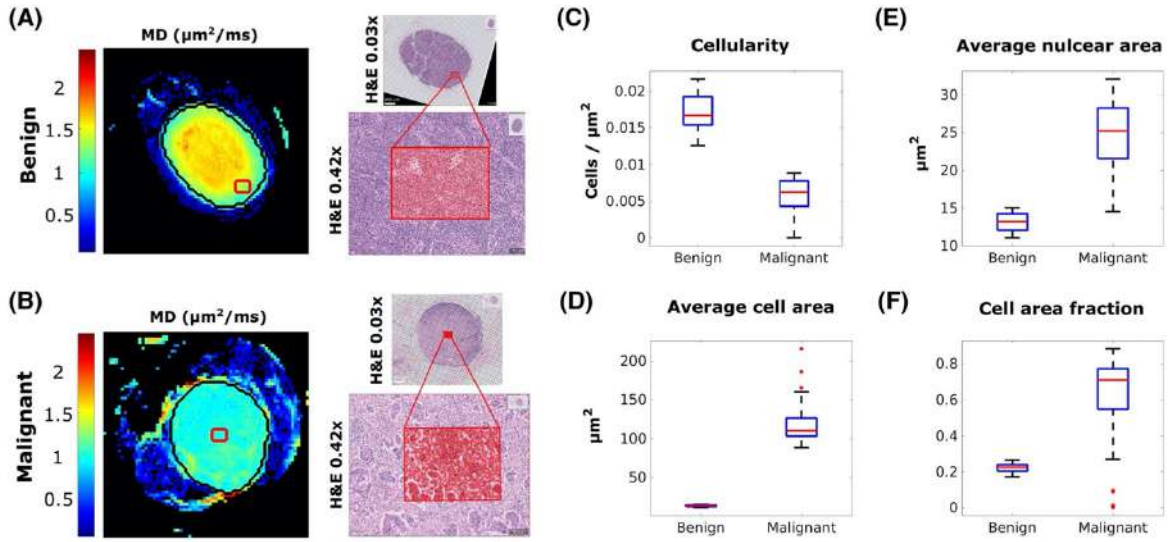

FIGURE 5 Example of corresponding ROIs between MRI and histology for (A) benign node and (B) malignant nodes. Comparison of histology features between benign and malignant nodes: (C) cellularity, (C) average cell area, (E) average nuclear area, and (F) cell area fraction

the microstructural differences. Whereas benign nodes are largely comprised of leucocytes, which are predominantly round, small, and practically devoid of cytoplasm, malignant nodes predominantly contain large and goblet-shaped malignant cells and exhibit a wide range of malignancy patterns including solid infiltration, necrosis, and desmoplasia, with or without associated inflammatory infiltrate. This wide range of cellular structure could give rise to high diffusion heterogeneity poorly captured by ADC.

Previous studies characterizing the diffusion properties of ex vivo lymph nodes have mainly employed ADC[48,58,59]; however, the results have shown variable outcome, with a very large spread in ADC values,[48] as well as poor correlation between in vivo and ex vivo lymph nodes.[58] Our study is consistent with these findings: the results evidenced a very large spread of ADC even for benign nodes (Figure 6). Potential sources for this high variability could include variable microstructure; fixation effects; or interactions with internal, susceptibility-induced fields. Regarding the latter, a large proportion of the lymph nodes analyzed in this study have also been imaged using a multi-gradient echo acquisition,[9] which was used to map T_2^* values that reflect the field inhomogenity. Similar to ADC, the T_2^* values from Ref. 9 also exhibited a large spread in the same benign nodes; however, no significant correlations have been found between ADC and T_2^* values, as illustrated in Supporting Information

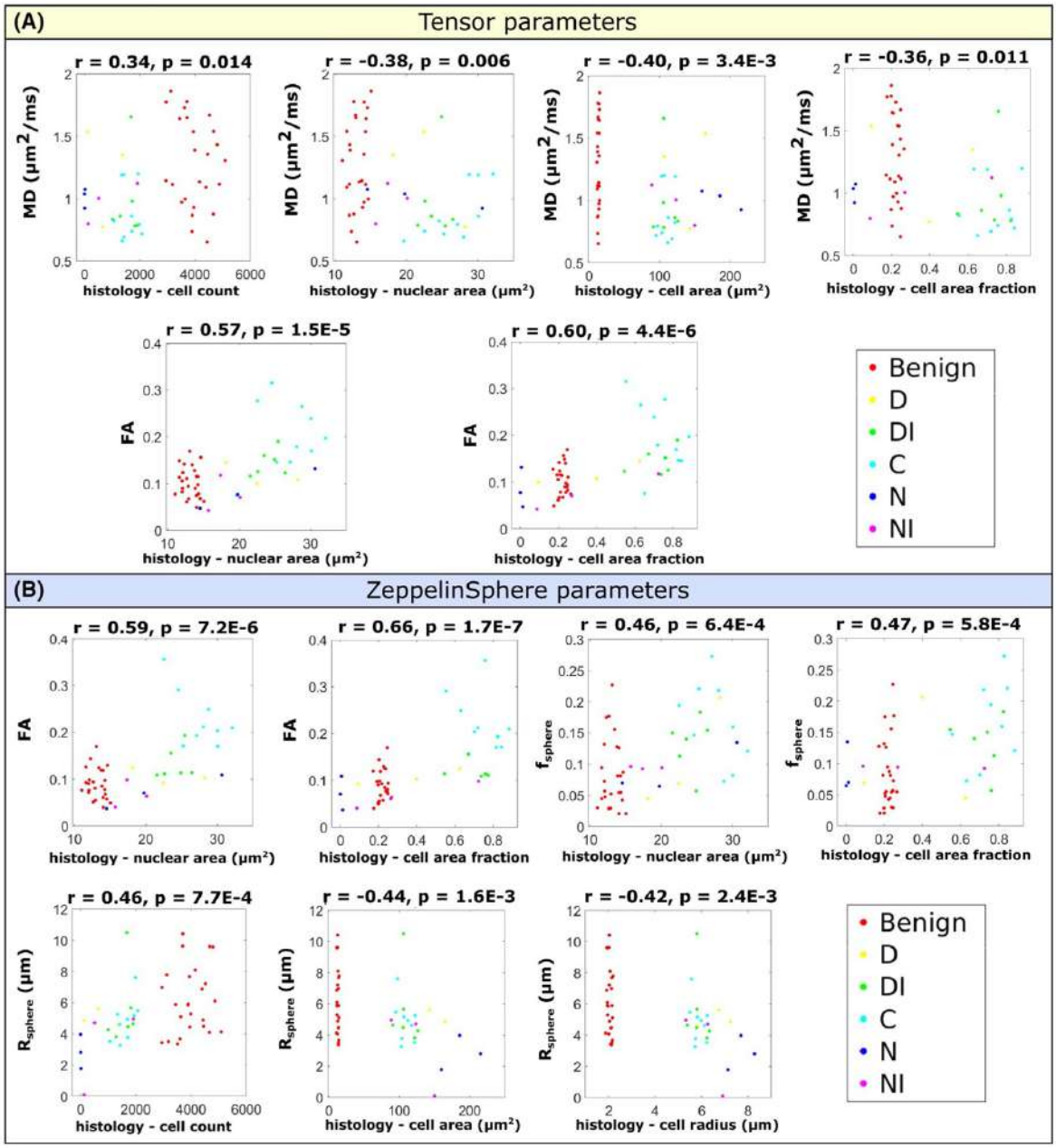

FIGURE 6 Correlation between MRI-derived model parameters and histology features for the (A) Tensor model and (B) ZeppelinSphere model. Only parameters with significant correlations with $r > 0.3$ are depicted. For the R_{sphere} parameter, we also show the correlation with the estimated cell radius from histology, which is calculated from the average cell area assuming a circular shape. Different marker colors represent different node types. Benign nodes are depicted in red, whereas malignant nodes are depicted in different colors depending on their malignancy pattern (D: desmoplastic; DI: desmoplastic with inflammation; C: cellular; N: necrotic; NI: necrotic with inflammation). The following correlation strengths are assumed based on the values of the correlation coefficient r: < 0.3 = negligible; 0.3 to 0.5 = weak; 0.5 to 0.7 = moderate; 0.7 to 0.9 = strong; 0.9 to 1.00 = very strong[63]

Figure S3. Regarding the effect of fixation duration, previous studies have shown variable results depending on the tissue type.[59-61] In our study, the fixation interval ranged from 2 weeks to 35 weeks (median 15 weeks); however, the correlation between MD values (or other metrics) and fixation period ($r = 0.33$, $P = .09$) was not significant. Thus, the preparation cannot account for the full variability observed in the benign nodes.

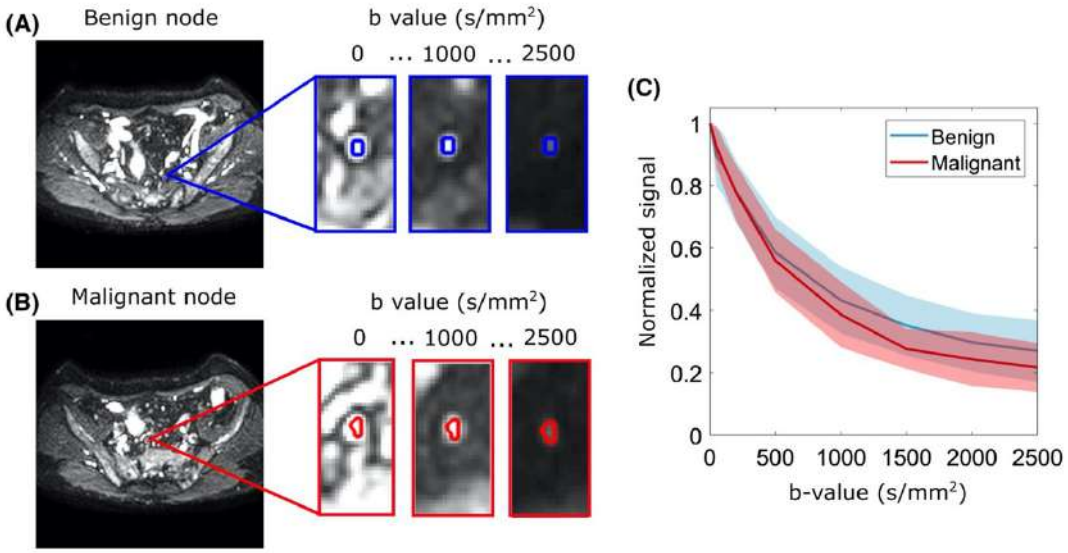

FIGURE 7 (A)-(B) Diffusion-weighted images of a benign and a malignant lymph node, respectively, with full FOV B_0 images and details of the lymph node ROI delineation for 3 b-values (0, 1000, and 2500 s/mm^2). (C) Average signal decay for benign and malignant lymph nodes as a function of b-value

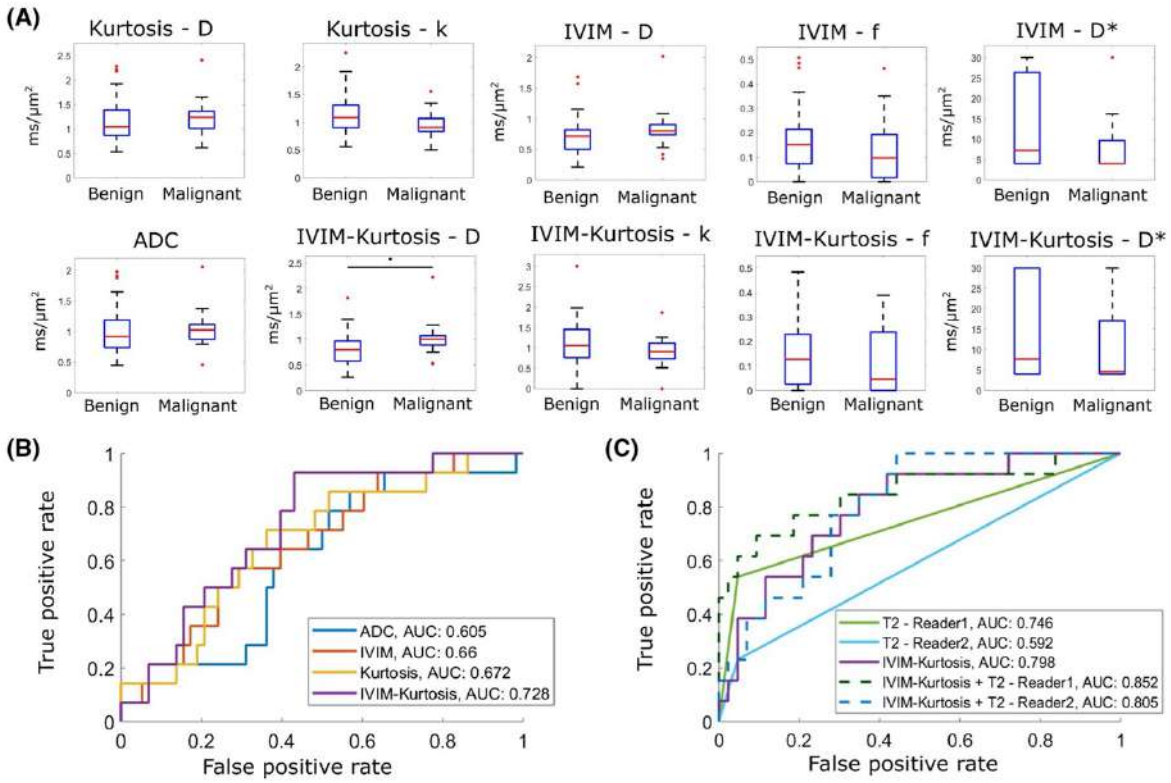

FIGURE 8 (A) Estimated parameter values of the various diffusion model for benign and malignant lymph nodes (Kurtosis and IVIM in the top row; ADC and IVIM-Kurtosis in the bottom row). (B) ROC curves for the ADC, IVIM, Kurtosis, and IVIM-Kurtosis models. (C) ROC curves for the IVIM-Kurtosis model, as well as for the node classification provided by 2 different radiologists. This ROC curve is evaluated on a subset of 56 nodes. ADC, apparent diffusion coefficient; IVIM, intravoxel incoherent motion

TABLE 2 Parameter values for benign and malignant nodes given by the ADC, IVIM, kurtosis and IVIM-kurtosis models applied to clinical data

	ADC	IVIM			Kurtosis		IVIM-Kurtosis			
	D ($ms/\mu m^2$)	f	D ($ms/\mu m^2$)	D* ($ms/\mu m^2$)	D ($ms/\mu m^2$)	k	D ($ms/\mu m^2$)	f	D* ($ms/\mu m^2$)	k
Benign	0.96 ± 0.34	0.16 ± 0.12	0.70 ± 0.28	12.9 ± 10.9	1.12 ± 0.39	1.14 ± 0.34	**0.80 ± 0.30**	0.15 ± 0.13	13.7 ± 11	1.09 ± 0.62
Malignant	1.08 ± 0.36	0.13 ± 0.15	0.85 ± 0.39	8.0 ± 7.5	1.27 ± 0.42	0.94 ± 0.27	**1.02 ± 0.41**	0.11 ± 0.13	10.1 ± 8.2	0.88 ± 0.49
P value	0.26	0.66	0.11	0.074	0.22	0.12	**0.030 (*)**	0.32	0.24	0.32

Abbreviations: ADC, apparent diffusion coefficient; IVIM, intravoxel incoherent motion.

Another interesting finding of the preclinical aspect of this study is that even the best-fitting model, despite its success in characterizing the diffusion signal decay and differentiating between malignant/benign nodes, correlates only moderately with the histological features. In malignant nodes, the restriction size R_{sphere} has similar values to cellular sizes in histology, with an average underestimation of 21 ± 32%; however, for benign lymph nodes, the restriction size has an average overestimation of 203 ± 110%, with a large spread of values, suggesting that the model is not necessarily adequate in benign lymph nodes. The highest correlation coefficient was observed between the FA values and the intracellular area fraction from histology, suggesting that the packing is somehow captured by the FA, whereas the restriction effects fitted by the models average out other histological properties, which are not directly visible in H&E staining and therefore correlate worse with the specific features they aim to represent such as cell size.

Taken together, the above-mentioned features highlight the simplistic nature of tissue modeling in terms of *specificity* and calls for caution when interpreting the model parameters (e.g., the model's spherical radii assigned to cellular spaces). Indeed, several assumptions are made: For example, the models assume nonexchanging water pools. However, as the diffusion times were varied up to 150 ms, exchange between compartments cannot be completely ruled out,[62,63] which potentially leads to an underestimation of the restriction fraction.[50] Another assumption is having the same diffusivity inside and outside the sphere, with time-dependence originating only from restricted diffusion, which might once again lead to bias.[46,64] Nevertheless, this assumption has been successfully applied in the past to model various tumor types,[33,37,40] with fitted parameters showing a good correlation with histology features.[33,41]

It is important to stress that, even if the estimated model parameters do not naturally correspond to features visible to histology, the modeling approach successfully captured the higher-order effects in the signal decay and recovered parameters, which were *useful* for lymph node classification, whereas the ADC approach was much less sensitive. In the future, more data could be acquired, thereby enabling increasingly complex models to be fit to the data, especially if single-shot acquisitions would be performed, leading to much more rapid acquisitions. Additionally, the sample preparation for ex vivo scanning could be improved in future experiments. In this study, some excluded nodes presented with poor quality images due to susceptibility artefacts, which we related to the accumulation of blood degradation products at their cut surface; as well as image distortions, which we retrospectively related to imperfect shimming. We believe imaging intact lymph nodes and limiting the amount of surrounding fat by more attentive dissection might minimize susceptibility and distortion in future experiments, respectively.

The second part of this study aimed at investigating some of the diffusion properties described above for clinical characterization of mesorectal lymph nodes in patients with rectal cancer at 1.5T. Given the clinical constraints, modeling anisotropy and restriction was not feasible, and perfusion effects had to be considered. Nevertheless, higher-order effects, shown to be important in the preclinical study, were accounted for in Kurtosis models. The results show that ADC alone does not faithfully distinguish between malignant and benign nodes, whereas an increase in the area under the ROC curve was noted for the IVIM-Kurtosis model compared with the standard ADC ($P = .19$). Moreover, combining IVIM-Kurtosis and T_2-weighted images provided a significant increase over the standard clinical classification based on T_2-weighted images alone ($P = .08$ for reader 1; $P < .01$ for reader 2). These results show that it is important to disentangle the various signal contributions, which are reflected in the ADC values, in order to better characterize and distinguish between node types.

The diffusion parameters obtained in this analysis for the ADC, IVIM, and Kurtosis models, i.e. higher ADC and D and lower D* and k in malignant nodes, are consistent with 2 recent studies employing IVIM and Kurtosis, respectively, to image lymph nodes in patients with rectal cancer,[25,28] however, in contradiction to the IVIM results from Ref. 29, in which the diffusivity in the malignant nodes is lower. The wide range of ADC and IVIM parameters are likely due to the heterogeneity of the lymph nodes as well as possible influences from the acquisition protocol. Moreover, in these studies there is no mention of any measures taken to minimize susceptibility and movement artifacts, which are common in pelvic MRI and whose avoidance was very important in our experiment.

Indeed, this study utilized state-of-the-art techniques to minimize motion artifacts, specifically, patients received a spasmolytic agent to minimize bowel movement, and a pressure belt was used to minimize artifacts due to respiratory motion. Nevertheless, some motion artifacts and partial volume could still be detected, especially when considering such small structures as lymph nodes. To further reduce the impact of motion on the data analysis, the dMRI parameter quantification was performed on ROIs, which were slightly translated for each part of the acquisition. Motion artifacts then lead to the exclusion of only 4 lymph nodes from the analysis, which we consider a good outcome for such MRI-challenging structures.

One limitation of this clinical study is the relatively small number of patients (N = 10) and the fact that half of malignant lymph nodes (7 of 14) originate from only 1 patient. Nevertheless, this effect was accounted for in the statistical model. Another limitation is related to the diffusion times and b-values clinically achievable. Although the preclinical results revealed that models with restriction and anisotropy best explain the diffusion properties of the tissue, such models were too complex to be fitted to the clinical data, which was constrained to measurements in 3 orthogonal directions averaged directly on the scanner and similar diffusion times for the different b-values. With the current imaging resolution, it was not feasible to assess the heterogeneity of diffusion parameters in the lymph nodes, with some nodes consisting only of a few voxels. Moreover, partial volume and motion effects, as well as different contrast between b_0 and diffusion-weighted images, make image registration a very difficult problem; thus, the analysis was performed at ROI level that is more robust but does not inform on parameter heterogeneity. Recent technical improvements in clinical scanners (slew rate, gradient strength, 3T field strength) would enable future studies to acquire dMRI measurements with multiple directions and diffusion times with a reasonable scan duration, which is required to characterize restriction and anisotropy in the tissue, as well as higher resolution images that could better inform about tissue heterogeneity. Nevertheless, these diffusion properties and their heterogeneity are to some extent reflected in the higher-order kurtosis models. Although the ex vivo and clinical studies cannot be directly compared because they include different patients, drastically different field strengths and image resolution, as well as different diffusion acquisitions and models, in both cases the results show that models including higher-order diffusion effects provide the best differentiation between benign and malignant nodes. Moreover, these approaches show a similar performance for the clinical data and ex vivo data when considering parameters averaged over the entire node.

5 | CONCLUSION

This work shows the potential of higher-order dMRI models to characterize and differentiate benign from malignant lymph nodes in rectal cancer patients, both ex vivo at ultra-high field and in vivo at 1.5T, paving the way for future oncologic studies on lymph node staging.

ACKNOWLEDGMENT

The authors would like to thank the following for their contributions: Lara Castanheira, Alexandra Ferreira and Ana Santos from the Pathology Department of the Champalimaud Centre for the Unknown; Nuno Figueiredo and José Filipe Cunha from the Digestive Unit of the Champalimaud Centre for the Unknown; Carlos Leichsenring, Vasco Geraldes and Cisaltina Sobrinho, from the Department of Surgery of the Hospital Fernando Fonseca, EPE; Maria Lisitskaya, a fellow radiologist at the Computational Clinical Imaging Group, Champalimaud Centre for the Unknown; Nickolas Papanikolaou from the Computational Clinical Imaging Group, Champalimaud

Centre for the Unknown; Eleftheria Panagiotaki from the Centre for Medical Image Computing, University College London; All the staff from the Radiology Department of the Champalimaud Centre for the Unknown; and the researchers from the Neuroplasticity and Neural Activity MRI Lab, Champalimaud Centre for the Unknown.

CONFLICT OF INTEREST

Paula Montesinos, Nuno Loução, Javier Gonzales-Sanchez are employees of Philips Healthcare.

ORCID

Andrada Ianuş https://orcid.org/0000-0001-9893-1724
Noam Shemesh https://orcid.org/0000-0001-6681-5876

REFERENCES

1. Yao Y-F, Wang L, Liu Y-Q, et al. Lymph node distribution and pattern of metastases in the mesorectum following total mesorectal excision using the modified fat clearing technique. *J Clin Pathol*. 2011;64:1073–1077.
2. Sauer R, Becker H, Hohenberger W, et al. Preoperative versus postoperative chemoradiotherapy for rectal cancer. *N Engl J Med*. 2004;351:1731–1740.
3. Munn LL, Padera TP. Imaging the lymphatic system. *Microvasc Res*. 2014;96:55–63.
4. Yankeelov TE, Pickens DR, Price RR. *Quantitative MRI in Cancer*. Boca Raton, FL: CRC Press; 2012.
5. Bipat S, Glas AS, Slors FJM, et al. Rectal cancer: local staging and assessment of lymph node involvement with endoluminal US, CT, and MR imaging. *Radiology*. 2004;232:773–783.
6. Jhaveri KS, Hosseini-Nik H. MRI of rectal cancer: an overview and update on recent advances. *Am J Roentgenol*. 2015;205:42–55.
7. Loftås P, Sturludóttir M, Hallböök O, Almlöv K, Arbman G, Blomqvist L. Assessment of remaining tumour involved lymph nodes with MRI in patients with complete luminal response after neoadjuvant treatment of rectal cancer. *Br J Radiol*. 2018;91:20170938.
8. Yang X, Chen Y, Wen Z, et al. Role of quantitative dynamic contrast-enhanced MRI in evaluating regional lymph nodes with a short-axis diameter of less than 5 mm in rectal cancer. *Am J Roentgenol*. 2019;212:77–83.
9. Santiago I, Santinha J, Ianuş A, et al. Susceptibility perturbation MRI (SPI) maps tumor infiltration into mesorectal lymph nodes. *Cancer Res*. 2019;79:2435–2444.
10. Herneth AM, Mayerhoefer M, Schernthaner R, et al. Diffusion weighted imaging: lymph nodes. *Radiology*. 2010;76:398–406.
11. Koh DM, Collins D. Diffusion-weighted MRI in the body: applications and challenges in oncology. *Am J Roentgenol*. 2007;188:1622–1635.
12. Reynaud O. Time-dependent diffusion MRI in cancer: tissue modeling and applications. *Front. Phys*. 2017;5:58.
13. Padhani AR, Liu G, Koh DM, et al. Diffusion-weighted magnetic resonance imaging as a cancer biomarker: consensus and recommendations. *Neoplasia*. 2009;11:102–125.
14. Surov A, Meyer HJ, Wienke A. Correlation between apparent diffusion coefficient (ADC) and cellularity is different in several tumors: a meta-analysis. *Oncotarget*. 2017;8:59492–59499.
15. Sui WF, Chen X, Peng ZK, et al. The diagnosis of metastatic axillary lymph nodes of breast cancer by diffusion weighted imaging: a meta-analysis and systematic review. *World J Surg Oncol*. 2016;14:155.
16. Pekçevik Y, Çukurova I, Arslan IB. Apparent diffusion coefficient for discriminating metastatic lymph nodes in patients with squamous cell carcinoma of the head and neck. *Diagn Interv Radiol*. 2015;21:397–402.
17. Lim HK, Lee JH, Baek HJ, et al. Is diffusion-weighted MRI useful for differentiation of small non-necrotic cervical lymph nodes in patients with head and neck malignancies? *Korean J Radiol*. 2014;15:810–816.
18. Hasbahceci M, Akcakaya A, Memmi N, et al. Diffusion MRI on lymph node staging of gastric adenocarcinoma. *Quant Imaging Med Surg*. 2015;5:392–400.
19. Cho EY, Kim SH, Yoon J-H, et al. Apparent diffusion coefficient for discriminating metastatic from non-metastatic lymph nodes in primary rectal cancer. *Eur J Radiol*. 2013;82:e662–e668.
20. Jensen JH, Helpern JA, Ramani A, et al. Diffusional kurtosis imaging: the quantification of non-gaussian water diffusion by means of magnetic resonance imaging. *Magn Reson Med*. 2005;53:1432–1440.
21. Rosenkrantz AB, Padhani AR, Chenevert TL, et al. Body diffusion kurtosis imaging: basic principles, applications, and considerations for clinical practice. *J Magn Reson*. 2015;42:1190–1202.
22. Shen LU, Zhou G, Tang F, et al. MR diffusion kurtosis imaging for cancer diagnosis: a meta-analysis of the diagnostic accuracy of quantitative kurtosis value and diffusion coefficient. *Clin Imaging*. 2018;52:44–56.
23. Jansen JFA, Stambuk HE, Koutcher JA, Shukla-Dave A. Non-gaussian analysis of diffusion-weighted MR imaging in head and neck squamous cell carcinoma: a feasibility study. *Am J Neuroradiol*. 2010;31:741–748.
24. Yamada I, Sakamoto J, Kobayashi D, et al. Diffusion kurtosis imaging of endometrial carcinoma: correlation with histopathological findings. *Magn Reson Imaging*. 2019;57:337–346.
25. Yu J, Dai X, Zou H-H, et al. Diffusion kurtosis imaging in identifying the malignancy of lymph nodes during the primary staging of rectal cancer. *Colorectal Dis*. 2018;20:116–125.
26. Le Bihan D, Breton E, Lallemand D, et al. Separation of diffusion and perfusion in intravoxel incoherent motion MR imaging. *Radiology*. 1988;168:497–505.
27. Iima M, Le Bihan D. Clinical intravoxel incoherent motion and diffusion MR imaging: past, present, and future. *Radiology*. 2016;278:13–32.
28. Qiu L, Liu X-L, Liu S-R, et al. Role of quantitative intravoxel incoherent motion parameters in the preoperative diagnosis of nodal metastasis in patients with rectal carcinoma. *J Magn Reson Imaging*. 2016;44:1031–1039.
29. Yu X-P, Wen LU, Hou J, et al. Discrimination between metastatic and nonmetastatic mesorectal lymph nodes in rectal cancer using intravoxel incoherent motion diffusion-weighted magnetic resonance imaging. *Acad Radiol*. 2016;23:479–485.
30. Wu W-C, Yang S-C, Chen Y-F, et al. Simultaneous assessment of cerebral blood volume and diffusion heterogeneity using hybrid IVIM and DK MR imaging: initial experience with brain tumors. *Eur Radiol*. 2017;27:306–314.
31. Fujima N, Sakashita T, Homma A, et al. Utility of a hybrid IVIM-DKI model to predict the development of distant metastasis in head

and neck squamous cell carcinoma patients. *Magn Reson Med Sci*. 2018;17:21–27.
32. Lu Y, Jansen J F, Mazaheri Y, et al. Extension of the Intravoxel Incoherent Motion Model to Non-Gaussian Diffusion in Head and Neck Cancer. *J Magn Reson Imaging*. 2012;36:1088–1096.
33. Panagiotaki E, Walker-Samuel S, Siow B, et al. Noninvasive quantification of solid tumor microstructure using VERDICT MRI. *Cancer Res*. 2014;74:1902–1912.
34. White NS, McDonald CR, Farid N, et al. Diffusion-weighted imaging in cancer: physical foundations and applications of restriction spectrum imaging. *Cancer Res*. 2014;74:4638–4652.
35. Reynaud O, Winters KV, Hoang DM, et al. Surface-to-volume ratio mapping of tumor microstructure using oscillating gradient diffusion weighted imaging. *Magn Reson Med*. 2016;76:237–247.
36. Jiang X, Li H, Xie J, et al. In vivo imaging of cancer cell size and cellularity using temporal diffusion spectroscopy. *Magn Reson Med*. 2017;78:156–164.
37. Liang S, Panagiotaki E, Bongers A, et al. Information-based ranking of 10 compartment models of diffusion-weighted signal attenuation in fixed prostate tissue. *NMR Biomed*. 2016; 29:660–671.
38. Szczepankiewicz F, van Westen D, Englund E, et al. The link between diffusion MRI and tumor heterogeneity: mapping cell eccentricity and density by diffusional variance decomposition (DIVIDE). *NeuroImage*. 2016;142:522–532.
39. Liang C-Y, Chen M-D, Zhao X-X, et al. Multiple mathematical models of diffusion-weighted magnetic resonance imaging combined with prognostic factors for assessing the response to neoadjuvant chemotherapy and radiation therapy in locally advanced rectal cancer. *Eur J Radiol*. 2019;110:249–255.
40. Xu J, Jiang X, Li H, et al. Magnetic resonance imaging of mean cell size in human breast tumors. 2019 arXiv:1905.07818 [physics.bio-ph].
41. Bonet-Carne E, Tariq M, Pye H, et al. Histological validation of in-vivo VERDICT MRI for prostate using 3D personalised moulds. In Proceedings of the 26th Annual Meeting of ISMRM, Paris, France, 2018. Abstract 0133.
42. Bailey C, Bourne RM, Siow B, et al. VERDICT MRI validation in fresh and fixed prostate specimens using patient-specific moulds for histological and MR alignment. *NMR Biomed*. 2019;32:e4073.
43. Panagiotaki E, Chan R, Dikaios N, et al. Microstructural characterisation of normal and malignant human prostate tissue with VERDICT MRI. *Invest Radiol*. 2014;50:218–222.
44. Johnston EW, Bonet-Carne E, Ferizi U, et al. VERDICT MRI for prostate cancer: intracellular volume fraction versus apparent diffusion coefficient. *Radiology*. 2019;291:391–397.
45. Zaccagna F, Riemer F, Priest AN, et al. Non-invasive assessment of glioma microstructure using VERDICT MRI: correlation with histology. *Eur J Radiol*. 2019;29:5559–5566.
46. Reynaud O, Winters KV, Hoang DM, et al. Pulsed and oscillating gradient MRI for assessment of cell size and extracellular space (POMACE) in mouse gliomas. *NMR Biomed*. 2016;29:1350–1363.
47. Jiang X, Li H, Xie J, et al. Quantification of cell size using temporal diffusion spectroscopy. *Magn Reson Med*. 2016;75:1076–1085.
48. Sahalan M. *Diffusion-weighted Imaging of Lymph Node Tissue*. [Dissertation]. Sydney, Australia: University of Sydney; 2019.
49. Panagiotaki E, Schneider T, Siow B, et al. Compartment models of the diffusion MR signal in brain white matter: a taxonomy and comparison. *NeuroImage*. 2012;59:2241–2254.
50. Li H, Jiang X, Xie J, et al. Impact of transcytolemmal water exchange on estimates of tissue microstructural properties derived from diffusion MRI. *Magn Reson Med*. 2017;77:2239–2249.
51. Alexander DC, Dyrby TB.Diffusion imaging with stimulated echoes: signal models and experiment design. arXiv:1305.7367 2013.
52. Neuman CH. Spin echo of spins diffusing in a bounded medium. *J Chem Phys*. 1974;60:4508.
53. Merboldt KD, Hanicke W, Frahm J. Self-diffusion NMR imaging using stimulated echoes. *J Magn Reson*. 1985;64:479–486.
54. Teruel JR, Cho GY, Moccaldi RM, et al. Stimulated echo diffusion tensor imaging (STEAM-DTI) with varying diffusion times as a probe of breast tissue. *J Magn Reson Imaging*. 2017;45:84–93.
55. Nolte UG, Finsterbusch J, Frahm J. Rapid isotropic diffusion mapping without susceptibility artifacts: whole brain studies using diffusion-weighted single-shot STEAM MR imaging. *Magn Reson Med*. 2000;44:731–736.
56. DeLong ER, DeLong DM, Clarke-Pearson DL. Comparing the areas under two or more correlated receiver operating characteristic curves: a nonparametric approach. *Biometrics*. 1988;44:837–845.
57. Beets-Tan RGH, Lambregts DMJ, Maas M, et al. Magnetic resonance imaging for clinical management of rectal cancer: updated recommendations from the 2016 European Society of Gastrointestinal and Abdominal Radiology (ESGAR) consensus meeting. *Eur Radiol*. 2018;28:1465–1475.
58. Fan X, Macleod K, Mustafi D, et al. Correlation of in vivo and ex vivo ADC and T2 of in situ and invasive murine mammary cancers. *PLoS ONE*. 2015;10:e0129212.
59. Korteweg MA, Zwanenburg JJM, van Diest PJ, et al. Characterization of ex vivo healthy human axillary lymph nodes with high resolution 7 Tesla MRI. *Eur Radiol*. 2011;21:310–317.
60. Giannakidis A, Gullberg GT, Pennell DJ, Firmin DN. Value of formalin fixation for the prolonged preservation of rodent myocardial microanatomical organization: evidence by MR diffusion tensor imaging. *Anat Rec (Hoboken)*. 2016;299:878–887.
61. Shatil AS, Uddin MN, Matsuda KM, Figley CR. Quantitative ex vivo MRI changes due to progressive formalin fixation in whole human brain specimens: longitudinal characterization of diffusion, relaxometry, and myelin water fraction measurements at 3T. *Front Med (Lausanne)*. 2018;5:31.
62. Pfeuffer J, Flögel U, Dreher W, Leibfritz D. Restricted diffusion and exchange of intracellular water: theoretical modelling and diffusion time dependence of 1H NMR measurements on perfused glial cells. *NMR Biomed*. 1998;11:19–31.
63. Tian X, Li H, Jiang X, et al. Evaluation and comparison of diffusion MR methods for measuring apparent transcytolemmal water exchange rate constant. *J Magn Reson*. 2017;275:29–37.
64. Lee HH, Fieremans E, Novikov DS. What dominates the time dependence of diffusion transverse to axons: intra- or extra-axonal water? *NeuroImage*. 2018;182:500–510.

SUPPORTING INFORMATION

Additional supporting information may be found online in the Supporting Information section.

FIGURE S1 Flow chart illustrating the number of patients and lymph nodes as well as the exclusion criteria for the ex-vivo (left) and clinical (right) studies

FIGURE S2 A) Parameter maps derived from the Diffusion Tensor model (MD and FA) for the same benign and malignant lymph nodes presented in Figure 3. B) MD and FA comparison for benign and malignant nodes

FIGURE S3 A-B) Parameter maps of MD and T_2^*, respectively; C) correlation plot between T_2^* and MD

FIGURE S4 Comparison of diffusion parameters in the capsule and parenchyma of a benign (A-C) and a malignant (D-F) node. A), D) FA maps illustrating the capsule and parenchyma ROIs; B), E) Histology images highlighting the stromal organization in the capsule; C), F) Boxplots of MD and FA values. All P values << .01

TABLE S1 Description of the diffusion models fitted to the pre-clinical ex-vivo data including model name, equation, number of fitted parameters and the range of parameter values

TABLE S2 Description of the diffusion models fitted to the clinical data including model name, equation, number of fitted parameters and the range of parameter values

How to cite this article: Ianuş A, Santiago I, Galzerano A, et al. Higher-order diffusion MRI characterization of mesorectal lymph nodes in rectal cancer. *Magn Reson Med.* 2019;00:1–17. https://doi.org/10.1002/mrm.28102

4.5 Advances in knowledge

We developed two new methods to distinguish normal from tumour-infiltrated mesorectal lymph nodes in rectal cancer - Susceptibility Perturbation MR Imaging and Higher-order Diffusion MR Imaging. We first tested the methods ex-vivo at ultra-high field (16.4 Tesla) and co-registered the high resolution "virtual histology" images with those of actual histology for microarchitectural comprehension. Then, we tested the node-by-node diagnostic accuracy in-vivo, upon patient staging, in a 1.5 Tesla clinical scanner. Finally, we confronted it with visual analysis by specialized radiologists according to current European Society of Gastrointestinal and Abdominal Radiology guidelines, to determine their added value. We will now summarize the advances in knowledge for each new method:

Susceptibility Perturbation MR Imaging (SPI)

- SPI accurately improved specificity toward microstructural lymph node characterization – the significant quantitative differences in its extracted parameters were, at least in part, explained by differences in cellularity and cell size between benign and malignant tissue, as opposed to iron content or oxygenation state.
- Malignant lymph node tissue presented with 3 main phenotypes at histology: solid infiltration, necrosis and desmoplasia, which in turn translated into variations of the SPI contrast.
- SPI increased the accuracy of lymph node characterization upon clinical staging at 1.5 Tesla, with a significant improvement in sensitivity compared to standard visual assessment by specialized radiologists.
- Combined SPI + radiologist analysis reached AuROCs of 0.80/0.87, coming close to those of Gadofoveset® or USPIO-based assessment and without their inconveniences.

Higher-order diffusion MR imaging

- The 8 compartment models used to analyze the rich ex-vivo diffusion MR imaging data showed an important spatial variation across lymph node tissue.

- The ZeppelinSphere model, which accounts for both diffusion anisotropy and restriction in the tissue, provided overall the best fit and translated into significant differences between

benign and malignant tissue, which we could at least in part justify based on differences in cell size and density.

- Intravoxel-Incoherent-Motion–Kurtosis was the most suitable of the 4 models tested in--vivo, with an AuROC of 0.80 for the differentiation between benign and malignant tissue, superior to visual analysis by specialized radiologists.

- ADC, the simplest and best known model in clinical practice, showed the worst performance for the in-vivo dataset.

- Combined Intravoxel-Incoherent-Motion–Kurtosis + radiologist evaluation resulted in AuROCS of 0.89/0.80, once again coming close to those of Gadofoveset® or USPIO-based assessment and without their inconveniences.

Susceptibility Perturbation MR Imaging and Higher-order Diffusion MR Imaging were able to characterize and differentiate benign from malignant lymph nodes in rectal cancer, both ex-vivo at 16.4 Tesla and in-vivo at 1.5 Tesla. These new methods may have the potential to aid in risk stratification and patient selection for neoadjuvant therapy.

PART II

SUSTAINED CLINICAL COMPLETE RESPONSE AT MR IMAGING AFTER NEOADJUVANT THERAPY

5.1 Re-staging and follow-up of rectal cancer patients with MR imaging when "Watch-and-Wait" is an option – A practical guide

Total mesorectal excision, as proposed by Heald *et al* in 1982, is now standard surgery for rectal cancer patients and contributed to an increase in 5-year survival rates from 30% to 68% and to a decrease in local recurrence from 40% to less than 5% (1). However, the morbidity of standard radical surgery is significant, with over a third of patients reporting urologic and/or sexual dysfunction and/or fecal incontinence (2,3). A series of landmark clinical trials support the use of neoadjuvant therapy to further improve oncologic outcomes in locally-advanced rectal cancer patients. It leads to a variable percentage of pathologic complete responses, ranging from 10 to 40% for long-course chemoradiation and 8–9% for short-course radiotherapy when surgery is performed 4–8 weeks after the end of radiotherapy (4–12). The need for radical surgery in such patients with no evidence of residual disease has been questioned, and a non-operative "Watch-and-Wait" approach is now established policy in dedicated centers worldwide (13). This approach demands a strict surveillance protocol based largely on endoscopy and MR imaging given regrowth on follow-up occurs in about one fourth of cases (14). In the following educational review, a practical guide for radiologists interested in "Watch-and-Wait" is provided.

References

1) Heald R, Ryall R. Recurrence and survival after total mesorectal excision for rectal cancer. Lancet. 1986. 1:1479–1482.

2) Schneider E, Hyder O, Brooke B et al. Patient readmission and mortality after colorectal surgery for colon cancer: impact of length of stay relative to other clinical factors. J Am Coll Surg. 2012. 214:390–398.

3) Chiappa A, Bertani E, Ferrari C et al. The impact of total mesorectal excision for rectal cancer on survival. Eur J Surg Oncol. 2014. 40(11):S97.

4) Maas M, Nelemans P, Valentini V et al. Long-term outcome in patients with a pathological complete response after chemoradiation for rectal cancer: a pooled analysis of individual patient data. Lancet Oncol. 2010. 11:835–844.

5) Garcia-Aguilar J, Shi Q, Thomas C et al. A phase II trial of neoadjuvant chemoradiation and local excision for T2N0 rectal cancer: preliminary results of the ACOSOG Z6041 trial. Ann Surg Oncol. 2012. 19:384–391.

6) Habr-Gama A, Perez R, Proscurshim I et al. Patterns of failure and survival for nonoperative treatment of stage c0 distal rectal cancer following neoadjuvant chemoradiation therapy. J Gastrointest Surg. 2006. 10:1319–1328.

7) Park I, Yu C. Current issues in locally advanced colorectal cancer treated by preoperative chemoradiotherapy. World J Gastroenterol. 2014. 20:2023–2029.

8) Chan A, Wong A, Jenken D et al. Posttreatment TNM staging is a prognostic indicator of survival and recurrence in tethered or fixed rectal carcinoma after preoperative chemotherapy and radiotherapy. Int J Radiat Oncol Biol Phys. 2005. 61: 665–677.

9) Glynne-Jones R, Wallace M, Livingstone J et al. Complete clinical response after preoperative chemoradiation in rectal cancer: is a "wait and see" policy justified? Dis Colon Rectum. 2008. 51:10–19.

10) Hatfield P, Hingorani M, Radhakrishna G et al. Short-course radiotherapy, with elective delay prior to surgery, in patients with unresectable rectal cancer who have poor performance status or significant co-morbidity. Radiother Oncol. 2009. 92(2):210–214.

11) Radu C, Berglund A, Påhlman L et al. Short-course preoperative radiotherapy with delayed surgery in rectal cancer – a retrospective study. Radiother Oncol. 2008. 87(3):343–349.

12) Pettersson D, Holm T, Iversen H et al. Preoperative short-course radiotherapy with delayed surgery in primary rectal cancer. Br J Surg. 2012. 99(4):577–583.

13) São Julião G, Habr-Gama A, Vailati B et al. The good, the bad and the ugly: rectal cancers in the twenty-first century. Tech Coloproctol. 2017. 21:573–575.

14) Socha J, Kępka L, Michalski W et al. The risk of distant metastases in rectal cancer managed by a watch-and-wait strategy – A systematic review and meta-analysis. Radiother Oncol. 2020. 144:1-6.

Santiago *et al. Insights Imaging* (2021) 12:114
https://doi.org/10.1186/s13244-021-01055-w

Insights into Imaging

EDUCATIONAL REVIEW

Open Access

Re-staging and follow-up of rectal cancer patients with MR imaging when "Watch-and-Wait" is an option: a practical guide

Inês Santiago[1,2*], Bernardete Rodrigues[3], Maria Barata[1], Nuno Figueiredo[4], Laura Fernandez[4], Antonio Galzerano[5], Oriol Parés[6] and Celso Matos[1]

Abstract

In the past nearly 20 years, organ-sparing when no apparent viable tumour is present after neoadjuvant therapy has taken an increasingly relevant role in the therapeutic management of locally-advanced rectal cancer patients. The decision to include a patient or not in a "Watch-and-Wait" program relies mainly on endoscopic assessment by skilled surgeons, and MR imaging by experienced radiologists. Strict surveillance using the same modalities is required, given the chance of a local regrowth is of approximately 25–30%, almost always surgically salvageable if caught early. Local regrowths occur at the endoluminal aspect of the primary tumour bed in almost 90% of patients, but the rest are deep within it or outside the rectal wall, in which case detection relies solely on MR Imaging. In this educational review, we provide a practical guide for radiologists who are, or intend to be, involved in the re-staging and follow-up of rectal cancer patients in institutions with an established "Watch-and-Wait" program. First, we discuss patient preparation and MR imaging acquisition technique. Second, we focus on the re-staging MR imaging examination and review the imaging findings that allow us to assess response. Third, we focus on follow-up assessments of patients who defer surgery and confer about the early signs that may indicate a sustained/non-sustained complete response, a rectal/extra-rectal regrowth, and the particular prognosis of the "near-complete" responders. Finally, we discuss our proposed report template.

Keywords: Rectal cancer, Magnetic resonance imaging, Neoadjuvant therapy, Re-staging, "Watch-and-Wait"

Key points

- MR Imaging is one of the pillars for the selection and follow-up of patients when "Watch-and-Wait" is an option.
- Radiologists participating in "Watch-and-Wait" programs should be familiar with the imaging findings that indicate a poor/incomplete response, a complete response and a "near-complete" response.
- Given deep rectal and extra-rectal regrowth detection relies on MR imaging only, radiologists should combine a high index of suspicion with a high precision, to propel salvage surgery only when needed.

Introduction

The concept of "locally-advanced rectal cancer" is intrinsically linked with a clinical indication for neoadjuvant therapy (NAT). It traditionally applies to all clinically staged T3/T4 and/or N+ tumours, although in the UK

*Correspondence: ines.santiago@neuro.fchampalimaud.org
[1] Radiology Department, Champalimaud Foundation, Avenida Brasília, 1400-038 Lisbon, Portugal
Full list of author information is available at the end of the article

and other centres across Europe criteria may be more strict [1, 2]. NAT regimens were initially designed with the sole purpose of downsizing/downstaging tumours in order to increase the likelihood of an R0 resection and diminish the risk of local recurrence [3], but the 10–25% pathologic complete response (pCR) rates have led clinicians to question the utility of radical surgery itself in such cases [4]. In fact, the real pCR odds may be even higher, given most patients included in reported studies were operated at 6–8 weeks while pCR rates increase significantly when the interval to surgery is lengthened to > 12 weeks post-radiotherapy (RT) [5]. This means that if patients are re-staged and no signs of tumour persistence are present, deferral of surgery may be a reasonable option, and "Watch-and-Wait" (W&W) programs have grown increasingly available and popular during the past almost 20 years [4]. For willing and able patients, this decision is largely based on re-staging rectal endoscopy and MR imaging assessments [6]. Strict follow-up afterwards is founded on the same grounds [6]. The overall survival of clinical complete responders appears similar to that of patients who undergo surgery and have a pCR [7]. Furthermore, out of the approximately 30% clinical complete responders who later on present with tumour regrowth, 95% are salvageable [8]. However, patients with local regrowth may present with a higher rate of distant metastatic disease compared to sustained clinical complete responders [9]. Whether this phenomenon is a reflection of the tumour biology or a consequence of an uncontrolled primary is not yet known [9]. Magnetic resonance (MR) imaging, as part of response assessment, should aim to distinguish "true" complete responders from patients with persistent, even if subclinical, disease, who need surgery for cure as early as possible. This educational review has three purposes: the first is to provide radiologists with the main relevant information to re-stage rectal cancer patients after NAT based on standard MR imaging; the second is to guide them through W&W follow-up MR imaging assessments in order to detect pelvic regrowths /recurrences as early as possible; the third is to present and discuss our proposed report template.

MR imaging preparation and acquisition technique

Before MR imaging acquisition, there are two preparatory steps which may significantly contribute to improve image quality. The first step is to ask patients to perform a small enema for rectal emptying before entering the MR equipment [10]. The second is to administer a spasmolytic agent such as butylscopolamine or glucagon before acquisition [10]. These two preparation steps are meant to minimise susceptibility artefacts due to air content and movement artefacts from peristalsis, respectively, given both adversely impact image interpretation, of diffusion-weighted imaging (DWI) in particular [10]. They are considered optional according to both ESGAR and SAR guidelines [11, 12]. When despite these measures patients still present with rectal air at tumour bed level and if they agree, a lubricated cannula can be inserted in the rectum for further emptying, and then removed before acquisition.

The use of endoluminal gel is not advocated routinely because distension of the rectum may result in misinterpretation of the distance between the tumour bed and circumferential resection margin (CRM), an essential re-staging information when surgery is a possibility [13]. If considered useful, gel should not exceed 60 ml to prevent excessive compression of the mesorectal fat [14].

Regarding technique, examinations should be performed on a 1.5T or 3T equipment using an external coil [11, 12]. 2D high-resolution T2-WI with a slice thickness ≤3 mm should be acquired in sagittal, axial and coronal planes, the two latter angulated perpendicular and parallel to the long axis of the tumour, respectively [11, 12]. In low tumours, additional high-resolution T2-WI angulated perpendicular and parallel to the anal canal may be acquired to better assess its involvement [11, 12]. A DWI acquisition including a high b value (≥800) should also be acquired, preferably with the same orientation as the axial high resolution T2-WI to ease finding co-localisation [11, 12]. Intravenous paramagnetic contrast administration is not routinely recommended [11, 12] but it may be useful in particular situations such as pelvic sepsis or fistulisation. Detailed acquisition protocols for our 1.5T and 3T Ingenia Philips Healthcare®, Best, The Netherlands clinical scanners are provided in Table 1.

Re-staging after neoadjuvant therapy

The issue of when to first assess tumour response is controversial. While the rate of pCR may increase after 12 weeks post-RT [5] some surgical teams are reluctant to operate beyond 8 weeks due to concerns about radiation-induced pelvic fibrosis and related surgical complications [15], which implies identifying poor/incomplete responders early. To move the decision timepoint from 6–8 weeks to 10–12 weeks post-RT may have no impact on surgery-related morbidity or mortality [16], and the extended period of surveillance may allow the start of consolidation chemotherapy on metastatic high-risk patients that may benefit from total NAT.

Although clinical and laboratory evaluation is relevant, re-staging relies heavily on rectal endoscopy and MR imaging. If the two are to be performed on the same day and given endoscopy requires the insufflation of air into the rectum, to perform MR imaging first may be

Table 1 Re-staging pelvic MR imaging acquisition parameters at 1.5T and 3T Ingenia Philips Healthcare®, Best, The Netherlands

	Oblique axial T2-W turbo spin-echo		Oblique coronal T2-W turbo spin-echo		Sagittal T2-W turbo spin-echo		Oblique axial single-shot spin-echo echo-planar diffusion		Axial T1-weighted gradient echo imaging	
	1.5T	3T	1.5T	3T	1.5T	3T	1.5T	3T	1.5T	3T
Echo time (msec)	115	105	115	105	105	100	92	95	10	15
Repetition time (msec)	4206	3943	4206	3943	2433	4672	6779	4140	683	734
Echo train length	17	19	17	19	17	17	–	–	5	7
Slice thickness (mm)	3	3	3	3	3	3	4	4	45	4
Gap (mm)	0	0	0	0	0	0	0	0	1	0.8
Matrix	400 x 333	400 x 259	400 x 333	400 x 259	252 x 223	252 x 237	76 x 65	80 x 65	376 x 390	404 x 415
Field-of-view (mm)	200 x 200	200 x 200	200 x 200	200 x 200	200 x 200	200 x 200	200 x 200	200 x 200	300 x 350	300 x 350
In-plane resolution (mm)	0.5 x 0.6	0.5 x 0.6	0.5 x 0.6	0.5 x 0.6	0.8 x 0.8	0.8 x 0.8	2.6 x 3.01	2.5 x 3.1	0.8 x 0.9	0.74 x 0.82
Signal averages	2	2	2	2	2	1	14	13	1	1
B value	–	–	–	–	–	–	1500	2000	–	–

Oblique axial scans are oriented perpendicularly to the long axis of the rectal wall at tumour location; [+]Spectral pre-saturation with inversion recovery is utilised for fat saturation

preferable in order to minimise air-induced susceptibility artefacts.

Endoscopic assessment [16] may be standardised according to a 5-point ordinal scale defined by the international W&W database consortium: responses may be graded, from best to worse response, as 0 (flat white scar with telangiectasia), 1 (shallow ulcer/red scar), 2 (ulcerated residual lesion or adenomatous residual mucosal abnormality), 3 (excavated ulcer with elevated edges) or 4 (persistent infiltrative lesion).

To identify the incomplete/poor responders

Approximately 20% of locally advanced rectal cancer patients show a poor response to neoadjuvant therapy, which may imply a shift in the neoadjuvant treatment scheme or early surgery [17, 18]. Poor responses generally present with endoscopic gradings of 3–4 and on MR imaging are characterised by (Fig. 1a–c):

1. Little reduction in tumour size

A tumour volume reduction below 70%, as based on slice-by-slice segmentation on T2-WI, is associated with a poor response [19–22]. Given tumour volume measurement is difficult and time-consuming, cranio-caudal length was suggested as an alternative [12]. Based on mrRECIST, less than 30% reduction in cranio-caudal tumour length is associated with a poor response [23]. However, this criteria was not validated prospectively [24].

2. MR Tumour regression grades (mrTRG) 3–5

MrTRG is an ordinal scale developed by Patel et al.to assess response on MR T2-WI in a parallel manner to the Mandard pathological TRG score [23, 25] and is presented in Table 2 [18].

There are multiple ordinal scales in the literature that represent variations or adaptations to it but in general, when T2-WI intermediate "tumour" signal predominates over hypointense fibrosis or clear hyperintense "acellular mucin" (mrTRG4-5, mrTRG5 hardly ever being observed in our experience), a poor response is assumed, and the 3-year disease free survival is 21% inferior compared to favourable mrTRG1-3s [23]. mrTRG3 may fall on the "good side" regarding long-term outcome [26] but the likelihood of a pCR or cCR when T2-intermediate clearly "tumoural" signal remains after neoadjuvant treatment is low, and it is therefore considered a sign of an incomplete response [27].

3. Significant restriction to diffusion on Diffusion-weighted Imaging (DWI)

DWI is highly sensitive to susceptibility artefacts and dependent on good acquisition technique. Good patient preparation is essential as well as adequate training in image reading. T2-shine through effects from luminal content, which will present with high signal intensity on high b value images and high signal intensity in the ADC map, should not to be mistaken for true restriction, which will present with high signal intensity on high b value images and low signal intensity in the ADC map; or with dense fibrosis, which will present with low signal intensity in both high b value images and ADC map. While on T2-WI mrTRG the

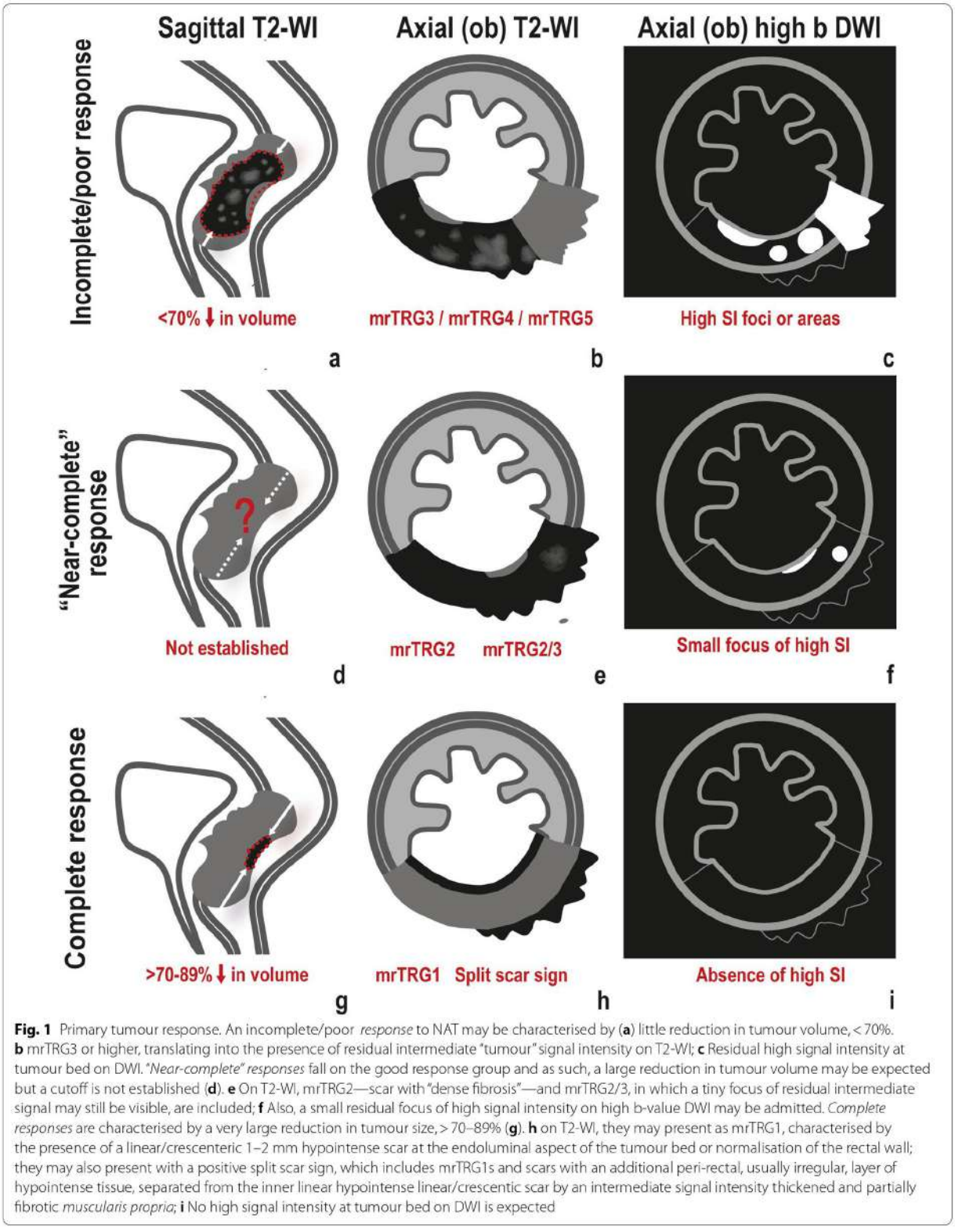

Fig. 1 Primary tumour response. An incomplete/poor *response* to NAT may be characterised by (**a**) little reduction in tumour volume, < 70%. **b** mrTRG3 or higher, translating into the presence of residual intermediate "tumour" signal intensity on T2-WI; **c** Residual high signal intensity at tumour bed on DWI. "*Near-complete" responses* fall on the good response group and as such, a large reduction in tumour volume may be expected but a cutoff is not established (**d**). **e** On T2-WI, mrTRG2—scar with "dense fibrosis"—and mrTRG2/3, in which a tiny focus of residual intermediate signal may still be visible, are included; **f** Also, a small residual focus of high signal intensity on high b-value DWI may be admitted. *Complete responses* are characterised by a very large reduction in tumour size, > 70–89% (**g**). **h** on T2-WI, they may present as mrTRG1, characterised by the presence of a linear/crescenteric 1–2 mm hypointense scar at the endoluminal aspect of the tumour bed or normalisation of the rectal wall; they may also present with a positive split scar sign, which includes mrTRG1s and scars with an additional peri-rectal, usually irregular, layer of hypointense tissue, separated from the inner linear hypointense linear/crescentic scar by an intermediate signal intensity thickened and partially fibrotic *muscularis propria*; **i** No high signal intensity at tumour bed on DWI is expected

Table 2 mrTRG and corresponding MR imaging findings [23]

mrTRG—Findings on MR imaging
1. Complete response (linear/crescentic 1–2 mm scar in mucosa or submucosa only, or normalisation of the rectal wall)
2. Good response (dense fibrosis; no obvious residual tumour, signifying minimal residual disease or no tumour)
3. Moderate response (> 50% fibrosis or mucin, and visible intermediate signal)
4. Slight response (little areas of fibrosis or mucin but mostly tumour)
5. No response (intermediate signal intensity, same appearances as original tumour/tumour regrowth)

proportion of intermediate "tumour" signal at tumour bed is taken into consideration, in most studies focusing on response assessment using DWI, assessment is binary—restriction indicates viable tumour whereas its absence suggests a complete response [28–31]. Also, DWI performance is generally evaluated in addition to T2-WI, and combined reading appears to perform significantly better for most readers [28–31]. Diffusion restriction may also be present in radiation-induced proctitis or hemorrhage/inflammation post-biopsy and when these procedures are performed before MR imaging, the radiologist should be notified. Also, restriction may be absent in incomplete responses, and according to Lambregts et al., in clear T2-WI intermediate-signal residual masses and in T2-hypointense "fibrotic" circumferential tumour scars, irrespective of DWI findings, the likelihood of viable tumour is very high (≥ 80%) [32].

Mucinous tumours have an intrinsically higher ADC compared to non-mucinous tumours, making response assessment based on DWI more difficult and less reliable [33].

An example of a poor tumour response is given in Fig. 2.

With respect to mesorectal lymph nodes, lymph nodes with incomplete/poor response usually present with (Fig. 3a–c):

1. *Short axis ≥ 5 mm*, which may be associated with a likelihood of residual disease up to 63% [12, 34].
2. *Residual intermediate "tumour" signal intensity or heterogeneous signal intensity on T2-WI*, which usually represents residual macroscopic tumour [34].

Residual high signal intensity on high b value DWI with low ADC does not aid in the identification of viable tumour in lymph nodes given it may be observed in both lymphoid and tumour tissue.

3. *Residual high "mucin" signal on high b-value T2-WI* — Mucinous tumours with lymph node involvement present with a higher frequency of residual viable tumour after neoadjuvant therapy and as such, lymph nodes with visible "mucin" high signal intensity on T2-WI at re-staging MR imaging are frequently positive [35].

An example of a poor lymph node response is given in Fig. 4.

Involvement of lateral pelvic sidewall lymph nodes is more likely to occur in tumours located at the level or below the peritoneal reflection, particularly if ≥ T3 [36]. The lower the location of the primary lesion, the higher the risk and in tumours < 4 cm from the anal verge, it may exceed 30% [36]. Lymph nodes with mixed signal intensity, irregular borders or short axis ≧ 5, 7 or 8 mm (different cutoffs are considered in different studies) on staging examinations were associated with a higher likelihood of harbouring metastasis [37, 38]. On re-staging MR imaging, criteria associated with residual tumour may be:

1. *Size reduction < 33%* between pre and post-neoadjuvant treatment [31].
2. *Short axis > 5 mm* on post-neoadjuvant therapy MR [38].
3. *Residual "tumour" signal intensity or heterogeneous signal intensity on T2-W,I* just the same as applied to mesorectal lymph nodes.

Regarding response of extramural venous invasion (EMVI) to neoadjuvant therapy, Chand et al.have established a specific TRG score for EMVI (mr-vTRG) on T2-WI and concluded grades 4 (< 25% fibrosis) and 5 (minimal fibrosis) were associated with higher local recurrence rates (44%) and lower disease-free survival (46%) compared to grades 1–3 (50% fibrosis or more)—9% local recurrence and 88% 3-year disease-free survival [39]. In our experience assessment of percentage of conversion to fibrosis may be difficult but indeed residual intermediate "tumour" signal intensity within EMVI after neoadjuvant therapy should signify viable tumour and a consequent poor or incomplete response, remaining restriction to diffusion supporting

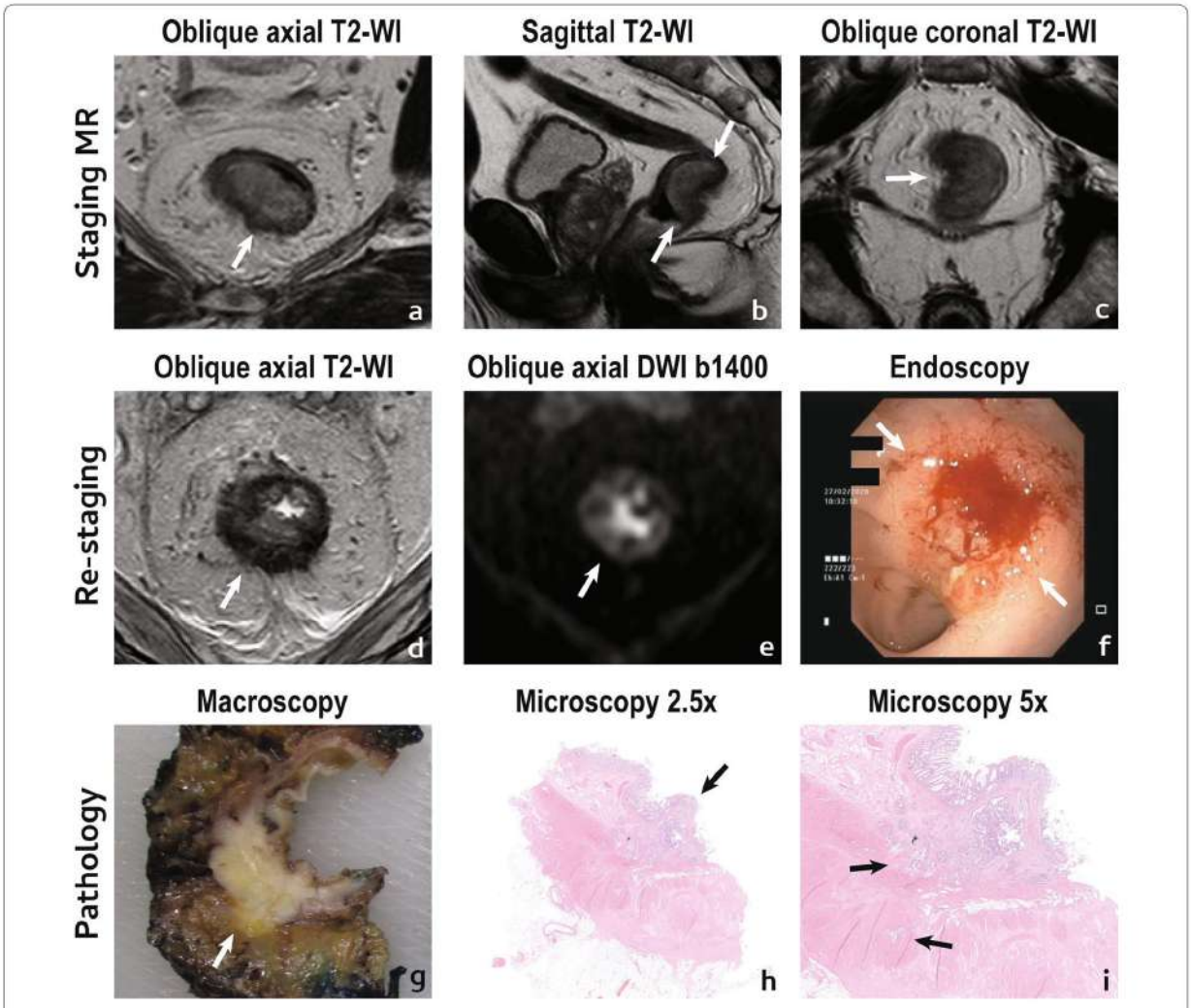

Fig. 2 Incomplete/poor tumour response. A 75 year-old male presented with a low mrT3a mrN0 EMVI + (not shown) CRM-rectal cancer (arrows in **a**–**c**). He underwent NAT and was re-staged at 12 weeks with MR imaging (**d**, **e**) and endoscopy (**f**). Reduction in size was estimated as < 50%, as may be inferred in **d** vs **a**. On T2-WI, the tumour scar was composed largely of intermediate signal intensity tissue (**d**), classified as mrTRG4 with absent split scar sign. On high b value DWI (**e**), a thick layer of high signal intensity was apparent at the endoluminal aspect of the tumour bed and a persistent infiltrative lesion was visible on endoscopy (between arrows in **f**). Patient underwent surgery and specimen was staged as a ypT3 (extension into mesorectal fat visible at macroscopy in **g**) N1c (not shown) TRG3 R0. At microscopy, viable tumour was predominantly mucosal/submucosal (arrow in **h**) but there were niches of viable tumour cells within the muscularis propria (arrows in **i**) and also at perirectal fat (not shown)

it. Although we found no data on the response of extranodal tumour deposits, similar criteria may apply.

Given incomplete/poor responders may undergo early surgery, it is particularly important that their identification is followed by detailed information on residual tumour location and relations. The most important of all items is the re-evaluation of the circumferential resection margin (CRM) given a clearance of the margin on re-staging high-resolution T2-WI has a positive predictive value of up to 90% for a clear margin at pathology, which may justify a shift towards less mutilating surgery [40–42]. On the other hand, if the margin is reached by dense hypointense fibrosis, the likelihood of tumour at pathology is lower than when it is reached by intermediate "tumour" signal intensity but is still significant, and as such it should be considered involved [40–42].

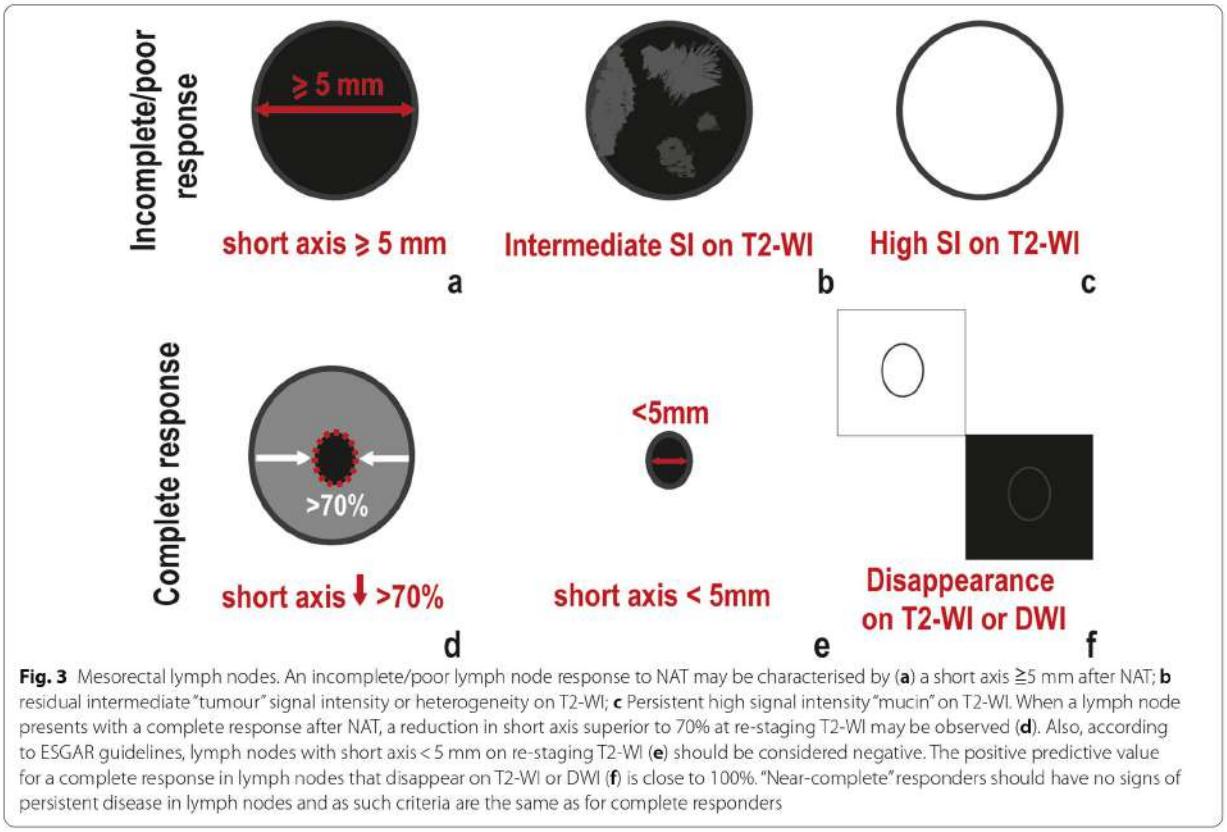

Fig. 3 Mesorectal lymph nodes. An incomplete/poor lymph node response to NAT may be characterised by (**a**) a short axis ≧5 mm after NAT; **b** residual intermediate "tumour" signal intensity or heterogeneity on T2-WI; **c** Persistent high signal intensity "mucin" on T2-WI. When a lymph node presents with a complete response after NAT, a reduction in short axis superior to 70% at re-staging T2-WI may be observed (**d**). Also, according to ESGAR guidelines, lymph nodes with short axis < 5 mm on re-staging T2-WI (**e**) should be considered negative. The positive predictive value for a complete response in lymph nodes that disappear on T2-WI or DWI (**f**) is close to 100%. "Near-complete" responders should have no signs of persistent disease in lymph nodes and as such criteria are the same as for complete responders

To identify the complete responders

Approximately 10–25% of patients with locally-advanced rectal cancer undergoing NAT prior to surgery achieve a pCR [4], escalating to even higher rates when more intense RT and/or chemotherapy regimens are employed [4].

There are some factors at staging MR that may be associated with a higher likelihood of a pCR, namely tumour length < 4 cm, tumour circumference < 180°, distance to anal verge < 45 mm and mrT stage ≤ 3 [43, 44]. Also, pCR rate increases with increasing interval to surgery to > 12 weeks [5], which means signs of a clinical complete response (cCR) on re-staging MR imaging are expected more often with longer intervals as well. Clinical complete response is characterised by a flat white scar with telangiectasia on endoscopy (endoscopy 0). At re-staging MR imaging the following are expected regarding the primary tumour (Fig. 1g–i):

1. Very large reduction in tumour size

Volume reduction > 70–89% at T2-WI (T2-hypointense "fibrosis" included in the measurements) and > 95–98% at DWI (only high signal intensity on high b value images measured) associate with a complete response to treatment [45–47].

2. mrTRG 1

Conversion to a linear/crescentic, 1–2 mm scar in the mucosa or submucosa or normalisation of the rectal all have very high specificity for complete response, in the range of 92–98% [48].

3. Positive split scar sign

The split scar sign has a very high specificity (97%) and positive predictive value (93/94%) for a sustained complete response [46], but it was not yet validated prospectively. It may be found on high resolution T2-WI and is characterised by an organised layered morphologic pattern of the tumour bed after neoadjuvant therapy, composed of an inner thin and regular hypointense band corresponding to the fibrosed submucosa; an intermediate signal intensity layer immediately underneath it, corresponding to a thickened and partially fibrosed *muscularis propria*; and an outer, irregular, hypointense layer of mesorectal fibrosis, which may be absent and usually

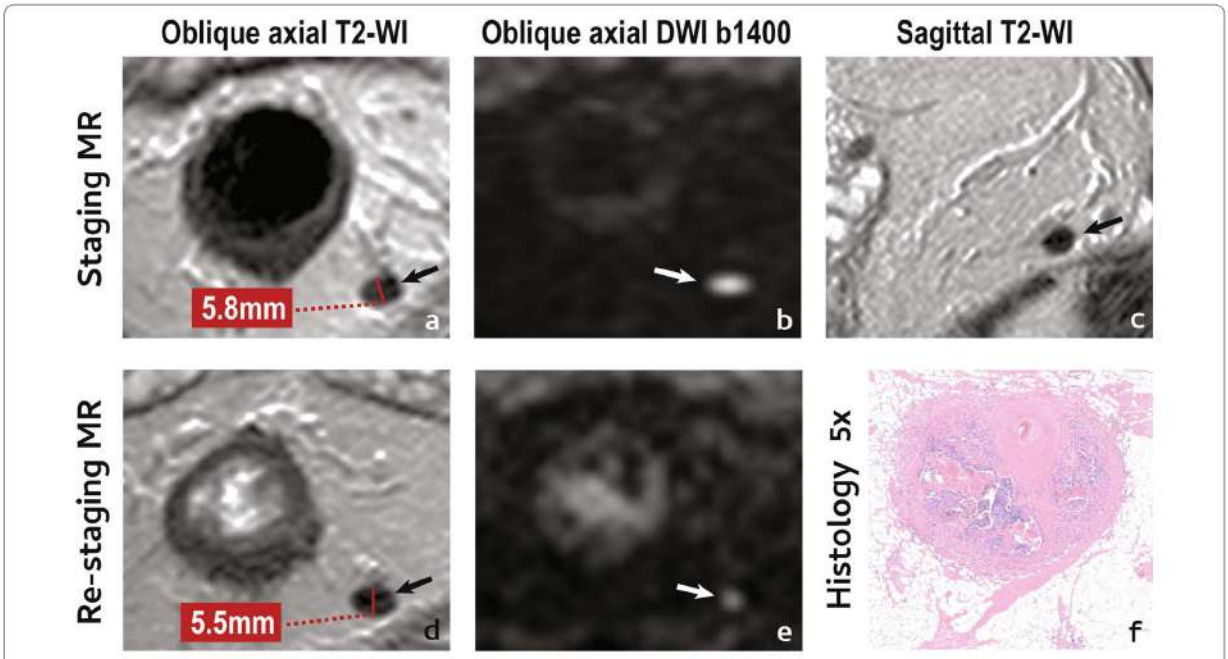

Fig. 4 Incomplete/poor lymph node response. A 65 year-old male presented with a low mrT3b (not shown) mrN1 (arrow in **a**–**c**) EMVI− CRM+ rectal cancer. He underwent NAT and was re-staged. Lymph node reduction in size was practically inexistent and post-NAT, short axis was > 5 mm (**d**). On T2-WI, the lymph node still looked heterogeneous, with areas of intermediate signal intensity (**d**). High signal intensity on high b value images was less but still present (**e**) (please note that visibility on high b value post-NAT imaging does not exclude good or even complete response). Patient underwent surgery and no residual lymphoid tissue was found within the lymph node in the pathology specimen, only tumour surrounded by fibrosis, adjacent to a vessel (**f**)—patient was therefore staged as a ypT3 N1c TRG3 R0

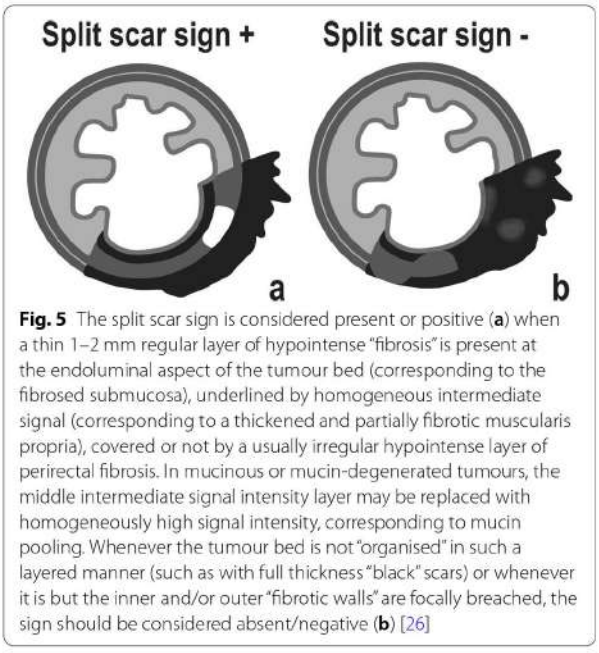

Fig. 5 The split scar sign is considered present or positive (**a**) when a thin 1–2 mm regular layer of hypointense "fibrosis" is present at the endoluminal aspect of the tumour bed (corresponding to the fibrosed submucosa), underlined by homogeneous intermediate signal (corresponding to a thickened and partially fibrotic muscularis propria), covered or not by a usually irregular hypointense layer of perirectal fibrosis. In mucinous or mucin-degenerated tumours, the middle intermediate signal intensity layer may be replaced with homogeneously high signal intensity, corresponding to mucin pooling. Whenever the tumour bed is not "organised" in such a layered manner (such as with full thickness "black" scars) or whenever it is but the inner and/or outer "fibrotic walls" are focally breached, the sign should be considered absent/negative (**b**) [26]

is in staged ≦ T2 tumours [49]. The split scar sign is explained in greater detail in Fig. 5.

4. Absence of high signal intensity on high b value DWI

Complete response on DWI is supported by the absence of high signal intensity at high b-value DWI images (using normal rectum as reference) [28–31] and it may be particularly valuable in small, subcircunferencial scars [32], whereas as previously discussed, in thick, circumferential T2-hypointese "fibrotic" responses, the likelihood of incomplete response is high even if DWI is negative [32].

An example of a complete tumour response is given in Fig. 6.

With respect to mesorectal lymph nodes, a complete response may present with (Fig. 3d–f):

1. *Significant size reduction or disappearance on T2-WI.* A ≥ 70% short axis reduction or disappearance of the LN on T2-WI may indicate ypN0 status in 100% of cases [34] and according to ESGAR guidelines, LNs < 5 mm after neoadjuvant therapy should be assumed as negative [12].

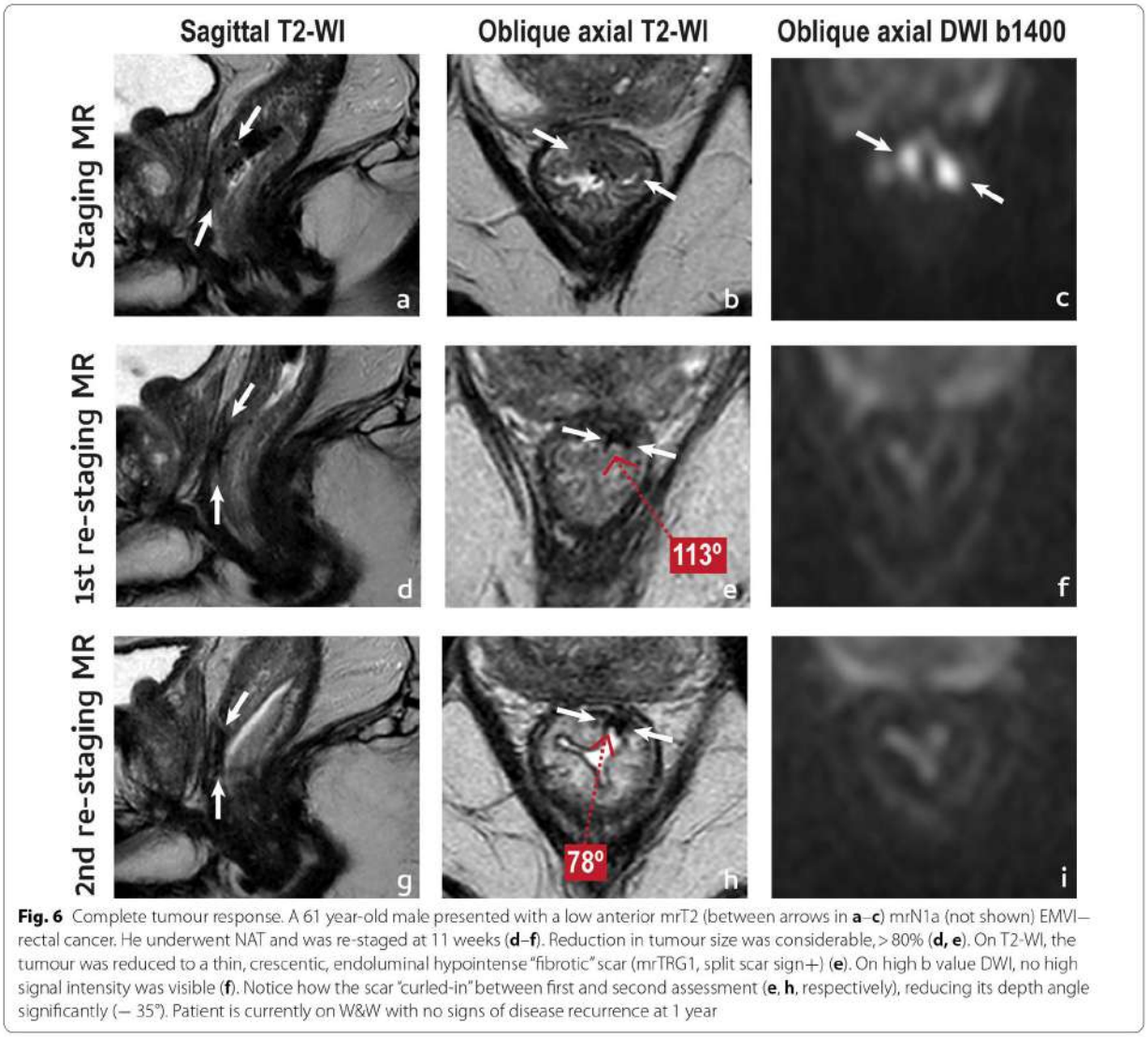

Fig. 6 Complete tumour response. A 61 year-old male presented with a low anterior mrT2 (between arrows in **a**–**c**) mrN1a (not shown) EMVI– rectal cancer. He underwent NAT and was re-staged at 11 weeks (**d**–**f**). Reduction in tumour size was considerable, > 80% (**d, e**). On T2-WI, the tumour was reduced to a thin, crescentic, endoluminal hypointense "fibrotic" scar (mrTRG1, split scar sign+) (**e**). On high b value DWI, no high signal intensity was visible (**f**). Notice how the scar "curled-in" between first and second assessment (**e**, **h**, respectively), reducing its depth angle significantly (– 35°). Patient is currently on W&W with no signs of disease recurrence at 1 year

2. *Disappearance on DWI*—Absence of visible lymph nodes in high b value DWI may be a reliable predictor of ypN0 status [50] but if high signal persists, a complete response may not be excluded.

An example of a complete lymph node response is provided in Fig. 7.

Lateral pelvic sidewall lymph nodes that shrink to 4 mm or less in short axis on re-staging MR imaging present no risk of local recurrence at 3 years according to Ogura et al. [51]. Disappearance or homogenous hypointensity on T2-WI and no visibility on high b value DWI may also favour a complete response.

Regarding response of extramural venous invasion, as stated above, mrV-TRG grades 1–3 (50% fibrosis or more) are associated with a good response, with only 9% LR rate and 88% 3-year DFS [39]. Even without concrete data on the subject, it appears reasonable to consider that normalisation of vessels or conversion to hypointense "fibrotic" signal intensity on T2-WI without high signal intensity on DWI would favour a complete response of extramural venous invasion, the same applying to extranodal tumour deposits.

Complete responders may be offered the possibility of entering a specialised surveillance program for organ preservation.

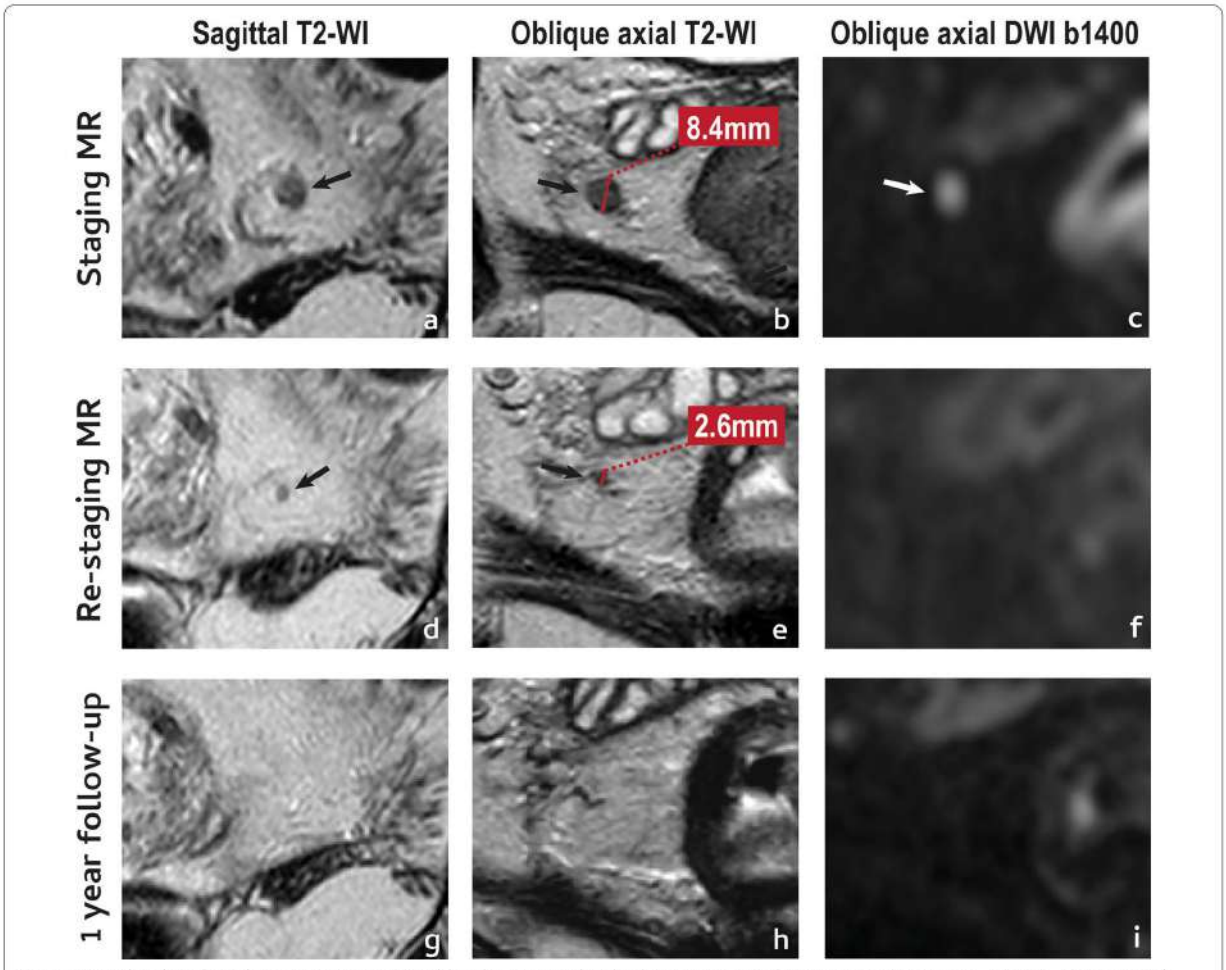

Fig. 7 Complete lymph node response. A 42 year-old male presented with a low mrT3a (not shown) mrN1a (arrow in **a**–**c**) EMVI− CRM+ rectal cancer. He underwent NAT and was re-staged. The positive lymph node showed a pronounced reduction in size after NAT, with a short axis reduction of 70% and a short axis < 5 mm (**e**). On T2-WI, the lymph node became too small to characterise (**e**). The lymph node was not visible on re-staging high b value DWI (**f**) and disappeared also on T2-WI at 1-year follow up MR imaging (**g**–**i**). Patient is currently under W&W with no clinical signs of viable local or distant disease

To identify the "near-complete" responders

The criteria presented above are very specific but not very sensitive for a complete response. The concept of "near-complete response" was introduced more recently, driven by the observation that a significant proportion of patients presenting with a very good but incomplete response at first assessment may convert into a cCR if given a longer interval and re-assessment [52]. This concept is, however, controversial. The scarce literature regarding this group of patients considers that they may present with endoscopic gradings 1–2 and/or up to high-grade dysplasia at histopathology when biopsy is performed [52–54]. However, given a negative biopsy is not equivalent to a complete clinical response, particularly in the presence of clinically residual abnormalities, its utility may be put to question [55]. Regarding the MR criteria (Fig. 1d–f):

mrTRG2-2/3

Patients with dense fibrosis or with dense fibrosis and minimal residual intermediate signal may be considered near-complete responders [52, 53].

Small focal area of high signal intensity on high b value DWI

A small focal area of high signal intensity on high b value DWI is admissible for a near-complete response [53].

There is no evidence regarding expected tumour size reduction for these patients.

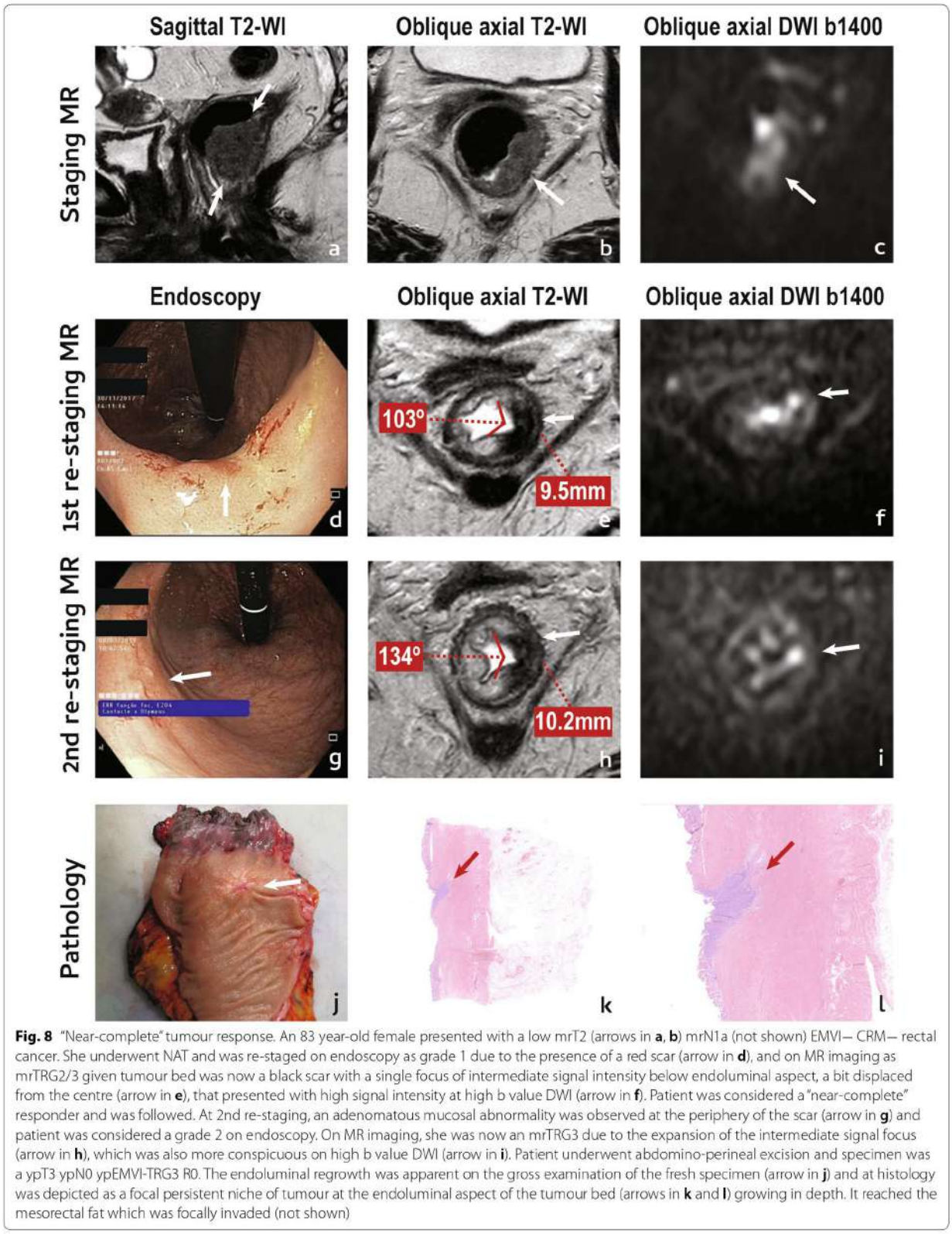

Fig. 8 "Near-complete" tumour response. An 83 year-old female presented with a low mrT2 (arrows in **a**, **b**) mrN1a (not shown) EMVI− CRM− rectal cancer. She underwent NAT and was re-staged on endoscopy as grade 1 due to the presence of a red scar (arrow in **d**), and on MR imaging as mrTRG2/3 given tumour bed was now a black scar with a single focus of intermediate signal intensity below endoluminal aspect, a bit displaced from the centre (arrow in **e**), that presented with high signal intensity at high b value DWI (arrow in **f**). Patient was considered a "near-complete" responder and was followed. At 2nd re-staging, an adenomatous mucosal abnormality was observed at the periphery of the scar (arrow in **g**) and patient was considered a grade 2 on endoscopy. On MR imaging, she was now an mrTRG3 due to the expansion of the intermediate signal focus (arrow in **h**), which was also more conspicuous on high b value DWI (arrow in **i**). Patient underwent abdomino-perineal excision and specimen was a ypT3 ypN0 ypEMVI-TRG3 R0. The endoluminal regrowth was apparent on the gross examination of the fresh specimen (arrow in **j**) and at histology was depicted as a focal persistent niche of tumour at the endoluminal aspect of the tumour bed (arrows in **k** and **l**) growing in depth. It reached the mesorectal fat which was focally invaded (not shown)

An example of a near-complete tumour response is provided in Fig. 8.

Regarding lymph node involvement, the only study on near-complete response mentioning lymph nodes considers "suspicious" lymph nodes, whether mesorectal or sidewall, should not be present on re-staging MR imaging [53]. As such, the *same criteria as for complete responders* should be applied (Fig. 3d–f). Although again no data was found on the matter, the same may work for EMVI and extranodal tumour deposits.

Follow-up of patients who deferred surgery

Question 1: Can we anticipate a clinical complete response is going to be sustained?

There are some signs at re-staging MR imaging that, although not validated, may favour a sustained complete response:

1. *Normalisation of the rectal wall* at re-staging MR imaging has a 100% specificity for a sustained complete response according to the pattern base approach by Lambregts et al. [32].
2. *A positive split scar sign* at first re-staging MR imaging may indicate a sustained complete response for a minimum period of 1 year with a specificity of 97%, as per our data [49] (Figs. 5, 6).
3. *Hypointense "fibrosis" on T2-WI without high signal intensity on high b value DWI in semicircular tumours* is, according to Lambregts et al., associated with a sustained complete response with a 91% specificity [32].

Question 2: When we observe a clinical complete response, can we anticipate a local regrowth is going to occur later on?

There are some signs at re-staging MR imaging that, although not validated, may associate with a higher likelihood of a local regrowth:

1. Tumour scar depth angle increase > 21° between 1st and 2nd post-NAT MR imaging

The scar depth angle is a measure of tumour bed contraction/dilation over time on T2-WI. For patients who enroll W&W, a scar depth angle increase of 21° or more between the first re-staging MR imaging examination (median 10 weeks post-RT) and the following (median 23 weeks post-RT) signaled a non-sustained complete response with a very high specificity (91/94%) [56]. To measure it, the central axial slice of the tumour must first be chosen using sagittal/coronal planes as reference. Then, within the central axial slice, the endoluminal centre of the scar should serve as pivot while the angle lines cross the endoluminal extremities of the scar (Fig. 9). For scars taking more than 180° of the rectal wall, the angle lines should cross the endoluminal aspect of the scar at 180°. The same applies to circumferential tumours, in which case the pivot should be placed at the endoluminal aspect of the point where it is most invasive (or randomly, if there is none). The most important thing to keep in mind is to keep the exact same measurement location between examinations. Figure 8 provides an example of tumour depth angle measurements and their significance—residual tumour focus grows into the lumen of the scar at second assessment, elevating pivot for angle measurement. Although it creates a sulc beside it, the scar as a whole "opens up". Please note that these results come from a single institution and have not yet been validated prospectively [56].

Fig. 9 Scar depth angle and thickness measurements should be performed on the axial central slice of the tumour. For scar depth angle measurements of small (< 180°) tumour scars, the endoluminal centre of the scar serves as pivot while the angle lines cross the endoluminal extremities of the scar (in blue). In > 180° scars, the pivot should also be central but the angle lines should cross the endoluminal aspect of the scar at 180° of the rectal circumference and no more than that. The same applies to circumferential scars but in such cases, the pivot should be placed at the most invasive tumour front if there is one, or randomly if there isn't. The most important thing to keep in mind is measuring at the exact same location in both first and second post-NAT MR imaging examinations. Scar thickness should be measured at pivot level, at the second MR imaging assessment. Measurement corresponds to a line that transverses tumour scar in depth, perpendicularly to it (in yellow), from inner to outer surface, irrespectively of it signal intensity

2. Scar thickness > 10 mm at 2nd MR imaging assessment.

For patients who enroll W&W, a scar thickness > 10 mm in the first follow-up examination (median

23 weeks post-RT) was > 90% specific for a non-sustained complete response, irrespective of other findings, according to the results of the same study as above [56]. Tumour scar thickness measurement should be performed at pivot level and corresponds to the in-depth measurement of the tumour bed, perpendicularly to it, from its inner to outer surface (Fig. 9) (Case in Fig. 8 also presents with scar thickness > 10 mm at 2nd assessment).

Question 3: How do we spot a rectal local regrowth?

In upfront clinical complete responders, we may expect a bit of scar "contraction" and/or scar "thinning" over time [56] but overall, patient preparation and acquisition technique assured, stable MR imaging findings are good MR imaging findings. Any change, even if subtle, should be reported but we should always make sure, before interpreting the findings, that no endoscopic procedures like biopsy, mucosectomy or local excision were performed given their potential false positive results. Subtle changes may include:

1. *Scar thickening* Scar thickening may be the first hint to a local regrowth and may present before any other MR imaging or endoscopic signs of macroscopic tumour [56].
2. *Depth angle increase* Depth angle increase may also be present before any obvious signs of a local regrowth on MR imaging or endoscopy and in fact 1. and 2. may be observed together [56].

More obvious changes indicating a local regrowth are:

3. *Intermediate "tumour" signal intensity/heterogeneity* "de novo" *at tumour scar on T2-WI* An mrTRG of 5 should be given when intermediate "tumour" signal appears de novo at tumour bed on W&W follow-up.
4. *High signal intensity at high b value DWI* "de novo" A bright spot or area de novo at tumour bed may indicate tumour regrowth with high specificity at it is particularly important when observed in depth, because it will be out of the scope of endoscopy.

Question 4: How do we spot an extra-rectal local regrowth?

Extra-rectal local regrowth is uncommon (3%) [55]. Its early detection, whether in lymph nodes, extra-nodal tumour deposits or EMVI, is dependent on careful comparison with previous examinations.

1. *Conformation change*, such as apparently "sterilised" lymph nodes/tumour deposits that become rounder or more irregular.
2. *Increase in size*, which may be subtle and require zoomed-in measurement in multiple planes.
3. *Intermediate "tumour" signal intensity/heterogeneity on T2-WI* de novo.
4. *Focus/foci of high* signal *intensity on high b-value DWI* de novo.

It is important to state that not all extra-rectal pelvic recurrences are clear regrowths. Uncommonly, disease may emerge in lymph nodes classified as innocent upon staging or as extranodal tumour deposits in a location in which only fat/vessels were present before, so carefull evaluation of the whole pelvis is imperative (Fig. 10).

Question 5: Upon conversion of a "near-complete" response to a clinical complete response, is patient prognosis the same compared to upfront clinical complete responders?

It is important to state that the management for this group of patients is controversial. In the study by Simpson et al. [53], 63% of the "near-complete" responders evolved to a cCR within a median time of 8.5 months. Compared to upfront clinical complete responders, there was an increase in the local regrowth rate from 14 to 18% and the disease-free survival dropped from a median 60.5 to 33 months [53]. Hupkens et al. [52] reported a 90% conversion of "near-complete" responders at first assessment to a clinical complete response if given 6–12 additional weeks, but with an increase in local regrowth rate from 15.9 to 27.1%. No impact on OS was reported in either studies [52, 53]. The incidence of distant metastasis is higher in patients with local regrowth (17.8%) than in sustained complete responders (4.9%) [55]. In summary, late complete responses may come at the cost of a higher rate of local regrowths, which in turn may be associated with a higher incidence of metachronous metastases. Whether the latter result from upfront differences in tumour biology or as a consequence of an uncontrolled primary is not yet known.

Re-staging and follow-up reporting template

Our proposed re-staging and follow-up reporting template is shown in Fig. 11. Please keep in mind that it is a mere suggestion and has not been validated in a prospective and multi-institutional setting.

Compared to the re-staging report template provided by ESGAR [10], ours is more complex, time-consuming and cumbersome to use because it includes multiple methods reported for response assessment and also contemplates follow-up imaging after re-staging. It involves recording thickness, volume, depth angle and their variation compared to the previous examination, given its potential, unvalidated utility in the early prediction of a

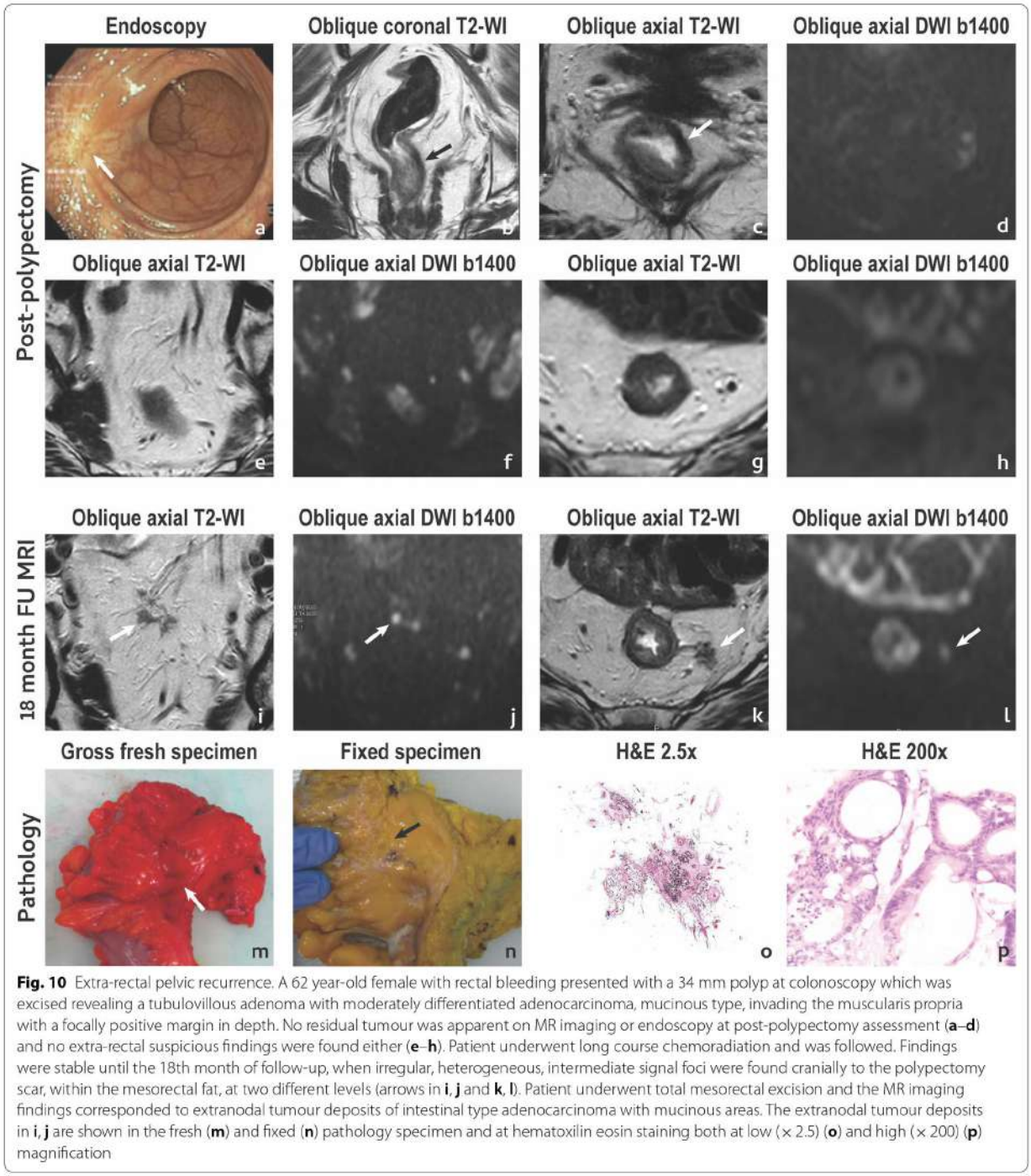

Fig. 10 Extra-rectal pelvic recurrence. A 62 year-old female with rectal bleeding presented with a 34 mm polyp at colonoscopy which was excised revealing a tubulovillous adenoma with moderately differentiated adenocarcinoma, mucinous type, invading the muscularis propria with a focally positive margin in depth. No residual tumour was apparent on MR imaging or endoscopy at post-polypectomy assessment (**a**–**d**) and no extra-rectal suspicious findings were found either (**e**–**h**). Patient underwent long course chemoradiation and was followed. Findings were stable until the 18th month of follow-up, when irregular, heterogeneous, intermediate signal foci were found cranially to the polypectomy scar, within the mesorectal fat, at two different levels (arrows in **i**, **j** and **k**, **l**). Patient underwent total mesorectal excision and the MR imaging findings corresponded to extranodal tumour deposits of intestinal type adenocarcinoma with mucinous areas. The extranodal tumour deposits in **i**, **j** are shown in the fresh (**m**) and fixed (**n**) pathology specimen and at hematoxilin eosin staining both at low (× 2.5) (**o**) and high (× 200) (**p**) magnification

non-sustained complete response, as discussed above. Also, our response assessment of the primary tumour is based on separate mrTRG, split scar sign and 3-point ordinal scale DWI evaluation, while ESGAR recommends using a 3-point combined T2-WI/DWI ordinal scale.

Conclusion

"Watch-and-Wait" rectal cancer programs are growing around the world and revolve around endoscopy and pelvic MR imaging, both for re-staging and patient follow-up. Radiologists involved in such programs should be

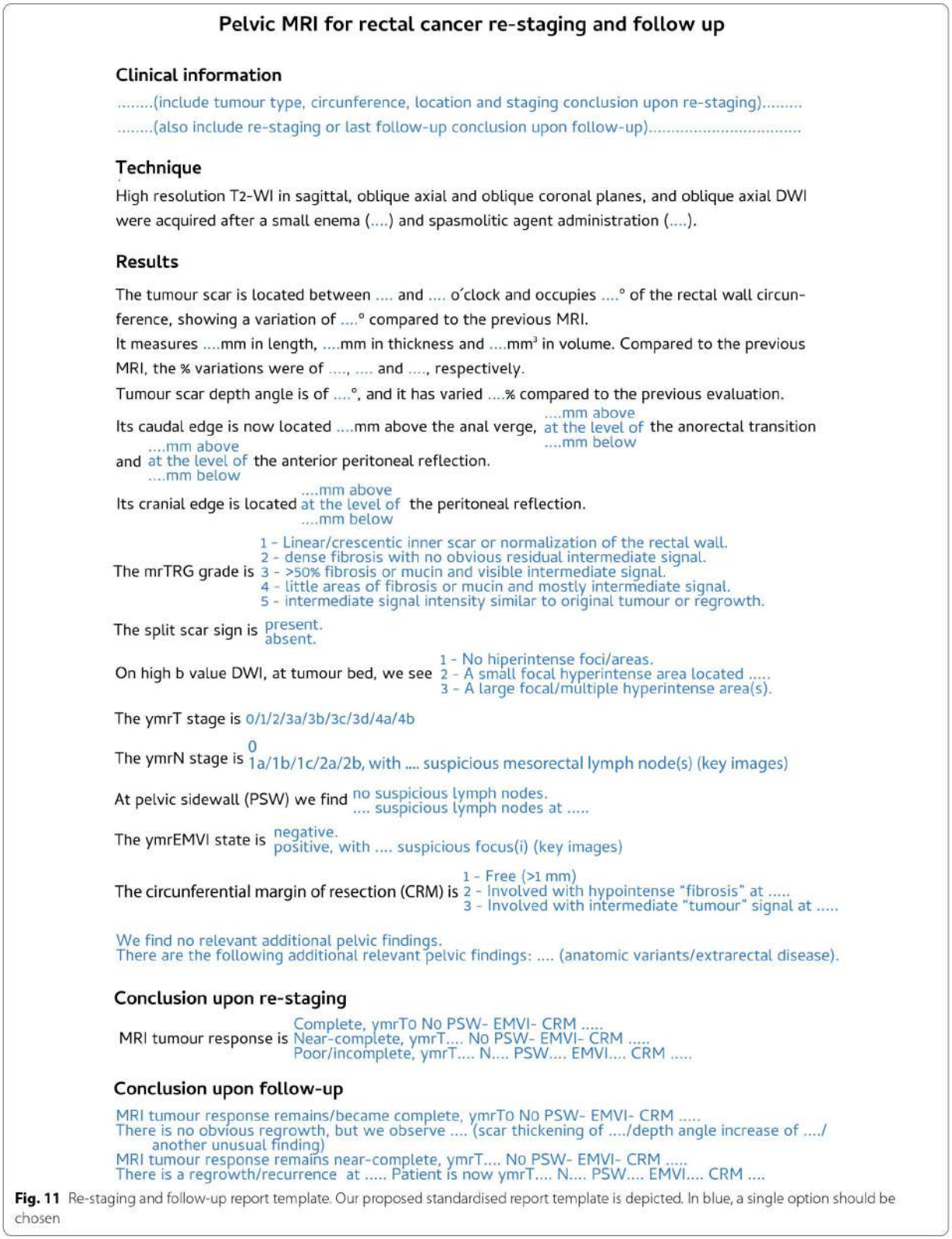

Pelvic MRI for rectal cancer re-staging and follow up

Clinical information

.....(include tumour type, circunference, location and staging conclusion upon re-staging).....

.....(also include re-staging or last follow-up conclusion upon follow-up).....

Technique

High resolution T2-WI in sagittal, oblique axial and oblique coronal planes, and oblique axial DWI were acquired after a small enema (....) and spasmolitic agent administration (....).

Results

The tumour scar is located between .... and .... o´clock and occupies ....° of the rectal wall circunference, showing a variation of ....° compared to the previous MRI.

It measures ....mm in length, ...mm in thickness and ....mm³ in volume. Compared to the previous MRI, the % variations were of ...., ... and ...., respectively.

Tumour scar depth angle is of ....°, and it has varied ....% compared to the previous evaluation.

Its caudal edge is now located ....mm above the anal verge, ...mm above / at the level of / ....mm below the anorectal transition and ....mm above / at the level of / ....mm below the anterior peritoneal reflection.

Its cranial edge is located ....mm above / at the level of / ....mm below the peritoneal reflection.

The mrTRG grade is
1 - Linear/crescentic inner scar or normalization of the rectal wall.
2 - dense fibrosis with no obvious residual intermediate signal.
3 - >50% fibrosis or mucin and visible intermediate signal.
4 - little areas of fibrosis or mucin and mostly intermediate signal.
5 - intermediate signal intensity similar to original tumour or regrowth.

The split scar sign is present. / absent.

On high b value DWI, at tumour bed, we see
1 - No hiperintense foci/areas.
2 - A small focal hyperintense area located .....
3 - A large focal/multiple hyperintense area(s).

The ymrT stage is 0/1/2/3a/3b/3c/3d/4a/4b

The ymrN stage is 0 / 1a/1b/1c/2a/2b, with .... suspicious mesorectal lymph node(s) (key images)

At pelvic sidewall (PSW) we find no suspicious lymph nodes. / .... suspicious lymph nodes at .....

The ymrEMVI state is negative. / positive, with .... suspicious focus(i) (key images)

The circunferential margin of resection (CRM) is
1 - Free (>1 mm)
2 - Involved with hypointense "fibrosis" at .....
3 - Involved with intermediate "tumour" signal at .....

We find no relevant additional pelvic findings.
There are the following additional relevant pelvic findings: .... (anatomic variants/extrarectal disease).

Conclusion upon re-staging

MRI tumour response is
Complete, ymrT0 N0 PSW- EMVI- CRM .....
Near-complete, ymrT.... N0 PSW- EMVI- CRM .....
Poor/incomplete, ymrT.... N.... PSW.... EMVI.... CRM .....

Conclusion upon follow-up

MRI tumour response remains/became complete, ymrT0 N0 PSW- EMVI- CRM .....
There is no obvious regrowth, but we observe .... (scar thickening of ..../depth angle increase of ..../another unusual finding)
MRI tumour response remains near-complete, ymrT.... N0 PSW- EMVI- CRM .....
There is a regrowth/recurrence at ..... Patient is now ymrT.... N.... PSW.... EMVI.... CRM ....

Fig. 11 Re-staging and follow-up report template. Our proposed standardised report template is depicted. In blue, a single option should be chosen

familiar with the imaging findings that suggest a poor/incomplete response, a complete response or a "near-complete" response and their prognostic implications. They should also be equipped for the early detection of local regrowths, in depth at tumour bed or extra-rectal in particular, given their invisibility at rectoscopy.

Abbreviations

CRM: Circumferential resection margin; DWI: Diffusion-weighted imaging; EMVI: Extramural venous invasion; MR: Magnetic resonance; mrTRG: Magnetic resonance tumour regression grade; mr-vTRG: Magnetic resonance venous tumour regression grade; NAT: Neoadjuvant therapy; pCR: Pathologic complete response; RT: Radiotherapy; W&W: Watch and Wait.

Acknowledgements

We are grateful to all staff composing the Imaging Department, the Colorectal Cancer Unit, and The Pathology Department of the Champalimaud Foundation. We would also like to thank Nuno Loução from Philips Healthcare (R) for the outstanding technical support.

Authors' contributions

IS designed and wrote the review. AG was responsible for the pathology image interpretation in figures. BR, MJB, NF, LF and CM revised the manuscript. All authors read and approved the final manuscript.

Funding

This research did not receive any specific grant from funding agencies in the public, commercial, or not-for-profit sectors.

Availability of data and materials

Not applicable.

Declarations

Ethics approval and consent to participate

Not applicable.

Consent for publication

Not applicable.

Competing interests

None of the authors have financial or non-financial competing interests to declare.

Author details

[1]Radiology Department, Champalimaud Foundation, Avenida Brasília, 1400-038 Lisbon, Portugal. [2]Nova Medical School, Campo Mártires da Pátria 130, 1169-056 Lisbon, Portugal. [3]Centro Hospitalar de Tondela-Viseu, EPE, Av. Rei Duarte, 3504-509 Viseu, Portugal. [4]Colorectal Surgery, Digestive Unit, Champalimaud Foundation, Avenida Brasília, 1400-038 Lisbon, Portugal. [5]Pathology Department, Champalimaud Foundation, Avenida Brasília, 1400-038 Lisbon, Portugal. [6]Radiation Oncology Department, Champalimaud Foundation, Avenida Brasília, 1400-038 Lisbon, Portugal.

Received: 28 April 2021 Accepted: 30 June 2021
Published online: 09 August 2021

References

1. Ali F, Keshinro A, Wesiser M (2020) Advances in the treatment of locally advanced rectal cancer. Ann Gastroenterol Surg 5(1):32–38
2. Glynne-Jones R, Wyrwicz L, Tiret E et al (2017) Rectal cancer: ESMO Clinical Practice Guidelines for diagnosis, treatment and follow-up. Ann Oncol 28(4):iv22–iv40
3. Lambregts D, Boellaard T, Beets-Tan R (2019) Response evaluation after neoadjuvant treatment for rectal cancer using modern MR imaging: a pictorial review. Insights Imaging 10(1):15
4. López-Campos F, Martín-Martín M, Fornell-Pérez R et al (2020) Watch and wait approach in rectal cancer: current controversies and future directions. World J Gastroenterol 26(29):4218–4239
5. Macchia G, Gambacorta M, Masciocchi C et al (2017) Time to surgery and pathologic complete response after neoadjuvant chemoradiation in rectal cancer: a population study on 2094 patients. Clin Transl Radiat Oncol 4:8–14
6. Maas M, Lambregts D, Nelemans P et al (2015) Assessment of clinical complete response after chemoradiation for rectal cancer with digital rectal examination, endoscopy, and MRI: selection for organ-saving treatment. Ann Surg Oncol 22:3873–3880
7. Wang Q, Zhang R, Xiao W et al (2021) The watch-and-wait strategy versus surgical resection for rectal cancer patients with a clinical complete response after neoadjuvant chemoradiotherapy. Radiat Oncol 16:16
8. Dossa F, Chesney TR, Acuna SA, Baxter NN (2017) A watch-and-wait approach for locally advanced rectal cancer after a clinical complete response following neo-adjuvant chemoradiation: a systematic review and meta-analysis. Lancet Gastroenterol Hepatol 2:501–513
9. Smith J, Strombom P, Chow O et al (2019) Assessment of a watch-and-wait strategy for rectal cancer in patients with a complete response after neo-adjuvant therapy. JAMA Oncol 5(4):e185896
10. Van Griethuysen J, Bus E, Hauptmann M et al (2018) Gas-induced susceptibility artefacts on diffusion-weighted MRI of the rectum at 1.5 T—effect of applying a micro-enema to improve image quality. Eur J Radiol 99:131–137
11. Gollub M, Arya S, Beets-Tan R et al (2018) Use of magnetic resonance imaging in rectal cancer patients: Society of Abdominal Radiology (SAR) rectal cancer disease-focused panel (DFP) recommendations 2017. Abdom Radiol (NY) 43(11):2893–2902
12. Beets-Tan R, Lambregts D, Maas M et al (2018) Magnetic resonance imaging for clinical management of rectal cancer: updated recommendations from the 2016 European Society of Gastrointestinal and Abdominal Radiology (ESGAR) consensus meeting. Eur Radiol 28:1465–1475
13. Slater A, Halligan S, Taylor SA, Marshall M (2006) Distance between the rectal wall and mesorectal fascia measured by MRI: effect of rectal distension and implications for preoperative prediction of a tumour-free circumferential resection margin. Clin Radiol 61:65–70
14. Dal Lago A, Minetti AE, Biondetti P, Corsetti M, Basilisco G (2005) Magnetic resonance imaging of the rectum during distension. Dis Colon Rectum 48:1220–1227
15. Goodman K (2016) Timing is everything: what is the optimal duration after chemoradiation for surgery for rectal cancer? J Clin Oncol 34:3724–3728
16. Figueiredo N, Panteleimonitis S, Popeskou S et al (2018) Delaying surgery after neoadjuvant chemoradiotherapy in rectal cancer has no influence in surgical approach or short-term clinical outcomes. Eur J Surg Oncol 44(4):484–489
17. Habr-Gama A, Sabbaga J, Gama-Rodrigues J et al (2013) Watch and wait approach following extended neoadjuvant chemoradiation for distal rectal cancer: are we getting closer to anal cancer management? Dis Colon Rectum 56(10):1109–1117
18. Bhoday J, Balyasnikova S, Wale A, Brown G (2017) How should imaging direct/orient management of rectal cancer? Clin Colon Rectal Surg 30:297–312
19. Nougaret S, Rouanet P, Molinari N et al (2012) MR volumetric measurement of low rectal cancer helps predict tumor response and outcome after combined chemotherapy and radiation therapy. Radiology 263(2):409–418
20. Kim Y, Kim D, Kim T et al (2005) Usefulness of magnetic resonance volumetric evaluation in predicting response to preoperative concurrent chemoradiotherapy in patients with resectable rectal cancer. Int J Radiat Oncol Biol Phys 62(761–768):1
21. Barbaro B, Fiorucci C, Tebala C et al (2009) Locally advanced rectal cancer: MR imaging in prediction of response after preoperative chemotherapy and radiation therapy. Radiology 250:730–739
22. Dresen R, Beets G, Rutten H et al (2009) Locally advanced rectal cancer: MR imaging for restaging after neoadjuvant radiation therapy with

concomitant chemotherapy. Part I. Are we able to predict tumor confined to the rectal wall? Radiology 252:71–80
23. Patel U, Brown G, Rutten H et al (2012) Comparison of magnetic resonance imaging and histopathological response to chemoradiotherapy in locally advanced rectal cancer. Ann Surg Oncol 19(09):2842–2852
24. Martens M, van Heeswijk M, van den Broek J et al (2015) Prospective, multicenter validation study of magnetic resonance volumetry for response assessment after preoperative chemoradiation in rectal cancer: can the results in the literature be reproduced? Int J Radiat Oncol Biol Phys 93(5):1005–1014
25. Shihab O, Taylor F, Salerno G et al (2011) MRI predictive factors for long-term outcomes of low rectal tumours. Ann Surg Oncol 18(12):3278–3284
26. Patel U, Taylor F, Blomqvist L et al (2011) Magnetic resonance imaging-detected tumor response for locally advanced rectal cancer predicts survival outcomes: MERCURY experience. J Clin Oncol 29:3753–3760
27. Fayaz M, Demian G, Fathallah W et al (2016) Significance of magnetic resonance imaging-assessed tumor response for locally advanced rectal cancer treated with preoperative long-course chemoradiation. J Glob Oncol 2(4):216–221
28. Sassen S, de Booij M, Sosef M et al (2013) Locally advanced rectal cancer: is diffusion weighted MRI helpful for the identification of complete responders (ypT0N0) after neoadjuvant chemoradiation therapy? Eur Radiol 23:3440–3449
29. Kim S, Lee J, Hong SH et al (2009) Locally advanced rectal cancer: added value of diffusion-weighted MR imaging in the evaluation of tumor response to neoadjuvant chemo and radiation therapy. Radiology 253:116–125
30. Song I, Kim SH, Lee SJ, Choi JY, Kim MJ, Rhim H (2012) Value of diffusion-weighted imaging in the detection of viable tumor after neoadjuvant chemoradiation therapy in patients with locally advanced rectal cancer: comparison with T2 weighted and PET/CT imaging. Br J Radiol 85:577–586
31. Lambregts D, Vandecaveye V, Barbaro B et al (2011) Diffusion-weighted MRI for selection of complete responders after chemoradiation for locally advanced rectal cancer: a multicenter study. Ann Surg Oncol 18:2224–2231
32. Lambregts D, Pizzi A, Maas M et al (2018) A pattern-based approach combining tumor morphology on mri with distinct signal patterns on diffusion-weighted imaging to assess response of rectal tumors after chemoradiotherapy. Dis Colon Rectum 61(3):328–337
33. Allen SD, Padhani AR, Dzik-Jurasz AS, Glynne-Jones R (2007) Rectal carcinoma: MRI with histologic correlation before and after chemoradiation therapy. AJR Am J Roentgenol 188(2):442–451
34. Heijnen L, Maas M, Beets-Tan R et al (2016) Nodal staging in rectal cancer: why is restaging after chemoradiation more accurate than primary nodal staging? Int J Colorectal Dis 31:1157–1162
35. Simha V, Kapoor R, Gupta R, Bahl A, Nada R (2014) Mucinous adenocarcinoma of the rectum: a poor candidate for neo-adjuvant chemoradiation? J Gastrointest Oncol 5(4):276–279
36. Santiago I, Figueiredo N, Parés O, Matos C (2020) MRI of rectal cancer—relevant anatomy and staging key points. Insights Imaging 11:100
37. Kim M, Hur B, Lee E et al (2018) Prediction of lateral pelvic lymph node metastasis in patients with locally advanced rectal cancer with preoperative chemoradiotherapy: focus on MR imaging findings. PLoS ONE 13(4):e0195815
38. Wong JS, Tan GH, Chia CS, Ong CA, Teo MC (2020) Management of synchronous lateral pelvic nodal metastasis in rectal cancer in the era of neoadjuvant chemoradiation: a systemic review. World J Gastrointest Surg 12(5):247–258
39. Chand M, Swift RI, Tekkis PP, Chau I, Brown G (2013) Extramural venous invasion is a potential imaging predictive biomarker of neoadjuvant treatment in rectal cancer. Br J Cancer. 110(1):19–25
40. Vliegen R, Beets G, Lammering GT et al (2008) Mesorectal fascia invasion after neoadjuvant chemotherapy and radiation therapy for locally advanced rectal cancer: accuracy of MR imaging for prediction. Radiology 246(2):454–462
41. Kulkarni T, Gollins S, Maw A, Hobson P, Byrne R, Widdowson D (2008) Magnetic resonance imaging in rectal cancer downstaged using neoadjuvant chemoradiation: accuracy of prediction of tumour stage and circumferential resection margin status. Colorectal Dis 10:479–489
42. Fokas E, Liersch T, Fietkau R et al (2014) Tumor regression grading after preoperative chemoradiotherapy for locally advanced rectal carcinoma revisited: updated results of the CAO/ARO/AIO-94 Trial. J Clin Oncol 32(15):1554–1562
43. Zhang J, Cai Y, Xie X et al (2020) Nomogram for predicting pathological complete response and tumor downstaging in patients with locally advanced rectal cancer on the basis of a randomized clinical trial. Gastroenterol Rep 8(3):234–241
44. Peng H, Wang C, Xiao W et al (2018) Analysis of Clinical characteristics to predict pathologic complete response for patients with locally advanced rectal cancer treated with neoadjuvant chemoradiotherapy. J Cancer 9(15):2687–2692
45. Curvo-Semedo L, Lambregts D, Maas M et al (2011) Rectal cancer: assessment of complete response to preoperative combined radiation therapy with chemotherapy—conventional MR volumetry versus diffusion-weighted MR imaging. Radiology 260(3):734–743
46. Sathyakumar K, Chandramohan A, Masih D, Jesudasan MR, Pulimood A, Eapen A (2016) Best MRI predictors of complete response to neoadjuvant chemoradiation in locally advanced rectal cancer. Br J Radiol 89(1060):20150328
47. Kang J, Kim Y, Kim H et al (2010) Tumor volume changes assessed by three-dimensional magnetic resonance volumetry in rectal cancer patients after preoperative chemoradiation: the impact of the volume reduction ratio on the prediction of pathologic complete response. Int J Radiat Oncol Biol Phys 76(4):1018–1025
48. Jang J, Choi S, Park S et al (2020) MR tumor regression grade for pathological complete response in rectal cancer post neoadjuvant chemoradiotherapy: a systematic review and meta-analysis for accuracy. Eur Radiol 30:2312–2323
49. Santiago I, Barata M, Figueiredo N et al (2019) The split scar sign as an indicator of sustained complete response after neoadjuvant therapy in rectal cancer. Eur Radiol 30(1):224–238
50. Van Heeswijk M, Lambregts D, Palm W et al (2017) DWI for assessment of rectal cancer nodes after chemoradiotherapy: is the absence of nodes at DWI proof of a negative nodal status? AJR Am J Roentgenol 208:W79–W84
51. Ogura A, Konishi T, Beets GL et al (2019) Lateral nodal features on restaging magnetic resonance imaging associated with lateral local recurrence in low rectal cancer after neoadjuvant chemoradiotherapy or radiotherapy. JAMA Surg 154(9):e192172
52. Hupkens B, Maas M, Martens M et al (2019) Organ preservation in rectal cancer after chemoradiation: should we extend the observation period in patients with a clinical near-complete response? Ann Surg Oncol 25(1):197–203
53. Simpson G, Hopley P, Wilson J et al (2020) Long-term outcomes of real world 'watch and wait' data for rectal cancer after neoadjuvant chemoradiotherapy. Colorectal Dis 22:1568–1576
54. Lynn P, Strombom P, Garcia-Aguilar J (2017) Organ-preserving strategies for the management of near-complete responses in rectal cancer after neoadjuvant chemoradiation. Clin Colon Rectal Surg 30(5):395–403
55. van der Valk M, Hilling D, Bastiaannet E et al (2018) IWWD Consortium. Long-term outcomes of clinical complete responders after neoadjuvant treatment for rectal cancer in the International Watch & Wait Database (IWWD): an international multicentre registry study. Lancet 391(10139):2537–2545
56. Santiago I, Barata MJ, Figueiredo N, Parés O, Matos C (2021) Early conformational changes at tumour bed and long term response after neoadjuvant therapy in locally-advanced rectal cancer. Eur J Radiol. 140:109742

Publisher's Note

5.2 Why is there a need to improve the early identification of sustained complete responders?

Current guidelines recommend rectal cancer response assessment to be based on endoscopy and MR imaging if organ-preservation is to be considered (1,2). Biopsies are not routinely employed, given, on one hand, the inherent sampling errors and, on the other hand, the false-positive cases due to the non-immediate process of tumour cell death after radiotherapy (3).

The endoscopic evaluation of residual mucosal abnormality was the earliest criterium used to identify patients with a complete response. Indeed, normalization of the mucosa on endoscopy is considered very specific (4-7). However, residual mucosal abnormalities are present in the majority (88– 89%) of unrecognized complete responders (3,8) and even in 61–74% of surgical specimens with a complete response. As such, many complete responses may be missed based on this method alone (8,9). Another limitation is that it does not allow in-depth scar or nodal disease observation having therefore the potential to, on the other side of the spectrum, miss residual disease in such locations (4).

Assessment of the relative proportion of intermediate signal intensity at the tumour bed on T2-weighted imaging (mrTRG or a variant) is the most widely accepted MR imaging method to assess response to neoadjuvant therapy. It has demonstrated the ability to predict patients' long-term survival in the MERCURY trial (10). However, according to the same research group, its specificity for pathologic complete response is relatively low (62.8%) and agreement with pathology is only fair (k = 0.24) (11). Its summary sensitivity and specificity for complete response are, according to a recent meta-analysis by Park *et al*, 0.49 (95%CI,0.33–0.65) and 0.86 (95%CI,0.74–0.93), respectively (12). Reported interobserver agreement is variable, ranging from poor to good, likely due to both the diverseness in assessment criteria and the heterogeneity of tumour response patterns (4,13-15). Adding diffusion-weighted imaging (DWI) to standard T2-weighted MR imaging assessment improves accuracy and is recommended by all international guidelines, but this method is highly dependent on patient preparation, acquisition protocol and reader's experience (16-19).

Artificial intelligence tools are now trendy in radiology journals. Radiomics analysis of combined T2-weighted imaging, DWI and contrast-enhanced T1-weighted imaging of pre-treatment MR imaging, for instance, performed extremely well for the identification of complete response, with specificity of 0.89 and AuROC values of ≥ 0.94, in a series of 186 patients who underwent surgery as curative treatment (20). However, this and other similar promising methods still rely on time-consuming image segmentation by radiologists (conveying a selection bias for data analysis), are based on

complex and sometimes flawed statistical methods, and are still missing validation, particularly with adequate external datasets (21).

But perhaps even more important than to identify a complete response after neoadjuvant therapy is to predict whether that clinical complete response will be sustained over time. We know that regrowth will occur in roughly one fourth of cases (22) and is practically always salvageable with surgery, so in itself, it might not be a problem. However, Smith *et al* and Fernandez *et al* found an excess rate of distant metastases in these patients compared to sustained complete responders, of 36% vs 1% and 17.8% vs 4.9%, respectively. Whether a higher risk is already present at baseline or metastases emerge as a consequence of the uncontrolled primary tumour is not yet known (22,23). A combined morphologic and functional visual pattern approach based on T2-weighted and DWI MR imaging provided a positive predictive value and a specificity for a sustained complete response over time of 87% and 94%, respectively, in a series of 222 patients. However, mucinous tumours were excluded from the analysis and they may constitute up to 10% of all rectal cancer cases (25).

In summary, optimal management requires the early differentiation of rectal cancer patients who will need surgery for cure from those who will sustain a complete response. Standard assessment tools, namely endoscopy, mrTRG and DWI appear insufficient for that purpose (5,16,24). Driven by the need for new methods that may be applicable to all rectal cancer patients, including those with mucinous tumours, we hereby introduce 3 imaging biomarkers as original research.

References

1) Beets-Tan R, Lambregts D, Maas M et al. Magnetic resonance imaging for clinical management of rectal cancer: Updated recommendations from the 2016 European Society of Gastrointestinal and Abdominal Radiology (ESGAR) consensus meeting. Eur Radiol. 2018. 28(4):1465-1475.

2) Gollub M, Arya S, Beets-Tan R et al. Use of magnetic resonance imaging in rectal cancer patients: Society of Abdominal Radiology (SAR) rectal cancer disease-focused panel (DFP) recommendations. Abdom Radiol. 2017. 43(11):2893-2902.

3) Nahas S, Nahas C, Marques C et al. Pathologic complete response in rectal cancer: can we detect it? Lessons learned from a proposed randomized trial of watch-and- wait treatment of rectal cancer. Dis Colon Rectum. 2016. 59:255–263.

4) Bhoday J, Smith F, Siddiqui M et al. Magnetic resonance tumor regression grade and residual mucosal abnormality as predictors for pathological complete response in rectal cancer post-neoadjuvant chemoradiotherapy. Dis Colon Rectum. 2016. 59(10): 925–933.

5) Smith F, Wiland H, Mace A et al. Clinical criteria underestimate complete pathological response in rectal cancer treated with neoadjuvant chemoradiotherapy. Dis Colon Rectum. 2014. 57(3):311–315.

6) Smith F, Chang K, Sheahan K et al. The surgical significance of residual mucosal abnormalities in rectal cancer following neoadjuvant chemoradiotherapy. Br J Surg. 2012. 99:993–1001.

7) Smith F, Winter D. Watch and wait for rectal cancer: where are we really at? Colorectal Dis. 2014. 16:332–334.

8) Van der Sande ME, Beets G, Hupkens B et al. Response assessment after (chemo)radiotherapy for rectal cancer: why are we missing complete responses with MRI and endoscopy? Eur J Surg Oncol. 2018. S0748-7983(18):32017–32011.

9) Van der Valk M, Hilling D, Bastiaannet E et al. Long- term outcomes of clinical complete responders after neoadjuvant treatment for rectal cancer in the International Watch & Wait Database (IWWD): an international multicenter registry study. Lancet. 2018. 391(10139):2537–2545.

10) Patel U, Taylor F, Blomqvist L et al. Magnetic resonance imaging–detected tumor response for locally advanced rectal cancer predicts survival outcomes: MERCURY experience. J Clin Oncol. 2011. 29(28):3753–3760.

11) Sclafani F, Brown G, Cunningham D et al. Comparison between MRI and pathology in the assessment of tumor regression grade in rectal cancer. Br J Cancer. 2017. 21:1–8

12) Park S, Cho S, Choi S et al. MRI Assessment of Complete Response to Preoperative Chemoradiation Therapy for Rectal Cancer: 2020 Guide for Practice from the Korean Society of Abdominal Radiology. Korean J Radiol. 2020. 21(7):812-828.

13) Sidiqui M, Gormly K, Bhoday J et al. Interobserver agreement of radiologists assessing the response of rectal cancers to preoperative chemoradiation using the MRI tumour regression grading (mrTRG). Clin Radiol. 2016. 71:854–862.

14) Yoen H, Park H, Kim S et al. Prognostic Value of Tumour Regression Grade on MR in Rectal Cancer: A Large-Scale, Single-Center Experience. Korean J Radiol. 2020. 10.3348.

15) Nagtegaal I, Glynne-Jones R. How to measure tumour response in rectal cancer? An explanation of T discrepancies and suggestions for improvement. Cancer Treat Rev. 2020. 84:101964.

16) Sassen S, de Booij M, Sosef M et al. Locally advanced rectal cancer: is diffusion weighted MRI helpful for the identification of complete responders (ypT0N0) after neoadjuvant chemoradiation therapy? Eur Radiol. 2013. 23:3440–3449.

17) Kim S, Lee J, Hong S et al. Locally advanced rectal cancer: added value of diffusion-weighted MR imaging in the evaluation of tumor response to neoadjuvant chemo and radiation therapy. Radiology. 2009. 253:116–125.

18) Song I, Kim S, Lee S et al. Value of diffusion-weighted imaging in the detection of viable tumor after neoadjuvant chemoradiation therapy in patients with locally-advanced rectal cancer: comparison with T2 weighted and PET/CT imaging. Br J Radiol. 2012. 85:577–586.

19) Lambregts D, Vandecaveye V, Barbaro B et al. Diffusion- weighted MRI for selection of complete responders after chemoradiation for locally advanced rectal cancer: a multicenter study. Ann Surg Oncol. 2011. 18:2224–2231.

20) Cui Y, Yang X, Shi Z et al. Radiomics analysis of multiparametric MRI for prediction of pathological complete response to neoadjuvant chemoradiotherapy in locally advanced rectal cancer. Eur Radiol. 2018. 29(3):1211–1220.

21) Moreira J, Santiago I, Santinha J et al. Challenges and Promises of Radiomics for Rectal Cancer. Curr Colorectal Cancer Rep. 2019. 15:175–180.

22) Smith J, Strombom P, Chow O, et al. Assessment of a watch-and-wait strategy for rectal cancer in patients with a complete response after neoadjuvant therapy. JAMA Oncol. 2019. 5(4):e185896.

23) Fernandez L, São Julião G, Figueiredo N et al Conditional recurrence-free survival of clinical complete responders managed by watch and wait after neoadjuvant chemoradiotherapy for rectal cancer in the International Watch & Wait Database: a retrospective, international, multicentre registry study. Lancet Oncol. 2021. 22(1):43-50.

24) Ryan J, Warrier S, Lynch A et al. Assessing pathological complete response to neoadjuvant chemoradiotherapy in locally advanced rectal cancer: a systematic review. Colorectal Dis. 2015. 17:849–861.

25) Lambregts D, Delli Pizzi A, Lahaye M et al. A pattern-based approach combining tumor morphology on mri with distinct signal patterns on diffusion-weighted imaging to assess response of rectal tumors after chemoradiotherapy. Dis Colon Rectum 2018. 61(3): 328–337.

5.3. The split scar sign as an indicator of sustained complete response after neoadjuvant therapy in rectal cancer

European Radiology (2020) 30:224–238
https://doi.org/10.1007/s00330-019-06348-9

GASTROINTESTINAL

Check for updates

The split scar sign as an indicator of sustained complete response after neoadjuvant therapy in rectal cancer

Inês Santiago[1,2] · Maria Barata[1] · Nuno Figueiredo[3] · Oriol Parés[4] · Vanessa Henriques[5] · António Galzerano[5] · Carlos Carvalho[6] · Celso Matos[1] · Richard J. Heald[3]

Received: 6 April 2019 / Revised: 11 June 2019 / Accepted: 27 June 2019 / Published online: 26 July 2019

Abstract

Objectives To measure the diagnostic performance of a new radiologic pattern on restaging magnetic resonance (MR) high-resolution T2-weighted imaging (T2-WI)—the split scar sign—for the identification of sustained complete response (SCR) after neoadjuvant therapy in rectal cancer.

Methods Institutional review board approval was obtained for this retrospective study and the informed consent requirement was waived. Fifty-eight consecutive patients with rectal cancer who underwent neoadjuvant therapy were enrolled. Two radiologists blindly and independently reviewed restaging pelvic MR imaging and recorded the presence/absence of the split scar sign (mrSSS). On a second round, they also assessed the relative proportion of intermediate signal intensity on T2-WI (mrT2) and of high signal intensity on high *b*-value diffusion-weighted imaging (mrDWI). Endoscopic response grading records were retrieved. Qui-square test was employed in search for associations between SCR, defined as pathologic complete response or long-term recurrence-free clinical follow-up, and mrSSS, mrT2, mrDWI and endoscopy. Interobserver agreement for imaging parameters was estimated using Cohen's kappa (*k*).

Results mrSSS was significantly associated with SCR, with specificity = 0.97/0.97, sensitivity = 0.52/0.64, PPV = 0.93/0.94, NPV = 0.73/0.78, and AuROC = 0.78/0.83, for observers 1/2, respectively. mrDWI was significantly associated with SCR for observer 2, with specificity = 0.76, sensitivity = 0.60, PPV = 0.65, NPV = 0.71, and AuROC = 0.69. mrT2 and endoscopy were not discriminative. Interobserver agreement was substantial for mrSSS ($k = 0.69$), moderate for mrDWI ($k = 0.46$), and poor for mrT2 ($k = 0.17$).

Conclusion The split scar sign is a simple morphologic pattern visible on restaging T2-WI which, although not sensitive, is very specific for the identification of sustained complete responders after neoadjuvant therapy in rectal cancer.

Key Points

- *The split scar sign is a morphologic pattern visible on high-resolution T2-weighted MR imaging in rectal cancer patients after neoadjuvant therapy. It therefore does not require any changes to standard protocol.*
- *At first restaging pelvic MR imaging (mean: 9.1 weeks after the end of radiotherapy), the split scar sign identified patients who sustained a complete response with very high specificity (0.97) and positive predictive value (0.93–0.94).*
- *The split scar sign has the potential to improve patient selection for "watch-and-wait" after neoadjuvant therapy in rectal cancer.*

Keywords Rectal neoplasms · Neoadjuvant therapy · Watchful waiting · Magnetic resonance imaging

✉ Inês Santiago
ines.santiago@neuro.fchampalimaud.org

[1] Radiology Department, Champalimaud Foundation, Avenida Brasília, 1400-038 Lisbon, Portugal

[2] Nova Medical School, Campo Mártires da Pátria 130, 1169-056 Lisbon, Portugal

[3] Colorectal Surgery, Digestive Unit, Champalimaud Foundation, Avenida Brasília, 1400-038 Lisbon, Portugal

[4] Radiation Oncology Department, Champalimaud Foundation, Avenida Brasília, 1400-038 Lisbon, Portugal

[5] Pathology Department, Champalimaud Foundation, Avenida Brasília, 1400-038 Lisbon, Portugal

[6] Medical Oncology, Digestive Unit, Champalimaud Foundation, Avenida Brasília, 1400-038 Lisbon, Portugal

Eur Radiol (2020) 30:224–238

Abbreviations

mrDWI	Relative proportion of high signal intensity on high *b*-value diffusion-weighted images (≤25% vs >25%)
mrSSS	Split scar sign
mrT2	Relative proportion of intermediate signal intensity on T2-WI (≤25% vs >25%)
SCR	Sustained complete response

Introduction

Total mesorectal excision, as proposed by Heald et al in 1982, is now standard surgery for rectal cancer patients and contributed to an increase in 5-year survival rates from 30% to 68% and to a decrease in local recurrence from 40% to less than 5% [1]. However, the morbidity of standard radical surgery is around one quarter, with over a third of patients reporting consequent urologic or sexual dysfunction and/or fecal incontinence [2, 3]. A series of landmark clinical trials support the use of neoadjuvant radiation to further improve oncologic outcomes in high-risk patients. It leads to a variable percentage of pathologic complete responses (pCR), ranging from 10 to 40% for long-course chemoradiation and 8–9% for short-course radiotherapy when surgery is performed 4–8 weeks after the end of radiotherapy [4–12]. The need for radical surgery in such patients with no evidence of residual disease has been questioned, and a non-operative, "watch-and-wait" approach is now established policy in certain dedicated centers worldwide [13]. This approach demands a strict surveillance protocol based on clinical evaluation, endoscopy and imaging. Systematic reviews have shown similar outcomes in those spared operation to those undergoing radical surgery [14–16]. Complete responders in both groups enjoy much improved oncological outcomes, demonstrating that an excellent response to neoadjuvant therapy is a favorable prognostic feature in itself.

The need to select patients for "watch-and-wait" has generated different response assessment protocols. The clinical and endoscopic evaluation of residual mucosal abnormality was the earliest criterion used to identify patients with a complete response, but it does not allow in-depth scar or nodal disease observation [17]. Furthermore, up to 74% of patients with pCR still show residual mucosal abnormality [18]. Reliance on this would therefore miss many potential complete responses. Assessment of the relative proportion of intermediate signal intensity at the tumor location on T2-WI, as a surrogate of persistent viable tumor, has demonstrated variable sensitivity and specificity values for the detection of complete response, ranging from 21.1% to 55% and 76% to 93%, respectively [19]. Adding diffusion-weighted imaging (DWI) to standard T2-WI assessment improves accuracy, but results vary depending on the reader's experience [20].

We describe here a pattern of tumor response after neoadjuvant therapy not previously reported. We call it the split scar sign (mrSSS), and we find it quick and easy to survey on standard T2-WI. Our purpose is to assess its diagnostic performance for the early identification of patients who will sustain a complete response after neoadjuvant therapy in rectal cancer.

Materials and methods

Study population and institutional setting

The institutional review board approved this retrospective study and waived patient informed consent requirement. All consecutive patients with pathologically proven rectal adenocarcinoma between 1/10/2012 and 1/3/2017 were retrieved from our prospectively organized rectal cancer database. Inclusion criteria were neoadjuvant therapy including radiation therapy; restaging pelvic MR imaging performed at our institution, including T2-WI and DWI; available histopathology results from surgery; and/or a minimum clinical follow-up period of >1 year for patients followed according to the "watch-and-wait" policy. Exclusion criteria were MR imaging artifacts precluding assessment and non-oncologic death or loss of follow-up before 1 year for patients on "watch-and-wait."

All patients were staged according to the TNM classification and discussed at the multidisciplinary team meeting. Staging was based on clinical examination, endoscopy and imaging (including thoracic CT and contrast-enhanced abdominal MR imaging/CT).

Criteria for neoadjuvant therapy were threatened or involved circumferential resection margin (mrCRM); mrT3c-d or mrT4a-b, regardless of mrN stage; tumor bordering the intersphincteric or distal total mesorectal excision plane; and/or extramural venous invasion (mrEMVI) [21]. When these criteria were applied, approximately one third of our patients were selected for immediate surgery and no neoadjuvant treatment.

Neoadjuvant long-course chemoradiation consisted of external beam volumetric modulated arc therapy (VMAT) with a dose of 45 Gy to elective pelvic fields, including an integrated boost of 54–56 Gy, for 25 consecutive days with concurrent capecitabine. Short-course radiotherapy with the same technique, with a dose of 5 × 5 Gy administered in 5 consecutive days, was employed in selected cases (stage IV at diagnosis or higher risk of systemic than local recurrence). Consolidation chemotherapy using capecitabine and oxaliplatin was employed in selected patients with high risk of systemic disease.

Data on patient demographics, clinical staging and restaging, type of surgery and histopathology, when operated, and follow-up were introduced in the prospectively organized

rectal cancer database by a physician uninvolved in imaging reading (NF). Major clinical responses based on clinical, endoscopic, and imaging assessment [22] were selected for "watch-and-wait" and reassessed every 12 weeks during the first year, every 16 weeks during the second year and every 6 months thereafter. Whenever tumor regrowth was suspected, elective surgery was proposed to the patient, except in a palliative setting or when clinically/technically contraindicated.

Imaging technique

Patients performed a small enema 20 min before acquisition (Microlax® 5 ml, Jaba Recordati). Intravenous butylscopolamine 20 mg was administered, except when contraindicated. Acquisitions were performed on one of two 1.5-T equipment (Achieva/Ingenia Philips Healthcare®). Acquisition parameters are presented in Table 1.

Imaging analysis

Examinations were blindly and independently analyzed on a picture archiving and communication system workstation (Philips Healthcare® Intellispace PACS DCX) by two gastrointestinal radiologists (observer 1: MJB, 13 years of experience, and observer 2: IS, 10 years of experience). Initially, observers analyzed staging pelvic MR imaging and recorded tumor location, mrT, mrN, mrEMVI, and mrCRM [22]. Post-neoadjuvant pelvic MR imaging examinations, acquired with a mean interval of 9.1 weeks after the end of radiotherapy (minimum = 5 weeks; maximum = 19 weeks), were analyzed in confrontation with staging images, randomly and in 2 rounds, with a 2-week interval, to minimize recall bias.

In the first round, observers assessed:

– *mrSSS*

The presence of the split scar sign (mrSSS+)—a radiologic sign observed on T2-WI and characterized by a particular morphologic pattern of the tumor scar (Fig. 1a)—was considered indicative of a SCR. It is characterized by the appearance of an inner regular and markedly hypointense layer corresponding to the fibrosed submucosa, either covered by normal mucosa or denuded, and an underlying layer of homogeneous intermediate signal intensity corresponding to a markedly thickened and fibrosis-infiltrated *muscularis propria*. A peripheral markedly hypointense layer of variable regularity and thickness may also be present, corresponding to perirectal fibrosis, particularly in tumors that are initially advanced. It may be absent, particularly in early ≤ T2 stages. In mucinous tumors, the intermediate signal intensity may be replaced with high signal intensity, corresponding to mucin pooling (Fig. 1b). A pierced appearance of the outer hypointense layer may be apparent whenever vascular structures extend in or out of the tumor scar (Fig. 1c), but neither the inner nor the outer hypointense layer (when present) should be bulged or breached by intermediate signal intensity, in which case the sign is considered absent (mrSSS−) (Fig. 1d). It is also considered absent (mrSSS−) whenever the scar is completely hypointense (Fig. 1e) or heterogeneous, with a "disorganized" appearance (Fig. 1f).

In the second round, they analyzed:

– *mrT2*

mrT2 was also observed on T2-WI, but it does not take into consideration the morphologic pattern of the scar. It rather relies

Table 1 Staging and restaging pelvic MR imaging acquisition parameters

Parameter	Oblique axial T2-weighted turbo spin-echo* (A/I)	Oblique coronal T2-weighted turbo spin-echo (A/I)	Sagittal T2-weighted turbo spin-echo (A/I)	Single-shot spin-echo echo-planar diffusion-weighted⁺ (A/I)
Echo time (ms)	120/85	120/100	120/100	69/90
Repetition time (ms)	3000/5692	3700/2000	4800/3102	2000/4288
Echo train length	21/18	24/16	18/21	–
Slice thickness (mm)	3/3	3/3	4/3	3/5
Gap (mm)	0.5/0.3	0.5/0.3	1/0.3	1/0
Matrix	248 × 242//416 × 465	248 × 234/200 × 179	180 × 160/252 × 223	124 × 124/76 × 65
Field of view (mm)	200 × 200/250 × 328	200 × 200/160 × 160	180 × 180/200 × 200	370 × 370/200 × 200
In-plane resolution (mm^2)	0.8 × 0.8/0.6 × 0.7	0.8 × 0.85/0.8 × 0.8	1 × 0.88/0.8 × 0.8	3 × 3/2.6 × 3.01
Signal averages	3/1	4/2	4/2	4/7

(A/I) 1.5 T Achieva/1.5 T Ingenia Philips Healthcare®

*Oblique axial scans were perpendicular to the long axis of the rectal wall at tumor location

⁺ Spectral pre-saturation with inversion recovery was utilized for fat saturation. *B* values of 0, 200, 500, and 1000 and 0 and 1400 s/mm^2 were employed for Achieva and Ingenia 1.5 T equipment, respectively

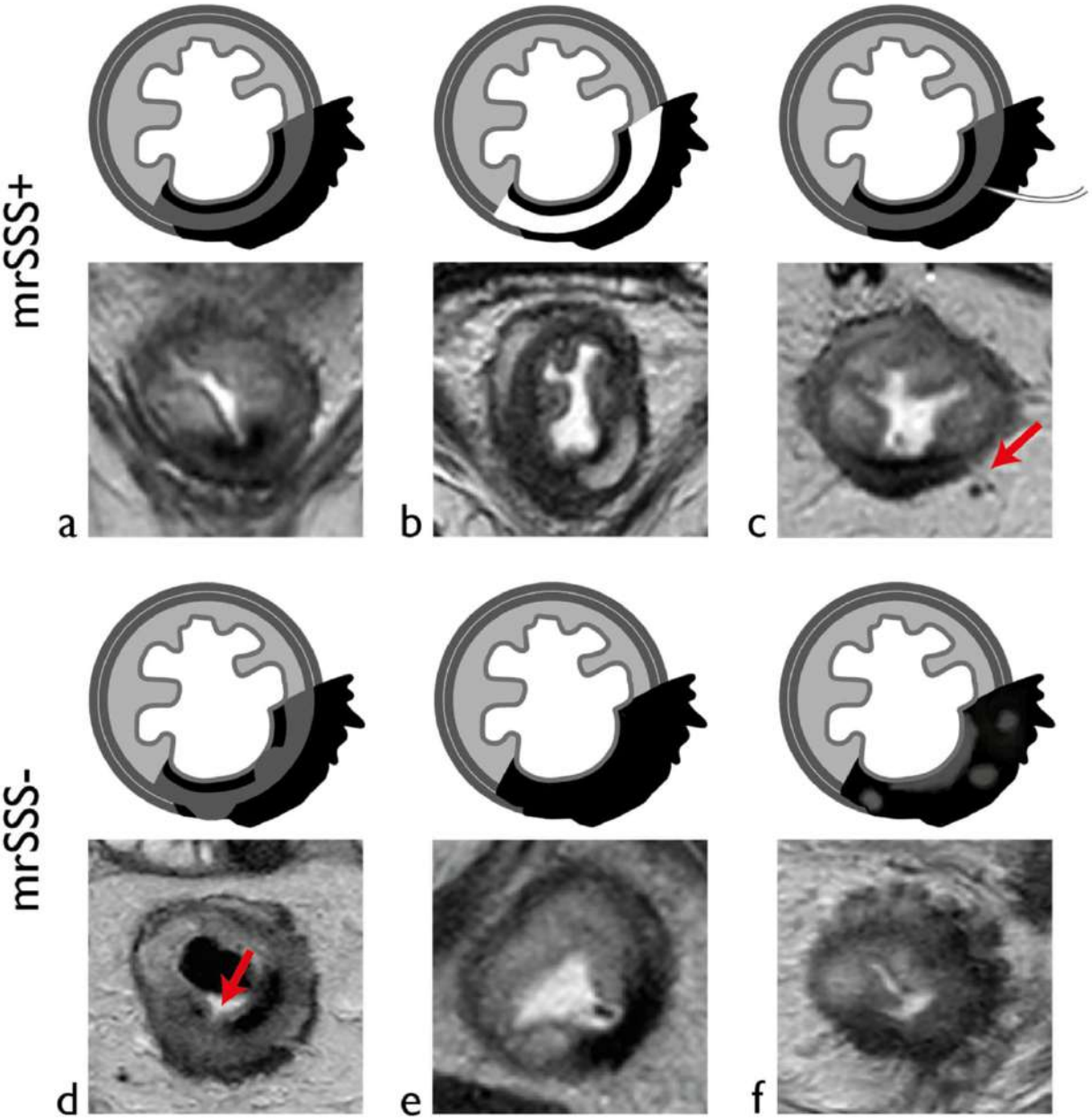

Fig. 1 Representative schemes and examples of positive (mrSSS+) and negative (mrSSS−) split scar sign cases. The split scar sign should be sought on high-resolution T2-WI. It is considered positive (mrSSS+) upon the presence of an inner, markedly T2-hypointense, regular layer of tissue at tumor location, corresponding to the fibrosed submucosa, covered by normal mucosa or denuded when ulceration is present; and a homogeneous intermediate signal intensity layer underneath it, corresponding to a markedly thickened and partially fibrotic *muscularis propria*. At the periphery, a T2-hypointense layer of variable regularity and thickness is usually apparent, translating perirectal fibrosis. It may, however, be absent, particularly in early-staged tumors (**a**). In mucinous tumors or tumors which respond with mucinous degeneration, the intermediate signal intensity may be replaced with high signal intensity, corresponding to mucin pooling (**b**). Vessels may pierce the outer hypointense layer in positive cases (arrow in **c**), but the sign is considered negative (mrSSS−) whenever the inner (arrow in **d**) or outer hypointense layers are bulged or breached by intermediate signal intensity, when the scar is homogeneously hypointense (**e**) or when the scar presents with a heterogeneous and disorganized appearance (**f**)

on the quantification of the relative proportion of intermediate signal intensity within it and is therefore an approximation to the MR tumor regression grade [23]. Cases with absent/minimal residual intermediate signal intensity on T2-WI (which would correspond to MR tumor regression grades (mrTRG) 1 and 2), were considered negative (mrT2−) and therefore likely sustained complete responders. Cases with a substantial proportion (> 25%) of intermediate signal or whenever tumor was

unchanged compared to baseline images (which would correspond to mrTRG3 to mrTRG5 [23]) were considered positive (mrT2+) and therefore likely non-sustained complete responders.

– *mrDWI*

mrDWI also does not take into consideration the morphologic pattern of the scar. It quantifies the relative surface area of high signal intensity in high-*b*-value DWI. Cases with absent/residual foci of high signal intensity on high-*b*-value images were considered negative (mrDWI−) and therefore indicative of a SCR. Cases with a substantial proportion of high signal intensity (> 25%) or tumor unchanged compared to staging images were considered positive (mrDWI+) and as likely non-SCR. Apparent diffusion coefficient (ADC) maps were interpreted side by side upon mrDWI classification, to aid in the differentiation between restricted diffusion and T2-shine through from luminal content.

Endoscopy

Endoscopy was performed upon patient restaging by a single dedicated surgeon (NF, 13 years of experience) according to a 5-point ordinal scale defined by the international "watch-and-wait" database consortium [22]. From the retrieved endoscopic records, responses graded as 0 (flat white scar with telangiectasia) or 1 (shallow ulcer/red scar) were considered Endo− and indicative of SCR, and responses graded as 2 (ulcerated residual lesion or adenomatous residual mucosal abnormality), 3 (excavated ulcer with elevated edges), or 4 (infiltrative lesion) were considered Endo+ and therefore indicative of a non-SCR.

Histopathology

Tumor p stage was retrieved from the pathology reports of patients who underwent surgery with curative intent, which were made according to the pTNM requirements from the 7th Edition of the College of American Pathologists.

Reference standard

The reference standard was SCR, defined as pathologic complete response or long-term local recurrence-free clinical follow-up (minimum follow-up period of 1 year).

Table 2 Clinical data on 58 patients with locally advanced rectal cancer who underwent neoadjuvant therapy

Variable	Total no. (%)	SCR no. (%)	Non-SCR no. (%)	*p* value*
Age (years)				1.00
< 60	29 (50%)	13 (45%)	16 (55%)	
≥ 60	29 (50%)	12 (41%)	17 (59%)	
Gender				1.00
Male	33 (57%)	14 (42%)	19 (58%)	
Female	25 (43%)	11 (44%)	14 (56%)	
Neoadjuvant treatment				1.00
Long-course chemoradiation	51(88%)	22 (43%)	29 (57%)	
Without consolidation CT	22 (39%)	14 (64%)	8 (36%)	
With consolidation CT	27 (47%)	13 (48%)	14 (52%)	
Short-course radiotherapy	7 (12%)	3 (43%)	4 (57%)	
Without consolidation CT	3 (5%)	1 (33%)	2 (67%)	
With consolidation CT	4 (7%)	3 (75%)	1 (25%)	
Surgery at any timepoint				< 0.01
Yes	34 (59%)	4 (12%)	30 (88%)	
LAR	21 (62%)	3 (14%)	18 (86%)	
APE	10 (29%)	0 (0%)	10 (100%)	
TEM	2 (6%)	1 (50%)	1 (50%)	
Col	1 (3%)	0 (0%)	1 (100%)	
No	24 (41%)	21 (88%)	3 (13%)	

CT, chemotherapy consolidation CT: chemotherapy administered after neoadjuvant therapy and before surgery if applicable

LAR low anterior resection, *APE* abdominoperineal excision, *TEM* transanal endoscopic microsurgery, *Col* derivative colostomy

*Pearson Qui-square test was employed except when Cochran's criteria were not met, in which case, Fisher's exact test was employed

Table 3 Initial staging tumor characteristics as defined retrospectively by the two observers on MR T2-WI and stratified by outcome

Variable	Total[a] no. (%)	SCR no. (%)	Non_SCR no. (%)	*p* value*	Total no. (%)	SCR no. (%)	Non_SCR no. (%)	*p* value*	
	Observer 1				Observer 2				IOA **
Location				0.79				0.79	0.85 ($p < 0.01$)
< 6 cm	27 (49%)	12 (44%)	15 (56%)		23 (42%)	9 (39%)	14 (61%)		
≥ 6 cm	28 (51%)	11 (39%)	17 (61%)		32 (58%)	14 (44%)	18 (56%)		
mrT				0.08				0.03	0.84 ($p < 0.01$)
≤ T3b	38 (69%)	19 (50%)	19 (50%)		34 (62%)	18 (53%)	16 (47%)		
≥ T3c	17 (31%)	4 (23%)	13 (77%)		21 (38%)	5 (24%)	16 (76%)		
mrN				0.73				0.35	0.23 ($p = 0.06$)
−	32 (58%)	14 (44%)	18 (56%)		20 (36%)	10 (50%)	10 (50%)		
+	23 (42%)	9 (39%)	14 (61%)		35 (64%)	13 (37%)	22 (63%)		
mrCMR				0.51				0.06	0.70 ($p < 0.01$)
−	39 (66%)	17 (45%)	21 (55%)		30 (55%)	16 (53%)	14 (47%)		
+	17 (31%)	6 (35%)	11 (65%)		25 (45%)	7 (28%)	18 (72%)		
mr EMVI				0.68				< 0.01	0.46 ($p < 0.01$)
−	44 (80%)	19 (43%)	25 (57%)		36 (66%)	20 (56%)	16 (44%)		
+	11 (20%)	4 (36%)	7 (64%)		19 (34%)	3 (16%)	16 (84%)		

Location represents distance to the anal verge. mrT represents T staging, ≤ mrT3b representing tumor extension of less than 5 mm into the mesorectal fat, and ≥ mrT3c representing tumor extension of 5 mm or more into the mesorectal fat and/or peritoneal and/or adjacent organ involvement [23]. mrN represents lymph node staging, one or more suspicious lymph nodes based on the ESGAR consensus meeting recommendations being considered N+ disease [24]. mrEMVI represents extramural venous invasion visible, intermediate signal in vessel lumen with slight vessel expansion, or irregular vessel contour being considered mrEMVI+[23]

*Pearson Qui-square test was employed except when Cochran's criteria were not met, in which case Fisher's exact test was employed

**Interobserver agreement was assessed using Cohen's kappa statistic

[a] In 3 cases, initial staging images were not available

Table 4 Results of the response assessment tools utilized to identify SCR at restaging pelvic MR imaging by the 2 observers

Variable	Total no. (%) Observer 1	SCR no. (%)	Non-SCR no. (%)	*p* value*	Total no. (%) Observer 2	SCR no. (%)	Non-SCR no. (%)	*p* value*	IOA**
	n (%)	*n* (%)	*n* (%)		*n* (%)	*n* (%)	*n* (%)		
mrT2				0.19				0.75	0.17 ($p = 0.12$)
−	31 (53%)	16 (52%)	15 (48%)		12 (21%)	6 (50%)	6 (50%)		
+	27 (47%)	9 (33%)	18 (67%)		46 (79%)	19 (41%)	27 (59%)		
mrDWI				0.18				< 0.01	0.46 ($p < 0.01$)
−	33 (57%)	17 (52%)	16 (48%)		23 (40%)	15 (65%)	8 (35%)		
+	25 (43%)	8 (32%)	17 (68%)		35 (60%)	10 (29%)	25 (71%)		
mrSSS				< 0.01				< 0.01	0.69 ($p < 0.01$)
+ (present)	14 (24%)	13 (93%)	1 (7%)		17 (29%)	16 (94%)	1 (6%)		
− (absent)	44 (76%)	12 (27%)	32 (73%)		41 (71%)	9 (22%)	32 (78%)		
Endoscopy[a]								0.59	
−	25 (47%)	13 (52%)	12 (48%)						
+	28 (53%)	12 (43%)	16 (57%)						

A negative classification (−) was considered indicative of a SCR for mrT2, mrDWI, and endoscopy. For the split scar sign (mrSSS), it was its presence (+) what was considered indicative of a SCR

*Pearson Qui-square test was employed except when Cochran's criteria were not met, in which case Fisher's exact test was employed

**Interobserver agreement was assessed using Cohens Kappa statistic

[a] Endoscopic records were unavailable in 5 patients

Table 5 Diagnostic performance of the response assessment tools for the identification of SCR at restaging pelvic MR imaging

Parameter	Observer	Sensitivity[CI]	Specificity[CI]	PPV[CI]	NPV[CI]	AuROC
mrSSS	*1*	*0.52[0.31–0.72]*	*0.97(0.84–1]*	*0.93[0.64–0.99]*	*0.73[0.64–0.80]*	*0.78[0.65–0.80]*
	2	*0.64[0.43–0.82]*	*0.97[0.84–1]*	*0.94[0.69–0.99]*	*0.78[0.68–0.86]*	*0.83[0.71–0.91]*
mrDWI	1	0.68[0.47–0.85]	0.51[0.34–0.69]	0.52[0.41–0.62]	0.68[0.52–0.80]	0.59[0.45–0.71]
	2	*0.60[0.39–0.79]*	*0.76[0.58–0.89]*	*0.65[0.49–0.79]*	*0.71[0.60–0.81]*	*0.69[0.55–0.80]*
mrT2	1	0.64[0.43–0.82]	0.55[0.36–0.72]	0.52[0.40–0.63]	0.67[0.52–0.79]	0.59[0.45–0.71]
	2	0.24[0.9–0.45]	0.82[0.65–0.93]	0.50[0.27–0.73]	0.59[0.52–0.65]	0.57[0.43–0.70]

Highlighted in italics are the diagnostic performance data on parameters in which there were statistically significant differences for the discrimination between SCR and non-SCR

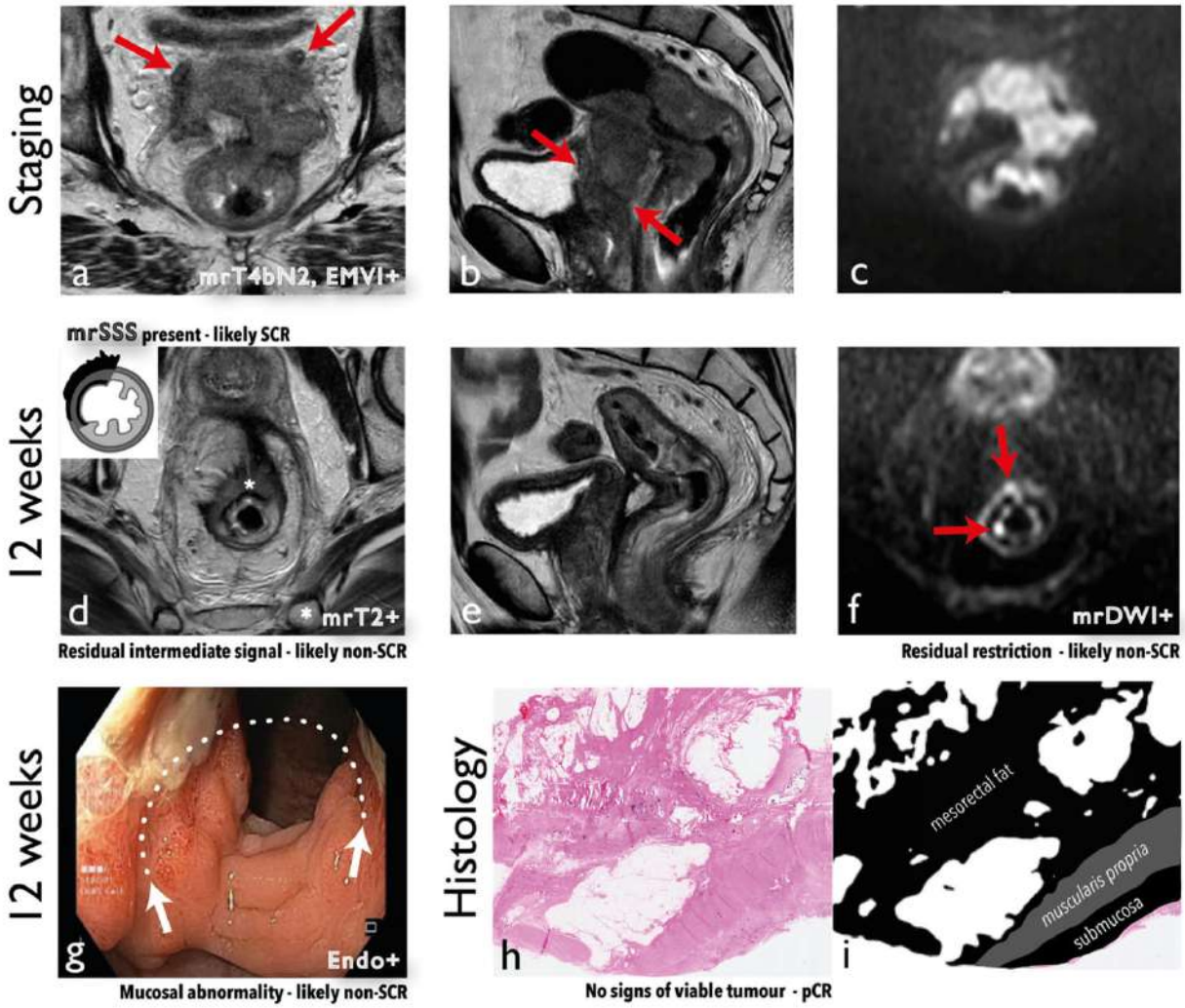

Fig. 2 57-year-old male patient with rectal adenocarcinoma. On staging MR imaging, tumor invaded the *vas deferens* (arrows in **a**), seminal vesicles and bladder (arrows in **b**) and the patient was staged as mrT4, mrN2, and mrEMVI+ (not shown). After long-course chemoradiation, marked tumor volume reduction was observed (**e**) but response was considered incomplete due to substantial intermediate signal on T2-WI (* in **d**); multiple foci of high signal intensity on DWI (arrows in **f**); and ulceration surrounded by adenomatous mucosal abnormality on endoscopy (between arrows in **g**). After resection, histopathology revealed a ypT0, ypN0, ypEMVI− specimen and the patient is currently disease-free, after 31 months of follow-up. In **h**, a hematoxylin & eosin-stained 4-μm cut slice through the tumor scar is depicted, and in **i**, a representative scheme of the same slice is shown. The split scar sign, clearly visible in **d**, translates into dense fibrosis in the submucosa (inner hypointense layer), markedly thickened *muscularis propria* (middle intermediate signal intensity layer), and dense fibrosis in the perirectal fat (outer hypointense layer, which, in this case, is markedly irregular)

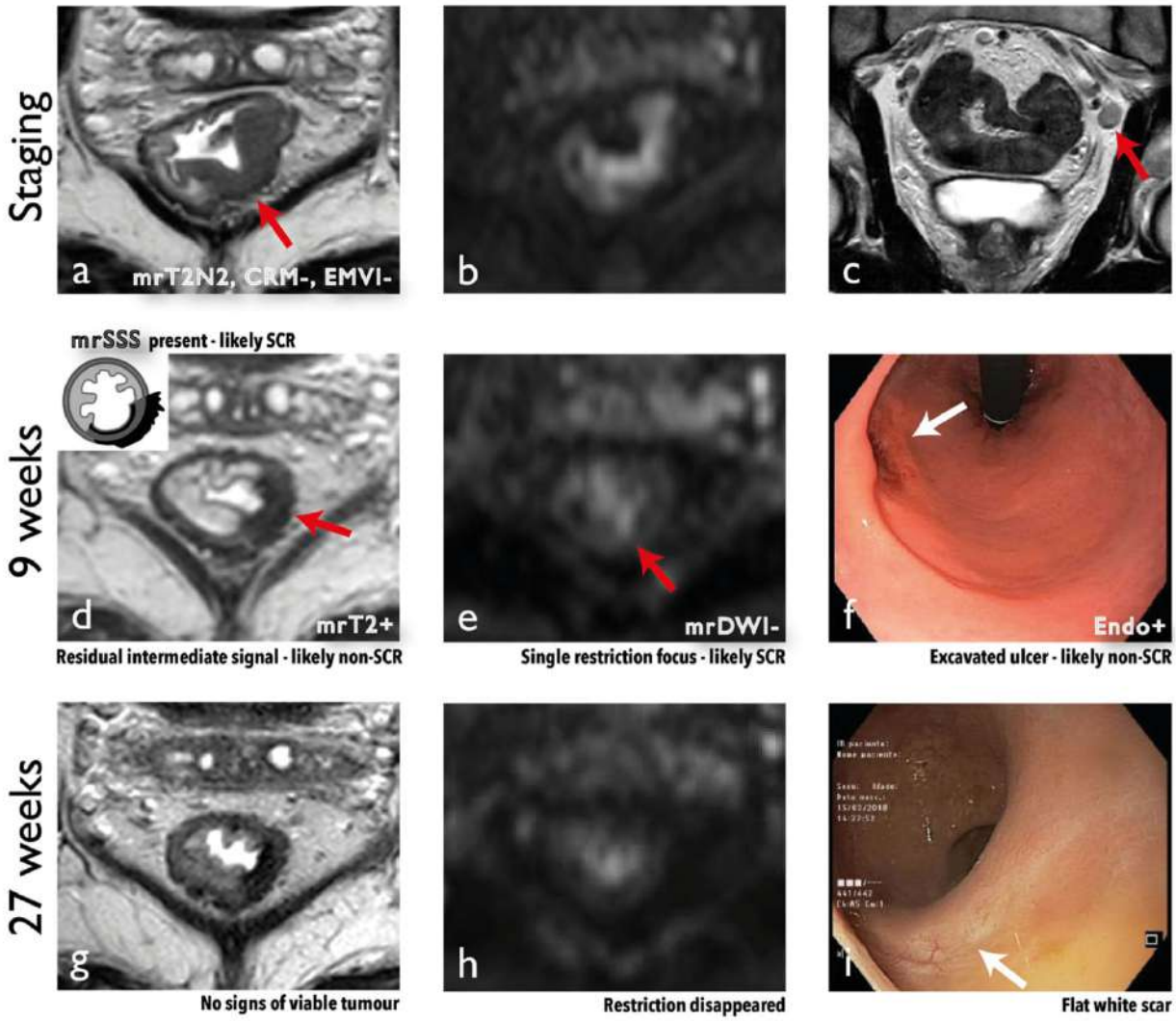

Fig. 3 A 58-year-old male patient with rectal cancer. Tumor was staged (**a**, **b**, **c**) as mrT2 (arrow in **a**), mrN2 involving the left lateral pelvic sidewall (arrow in **c**), mrCRM−, and mrEMVI−. The patient underwent long-course chemoradiation followed by consolidation chemotherapy. At the first reassessment, 9 weeks after the end of radiotherapy, the typical imaging pattern of mrSSS was present (arrow in **d**). Given substantial intermediate signal intensity was apparent, patients was classified as mrT2+ by both observers. There was a single focus of high signal intensity on high-*b*-value DWI within the scar, and the patient was considered mrDWI− (arrow in **e**). On endoscopy, a residual ulcerated lesion was apparent, and the patient was considered Endo+ (arrow in **f**). The patient was followed, and at 27 weeks, there were no signs of viable tumor at both lateral pelvic lymph node (not shown) and primary location on T2-WI or DWI (**g** and **h**, respectively). Residual ulcer had been replaced by a flat white scar with hovering telangiectasias on endoscopy (arrow in **i**). These findings were in accordance with a clinical complete response. The patient was followed, with no signs of local or distant disease recurrence up to date, 3.5 years after the end of radiotherapy

Statistical analysis

Data were recorded using an Excel spreadsheet (Microsoft Excel for Mac 011, version 14.2.1, Microsoft®) and analyzed using SPSS (version 23, IBM®). Qui-square test was employed in search of associations between SCR and mrSSS, mrT2, mrDWI, and endoscopy. Interobserver agreement for MR imaging parameters was estimated using Cohen's kappa statistic (0–0.20 = poor; 0.21–0.40 = fair; 0.41–0.60 = moderate; 0.61–0.80 = substantial; 0.81–1 = almost perfect).

Results

Study population characteristics

Complete data on 67 patients were retrieved from the database. Nine patients were excluded from the analysis: 7 due to susceptibility artifacts precluding evaluation of restaging DWI images, 1 due to loss to follow-up while on "watch-and-wait" before 1 year, and 1 due to non-oncologic death while on "watch-and-wait" before 1 year. Thus, 58 patients were

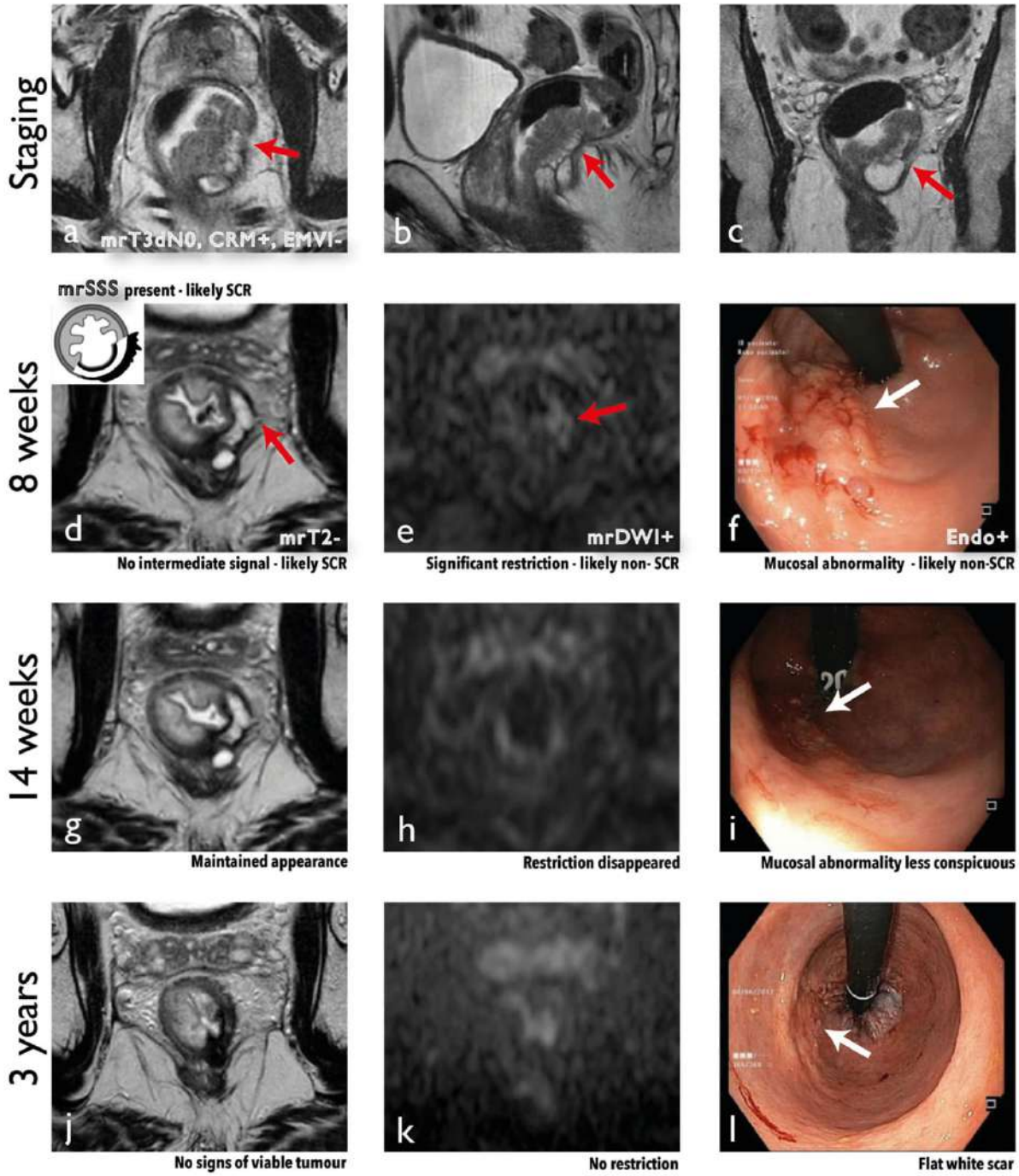

Fig. 4 A 68-year-old male patient with a mucinous rectal cancer staged as mrT3d mrN0, mrEMVI− and mrCRM+ due to involvement of the sphincteric complex (arrows in **a**, **b**, and **c**). The patient underwent neoadjuvant chemoradiation. At first reassessment, 8 weeks after the end of radiotherapy, response was considered mrT2− and mrSSS+ by both observers due to an absent intermediate signal intensity and a clear split scar sign (arrow in **d**), respectively. Some hyperintensity was still apparent within the scar on DWI and the patient was considered mrDWI+ (arrow in **e**). Adenomatous residual mucosal abnormality was apparent on endoscopy (endo+) (arrow in **f**). On the second follow-up, at 14 weeks, the appearance of the scar was the same on T2-WI (**g**), restriction to diffusion was no longer apparent (**h**), and mucosal abnormality was less conspicuous (arrow in **i**). On subsequent follow-ups, mucosal abnormality resolved and no signs of viable tumor were apparent. The patient enrolled in the "watch-and-wait" program and has so far completed 3 years of follow-up with no signs of local or distant disease recurrence. At last follow-up, the scar looked smaller and very hypointense on T2-WI (**j**), dark on DWI (**k**), and white and flat with hovering telangiectasias on endoscopy (arrow in **l**), in accordance with a clinical complete response

Eur Radiol (2020) 30:224–238

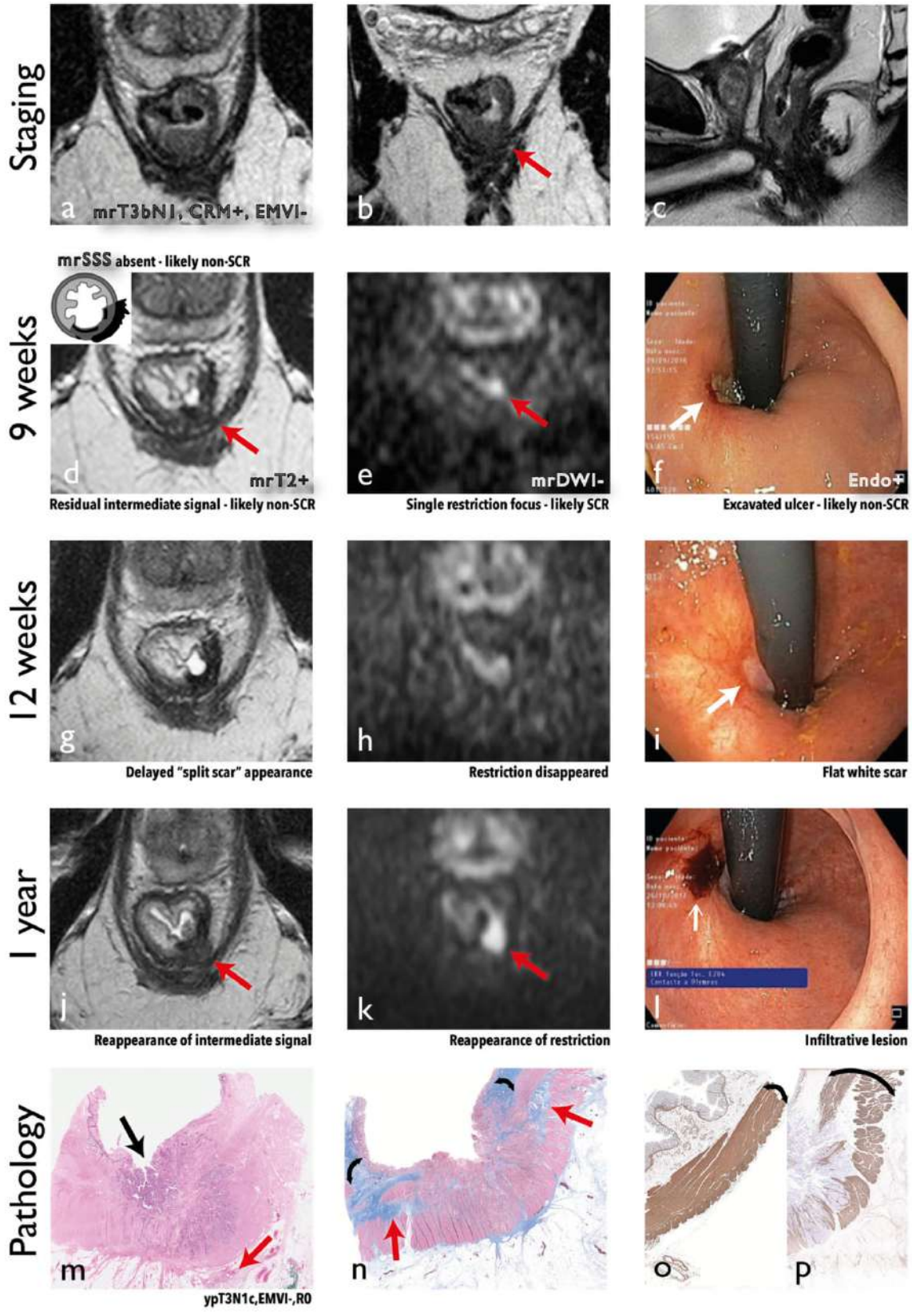

Fig. 5 A 62-year-old male patient with rectal cancer staged (**a**–**c**) as mrT3b abutting the left levator (arrow in **b**), mrN1, mrEMVI−. The patient underwent long-course chemoradiation and was assessed at 9 weeks (**d**–**f**). On T2-WI, substantial intermediate signal intensity was considered present (mrT2+) and mrSSS was considered negative (notice interruption of both hypointense layers (arrow in **d**)). On DWI, a single residual focus of high signal intensity was observed at the center of the scar (mrDWI−) (arrow in **e**), which corresponded to a fibrin-filled, excavated ulcer on endoscopy (arrow in **f**) (endo+). At 12 weeks, the tumor bed became layered, with a "split scar" appearance (**g**). No high signal intensity was observed on DWI (**h**), and the ulcer became flat (arrow in **i**). The patient was followed with no change, but at 1 year, a clear breach of the hypointense rims was again observed on T2-WI (arrow in **j**), extensive mural restriction to diffusion was present (arrow in **k**), and an infiltrative lesion became apparent on endoscopy (arrow in **l**). The patient underwent extralevator abdominoperineal resection, and pathology revealed a ypT3, ypN1c, ypEMVI−, R0 specimen. Histology using H&E (**m**) revealed the residual tumor extending from the ulcerated endoluminal aspect (black arrow) in depth to the mesorectal fat (red arrow). Masson's trichrome stain (**n**) depicts muscle and tumor in pink/red and collagen fibers in blue. Notice deep blue submucosa at the periphery of the tumor remnant (double curved arrow). It would correspond to the inner hypointense layer of the split scar sign, were it not clearly interrupted. When normal *muscularis propria* of the rectum (double curved arrow in **o**) is compared to the *muscularis propria* of the patient (double curved arrow in **p**) using desmin stain, marked thickening is observed, with a clear separation between inner circular and outer longitudinal layers in the latter and deposition of fibrosis (red arrows in **n**). This layer would correspond to the intermediate signal intensity layer of the split scar sign if tumor regrowth were absent. The patient is now disease-free, 17 months after the end of radiotherapy and 3 months after surgery

considered eligible (33 men and 25 women; mean age, 64.3 years; age range, 38–90 years). Three patients included in the analysis underwent surgery, had an incomplete response in the pathology specimen, and decided to be followed at other institutions. Mean follow-up for the remainder was 32.2 months (minimum = 12 months; maximum = 62 months). Patient clinical data are depicted in Table 2.

Out of our total of 58 patients, 25 (43%) presented with a SCR. Of these, 21 (84%) were patients on "watch-and-wait" who never underwent surgery; 2 (8%) were patients initially on "watch-and-wait" who presented with clinical signs of disease recurrence, underwent surgery but had a pCR; and 2 (8%) were patients who went straight to surgery and had pCR.

Of the 17 patients initially on "watch-and-wait" who presented with local persistence or regrowth, 16 (94%) were eligible for salvage surgery and went forward to an R0 resection. The R1 case, initially staged as mrT4, mrN2; mrCMR+; mrEMVI+, was judged a local regrowth 57 weeks after chemoradiation with symptoms of obstruction and invasion of the posterior margin of resection. Thirteen (22%) patients presented with distant metastatic disease, incidence being significantly lower ($p < 0.01$) for those who enrolled in "watch-and-wait" ($n = 4$ [31%] vs $n = 9$ [69%]). There were two oncologic deaths in our patient population, one in a patient with local and distant disease recurrence at 7 months after the end of radiotherapy who refused treatment and another in a patient presenting with synchronous multi-organ metastatic disease.

Out of the 33 non-SCRs, 30 underwent surgery and pathologic tumor regression grade (pTRG) records, based on the Dworak classification, were available in 28 of them: pTRG2 (dominant fibrotic changes with few tumor cells or groups) and pTRG1 (dominant tumor mass with obvious fibrosis and/or vasculopathy) predominated, comprising 35.7% and 32.1% of cases, respectively.

Staging tumor characteristics

Initial staging tumor characteristics, as assessed retrospectively by the two radiologists, are depicted in Table 3. In the initial staging MR imaging, no significant differences in tumor location or mrN stage were found between SCR and non-SCR, for both observers. For observer 2, there were statistically significant differences in mrT stage ($p = 0.03$), patients with stages ≤ mrT3b being more likely to present with SCR, and in mrEMVI, mrEMVI− patients being more likely to present with a SCR ($p < 0.01$). Interobserver agreement was almost perfect for tumor location ($k = 0.85$) and mrT stage ($k = 0.84$), substantial for mrCRM ($k = 0.70$), moderate for mrEMVI ($k = 0.46$), and fair for mrN staging ($k = 0.23$).

MR imaging analysis and endoscopy

Results of the MR imaging response assessment tools utilized are depicted in Table 4, as well as the results of endoscopic assessment. Significant differences between SCR and non-SCR were found for mrSSS ($p < 0.01$ for both observers). For observer 2, significant differences were also found for mrDWI ($p < 0.01$). No significant differences were found for mrT2 ($p = 0.19/0.75$ for observers 1/2) or endoscopy ($p = 0.59$). Agreement between observers was substantial for mrSSS ($k = 0.69$, $p < 0.01$), moderate for mrDWI ($k = 0.46$, $p < 0.01$), and poor for mrT2 ($k = 0.17$, $p = 0.12$). The diagnostic performance data on the imaging tools is presented in Table 5. For the identification of SCR and for observers 1/2, respectively, mrSSS presented with very high specificity (0.97 [95CI, 0.84–1]/0.97 [95CI, 0.84–1]) and PPV (0.93 [95CI, 0.64–0.99]/0.94 [95CI, 0.69–0.99]). Case examples of the split scar sign are depicted in Figs. 2, 3, and 4. Figures 5 and 6 depict examples of patients in which the split scar sign was absent who turned out to have persistent disease.

In 43 out of the 58 patients included in this study, mrSSS was also evaluated at the second timepoint after neoadjuvant therapy (mean interval from end of radiotherapy to MR imaging was 21 weeks; minimum = 10; maximum = 41). Sensitivity, specificity, PPV, and NPV for observers 1/2 were 0.68/0.72, 0.56/0.88, 0.68/0.90, and 0.56/0.70.

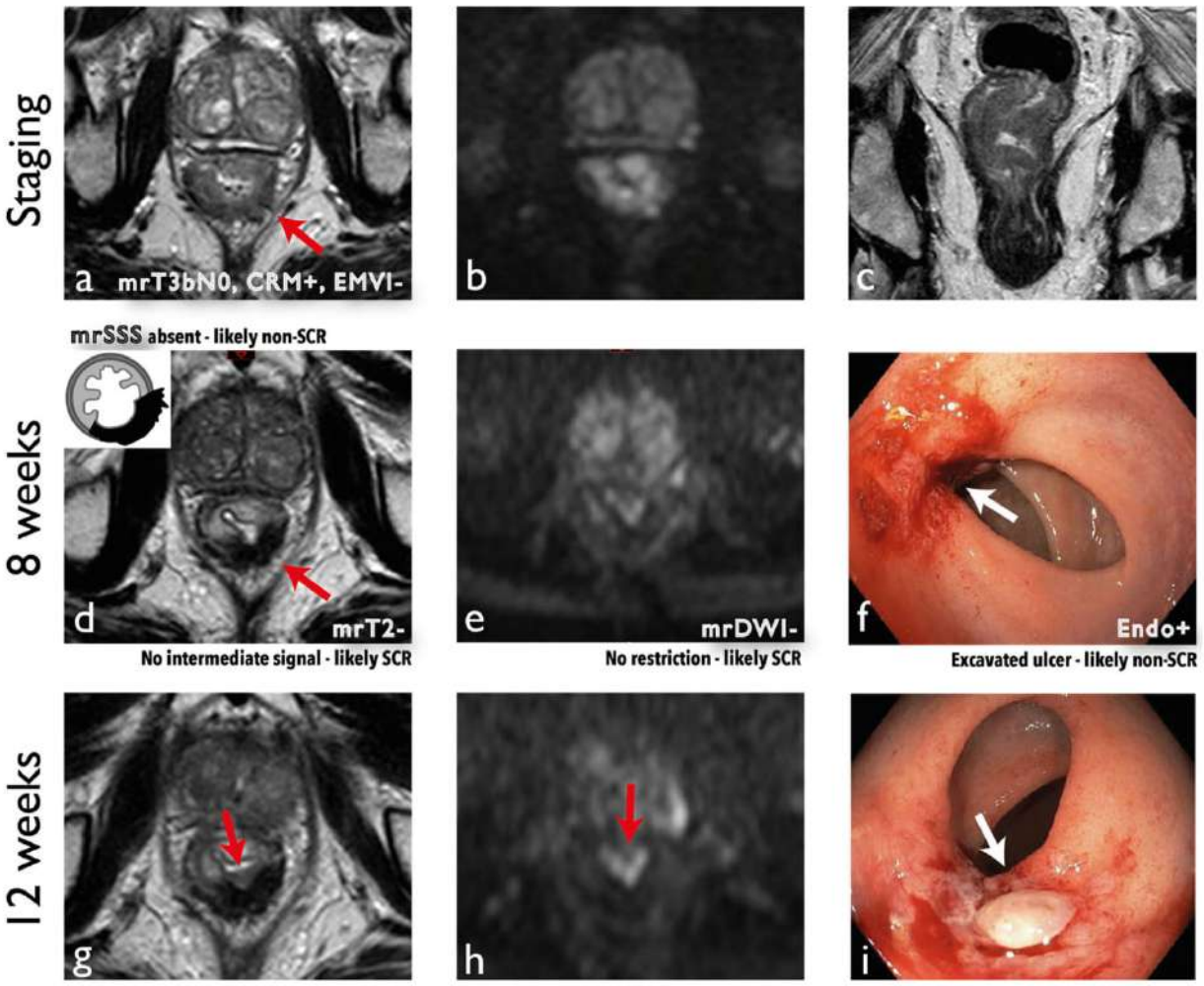

Fig. 6 A 76-year-old male patient with a similar low rectal cancer to the patient in Fig. 5, staged as T3b (arrow in **a**), N0, CRM+ and EMVI–. The patient underwent long-course chemoradiation and 8 weeks after (**d**–**f**), a black scar with no intermediate signal was apparent (mrT2−) (arrow in **d**) and the split scar sign was absent. No restriction to diffusion (mrDWI−) was observed, (**e**) but on endoscopy, an ulcerated residual lesion was visible (endo+) (arrow in **f**). The patient was again observed at 12 weeks (**g**–**i**) and on T2-WI, an endoluminal intermediate signal intensity regrowth was apparent (arrow in **g**). Restriction to diffusion was considered absent, given central star-shaped high signal intensity on high-*b*-value images is generally the result of luminal content (a pitfall) and was what was observed (**h**). On endoscopy, a fibrin-filled excavated ulcer with elevated edges was apparent, representing persistent disease, which was biopsy-confirmed

Discussion

In this study, we have focused on a unique morphologic pattern on MR T2-WI, which we named the split scar sign. The split scar sign is apparent at the first post-neoadjuvancy timepoint—the very time that the decision to operate is being made by the multidisciplinary team—and according to our results, it divides rectal cancer patients into 2 groups: those in which it is present, who have a 97% chance of achieving a SCR, and those in which it is absent, who have a 73–78% chance of failing to do so. Since the risk of regrowth is the most controversial aspect of the current controversies regarding "watch-and-wait," the existence of a single sign with such high specificity for SCR seems helpful to engage the MDT, and surgeons in particular, to accept surveillance as an option in rectal cancer management.

Conventional T2-WI-based assessment of response to neoadjuvant therapy relies on visual estimation of the relative proportion of intermediate signal intensity within the tumor scar. The value of this method to predict patients' long-term survival was established in the MERCURY trial [23]. However and according to the same group, its specificity for pCR is relatively low (62.8%) and agreement with pathology is fair ($k = 0.24$) [25]. Although series are not directly comparable due to the fact that our reference standard includes patients on clinical follow-up, our

results using this method seem to reflect these limitations, given no statistically significant differences between SCR and non-SCR were found. On the other hand, while visually estimating the relative proportion of high signal intensity on high-b-value DWI, differences between SCR and non-SCR were significant for one observer. These results may be in accordance with previously reported studies, in which DWI improved accuracy compared to standard T2-WI assessment [20, 24, 26, 27]. However, we did not combine the DWI and T2-WI assessment in our series so we cannot be sure. But rather than simple signal intensity proportion estimation, patterns of response, whether visual or computed, are being more and more frequently and successfully explored in rectal cancer. A combined morphologic and functional visual pattern approach, based on T2-WI and DWI respectively, improved NPV and sensitivity for residual tumor (equivalent to PPV and specificity for complete response) compared to previous studies, to 87% and 94%, respectively, in a series of 222 patients with non-mucinous tumors [28]. Radiomics analysis of combined T2-WI, DWI and contrast-enhanced T1-WI of pre-treatment MR performed extremely well for the identification of complete response, with specificity of 0.89 and AuROC values of ≥ 0.94, in another series of 186 patients who underwent surgery as curative treatment [29]. Ours is a simpler visual morphologic pattern approach, strictly based on restaging T2-WI, which was tested in both mucinous and non-mucinous tumors and in both operated and watch-and-wait patients. It has the advantages of bypassing the well-known artifacts and interpretation pitfalls of DWI [30] and the cumbersome image segmentation process of radiomics analysis [18].

Normalization of the mucosa on endoscopy is considered very specific for complete response [17, 18, 31, 32], but mucosal abnormalities are present in the majority (88–89%) of unrecognized complete responders [33, 34] and even in 61–74% of pCR surgical specimens [34, 35]. Biopsies are not routinely employed, given, on one hand, the inherent sampling errors and, on the other hand, the false-positive cases due to the non-immediate process of tumor cell death after radiotherapy [34]. We retrieved and analyzed the restaging endoscopies of our dataset. In our series, 57% of patients considered endo+ turned out to sustain a complete response, which is in line with the above-mentioned limitations of the modality. However, 48% of endo− patients did not sustain a complete response, defying its reported high specificity. We must keep in mind, however, that only 33% of our patients went straight to surgery, so unlike in the studies mentioned above, regrowths were included in our series.

The split scar sign may identify patients who sustain a complete response with higher specificity than conventional approaches and with equivalent specificity to that of the more complex methodologies in the studies mentioned above, albeit at the cost of missing a substantial proportion of SCRs. It might translate a process of rectal wall remodeling characterized by submucosal fibrosis leading to an inner hypointense layer, and thickening plus fibrotic remodeling of the *muscularis propria* leading to an underlying intermediate signal intensity layer. A visible outer hypointense layer is usually also present, representing perirectal fibrosis, but indeed, it may be absent, particularly in early T-staged tumors. Importantly, the very high specificity and PPV of the split scar sign for SCR appear to be dependent on an early presentation, given they dropped significantly when based on the second timepoint after neoadjuvant therapy.

There were some limitations in our study. First, it's retrospective nature could have introduced a selection bias. However, patients were retrieved from a prospectively organized database, minimizing bias effect. Second, the observers were dealing with cases from their own institution. However, the long follow-up period in the inclusion criteria minimized recall bias during blind reading of the images. Third, we did not perform an analysis of lymph node response and indeed it must be included in patients considered for "watch-and-wait." Fourth, the time interval between the end of chemoradiation and MR imaging varied across our patient population, which may have influenced the findings. Fifth, the minimum follow-up period was only 1 year while the most recurrences occur during the first 2 years [35]. However, our mean follow-up was close to 3 years (32.2 months). Finally, our radiotherapy modality is VMAT, which incorporates a dose boost for gross tumor volume. Given we do not know its influence on the tumor and rectal wall remodeling process, we cannot state that these results would apply to institutions where a different radiotherapy methodology is employed.

In conclusion, our results indicate that the split scar sign, a simple visual pattern visible on standard post-neoadjuvancy T2-WI, is very specific for a sustained complete response and may therefore be of great value for the selection of rectal cancer patients for "watch-and-wait." However, it misses a significant proportion of complete responders, which signals the need for complementary modalities with higher sensitivity. A prospective analysis of a greater number of patients in a multi-institutional setting is required to further explore, not only the general applicability and predictive value of this sign per se, but also of its combination with additional clinical and imaging parameters.

Acknowledgments The authors would like to thank all personnel from the Radiology Department and all personnel from the Digestive Unit of the Champalimaud Foundation.

Funding The authors state that this work has not received any funding and is in compliance with ethical standards.

Compliance with ethical standards

Guarantor The scientific guarantor of this publication is Richard J. Heald, MD, CBE, MChir, FRCS.

Conflict of interest The authors declare that they have no competing interest.

Statistics and biometry One of the authors has significant statistical expertise, and no complex statistical methods were necessary for this paper.

Informed consent Written informed consent was waived by the Institutional Review Board.

Ethical approval Institutional Review Board approval was obtained.

Methodology
- This is a retrospective
- observational
- cross sectional study

References

1. Heald RJ, Ryall RD (1986) Recurrence and survival after total mesorectal excision for rectal cancer. Lancet 1:1479–1482
2. Schneider EB, Hyder O, Brooke BS et al (2012) Patient readmission and mortality after colorectal surgery for colon cancer: impact of length of stay relative to other clinical factors. J Am Coll Surg 214:390–398
3. Chiappa A, Bertani E, Ferrari C, Venturino M, Andreoni B (2014) The impact of total mesorectal excision for rectal cancer on survival. Eur J Surg Oncol 40(11):S97
4. Maas M, Nelemans PJ, Valentini V et al (2010) Long-term outcome in patients with a pathological complete response after chemoradiation for rectal cancer: a pooled analysis of individual patient data. Lancet Oncol 11:835–844
5. Garcia-Aguilar J, Shi Q, Thomas CR Jr et al (2012) A phase II trial of neoadjuvant chemoradiation and local excision for T2N0 rectal cancer: preliminary results of the ACOSOG Z6041 trial. Ann Surg Oncol 19:384–391
6. Habr-Gama A, Perez RO, Proscurshim I et al (2006) Patterns of failure and survival for nonoperative treatment of stage c0 distal rectal cancer following neoadjuvant chemoradiation therapy. J Gastrointest Surg 10:1319–1328
7. Park IJ, Yu CS (2014) Current issues in locally advanced colorectal cancer treated by preoperative chemoradiotherapy. World J Gastroenterol 20:2023–2029
8. Chan AK, Wong A, Jenken D, Heine J, Buie D, Johnson D (2005) Posttreatment TNM staging is a prognostic indicator of survival and recurrence in tethered or fixed rectal carcinoma after preoperative chemotherapy and radiotherapy. Int J Radiat Oncol Biol Phys 61:665–677
9. Glynne-Jones R, Wallace M, Livingstone JI, Meyrick-Thomas J (2008) Complete clinical response after preoperative chemoradiation in rectal cancer: is a "wait and see" policy justified? Dis Colon Rectum 51:10–19
10. Hatfield P, Hingorani M, Radhakrishna G et al (2009) Short-course radiotherapy, with elective delay prior to surgery, in patients with unresectable rectal cancer who have poor performance status or significant co-morbidity. Radiother Oncol 92(2):210–214
11. Radu C, Berglund A, Påhlman L, Glimelius B (2008) Short-course preoperative radiotherapy with delayed surgery in rectal cancer - a retrospective study. Radiother Oncol 87(3):343–349
12. Pettersson D, Holm T, Iversen H, Blomqvist L, Glimelius B, Martling A (2012) Preoperative short-course radiotherapy with delayed surgery in primary rectal cancer. Br J Surg 99(4):577–583
13. São Julião GP, Habr-Gama A, Vailati BB, Perez RO (2017) The good, the bad and the ugly: rectal cancers in the twenty-first century. Tech Coloproctol 21:573–575
14. Pozo ME, Fang SH (2015) Watch and wait approach to rectal cancer: a review. World J Gastrointest Surg 7(11):306–312
15. Lorimer PD, Motz BM, Kirks RC et al (2017) Pathologic complete response rates after neoadjuvant treatment in rectal cancer: an analysis of the national cancer database. Ann Surg Oncol 24:2095–2103
16. Kong JC, Guerra GR, Warrier SK, Ramsay RG, Heriot AG (2017) Outcome and salvage surgery following "watch and wait" for rectal cancer after neoadjuvant therapy: a systematic review. Dis Colon Rectum 60(3):335–345
17. Bhoday J, Smith F, Siddiqui MR et al (2016) Magnetic resonance tumor regression grade and residual mucosal abnormality as predictors for pathological complete response in rectal cancer postneoadjuvant chemoradiotherapy. Dis Colon Rectum 59(10):925–933
18. Smith FM, Wiland H, Mace A, Pai RK, Kalady MF (2014) Clinical criteria underestimate complete pathological response in rectal cancer treated with neoadjuvant chemoradiotherapy. Dis Colon Rectum 57(3):311–315
19. Ryan JE, Warrier SK, Lynch AC, Heriot AG (2015) Assessing pathological complete response to neoadjuvant chemoradiotherapy in locally advanced rectal cancer: a systematic review. Colorectal Dis 17:849–861
20. Sassen S, de Booij M, Sosef M et al (2013) Locally advanced rectal cancer: is diffusion weighted MRI helpful for the identification of complete responders (ypT0N0) after neoadjuvant chemoradiation therapy? Eur Radiol 23:3440–3449
21. Nougaret S, Reinhold C, Mikhael HW, Rouanet P, Bibeau F, Brown G (2013) The use of MR imaging in treatment planning for patients with rectal carcinoma: have you checked the "DISTANCE"? Radiology 268(2):330–344
22. Beets GL, Figueiredo NL, Habr-Gama A, van de Velde CJ (2015) A new paradigm for rectal cancer: organ preservation: Introducing the International Watch & Wait Database (IWWD). Eur J Surg Oncol 41(12):1562–1564
23. Patel U, Taylor F, Blomqvist L et al (2011) Magnetic resonance imaging–detected tumor response for locally advanced rectal cancer predicts survival outcomes: MERCURY experience. J Clin Oncol 29(28):3753–3760
24. Kim SH, Lee JM, Hong SH et al (2009) Locally advanced rectal cancer: added value of diffusion-weighted MR imaging in the evaluation of tumor response to neoadjuvant chemo and radiation therapy. Radiology 253:116–125
25. Sclafani F, Brown G, Cunningham D et al (2017) Comparison between MRI and pathology in the assessment of tumor regression grade in rectal cancer. Br J Cancer 21:1–8
26. Song I, Kim SH, Lee SJ, Choi JY, Kim MJ, Rhim H (2012) Value of diffusion-weighted imaging in the detection of viable tumor after neoadjuvant chemoradiation therapy in patients with locally advanced rectal cancer: comparison with T2 weighted and PET/CT imaging. Br J Radiol 85:577–586
27. Lambregts DMJ, Vandecaveye V, Barbaro B et al (2011) Diffusion-weighted MRI for selection of complete responders after chemoradiation for locally advanced rectal cancer: a multicenter study. Ann Surg Oncol 18:2224–2231
28. Lambregts DMJ, Delli Pizzi A, Lahaye M et al (2018) A pattern-based approach combining tumor morphology on mri with distinct signal patterns on diffusion-weighted imaging to assess response of

rectal tumors after chemoradiotherapy. Dis Colon Rectum 61(3): 328–337

29. Cui Y, Yang X, Shi Z et al (2018) Radiomics analysis of multiparametric MRI for prediction of pathological complete response to neoadjuvant chemoradiotherapy in locally advanced rectal cancer. Eur Radiol 29(3):1211–1220
30. Lambregts DMJ, van Heeswijk MM, Delli Pizzi A et al (2017) Diffusion-weighted MRI to assess response to chemoradiotherapy in rectal cancer: main interpretation pitfalls and their use for teaching. Eur Radiol 27(10):4445–4454
31. Smith FM, Chang KH, Sheahan K, Hyland J, O'Connell PR, Winter DC (2012) The surgical significance of residual mucosal abnormalities in rectal cancer following neoadjuvant chemoradiotherapy. Br J Surg 99:993–1001
32. Smith FM, Winter D (2014) Watch and wait for rectal cancer: where are we really at? Colorectal Dis 16:332–334
33. van der Sande ME, Beets GL, Hupkens BJ et al (2018) Response assessment after (chemo)radiotherapy for rectal cancer: why are we missing complete responses with MRI and endoscopy? Eur J Surg Oncol S0748-7983(18):32017–32011
34. Nahas SC, Rizkallah Nahas CS, Sparapan Marques CF et al (2016) Pathologic complete response in rectal cancer: can we detect it? Lessons learned from a proposed randomized trial of watch-and-wait treatment of rectal cancer. Dis Colon Rectum 59:255–263
35. van der Valk MJM, Hilling DE, Bastiaannet E et al (2018) Long-term outcomes of clinical complete responders after neoadjuvant treatment for rectal cancer in the International Watch & Wait Database (IWWD): an international multicenter registry study. Lancet 391(10139):2537–2545

5.4. Early conformational changes at tumour bed and long term response after neoadjuvant therapy in rectal cancer

European Journal of Radiology 140 (2021) 109742

Contents lists available at ScienceDirect

European Journal of Radiology

journal homepage: www.elsevier.com/locate/ejrad

Early conformational changes at tumour bed and long term response after neoadjuvant therapy in locally-advanced rectal cancer

Inês Santiago [a,b,*], Maria-João Barata [a], Nuno Figueiredo [c], Oriol Parés [d], Celso Matos [a]

[a] Radiology Department, Champalimaud Foundation, Avenida Brasília, Lisbon, 1400-038, Portugal
[b] Nova Medical School, Campo Mártires da Pátria 130, Lisbon, 1169-056, Portugal
[c] Colorectal Surgery, Digestive Unit, Champalimaud Foundation, Avenida Brasília, Lisbon, 1400-038, Portugal
[d] Radiation Oncology Department, Champalimaud Foundation, Avenida Brasília, Lisbon, 1400-038, Portugal

ARTICLE INFO

Keywords:
Rectal neoplasms
Neoadjuvant therapy
Watchful waiting
Magnetic resonance imaging

ABSTRACT

Objectives: To evaluate how changes in tumour scar depth angle and thickness in the post-neoadjuvant period relate to long-term response in locally-advanced rectal cancer patients.
Methods: Informed consent was obtained from all patients and institutional review board approved this retrospective study. Sixty-nine consecutive locally-advanced rectal cancer patients who underwent neoadjuvant therapy and were selected for "Watch-and-Wait" were enrolled. Two radiologists, O1 and O2, blindly and independently reviewed the 1st and 2nd post-neoadjuvant therapy pelvic MRI T2-weighted images and recorded depth angle and thickness of the tumour scar. Value changes were calculated by simple subtraction (2nd-1st). Mann-Whitney *U* test was employed to assess for significant differences between sustained clinical complete responders (SCR), defined as patients with pathologic complete response or clinical complete response with a minimum follow-up of 1 year; and non-sustained complete responders (non-SCR). Interobserver agreement was estimated using intraclass correlation coefficient (ICC). Data on mrTRG, DWI and endoscopy at 1st and 2nd timepoints were retrieved for comparison.
Results: In SCR, depth angle change between 1st (med = 10 weeks after end of radiotherapy) and 2nd (med = 23 weeks after end of radiotherapy) timepoints was significantly different (O1:p = 0.004; O2:p = 0.010): the SCR group showed a depth angle reduction (O1:med=-4.45; O2:med=-2.35), whereas non-SCRs showed a depth angle increase (O1:med=+2.60; O2:med=+7.40). Also, at 2nd timepoint, SCR scars were significantly thinner both for O1 (p = 0.003; SCR:med = 7.05 mm; non-SCR:med = 9.4 mm) and O2 (p = 0.006; SCR:med = 6.45 mm; non-SCR:med = 8.2 mm). A depth angle increase >21° between 1st and 2nd timepoints and a scar thickness >10 mm at 2nd timepoint were not sensitive but were highly specific for a non-SCR (91/94 %) for both observers. Interobserver agreement was good for scar depth angle change (ICC = 0.65) and excellent for scar thickness at 2nd timepoint (ICC = 0.84). Of the retrieved data, only DWI at 2nd timepoint was discriminative (p = 0.043) providing a similar sensitivity (33 %) and a slightly lower specificity (87.5 %).
Conclusion: Tumour scar expansion >21° between 1st and 2nd post-neoadjuvancy MRI and a scar thickness >10 mm at 2nd post-neoadjuvancy MRI may consistently indicate a non-SCR with high specificity in locally-advanced rectal cancer patients.

1. Background

Recent rise in the incidence of colorectal cancer in young individuals (<50 years) appears to be largely driven by an increased incidence of rectal cancer [1–4]. Standard upfront treatment for locally-advanced rectal cancer is neoadjuvant therapy (NAT), which includes radiotherapy (RT) plus varied chemotherapy (CT) regimens [5]. The justification for its use has gone beyond tumour shrinkage to ease complete resection and reduce the chance of local recurrence, to include attempting to achieve a complete response (CR), which may occur in up

Abbreviations: CR, complete response; SCR, sustained complete response; Non-SCR, non-sustained complete response; mrTRG, MR imaging tumour regression grade; DWI, MR diffusion-weighted imaging; NAT, neoadjuvant therapy; RT, radiotherapy; CT, chemotherapy; W&W, watch and wait.

* Corresponding author at: Champalimaud Foundation, Avenida Brasília, Lisbon, 1400-038, Portugal.
E-mail address: ines.santiago@neuro.fchampalimaud.org (I. Santiago).

https://doi.org/10.1016/j.ejrad.2021.109742
Received 1 January 2021; Received in revised form 24 March 2021; Accepted 23 April 2021
Available online 30 April 2021

to 25 % of cases and drive organ preservation strategies [6]. Organ preservation may be especially relevant in low tumours, which require more mutilating surgical procedures. "Watch-and-wait" programs (W&W) have disseminated worldwide and rely on response assessment and follow-up with endoscopy and MRI by experienced teams. Patients may respond to NAT in one of three ways: 1. Sustained clinical CR - no signs of residual tumour initially and no signs of tumour regrowth on follow-up; 2. Clinical CR with regrowth - no macroscopic tumour initially and regrowth on follow-up (about 1/4th of cases) [7]; 3. Persistence - no or incomplete response on initial evaluations. From a practical point of view, 2. and 3. require surgery, whether standard or minimally invasive. "Salvage" surgery for regrowths, when patients comply to surveillance protocols, is highly effective with only 0.2–1 % incomplete resections [7–9]. However, Smith et al. found an excess rate of distant metastases in patients with local regrowth compared to sustained CR (36 % vs 1%) and whether a higher risk is already present at baseline or metastases emerge as a consequence of the uncontrolled primary tumour is not yet known [7,10]. As such, the desirable scenario would be to identify all patients that require surgery for local disease control in the early period that follows NAT – both clear tumour persistences and apparent CRs that regrow. Although other methods can be adopted, the most widely disseminated assessment methods - endoscopy, DWI, mrTRG and other ordinal scales based on visual analysis of T2-weighted images - have limitations and have been mostly explored to define response at the particular timepoint of the observation rather than to estimate the likelihood of a sustained vs non-sustained clinical CR [11–13]. We hypothesized that the conformational changes of tumour scars in the post-NAT period may differ between sustained clinical complete responders (SCR) and non-sustained clinical complete responders (non-SCR), and that those changes may be easily measured on T2-weighted imaging. The purpose of this study is to evaluate how scar depth angle and thickness in the post-NAT period relate to long-term tumour response in rectal cancer patients.

2. Methods

2.1. Study population and institutional setting

The Institutional Review Board approved this retrospective cross-sectional study and all patients signed an informed consent. All consecutive patients with biopsy-proven rectal adenocarcinoma diagnosed between 1/2/2013 and 1/5/2019 were retrieved from our prospectively organized rectal cancer database. Inclusion criteria were: NAT including radiation therapy; first and second restaging MRI performed at our institution; available histopathology results and/or a minimum follow-up of 1 year for patients on W&W. Exclusion criteria were MRI artefacts precluding assessment and non-oncologic death or loss of follow-up before 1 year for patients on W&W.

Patients were staged according to the TNM classification, based on clinical examination, endoscopy and imaging (thoracic CT and contrast-enhanced abdominal MRI/CT).

All patients were discussed at the multidisciplinary team meeting and patients with threatened/involved mesorectal fascia (MRF); mrT3c-d/mrT4a-b regardless of mrN stage; tumour bordering the intersphincteric or distal total mesorectal excision plane and/or extramural venous invasion were considered locally-advanced. [14]. Applying these criteria, approximately 2/3 of patients were selected for NAT.

Neoadjuvant long-course chemoradiation consisted of external beam Volumetric Modulated Arc Therapy (VMAT) with a dose of 45 Gy to elective pelvic fields, including an integrated boost of 54–56 Gy, for 25 consecutive days with concurrent capecitabine. Short-course RT used the same technique, with a dose of 5 × 5 Gy delivered in 5 consecutive days and was employed in selected cases (stage IV at diagnosis or higher risk of systemic than local recurrence). Selected patients with high-risk of systemic disease received consolidation chemotherapy with capecitabine and oxaliplatin.

Table 1
Staging and restaging pelvic MR imaging acquisition parameters. (A/I) 1.5 T Achieva / 1.5 T Ingenia Philips Healthcare®, Best, The Netherlands.

Parameter	Oblique axial T2-weighted turbo spin-echo* (A/I)	Oblique coronal T2-weighted turbo spin-echo (A/I)	Sagital T2-weighted turbo spin-echo (A/I)	Single-shot spin-echo echo-planar diffusion-weighted+ (A/I)
Echo time (msec)	120 / 85	120 / 100	120 / 100	69 / 90
Repetition time (msec)	3000 / 5692	3700 / 2000	4800 / 3102	2000 / 4288
Echo train length	21 / 18	24 / 16	18 / 21	–
Slice thickness (mm)	3 / 3	3 / 3	4 / 3	3 / 5
Gap (mm)	0.5 / 0.3	0.5 / 0.3	1 / 0.3	1 / 0
Matrix	248 × 242 / 416 × 465	248 × 234 / 200 × 179	180 × 160 / 252 × 223	124 × 124 / 76 × 65
Field-of-view (mm)	200 × 200 / 250 × 328	200 × 200 / 160 × 160	180 × 180 / 200 × 200	370 × 370 / 200 × 200
In-plane resolution (mm [2])	0.8 × 0.8 / 0.6 × 0.7	0.8 × 0.85 / 0.8 × 0.8	1 × 0.88 / 0.8 × 0.8	3 × 3 / 2.6 × 3.01
Signal averages	3 / 1	4 / 2	4 / 2	4 / 7

* Oblique axial scans were perpendicular to the long axis of the rectal wall at tumour location; +Spectral pre-saturation with inversion recovery was utilized for fat saturation. B-values of 0, 200, 500 and 1000 and 0 and 1400 s/mm^2 were employed for Achieva and Ingenia 1.5 T equipment, respectively.

Data on patient demographics, clinical staging and restaging, type of surgery and histopathology when operated; and follow-up were recorded prospectively by a physician uninvolved in image reading.

2.2. Imaging technique

Patients performed a small enema 20 min before acquisition (Microlax® 5 mL, Jaba Recordati). Intravenous butylscopolamine 20 mg was administered, except when contraindicated. Acquisitions were performed on 1.5 T equipments (Achieva/Ingenia Philips Healthcare®) as presented in Table 1.

2.3. Imaging analysis

We focused on the 1st and 2nd MRI evaluations, which took place at a median of 10 weeks (min = 3;max = 19 weeks) and 23 weeks (min = 9; max = 34 weeks) post-NAT, respectively. Examinations were blindly and independently read on a picture archiving and communication system workstation (Philips Healthcare® Intellispace PACS DCX) by two gastrointestinal radiologists (Observer 1:*BLINDED*, 9 years of experience and observer 2:*BLINDED*, 12 years of experience). The first and second post-NAT pelvic T2-weighted MR images were analysed with the patients' staging pelvic T2-weighted MR images as explained in Fig. 1.

2.4. Retrieved response assessment

MRI and endoscopy data collected from standardized reports performed by one of 2 trained radiologists (9 and 12 years of experience) and a surgeon (12 years of experience), respectively, were retrieved and analyzed for comparison. mrTRG classifications of 1 (linear scar only) or 2 (dense fibrosis with no obvious intermediate signal) were considered indicative of a SCR, whereas mrTRG3 (visible intermediate signal but >50 % fibrosis or mucin), mrTRG4 (>50 % intermediate signal) and mrTRG5 (no change compared to staging examination) were considered indicative of a non-SCR. Cases with absent/residual foci of high signal

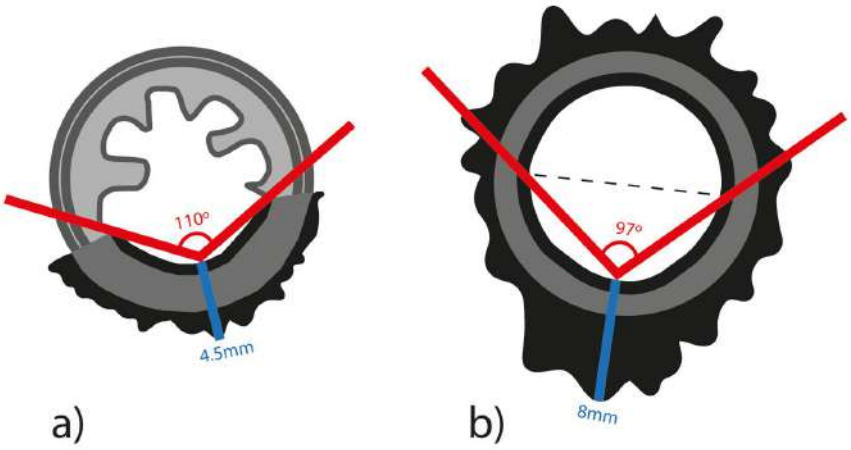

Fig. 1. Schematic representation of scar depth angle and thickness measurements made on the chosen axial central slice of the tumour. In small tumour scars (**a**), the endoluminal center of the scar serves as pivot for angle measurement and the lines cross the endoluminal extremities of the scar (in red). If tumour scar is circumferential (**b**), the pivot is placed at its most invasive front (or randomly, if tumour scar thickness is regular). For circumferential tumour scars or scars involving >180° of the rectal wall circumference, the lines then cross the endoluminal aspect of the scar at its opposing hemicircumference (in red). Pivots are also reference points for scar thickness measurement, which is performed perpendicularly to its inner surface (blue lines in **a** and **b**).

intensity on high-b-value DWI were considered indicative of a SCR, whereas cases with a substantial proportion of high signal intensity (>25 %) were considered indicative of a non-SCR. Endoscopic responses graded as 0 (flat white scar with telangiectasia) or 1 (shallow ulcer/red scar) were considered indicative of SCR and responses graded as 2 (ulcerated residual lesion or adenomatous residual mucosal abnormality), 3 (excavated ulcer with elevated edges) or 4 (infiltrative lesion) were considered indicative of a non-SCR.

All patients were discussed at the multidisciplinary team meeting and major clinical responses at first evaluation (median 10 weeks post-NAT), which included clinical complete responses (mrTRG1 and no high signal intensity on high b-value DWI and endoscopy 0) and near-complete responses (mrTRG2–2/3 and/or residual small focus of high signal intensity on high b-value DWI and/or endoscopy 1–2) [15,16] were selected for "Watch & Wait". Patients on "Watch & Wait" were reassessed every 12 weeks during the first year, every 16 weeks during the second year and every 6 months thereafter, as established by the International Watch & Wait Dababase Consortium [17]. Whenever a clinical CR was not achieved or a regrowth was suspected, elective surgery was proposed to the patient, except in palliative settings or when patients' co-morbidity/frailty contraindicated a major abdominal operation.

2.5. Histopathology

Tumour p-stage was retrieved from the pathology reports of patients who underwent surgery, made according with the pTNM requirements from the 7th Edition of the College of American Pathologists.

2.6. Reference standard

The reference standard was SCR, defined as pathologic CR or local recurrence-free clinical follow-up over a minimum of 1 year.

2.7. Statistical analysis

Data was recorded separately between O1 and O2 using an Excel spreadsheet (Microsoft Excel for Mac 011, version 14.2.1, Microsoft®) and analyzed using SPSS (version 23, IBM®). Subtraction was performed between 2nd and 1st timepoint reported values, both for depth angle and thickness of the tumour scar. Non-parametric tests were employed given the non-normality of the distributions. Mann-Whitney *U* test was employed in search for significant differences between SCR and non-SCR in depth angle at 1st timepoint, depth angle at 2nd timepoint, depth angle difference, thickness at 1st timepoint, thickness at 2nd timepoint and thickness difference. ROC curves were obtained and used to define optimal cutoff values. Interobserver agreement was estimated using the intraclass correlation coefficient (<0.4=poor; 0.4–0.59=fair; 0.6–0.74=good; >0.75=excellent reliability) [18]. Retrieved response assessment data was analyzed using the Chi-square test.

Table 2
Clinical data on 69 patients with locally advanced rectal cancer who underwent NAT. CRT: chemoradiation therapy; RT: radiotherapy; CT: chemotherapy; LAR: low anterior resection; APE: abdominoperineal excision; TAMIS: transanal minimally invasive surgery; Col: derivative colostomy.

Variable	Total nº (%)	SCR nº (%)	Non-SCR nº (%)	P value *
Age (years)				0.35
≦60	47 (68.1 %)	20 (42.6 %)	27 (57.4 %)	
>60	22 (31.9 %)	12 (54.5 %)	10 (45.5 %)	
Gender				0.14
male	43 (62.3 %)	17 (39.5 %)	26 (60.5 %)	
female	26 (37.7 %)	15 (57.7 %)	11 (42.3 %)	
Neoadjuvant treatment				0.31
Long-course CRT	28 (40.6 %)	11 (39.3 %)	17 (60.7 %)	
Short-course RT	1 (1.4 %)	0 (0%)	1 (100 %)	
Long-course CRT + consolidation CT	36 (52.2 %)	20 (55.6 %)	16 (44.4 %)	
Short-course RT + consolidation CT	4 (5.8 %)	1 (25 %)	3 (75 %)	
Surgery at any timepoint				**<0.01**
Yes	36 (52.2 %)	2 (5.6 %)	34 (94.4 %)	
No	33 (47.8 %)	30 (90.9 %)	3 (9.1 %)	
Type of surgery				1.0
LAR	15 (41.7 %)	2 (13.3 %)	13 (86.7%)	
APE	15 (41.7%)	0 (0%)	15 (100 %)	
TAMIS	4 (11.1 %)	0 (0%)	4 (100 %)	
Col	2 (5.9 5.6 %)	0 (0%)	2 (100 %)	

* Pearson Qui-Square test was employed except when Cochran's criteria were not met, in which case Fisher's Exact test was employed.

Table 3
Initial staging tumour characteristics as defined upon clinical staging, stratified by outcome.

Variable	Total[a] n°(%)	SCR n° (%)	Non_SCR n° (%)	P value*
Location				0.50
<6 cm	38 (55.1 %)	19 (50 %)	19 (50 %)	
≥ 6 cm	31 (44.9 %)	13 (41.9 %)	18(58.1 %)	
mrT				0.68
≤mrT2	22 (31.9 %)	11(50 %)	11 (50 %)	
≥mrT3	47 (68.1 %)	21 (44.7 %)	26 (55.3 %)	
mrN				0.15
–	24 (34.8 %)	14 (58.3 %)	10 (41.7 %)	
+	45 (65.2 %)	18 (40 %)	27 (60 %)	
mrCMR				0.50
–	46 (66.7 %)	20 (43.5 %)	26 (56.5 %)	
+	23 (33.3 %)	12 (52.2 %)	11 (47.8 %)	
mr EMVI				0.46
–	51 (73.9 %)	25 (49 %)	26 (51 %)	
+	18 (26.1 %)	7 (38.9 %)	11 (61.1 %)	

* Pearson Qui-Square test was employed except when Cochran's criteria were not met, in which case Fisher's Exact test was employed. Location represents distance to anal verge. mrT represents T staging, ≤mrT2 representing tumour confined to the rectal wall and ≥ mrT3 representing tumour extending into the mesorectal fat and/or peritoneal and/or adjacent organ involvement. mrN represents lymph node staging, one or more suspicious lymph nodes based on the staging examination being considered N + disease. mrEMVI represents extramural venous invasion, intermediate signal in vessel lumen with slight vessel expansion or irregular vessel contour being considered mrEMVI+(14).

3. Results

3.1. Study population and tumour staging characteristics

Eighty-one patients met inclusion criteria and were retrieved from the database. Twelve patients were excluded: 10 due to an inability to identify the tumour scar either due to normalization of the rectal wall (n = 7) or to diffuse massive rectal wall oedema (n = 3), one due to Crohn's disease affecting the rectum and 1 due to movement artefacts that compromised image analysis. Thus, 69 patients were considered eligible (43 men, 26 women; mean age:66 years, range:43–93 years). For patients with SCR, mean follow-up was 38 months (minimum = 12; maximum = 74).

Patients' clinical data is depicted in Table 2 and initial staging tumour characteristics are presented in Table 3. No significant differences between SCR and non-SCR were found for patient age, gender or type of neoadjuvant treatment. For obvious reasons, non-SCR were operated far more often, and low anterior resection comprised 43.5 % of all surgeries performed.

Twelve (17.4 %) patients with an initial major clinical response enrolled W&W but did not attain a clinical CR at 2nd assessment and therefore underwent surgery. Twenty-five (36.2 %) patients initially on W&W attained a clinical CR but later on presented with regrowth, which occurred at a mean 64 weeks post-RT (minimum = 29 weeks; maximum = 118 weeks). Thirty-two patients (46.4 %) presented with a SCR. Of the latter, 30 (93.8 %) were on W&W and never underwent surgery and 2 (6.3 %) underwent radical surgery and had a pathologic CR.

Three patients (all operated with an incomplete response at pathology, and as such considered non-SCR) went to other institutions and were lost to follow-up. There were significant differences in the rate of distant metastases of the remainder (p = 0.012), 35.3 % of non-SCR presenting with distant metastases vs only 9.4 % of SCR. Out of non-SCR patients with distant metastases (n = 12), 66.7 %(n = 8) were initial clinical CRs that presented later with regrowth.

3.2. MRI analysis

Scar depth angle measurements were significantly different between SCR and non-SCR for both observers (O1:p = 0.004; O2:p = 0.010). The SCR group showed a depth angle reduction (O1:med=-4.45°,IQR = 20.78°,95 %CI[6.86:-10.84]; O2:med=-2.35°,IQR = 18.35°,95 %CI [1.5:-8.92]) whereas the non-SCR group showed a depth angle increase

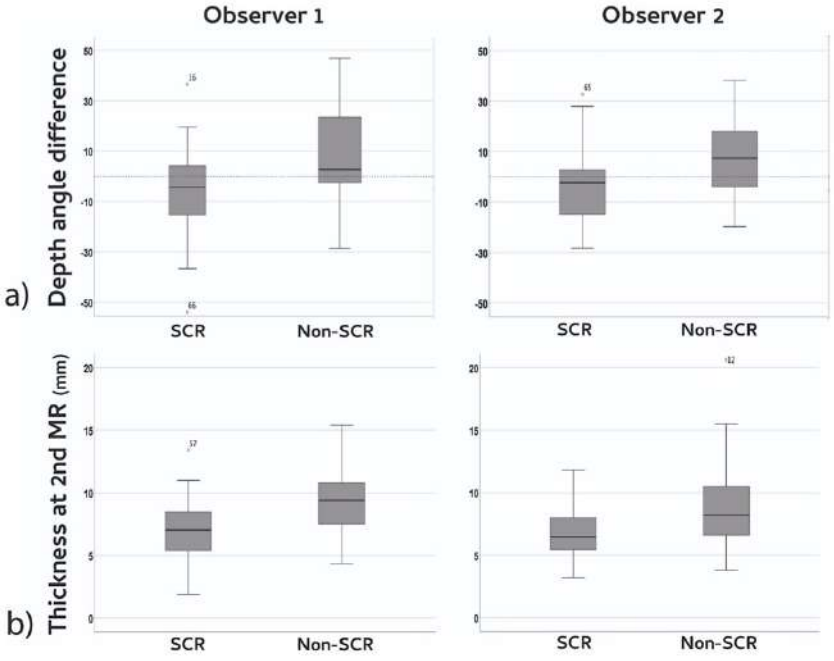

Fig. 2. a) Boxplots displaying tumour scar depth angle differences between SCR and non-SCR for Observers 1 and 2. In the majority of SCR cases and for both observers, the scar depth angle decreases between the 1st and 2nd MR imaging, reflecting scar contraction; whereas the opposite is observed for non-SCR. b) Boxplots displaying tumour scar thickness at 2nd timepoint (mean 23 weeks after the end of RT) between SCR and non-SCR for Observers 1 and 2. The scar thickness is significantly greater in non-SCR for both observers.

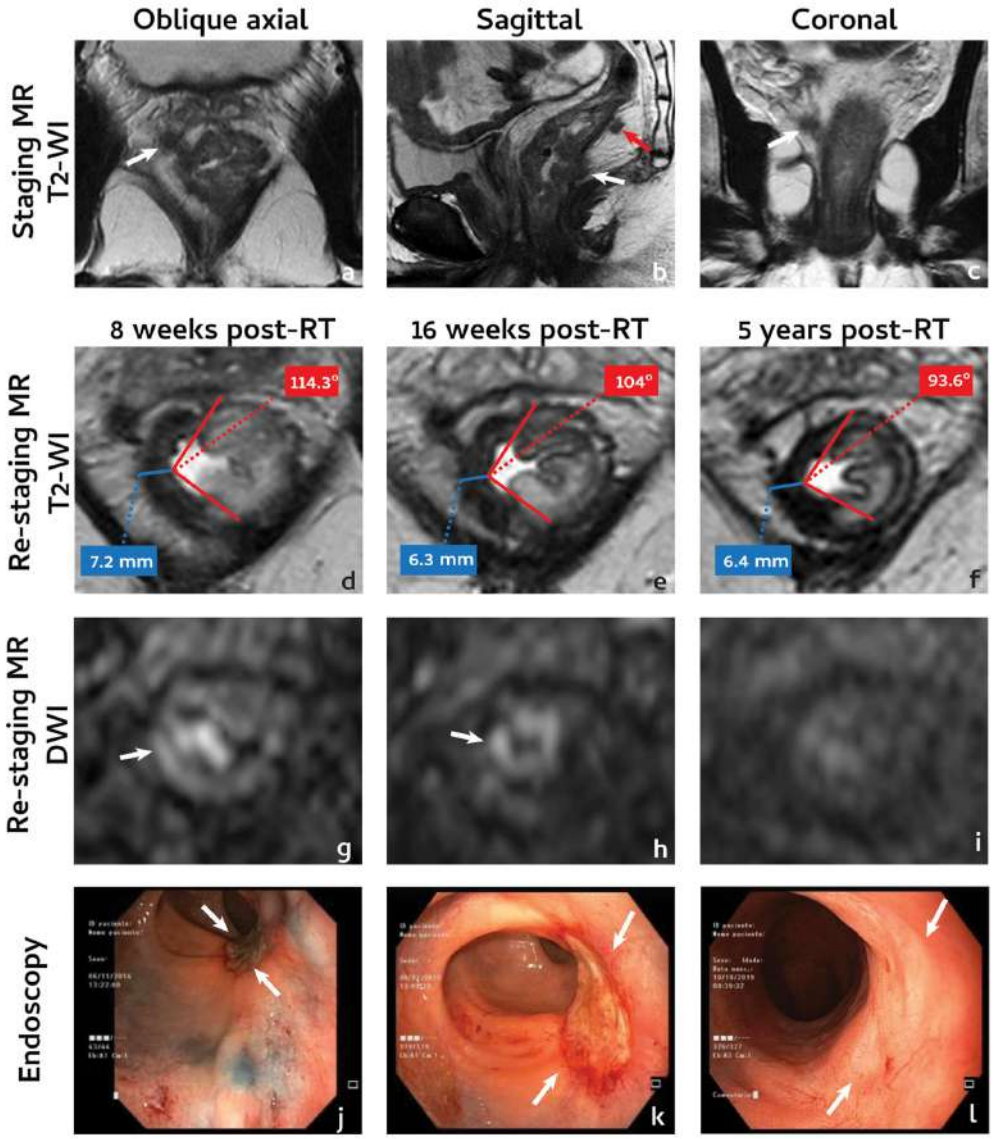

Fig. 3. Fifty-four years old male with a low rectal cancer, mrT3 mrN2 EMVI + MRF + . EMVI is depicted in a and c (white arrows). Notice extension of EMVI beyond the mesorectal fascia (arrow in a). Posterior mesorectal extension (white arrow) and a tumour deposit (red arrow) are depicted in b. Patient underwent CRT + adjuvant CT. At first re-evaluation, response was graded mrTRG3 (d), DWI was considered positive due to a substantial proportion of high signal at tumour bed on high b-value images (g) and was assessed as grade 2 on endoscopy (ulcerated residual lesion between arrows in j). At second assessment, high signal on high b-value DWI images was residual (arrow in h) whereas mrTRG and endoscopic evaluation remained stable (e,k). Tumour scar contracted (-10.3°) and became slightly thinner (-1.1 mm) compared to first assessment (e). Patient was followed while tumour scar became more fibrotic and concave (f), high signal on high b-value DWI disappeared (i) and the ulcer was replaced with a flat white scar – grade 0 (l). Patient remains a clinical complete responder, distant disease-free, at 5 years of follow-up.

(O1:med=+2.60°,IQR = 26.40°,95 %CI[3.73:20.95]; O2:med=+7.40°, IQR = 23.10°,95 %CI[0.18:-17.59) (Fig. 2a). At ROC analysis, we found that an angle increase of >21° from 1st to 2nd timepoint provided a low sensitivity (32 %/19 %) but a very high specificity for a non-SCR (91 %/94 %) (O1/O2).

Considering the 2nd timepoint only, SCR scars were significantly thinner than non-SCR scars (O1:p = 0.003; O2:p = 0.006). For O1, median scar thickness of SCR was 7.05 mm (IQR = 3 mm) vs 9.4 mm (IQR = 4 mm) in non-SCR. For O2, median scar thickness of SCR was 6.45 mm (IQR = 3 mm) vs 8.2 mm (IQR = 4 mm) in non-SCR (Fig. 2b). Considering a cutoff of 10 mm at ROC analysis, sensitivity for non-SCR was low for both observers (30 %/32 %) but specificity was very high (91 %/94 %). All cases with scar thickness >13 mm at 2nd timepoint were non-SCR.

Interobserver agreement was good for scar depth angle change (ICC = 0.65) and excellent for scar thickness at 2nd timepoint (ICC = 0.84).

Case examples of tumour scar behaviour for SCR and non-SCR are depicted in Figs. 3 and 4 and Figs. 5 and 6, respectively.

We also compared these results with those based on the recorded mrTRG 19, mrDWI and endoscopy data at 1st and 2nd evaluations post-NAT (endoscopy was performed within the same week of MRI on all patients). No significant differences were found between mrTRG1–2

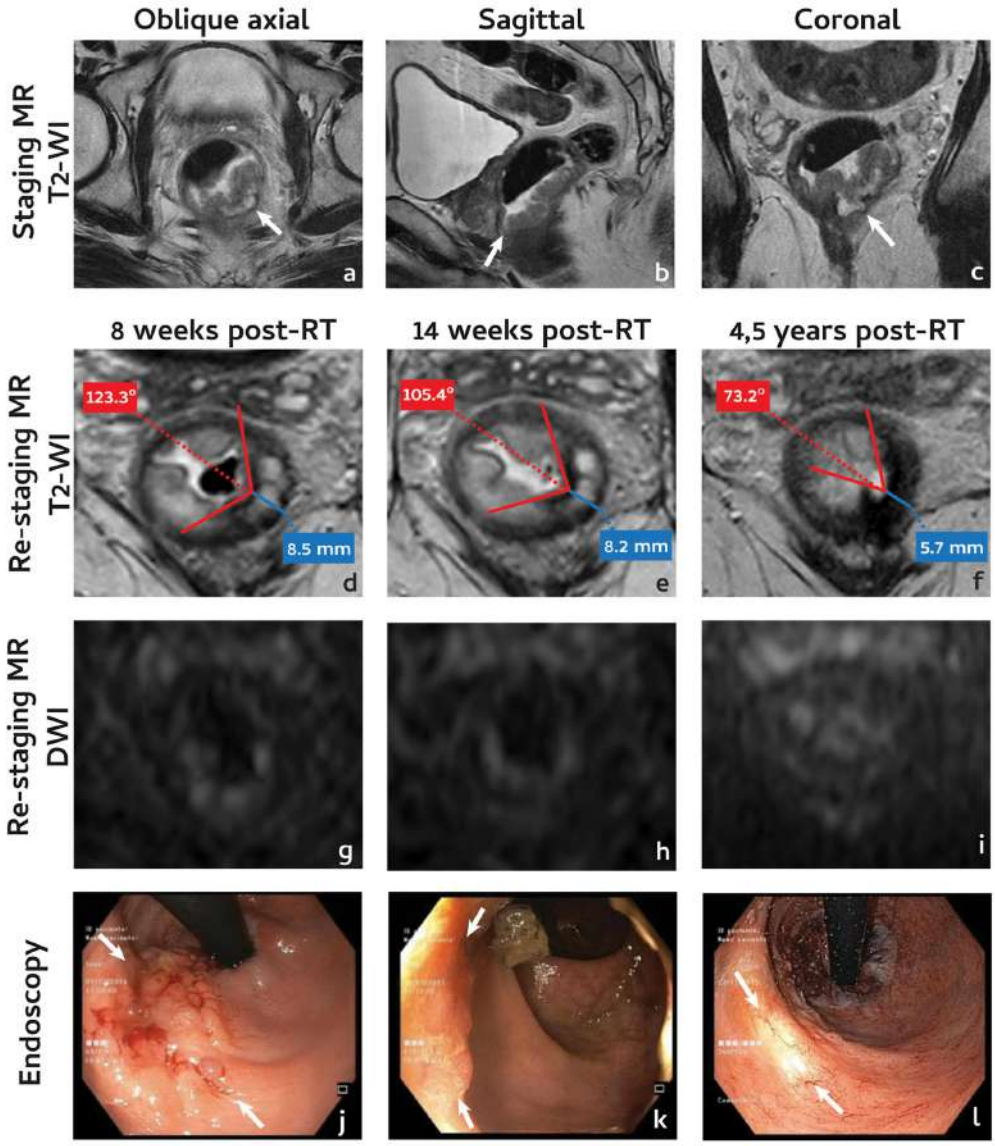

Fig. 4. Sixty-six years old male with a low mucinous rectal cancer, mrT3 mrN0 EMVI- MRF + . Tumour abutted the anorectal transition (arrow in b) and invaded left levator ani (arrows in a and c). Patient underwent CRT + adjuvant CT. At first assessment, response was graded mrTRG2 (d) and DWI was inconclusive due to susceptibility artefacts from luminal air (g). On endoscopy, an adenomatous residual mucosal abnormality (grade 2) was found (between arrows in j). At second assessment, DWI was negative and T2-WI and endoscopic findings remained stable (e,h,k) but a clear tumour scar contraction was present (-17.9°) (e). Patient is now at 4.5 years of follow up with a clinical CR and no distant disease recurrence. Now imaging shows a thinner, more fibrotic and concave scar (f) and endoscopy and DWI are negative (I, l).

and mrTRG3–5 at 1st and 2nd timepoint. mrDWI showed statistical significance only at 2nd timepoint ($p = 0.043$) with sensitivity = 33.33 %, specificity = 87.5 %, PPV = 75 % and NPV = 53.85 %. Interestingly, all mrDWI false positive cases at 2nd timepoint (n = 4) were negative on depth angle difference (<21°) and scar thickness (<10 mm) at 2nd timepoint. Endoscopic analysis did not reach statistical significance but came very close at 1st timepoint ($p = 0.057$) with sensitivity = 54.29 %, specificity = 68,75 %, PPV = 65.52 % and NPV = 57,89 %.

4. Discussion

In this study, we focused on how two indirect measures of rectal cancer scar arquitecture in the post-NAT period – depth angle and thickness – relate to long term tumour response. We found that depth angle increases >21° between the 1st and 2nd MRI (median 10 and 23 weeks post-RT, respectively) and scar thickness >10 mm at 2nd MRI, were two highly specific (>90 %) signs of non-SCR. Importantly, all cases with scar thickness at 2nd MRI > 13 mm were non-SCR. According to our data, depth angle and thickness may be reliable biomarkers (ICCs of 0.65 and 0.84, respectively) that permit early identification of patients who need surgery for disease control, with an improved performance compared to endoscopy and mrTRG. Their performance was only slightly better compared to retrieved DWI analysis at 2nd timepoint, and all 4 false positive DWI cases were negative for both scar depth angle and

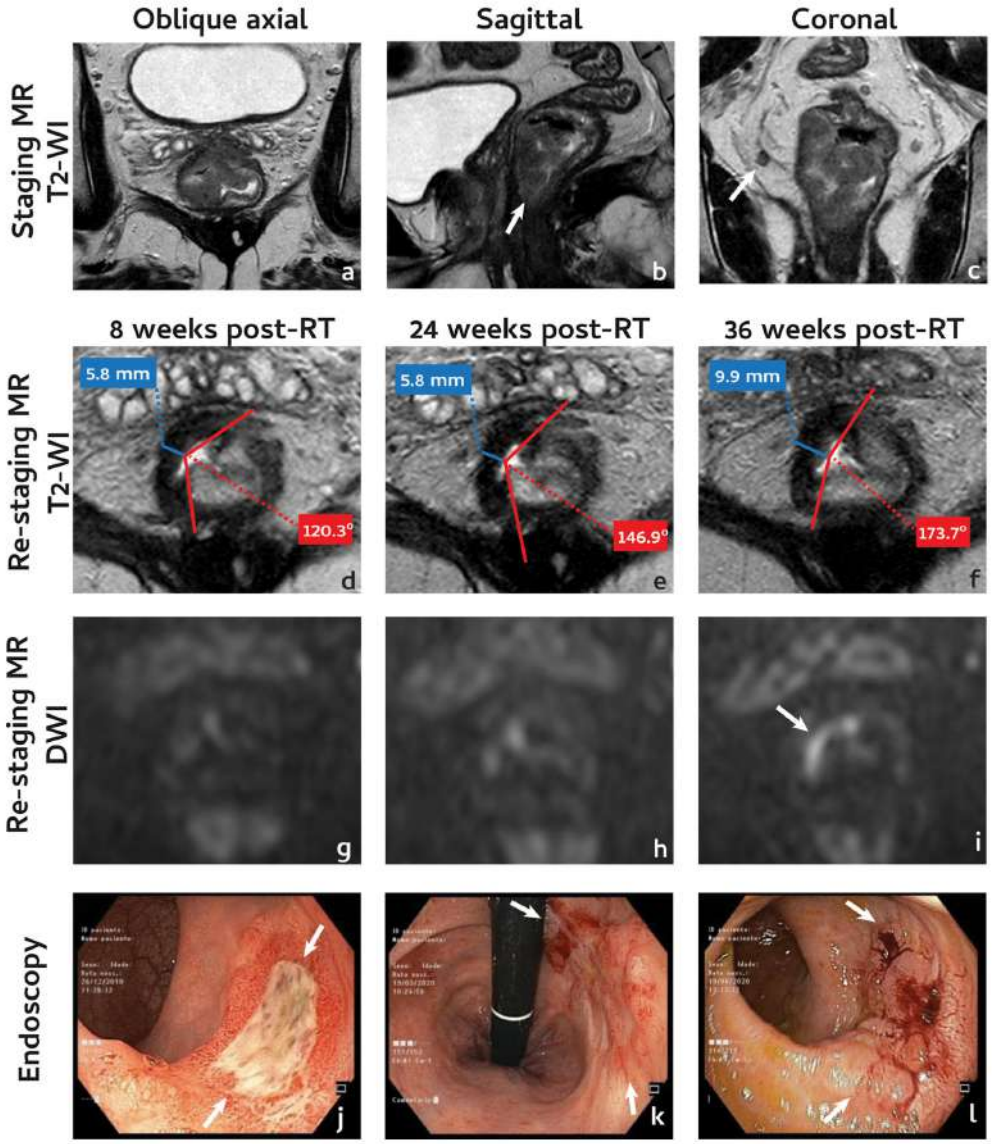

Fig. 5. Forty-two years old male with a low rectal cancer, mrT2 mrN1 EMVI- MRF-. Tumour was located anteriorly and abutted the anorectal transition (arrow in b). A positive lymph node is depicted in c (arrow). Patient underwent CRT + adjuvant CT. At first assessment, response was graded mrTRG2 (d), negative on DWI (g) and grade 3 on endoscopy (j). At second assessment, mrTRG and DWI remained stable (e,h) but the scar lost its concavity (+26.6°) (e). Scar thickness did not change (e). On endoscopy, an adenomatous residual mucosal abnormality (grade 2) was observed (k). At 36 weeks of follow-up, intermediate tumour signal became apparent on the endoluminal surface of the scar (f), DWI became positive at the same location (i) while scar thickness and angle further increased (f). Patient underwent an AAP and was staged as ypT2N0R0.

thickness, which may bode well for a combined analysis.

In an era in which organ preservation is sought by patients and W&W is gathering support from an increasing number of clinicians, many questions arise with respect to local regrowths. The degree of uncertainty regarding how a subclinical uncontrolled group of cancer cells might contribute to the increased rate of distant metastatic disease presses on the need to choose which patients benefit from an immediate operation in the early post-NAT period. As such, these two reliable, easy-to-read and highly specific biomarkers appear promising for clinical decision making.

Current guidelines recommend response assessment to be based on MRI and endoscopy if organ-preservation is to be considered [20,21]. The most widely accepted MRI parameter for that purpose is mrTRG (or a variant) and relies on visual estimation of the relative proportion of "tumour signal" vs fibrosis at tumour bed on T2-weighted images. Its summary sensitivity and specificity for a pathologic non-CR are, according to a recent meta-analysis by Park et al., 0.86 (95 %CI,0.74–0.93) and 0.49 (95 %CI,0.33–0.65), respectively [22]. Reported interobserver agreement is variable, ranging from poor to good, likely due to both the diverseness in assessment criteria and the heterogeneity of tumour response patterns [23–27]. Fragmentation, in which most of the tumour mass is destroyed but disperse small nests of tumour cells remain, may be present in 40–80 % of cases, in which case residual tumour may be well below the resolution capabilities of clinical MRI [27]. This

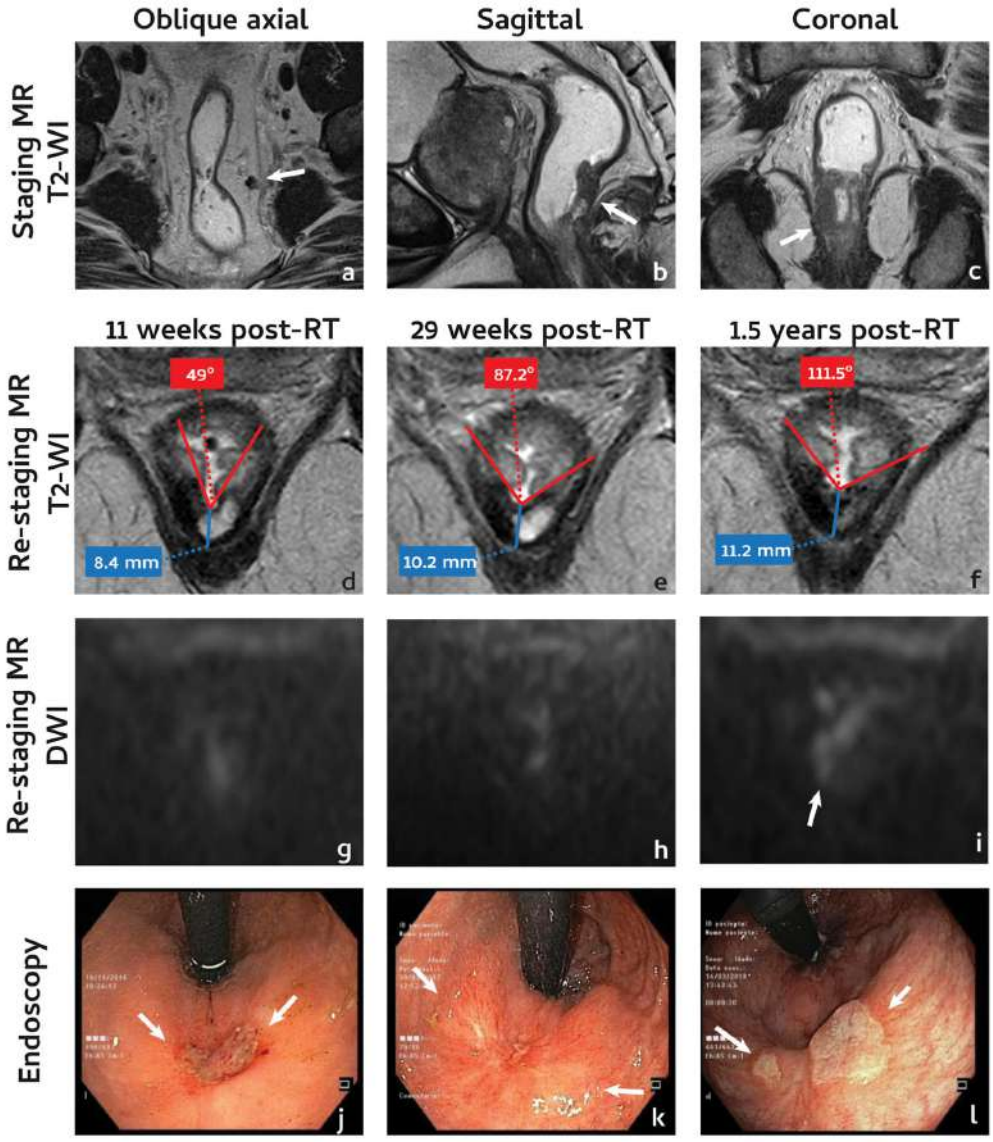

Fig. 6. Sixty-seven years old male with a mucinous low rectal cancer, mrT3 mrN1 EMVI- MRF + . Tumour was located posteriorly (arrow in b) and abutted the right levator ani (arrow in c). A positive lymph node is depicted in a (arrow). Patient underwent CRT. At first assessment, response was graded mrTRG2 (d), was negative on DWI(g) and grade 1 on endoscopy (shallow ulcer between arrows in j). At second assessment, mrTRG and DWI remained stable (e,h) as well as endoscopic grade (red scar between arrows in k). However, the scar lost its concavity (+ 38.2°) and increased in thickness, being higher than 10 mm (e). Patient was followed and at 1.5 years, intermediate tumour signal became apparent within the scar (f), DWI became faintly positive at the same location (arrow in i) while scar thickness and angle further increased (f). Patient underwent an APE and was staged as ypT2N0R0.

fenomenon may justify the significant number of apparent clinical CRs on initial evaluations that later develop a visible regrowth, and our results suggest scar depth angle and thickness might help foresee such cases. Hypothesis to justify our findings would be that nested subclinical viable tumour cells might preclude progressive fibrotic scar contraction and that thicker scars may be more frequent in more advanced tumours to begin with – those in which tumour fragmentation is more likely to occur [27] – and indeed in our sample, 79/93 % of scars >10 mm at 2nd assessment originated from mrT3-T4 tumours.

DWI was introduced more recently but is part of rectal cancer management guidelines across the world [20–22]. The presence of high signal intensity at tumour bed on high b-value images is generally indicative of a non-CR [22]. The diagnostic performance of combined T2-DWI MRI analysis appears beneficial compared to mrTRG (or similar) alone, but results are highly variable [13,28,29]. In our study, specificity of DWI alone at 2nd evaluation was very good (0.87) coming close to that of scar depth angle change and thickness at 2nd timepoint (0.91/0.94 for both), but we have no data on combined analysis to see if performance could be further improved.

Other approaches going beyond plain evaluation of the proportion of different signal intensities at tumour bed have been explored to differentiate SCR from non-SCR. These include the split scar sign, which is highly sensitive (sensitivity = 0.97) but not specific (specificity = 0.52/0.64); and the T2 + DWI pattern-based approach which is very sensitive

(0.94) and specificic (0.77) for non-SCR. The added value of depth angle change and thickness at 2nd assessment compared to these methods appears to lie in the higher specificity (0.94) for a non-SCR and in the applicability to mucinous tumours, which were excluded from the T2 + DWI pattern-based approach series. More complex artificial intelligence algorithms [23,30–34] present with impressive published results but require cumbersome and time-consuming image segmentation and post-processing.

Combining MRI with endoscopy increased sensitivity and specificity for non-CR when compared to MRI alone according to one study [34], whereas in the remainder, sensitivity increased while specificity decreased [35–38]. Those results may be due to the fact that mucosal abnormalities are present in the majority (88–89 %) of unrecognized CR and even in 61–74 % of pathologic CRs [38,39]. In our dataset, endoscopy alone came close to statistical significance at 1st timepoint ($p = 0.057$) with a specificity of 0.69 for non-SCR. Once again no data on combined analysis was available.

5. Limitations

Our study had limitations. First, observers were reading cases from their institution, but the long minimal follow-up requirements limited recall bias. Second, both observers are dedicated gastrointestinal radiologists with >5 years of experience and it is not clear if results may be attained by less experienced radiologists. Third, it was a retrospective study. However, patient data was introduced prospectively in the database, which controlled for selection bias. Forth, we use standard radiation doses to the elective pelvic fields with dose intensification (boost) to the primary tumour and eventual involved lymph nodes routinely to our patients, which may not be the reality in all institutions, and we have no data on whether it may convey morphologically different tumour responses. Fifth, there was variability in the period between the end of RT and the 1st and 2nd MRI and endoscopy evaluations, particularly the latter (min = 9; max = 34 weeks), which may have influenced the findings. Sixth, there was also some overlap in the time elapsed between the end of RT and the 1st and 2nd assessment MRIs, which may make the results difficult to apply universally. Seventh, our minimum follow-up was 1 year and some studies support a minimum follow-up of 2 years [37]. However, the majority of local regrowths do occur in the 1st year [40–42] and the probability of remaining free of local regrowth for an additional 2 years if a patient sustains a CR for 1 year is 88.1 %, as reported by Fernandez L et al. [42]. Finally, we did not evaluate lymph node, tumour deposit and EMVI response, on which clinical decisions also rely, but no extra-rectal pelvic recurrences were present in any of the patients in the SCR group.

6. Conclusions

We were able to extract from simple measurements performed on the standard T2-weighted images of the 1st two restaging MR examinations, specific and reliable information on the likelihood of an uncontrolled primary tumour. According to our results, patients with scars that expand by 21° or more between 1st and 2nd evaluation post-RT, or with a thickness of >10 mm at 2nd evaluation post-RT will very likely need surgery for cure, even if no clinical signs of tumour persistence are present. The low sensitivity precludes that we use these parameters alone but it may be that, together with other tools with high sensitivity for residual tumour, such as mrTRG, they may contribute to better rectal cancer patient selection for "W&W".

CRediT authorship contribution statement

Inês Santiago: Conceptualization, methodology, investigation, formal analysis, writing. **Maria Barata:** Conceptualization, methodology, investigation. **Nuno Figueiredo:** Data curation, review and editing. **Oriol Parés:** Review and editing. **Celso Matos:** Review and editing, supervision.

Funding

This research did not receive any specific grant from funding agencies in the public, commercial, or not-for-profit sectors.

Contributions

IS and MJB designed the study. NF and OP created the patient database. IS and MJB performed the image analysis. IS performed the statistics analysis. IS drafted the manuscript. MJB and CM revised the manuscript.

Ethics approval and consent to participate

This retrospective study was approved by the Champalimaud Foundation review board. Informed consent was obtained from all patients.

Consent for publication

Not applicable

Declaration of Competing Interest

The authors report no declarations of interest.

Acknowledgements

The authors would like to thank all personnel working in the Radiology Department and Digestive Unit of the Champalimaud Foundation.

References

[1] E. Ward, R. Sherman, S. Henley, et al., Annual report to the nation on the status of Cancer, featuring Cancer in men and women age 20-49 years, J. Natl. Cancer Inst. 111 (12) (2019) 1279.
[2] D. Davis, J. Marcet, J. Frattini, et al., Is it time to lower the recommended screening age for colorectal cancer? J. Am. Coll. Surg. 213 (3) (2011) 352.
[3] R. Meester, A. Mannalithara, I. Lansdorp-Vogelaar, et al., Trends in incidence and stage at diagnosis of colorectal cancer in adults aged 40 through 49 years, 1975-2015, JAMA 321 (19) (2019) 1933.
[4] D. Ahnen, S. Wade, W. Jones, et al., The increasing incidence of young-onset colorectal cancer: a call to action, Mayo Clin. Proc. 89 (2) (2014) 216–224.
[5] R. Bahadoer, E. Dijkstra, B. Van-Etten, et al., Short-course radiotherapy followed by chemotherapy before total mesorectal excision(TME) in locally advanced rectal cancer – the randomized RAPIDO trial, J. Clin. Oncol. 38 (15) (2020) 4006.
[6] Y. Tan, D. Fu, D. Li, et al., Predictors and risk factors of pathologic complete response following neoadjuvant C. hemoradiotherapy for rectal Cancer: a population-based analysis, Front. Oncol. 9 (2019) 497.
[7] J. Socha, L. Kepka, W. Michalski, et al., The risk of distant metastases in rectal cancer managed by a watch-and-wait strategy – a systematic review and meta-analysis, Radiother. Oncol. 144 (2020) 1–6.
[8] M. van-der-Valk, D. Hilling, E. Bastiaannet, et al., Long-term outcomes of clinical complete responders after neoadjuvant treatment for rectal cancer in the International Watch & Wait Database(IWWD): an international multicentre registry study, Lancet 391 (2018) 2537–2545.
[9] F. Dossa, T. Chesney, S. Acuna, et al., A watch-and-wait approach for locally advanced rectal cancer after a clinical complete response following neoadjuvant chemoradiation: a systematic review and meta-analysis, Lancet Gastroenterol. Hepatol. 2 (2017) 501–513.
[10] J. Smith, P. Strombom, O. Chow, et al., Assessment of a watch-and-wait strategy for rectal cancer in patients with a complete response after neoadjuvant therapy, JAMA Oncol. 5 (2019), e185896.
[11] F. Smith, H. Wiland, A. Mace, et al., Clinical criteria underestimate complete pathological response in rectal cancer treated with neoadjuvant chemoradiotherapy, Dis. Colon Rectum 57 (3) (2014) 311–315.
[12] J. Ryan, S. Warrier, A. Lynch, et al., Assessing pathological complete response to neoadjuvant chemoradiotherapy in locally advanced rectal cancer: a systematic review, Colorectal Dis. 17 (2015) 849–861.
[13] S. Sassen, M. de Booij, M. Sosef, et al., Locally advanced rectal cancer: is diffusion weighted MR imaging helpful for the identification of complete responders (ypT0N0) after neoadjuvant chemoradiation therapy? Eur. Radiol. 23 (2013) 3440–3449.

[14] S. Nougaret, C. Reinhold, H. Mikhael, et al., The use of MR imaging in treatment planning for patients with rectal carcinoma: have you checked the "DISTANCE"? Radiology 268 (2) (2013) 330–344.
[15] B. Hupkens, et al., Organ preservation in rectal cancer after chemoradiation: Should we extend the observation period in patients with a clinical near-complete response? Ann. Surg. Oncol. 25 (1) (2019) 197–203, 218.
[16] G. Simpson, P. Hopley, J. Wilson, et al., Long-term outcomes of real world 'watch and wait' data for rectal cancer after neoadjuvant chemoradiotherapy, Colorectal Dis. 22 (2020) 1568–1576.
[17] G. Beets, N.L. Figueiredo, A. Habr-Gama, et al., A new paradigm for rectal cancer: organ preservation: introducing the International Watch & Wait Database (IWWD), Eur. J. Surg. Oncol. 41 (12) (2015) 1562–1564.
[18] T. Koo, M. Li, A guideline of selecting and reporting intraclass correlation coefficients for reliability research, J. Chiropr. Med. 15 (2) (2016) 155–163.
[20] R. Beets-Tan, D. Lambregts, M. Maas, et al., Magnetic resonance imaging for clinical management of rectal cancer: updated recommendations from the 2016 European Society of Gastrointestinal and Abdominal Radiology (ESGAR) consensus meeting, Eur. Radiol. 28 (4) (2018) 1465–1475.
[21] M. Gollub, S. Arya, R. Beets-Tan, et al., Use of magnetic resonance imaging in rectal cancer patients: society of Abdominal Radiology(SAR) rectal cancer disease-focused panel(DFP) recommendations, Abdom. Radiol. 43 (11) (2017) 2893–2902.
[22] S. Park, S. Cho, S. Choi, et al., MRI assessment of complete response to preoperative chemoradiation therapy for rectal Cancer: 2020 guide for practice from the Korean society of abdominal radiology, Korean J. Radiol. 21 (7) (2020) 812–828.
[23] I. Santiago, M. Barata, N. Figueiredo, et al., The split scar sign as an indicator of sustained complete response after neoadjuvant therapy in rectal cancer, Eur. Radiol. 30 (1) (2020) 224–238.
[24] M. Sidiqui, K. Gormly, J. Bhoday, et al., Interobserver agreement of radiologists assessing the response of rectal cancers to preoperative chemoradiation using the MRI tumour regression grading (mrTRG), Clin. Radiol. 71 (2016) 854–862.
[25] H. Yoen, H. Park, S. Kim, et al., Prognostic value of tumour regression grade on MR in rectal cancer: a large-scale, single-center experience, Korean J. Radiol. (2020), 10.3348.
[26] J. Bhoday, F. Smith, M. Siddiqui, et al., Magnetic resonance tumour regression grade and residual mucosal abnormality as predictors for pathological complete response in rectal cancer postneoadjuvant chemoradiotherapy, Dis. Colon Rectum 59 (10) (2016) 925–933.
[27] I. Nagtegaal, R. Glynne-Jones, How to measure tumour response in rectal cancer? An explanation of T discrepancies and suggestions for improvement, Cancer Treat. Rev. 84 (2020), 101964.
[28] S. Kim, J. Lee, S. Hong, et al., Locally advanced rectal cancer: added value of diffusion-weighted MR imaging in the evaluation of tumour response to neoadjuvant chemo- and radiation therapy, Radiology. 253 (2009) 116–125.
[29] D. Lambregts, V. Vandecaveye, B. Barbaro, et al., Diffusion-weighted MRI for selection of complete responders after chemoradiation for locally advanced rectal cancer: a multicenter study, Ann. Surg. Oncol. 18 (2011) 2224–2231.
[30] D. Lambregts, A. Delli-Pizzi, M. Lahaye, et al., A pattern-based approach combining tumour morphology on mri with distinct signal patterns on diffusion-weighted imaging to assess response of rectal tumours after chemoradiotherapy, Dis. Colon Rectum 61 (3) (2018) 328–337.
[31] Y. Cui, X. Yang, Z. Shi, et al., Radiomics analysis of multiparametric MRI for prediction of pathological complete response to neoadjuvant chemoradiotherapy in locally advanced rectal cancer, Eur. Radiol. 29 (3) (2018) 1211–1220.
[32] Y. Xiaoping, P. Qian, Z. Youming, et al., MRI-based radiomics predicts tumour response to neoadjuvant chemoradiotherapy in locally advanced rectal Cancer, Front. Oncol. 9 (2019) 552.
[33] N. Horvat, H. Veeraraghavan, M. Khan, et al., MR imaging of rectal Cancer: radiomics analysis to assess treatment response after neoadjuvant therapy, Radiology 287 (3) (2018) 833–843.
[34] J. Bibault, P. Giraud, M. Housset, et al., Deep Learning and Radiomics predict complete response after neo-adjuvant chemoradiation for locally advanced rectal cancer, Sci. Rep. 8 (2018) 12611.
[35] M. Maas, D. Lambregts, P. Nelemans, et al., Assessment of clinical complete response after chemoradiation for rectal cancer with digital rectal examination, endoscopy, and MRI: selection for organ-saving treatment, Ann. Surg. Oncol. 22 (2015) 3873–3880.
[36] H. Ko, Y. Choi, J. Lee, et al., Combination assessment of clinical complete response of patients with rectal cancer following chemoradiotherapy with endoscopy and magnetic resonance imaging, Ann. Coloproctol. 35 (2019) 202–208.
[37] L. Kuo, J. Chiou, C. Tai, et al., Can we predict pathologic complete response before surgery for locally-advanced rectal cancer treated with preoperative chemoradiation therapy? Int. J. Colorectal Dis. 27 (2012) 613–621.
[38] S. Liu, G. Zhong, W. Zhou, et al., Can endorectal ultrasound, MRI, and mucosa integrity accurately predict the complete response for mid-low rectal cancer after preoperative chemoradiation? A prospective observational study from a single medical center, Dis. Colon Rectum 61 (2018) 903–910.
[39] M. van-der-Sande, G. Beets, B. Hupkens, et al., Response assessment after (chemo) radiotherapy for rectal cancer: why are we missing complete responses with MRI and endoscopy? Eur. J. Surg. Oncol. S0748-7983 (18) (2018), 32017–32011.
[40] M. Dattani, R.J. Heald, G. Goussous, et al., Oncological and survival outcomes in watch and wait patients with a clinical complete response after neoadjuvant chemoradiotherapy for rectal cancer: a systematic review and pooled analysis, Ann. Surg. 268 (6) (2018) 955–967.
[41] S. Chadi, L. Malcomson, J. Ensor, et al., Factors affecting local regrowth after watch and wait for patients with a clinical complete response following chemoradiotherapy in rectal cancer (InterCoRe consortium): an individual participant data meta-analysis, Lancet Gastroenterol. Hepatol. 3 (12) (2018) 825–836.
[42] L. Fernandez, G. São-Julião, N. Figueiredo, et al., Conditional recurrence-free survival of clinical complete responders managed by watch and wait after neoadjuvant chemoradiotherapy for rectal cancer in the International Watch & Wait Database: a retrospective, international, multicentre registry study, Lancet Oncol. 22 (1) (2021) 43–50.

5.5. Advances in knowledge

We described three new T2-weighted MR imaging methods to distinguish patients who will sustain a complete response over time from those who won´t, in the early period that follows radiotherapy – the split scar sign, the scar depth angle difference and the scar thickness at second assessment. The analysis was performed retrospectively, blindly and independently by two specialized radiologists, to all eligible patients in our prospectively-recorded rectal cancer database. Interobserver agreement was assessed and the new methods were confronted with standard assessment tools, namely endoscopy, mrTRG (or similar) and DWI, to determine their added value. We will now summarize the advances in knowledge for each of them:

Split Scar Sign

- The split scar sign is a morphologic pattern visible on high-resolution T2-weighted MR imaging in rectal cancer patients after neoadjuvant therapy. It therefore does not require any changes to standard protocol.
- At first restaging pelvic MR imaging (mean: 9.1 weeks after the end of radiotherapy), the split scar sign identified patients who sustained a complete response with very high specificity (0.97) and positive predictive value (0.93–0.94).
- Its interobserver agreement was substantial (k=0.69, p<0.01).
- The split scar sign performed better than conventional T2-weighted (p=0.19/0.75) and DWI (p=0.18/<0.01) assessments, and also better than endoscopy (p=0.59).
- The split scar sign may have the potential to improve patient selection for “Watch-and-Wait” after neoadjuvant therapy in rectal cancer.

Scar Depth Angle Difference

- The scar depth angle difference is based on simple measurements on T2-weighted MR imaging by specialized radiologists and as such does not imply any change in standard re-staging acquisition protocol.
- A tumour scar depth angle increase > 21º between the first and second MR Imaging assessments post-neoadjuvant therapy (med: 10 weeks and 23 weeks after the end of

radiotherapy, respectively) was highly specific for a non-sustained complete response (specificity=0.91/0.94).

- Inter-observer agreement was good (intraclass correlation coefficient of 0.65).
- Its performance was superior to that of the retrieved endoscopy and mrTRG assessments. It was equivalent to that of retrieved DWI but all false positive DWI evaluations were negative for scar depth angle change, boding well for a combined analysis.

Scar thickness at second assessment

- The scar thickness at second assessment (med: 23 weeks after the end of radiotherapy) is based on simple measurements on T2-weighted MR imaging by specialized radiologists.
- A thickness >10mm indicated a non-sustained complete response with very high specificity (0.91/0.94).
- Inter-observer agreement was excellent (intraclass correlation coefficient of 0.84).
- Its performance was superior to that of the retrieved endoscopy and mrTRG assessments. It was equivalent to that of retrieved DWI but all false positive DWI evaluations were negative for scar thickness at second assessment, boding well for a combined analysis.

The split scar sign, the scar depth angle difference and the scar thickness at second assessment are 3 promising imaging biomarkers to differentiate “true” complete responders from patients who will require surgery for cure, in the early period after neoadjuvant therapy. They are based on simple analysis of standard MR T2-weighted images, which may ease their clinical implementation, should they be validated prospectively.

6. Summary and perspectives

The present thesis focused on MR imaging in rectal cancer and was divided in two parts: In the first part, we targeted the "Achilles heel" of rectal cancer staging – lymph node classification. We elaborated on the development of two new methodologies ex-vivo at ultra-high MR field strength and in robust co-registration with histology, named Susceptibility Perturbation MR Imaging and Higher-order Diffusion MR Imaging. We then described the translation of the experiments to an in-vivo context, at 1.5 Tesla during patient staging, and their added value for lymph node classification; In the second part, we pinpointed the re-staging of locally-advanced rectal cancer after neoadjuvant therapy. We described 3 simple new methods, based on the visual analysis of standard high resolution T2-weighted images, to differentiate sustained complete responders from non-sustained complete responders. These methods, named the split scar sign, the scar depth angle difference and the scar thickness at second assessment, may have the potential to aid in patient selection for "Watch-and-Wait" versus curative resection.

The next steps regarding the research presented should be to test the methods prospectively at multiple institutions, using different MR equipment and acquisition protocols, with adequate validation: Susceptibility Perturbation MR Imaging and Higher-order Diffusion MR Imaging will require careful co-registration with histology; the split scar sign, the scar depth angle difference and the scar thickness at second assessment will require co-registration with pathology and/or long-term "Watch-and-Wait" follow-up. The impact of the use of any of these methods on long-term patient outcome should also be assessed.

The content of this thesis is not trendy, given it emerges in the middle of a deluge of radiology research on artificial intelligence and, when it comes to oncology, radiomics is a particularly appealing field. The latter consists of the extraction of a large number of quantitative features from radiological images in search of new signatures to improve tumour phenotyping and to predict and evaluate response to therapy. Although it is underlined with the premise that radiological images reflect pathophysiology, most of the quantitative features are agnostic, meaning they fail to be appreciated by the human eye. To jump beyond promising into clinical practice, these powerful tools will require a process of validation that includes some form of biological understanding. As such, a combined analysis with conventional semantics is encouraged, as well as integration with clinical data such as histology, immunohistochemistry, mutational status, immunologic phenotype, habitat subregional mapping and others. Not only will the integration provide more intelligible answers, but also increase specificity towards patient management. We believe radiomics and other

artificial intelligence algorithms will not halt innovation in image acquisition methods, given the latter can only feed the former with additional information. Also, we believe these algorithms may greatly assist radiologists on a relatively short run, complementing their conventional semantic analysis and their reasonableness to deal with the unexpected.